UNIVERSITY OF OXFORD

E-CADHERIN LOSS OF FUNCTION IN THE MURINE INTESTINE

Submitted for the Degree of Doctor of Philosophy

by

Julia Matheson

Balliol College
Oxford
Trinity 2012

E-CADHERIN LOSS OF FUNCTION IN THE MURINE INTESTINE

Submitted for the degree of Doctor of Philosophy

By
Julia Matheson
Balliol College
Trinity 2012

Thesis Abstract

E-cadherin (*Cdh1)*, is a major component of epithelial adherens junctions, binds the Wnt pathway effector β-catenin and is lost at the invasive edge of colon cancers. Crypt stem cells give rise to 4 cell lineages that, with the exception of Paneth cells, travel along the crypt-villus axis over 3 days and are shed by anoikis. Gain of function of the Wnt pathway by a mutation in Adenomatous Polyposis Coli (*Apc*) disrupts enterocyte turnover to result in adenoma formation. Homozygote null *Cdh1* is embryonic lethal, and heterozygote *Cdh1* can promote Apc^{1638N} induced adenoma formation, but we lack models that assess additional functions of *Cdh1* in the adenoma to carcinoma transition. The aim of this thesis was to evaluate the effect of *Cdh1* loss of function in the murine intestine, including in the setting of Wnt pathway activation. To do this, germline and intestinal specific conditional *Cdh1* loss of function models were generated.

Conditional homozygous deletion of *Cdh1* resulted in embryonic lethality using *Villin-Cre*. In adults, homozygous *Cdh1* loss using the tamoxifen inducible *Villin-*$CreER^{T2}$ led to intestinal inflammation, bacteraemia and disrupted crypt-villus architecture. Combined conditional homozygous deletion of *Cdh1* and *Apc* resulted in Wnt pathway upregulation assessed by β-catenin immunolabelling. Strain dependent effects of *Cdh1* heterozygosity were apparent on the *Apc* heterozygote background: $Apc^{Min/+}$ $Cdh1^{+/-}$ (C57BL/6J) had no effect on survival or adenoma phenotype compared to littermate $Apc^{Min/+}$; $Cdh1^{+/fl}$ increased adenoma burden in $Apc^{+/fl}$ *Vil-Cre* animals (B6D2/C57BL/6J).

Low frequency recombination of $Apc^{fl/fl}$ using *Lgr5-EGFP-IRES-*$CreER^{T2}$ bypasses the loss of heterozygosity event relied on in heterozygous *Apc* tumour models achieving a large adenoma burden within 4 weeks. *Cdh1* loss did not alter survival or adenoma phenotype in this model, including the development of large caecal tumours. Immunolabelling of tumours from $Apc^{fl/fl}$ $Cdh1^{fl/fl}$ animals showed persistent E-cadherin protein expression, suggesting incomplete recombination or that double homozygote enterocytes failed to survive. *In vitro* adenoma culture was used to test whether E-cadherin loss was incompatible with enterocyte survival in the setting of Wnt activation. $Apc^{fl/fl}$ $Cdh1^{+/+}$ and $Apc^{fl/fl}$ $Cdh1^{fl/fl}$ adenoma were cultured in matrigel and treated with an adenovirus expressing Cre recombinase under a CMV promoter (Ad-Cre). Ad-Cre had no effect on $Apc^{fl/fl}$ $Cdh1^{+/+}$ adenoma growth. Ad-Cre treated $Apc^{fl/fl}$ $Cdh1^{fl/fl}$ adenoma organoids showed cells where E-cadherin loss resulted in Wnt pathway upregulation as assessed by nuclear β-catenin and Axin2 expression, and epithelial mesenchymal transition shown by upregulation of fibronectin, twist and vimentin. This work supports a role for E-cadherin in modulation of the Wnt pathway. Further investigation is required to define the cell adhesion versus Wnt regulatory functions of E-cadherin.

Table of Contents

Acknowledgments

A decade ago, sitting in a lecture listening to Parry Guilford describe the story of finding E-cadherin mutations in a Maori kindred with gastric cancer, I remember being fascinated. Little did I know just how well I would get to know this gene. Thank you firstly to Bass, for the opportunity to tackle this work. Without his support, enthusiasm and encouragement this would not have been possible. The past four years have been an education not only in cancer biology and molecular genetics, but also by example in the challenges and rewards of being a clinician-scientist.

Everyone in the Hassan Lab has contributed to this journey in some way. Thanks must go to Jen for teaching me the ropes of mouse work, Emma for support with genotyping and *in vitro* work, and Dave and Vikki for being model senior DPhil students. Thank you also to Hans and David for help with constructs for the next phase of work. Enormous thanks must go to Claudia, who has taught me everything I know about imaging. Her support and wisdom have been vital to this project. Hats, Susana, and Andrea have provided key moral support over the past few months.

The Dunn School has been a fantastic Department. Kevin Maloy has been a helpful and enthusiastic advisor and the rest of the Maloy crew great lab neighbours. Thank you to the staff at PSB for their expert animal care, to Richard for providing excellent histology at high speed and to Hans Morreau for pathology input. Also thanks to Alan Wainman for assistance and patience setting up the live cell imaging. I am grateful to collaborators who have provided mice and reagents central to experiments.

I would like to acknowledge the Rhodes Trust, not only for financial support, but also for providing a wonderful supportive community in Oxford. Thanks to Balliol College for a generous scholarship and to Piers Nye and Jonathan Bard for being encouraging College advisors. I am also extremely appreciative of financial support from the Dunn School for the final year of the DPhil and to Cancer Research UK for providing core lab funding.

Enormous thanks must go to people behind the scenes who have inspired and believed in me. A wonderful mentor, Stephen Robertson, deserves special mention for encouraging me to be brave and tackle the bench. Friends in Oxford and at home have provided necessary laughter and light relief when the science has been tough. I am blessed with an incredible family. Huge thanks to Mum, Dad, Richard and Emma who have shared the highs and the lows of the past four years from afar and always supported me chasing my dreams. Finally, I cannot thank Trav enough. He has been there for every challenge and hurdle of this journey, with unwavering support and understanding. I could not have done it without him.

List of Tables

List of Figures

Abbreviations

4OHT	4-hydroxytamoxifen
aa	Amino acid
Ad-Cre	Adenovirus Cre recombinase
APC	Adenomatous polyposis coli
ATP	Adenosine triphosphate
ATP5a1	ATP synthase gene
βTrCP	Beta-transducin repeat containing protein
BCL9	B-cell lymphoma
BCP	1-bromo-3-chloropropane
Bmi-1	B lymphoma Mo-MLV insertion region 1 homolog
BMP	Bone morphogenetic protein
BrdU	Bromodeoxyuridine
C	Celcius
CBC	Crypt base columnar cell
CBP	CREB binding protein
CC3	Cleaved caspase 3
Cdh1	E-cadherin
CK1	Casein kinase 1
CMV	Cytomegalovirus
COMP	Cartilage oligomeric matrix protein
CRC	Colorectal cancer
CTOS	Cancer tissue-originated spheroid
DAB	3-,3-diaminobenzidine
DAPI	4',6-diamidino-2-phenylindole
DCC	Deleted in Colorectal Cancer
DEPC	Diethylpyrocarbonate
DGC	Diffuse gastric cancer
DKK	Dickkopf
DNA	Deoxyribonucleic acid
DPC4	Deleted in Pancreatic Carcinoma
Dsh	Dishevelled
DTT	DL-Dithiothreitol
E	Embryonic
EB1	End binding 1
EC	Extracellular
ECADCOMP	A recombinant E-cadherin ectodomain, pentamerized by the assembly domain of cartilage oligomeric matrix protein
EDTA	Ethylenediaminetetraacetic acid
EdU	5-ethynyl-2'-deoxyuridine
EGF	Epidermal growth factor
EGFR	Epidermal growth factor receptor
EMT	Epithelial mesenchymal transition
ENU	N-ethyl-N-nitrosourea
Eplin	Epithelial protein lost in neoplasm
ES	Embryonic stem
FACS	Fluorescence-activated cell sorting
FAP	Familial adenomatous polyposis
FFPE	Formalin fixed paraffin embedded
FLP	Flippase

FRP	Frizzled-related protein
FRT	Flippase recognition target
Fz	Frizzled receptor
GC	Gastric cancer
GFP	Green fluorescent protein
GMRG	Geometric mean reference genes
GOI	Gene of interest
GSK	Glycogen synthase kinase
H&E	Hematoxylin and eosin
HAV	Histidine-Alanine-Valine
HDAC	Histone deacetylases
HDGC	Hereditary diffuse gastric cancer
HDLG	Human disc large
HHT	Hereditary haemorrhagic telangiectasia
HMG	High mobility group
HNPCC	Hereditary nonpolyposis colorectal cancer
IgG	Immunoglobulin G
Int-1	Integration 1
IP	Intraperitoneal
JPS	Juvenile polyposis syndrome
L-CAM	Liver cell adhesion molecule
LEF	Lymphoid enhancer-binding factor 1
Lgr5	Leucine-rich repeat containing G-protein-coupled receptor
LNA	Locked nucleic acid
LOH	Loss of heterozygosity
LRP	Lipoprotein receptor-related protein
MAPK	Mitogen-activated protein kinase
Math1	Mouse atonal homologue 1
MET	Mesenchymal epithelial transition
MH	Mad-homology
miRNA	Micro RNA
MLH1	MutL homolog 1
MGI	Mouse genome informatics
MMTV	Mouse mammary tumour virus
MOI	Multiplicity of infection
Mom	Modifier of Min
NaCl	Sodium chloride
NBF	Neutral buffered formalin
NHEKs	Normal human epidermal keratinocytes
NMR	Nuclear magnetic resonance
NMU	N-Nitroso-N-methylurea
P	Postnatal
PBS	Phosphate buffered saline
PCR	Polymerase chain reaction
PFU	Plaque forming units
PGE2	Prostaglandin E2
PI3K	Phosphoinositide 3-kinase
PS1	Presenilin-1
QPCR	Quantitative polymerase chain reaction
QTL	Quantitative trait loci
RIN	RNA integrity number
Rint-1	Rad 50-interacting protein 1
RNA	Ribonucleic acid

RT	Reverse transcription
SAD	Smad4 activation domain
SDS	Sodium dodecyl sulfate
Ser	Serine
sFRPs	Secreted Frizzled-related proteins
SI	Small intestine
SIP1	Smad-Interacting Protein
SPF	Specific pathogen free
TAK1	TGFβ Activated Kinase 1
TBE	Tris/Borate/EDTA
TBS	Tris-buffered saline
TCF	T-cell factor
TGF	Transforming growth factor
UPL	Universal Probe Library
VEGF	Vascular endothelial growth factor
Vil-Cre	*Villin-Cre*
Vil-CreER^{T2}	*Villin-CreER^{T2}*
Wg	Wingless
WIF1	Wnt inhibitory factor
YFP	Yellow flurorescent protein

1 Introduction

Colorectal cancer (CRC) is a major cause of cancer mortality. Over a million new cases were diagnosed worldwide in 2002 and it is the second leading cause of cancer mortality in the United Kingdom (Parkin et al, 2005). It is estimated that over 12 billion dollars was spent on the care of patients with CRC in the United States of America in 2006 alone (National Cancer Institute, April 2010). Surgery remains the mainstay of treatment and whilst effective for localized disease, curative rates for metastatic disease are low even with adjuvant therapy. Although there has been much progress in understanding the molecular pathogenesis of CRC, this has been slow to translate into effective targeted molecular therapies (Cunningham et al, 2010). One of the main barriers to effective targeted molecular therapies has been the lack of *in vivo* models of the adenoma to carcinoma transition to identify key therapeutic targets.

Cdh1 encodes a protein called E-cadherin that is involved in cell adhesion and linked to the Wnt signalling pathway. Loss of E-cadherin has been implicated in the invasive stage of epithelial cancers, particularly gastric cancer and lobular breast cancer. Its role in CRC has been more contentious. This thesis uses mouse models to examine the effect of loss of E-cadherin in the normal intestine and intestinal tumourigenesis. It also examines the role of a second candidate gene for CRC invasion that can regulate E-cadherin, *Smad4*.

1.1 The intestinal epithelium

The intestinal epithelium is a barrier to the outside world and its correct functioning relies on carefully orchestrated homeostasis and rapid cell turnover. In humans the whole epithelium is renewed every 5 days making it the most proliferative tissue in the human body (Schuijers & Clevers, 2012). The structure of the intestinal epithelium reflects two main functions: absorption and immune defence. Effective absorption relies partly on a large surface area. Barrier function requires strong cell adhesion and an active mucosal immune system. The intestinal tract is effectively a three layered tube: an outer smooth muscle later for peristalsis, a middle stromal layer that includes immune cells, and an inner mucosal layer of a sheet of epithelial cells. In the small intestine, the epithelial sheet is folded into numerous luminal

projections called villi with submucosal invaginations called the crypts of Lieberkühn. The large intestine has a flat surface epithelium with crypts.

The crypt is the proliferative compartment where multipotent stem cells reside and the villus is the differentiated compartment. Intestinal villi form from embryonic day 15, but at birth mice only have shallow crypt pockets that develop in early postnatal weeks into mature crypt units (Crosnier et al, 2006). Leucine-rich repeat containing G-protein-coupled receptor (*Lgr5*) positive stem cells reside at the crypt base, flanked by Paneth cells which have a key function in maintaining the stem cell niche (Barker et al, 2007; Sato et al, 2011b). Stem cells create an immediate population of transit amplifying cells that undergo 4 to 5 cycles of cell division before entering the villus compartment as differentiated cells of four main epithelial lineages: enterocytes, the absorptive cells; goblet cells which produce mucus to protect the epithelium; enteroendocrine cells, the hormone-secreting cells; and Paneth cells which secrete antimicrobial peptides including lysozyme and maintain the stem cell niche. Paneth cells migrate to the bottom of the crypt where they reside for 3-6 weeks, whereas the other cell types away from the crypt, taking about 5 days (3 days in mice) to travel to the tip of the villus where they undergo anoikis and are exfoliated into the intestinal lumen (Pinto & Clevers, 2005; Sancho et al, 2004). The turnover is more impressive when the number of cells is taken into account: each villus has 2000-7000 cells (depending on the region of the intestine) and is circled by about 15 crypts, each with 350-550 cells. There are roughly a million crypts in a mouse small intestine (Pinto & Clevers, 2005).

Proliferation and cell fate decisions in the intestinal crypt are controlled by key signalling pathways. The Wnt pathway has been shown to be critical for stem cell regulation through a number of mouse models disrupting components of the Wnt signalling pathway that result in abrogated crypt development or proliferation (Schuijers & Clevers, 2012). Whilst coordinated Wnt activation is necessary for progenitor cell maintenance and proliferation, inappropriate Wnt activation is often seen in tumourigenesis, suggesting the two situations have much in common. For example, Wnt pathway activation is seen in over 90% of colorectal cancers (CRCs) (Cancer Genome Atlas Network, 2012). Additionally, 'lineage retracing' using the R26R-Confetti reporter mouse has recently shown that *Lgr5* cells constitute 5-10% of intestinal adenoma cells,

are flanked by Paneth cells as they are in intestinal crypts, and drive adenoma growth, supporting the concept of a cancer stem cell (Schepers et al, 2012).

I will come to the Wnt pathway in detail in the following section. Notwithstanding, a particular Wnt target gene, *Lgr5*, must be introduced here in the context of stem cell maintenance. For many years, two schools of thought existed as to location of the intestinal stem cell: the '+4 position model' and the 'stem cell zone model' (Barker et al, 2008). In the +4 position model, stem cells were believed to reside at cell position 4 from the base of the intestinal crypt. Evidence supporting their 'stemness' included rapid cycling and high sensitivity to radiation (Potten, 1977; Potten et al, 1974). The stem cell zone model was based on observations dating back to the 1970s, whereby electron microscopy was employed to show a population of thin cycling cells called crypt base columnar cells (CBCs) located between Paneth cells at the crypt base (Barker et al, 2008). *Lgr5*, confirmed as a Wnt target gene in microarray expression analysis of human CRC cell lines, was shown to mark the CBCs specifically (Van der Flier et al, 2007). Lineage tracing using *Lgr5* transgenes driving the expression of *GFP* and *CreER*^{T2}, crossed with *Rosa-LacZ* reporter mice, revealed a single *Lgr5* CBC could give rise to all differentiated cell lineages in the intestine. Furthermore, labelling was seen to persist over the lifetime of the animal, confirming the cells were multipotent and long-lived (Barker et al, 2007). Contrary to the classic stem cell definition *Lgr5* positive cells are not quiescent, dividing once every 24 hours (Barker et al, 2007).

Whilst *Lgr5* positive CBCs are now widely considered the intestinal stem cells, there is evidence that a second pool of stem cells exists. B lymphoma Mo-MLV insertion region 1 homolog (*Bmi-1*) has been identified as a marker of '4+' cells. Lineage tracing experiments have shown that such cells, though less common than *Lgr5* positive CBCs, are also multipotent and long-lived (Sangiorgi & Capecchi, 2008). With complete ablation of *Lgr5* expressing cells in mice, *Bmi-1* positive cells become highly proliferative and lineage tracing shows they can give rise to *Lgr5* positive cells (Tian et al, 2011). Thus, *Bmi-1* cells may be a reserve stem cell pool in the event of disturbed homeostasis.

In the past 2 years understanding of the stem cell niche has progressed markedly. Sato and colleagues showed Paneth cells constitute the *Lgr5* stem cell niche, providing essential growth

signals (Sato et al, 2011b). Whilst single *Lgr5* stem cells could be cultured to produce self-organizing crypt villus units, this required an exogenous Wnt supply (Sato et al, 2009). Co-culture of stem and Paneth cells greatly improved the efficiency of formation of these units (Sato et al, 2011a). Conditional removal of Paneth cells from the mouse intestine resulted in loss of *Lgr5* stem cells also and Paneth cells were shown to express factors vital to stem cell maintenance including epidermal growth factor (EGF), transforming growth factor alpha (TGF-α), Wnt3 and Notch ligands. Two recent studies, however, have shown *Lgr5* cells can survive *in vivo* in the absence of Paneth cells in mouse models with Mouse atonal homologue 1 (*Math1*) deficiency (Durand et al, 2012; Kim et al, 2012). This suggests that removing the stem cell dependence on Notch signalling can compensate for decreased Wnt supply *in vivo*.

Lgr5 is a member of the G-protein-coupled 7-transmembrane protein family and was an orphan protein receptor until the ligands Roof plate-specific (R) spondins were identified in 2011 (Schuijers & Clevers, 2012). R-spondins can increase Wnt signalling, particularly in culture where they provide the Wnt drive necessary for crypt formation (Sato et al, 2011a).

Whilst our understanding of intestinal crypt function and proliferative capacity in the intestine has improved dramatically in recent years, there has been less focus on the mechanisms underlying death and shedding of cells. Frisch and Francis coined the term 'anoikis', which in Greek means homelessness, for a form of apoptosis of epithelial cells induced by detachment from the extracellular matrix (Frisch & Francis, 1994). The execution of apoptosis following detachment can occur through the intrinsic or extrinsic apoptotic pathways, with caspase-3 activation (cleaved caspase-3, CC3) being the common event for both pathways (Taddei et al, 2012). Loss of E-cadherin is an early event during enterocyte anoikis and modulation of E-cadherin expression can alter the balance between apoptosis and survival (Fouquet et al, 2004). In normal enterocytes, E-cadherin loss occurs through endocytosis, in a process mediated by epidermal growth factor receptor (EGFR) (Lugo-Martínez et al, 2009). Accordingly, the balance between Wnt signalling at the bottom of the crypt-villus escalator, and E-cadherin-mediated anoikis as cells leave the escalator, may be important in maintaining a functional intestinal epithelium.

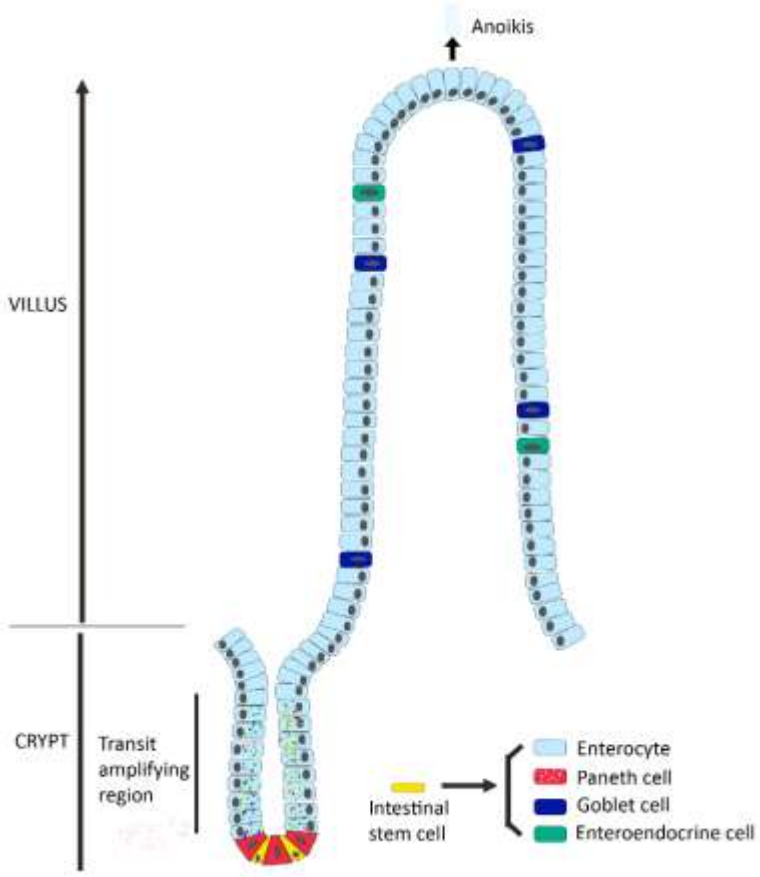

Figure 1. Intestinal crypt-villus structure
Schematic of a small intestinal crypt-villus unit. Lgr5+ intestinal stem cells (yellow) are flanked by Paneth cells (red) at the crypt base. Stem cell division leads to a population of cells in the transit amplifying region where they undergo differentiation into 4 cell lineages: enterocytes (the absorptive cells, light blue), goblet cells (mucus producing cells, dark blue), enteroendocrine cells (hormone secreting cells, green) and Paneth cells (secrete antimicrobial peptides, red). Enterocytes, goblet cells and enteroendocrine cells migrate along the crypt-villus axis, taking 3 days in the mouse to reach the villus tip where they are shed and undergo anoikis.

A number of signalling pathways have roles in maintaining the crypt-villus boundary and cell segregation (Crosnier et al, 2006). The Wnt pathway is my focus. As already outlined, it is active in the crypt, but not the villus of the intestine. The Notch pathway is also predominantly active in the crypt and has a role in determining differentiation of cells into an absorptive (enterocyte) or secretory (Paneth, goblet or enteroendocrine) lineage (Crosnier et al, 2006). Cells that adopt a secretory lineage express notch ligands; through lateral inhibition they prevent their neighbouring cells from adopting the same fate. *Math1* is expressed by precursor cells to all three secretory lineages. *Math1* null mice lack all secretory cells but have normal enterocytes. The Wnt and Notch pathways also together have a role in maintaining the stem cell niche.

The ephrin ligands and Eph receptors have key roles in cell segregation. EphB3 is expressed in Paneth cells. There is a gradient of EphB2 expression from high at the crypt base to low at the crypt-villus junction, and the reverse gradient for the ephrins. They are Wnt regulated genes and exert their segregation effects through repulsive forces between Eph and ephrin expressing cells, in a process mediated by E-cadherin (Cortina et al, 2007). *Eph3* null mice have Paneth cells misplaced throughout the crypt-villus axis, and *Eph2/Eph3* null mice lack a distinct crypt-villus boundary (Batlle et al, 2002).

The Hedgehog pathway also has a role in demarcating the villus from the crypt. Hedgehog signalling from the epithelium to the surrounding mesenchyme is necessary for villus formation and maintaining an appropriate distance between neighbouring crypts. The Bone morphogenetic protein (BMP) pathway has a role in controlling crypt formation. Noggin, a BMP inhibitor, is expressed by the mesenchymal cells surrounding the crypt and the BMP pathway is active in the epithelium of the villus. Overexpression of noggin or bone morphogenetic protein receptor, type IA (*Bmpr1a*) null mice both have increased numbers of crypts, adjacent to the villi in the former, or in the normal position with the latter. Hedgehog and BMP signalling appear to be coordinated to maintain Wnt signalling in the crypt, but repress it in the villus (Crosnier et al, 2006)

1.2 The Wnt pathway

The Wnt pathway has been identified as a key signalling pathway in all animal species. It has fundamental roles in development, an ongoing influence on tissue homeostasis throughout adult life, and frequent dysregulation in tumourigenesis. In 1973 a *Drosophila melanogaster* mutant lacking wings was described. The gene *Wingless (Wg)* was found to be responsible for this segment polarity defect (Nusslein-Volhard & Wieschaus, 1980). In 1982 Nusse and Varmus discovered that activation of a gene they called *integration 1 (Int-1)* by the Mouse Mammary Tumor Virus could cause breast tumours in mice (Nusse & Varmus, 1982). The genes *Integration* and *Wingless* were shown to be homologous and involved in an important signalling pathway, subsequently termed the Wnt pathway (an amalgam of *Wg* and *Int*) (Rijsewijk et al, 1987). Model systems have advanced our understanding of the Wnt pathway, particularly extensive work during development in *Drosophila melanogaster*, and also *Xenopus laevis* and *Mus musculus* models.

Early findings included the duplication of the *Xenopus* body axis following the injection of mouse *Wnt1* mRNA into embryos at the four-cell blastomere stage (McMahon & Moon, 1989). Genes identified in the signalling pathway that were able to induce axis duplication included Dishevelled, β-catenin (*armadillo* in *Drosophila*) and glycogen synthase kinase 3 (GSK3, *shaggy/zeste-white 3* in *Drosophila*) (Guger & Gumbiner, 1995). Many of the genes identified as being tightly regulated during discrete time points in development were subsequently shown to act as oncogenes and tumour suppressor genes when normal regulation was lost. In particular, the discovery that adenomatous polyposis coli (APC), a key tumour suppressor in colonic cancer, was part of the β-catenin destruction complex highlighted the importance of the Wnt pathway in cancer (Rubinfeld et al, 1993; Su et al, 1993).

Most mammals have 19 Wnt genes. Characterization of the proteins has proved challenging. It is known however that post-translational modifications including lipidation are important for both secretion and signalling (Clevers & Nusse, 2012). Successful secretion may rely on Wnt chaperones such as Wntless (Cadigan & Peifer, 2009). Wnt proteins bind to both a Frizzled receptor (Fz) and a lipoprotein receptor-related protein (LRP5 or LRP6) co-receptor at the

plasma membrane. Wnt proteins bind to a cysteine-rich amino terminal domain of seven-transmembrane receptors (Bhanot et al, 1996). Recently it has been shown that Wnt proteins have a structure akin to a hand with a thumb and index finger that grasp binding sites of the cysteine-rich domain with a prominent lipid group or a hydrophobic depression (Janda et al, 2012). A single Wnt protein can bind multiple Fz receptors and vice versa (Bhanot et al, 1996).

A number of inhibitors and activators of the Wnt-Fz interaction have been identified. Fz homologues that share an extracellular cysteine-rich domain with seven transmembrane repeats are one such group, some of which are able to bind Wnt ligands and act as Wnt inhibitors. Molecules have also been identified that lack the transmembrane repeats and are thus able to act as soluble Wnt antagonists, for example Frzb-1, Frzb and the secreted Frizzled-related proteins (sFRPs) (Leyns et al, 1997; Rattner et al, 1997; Wang et al, 1997). Frizzled-related protein has a region homologous to a Wnt-binding domain of frizzled and is a dominant negative receptor (Finch et al, 1997). Dickkopfs (DKKs) are the best characterized Wnt signalling inhibitors. They form a ternary complex with the receptor Kremen and LRP6 that is subsequently endocytosed making the Wnt receptor unavailable (Bafico et al, 2001; Glinka et al, 1998; Mao et al, 2002). Other inhibitors include Wnt inhibitory factor 1 (WIF1), Wise (binds to LRP) and SOST (Hsieh et al, 1999). Activators of the Wnt-Fz interaction include Norrin, which surprisingly has high affinity binding to Fz receptors despite no sequence homology with Wnts, and the R-spondins (Kazanskaya et al, 2004; Kim et al, 2005; Xu et al, 2004).

The mechanism by which Wnt binding to Fz/LRP mediates downstream signalling is insufficiently understood. Wnt stimulation leads to phosphorylation of motifs on the cytoplasmic tail of LRP by GSK3 and casein kinase 1 gamma (CK1γ), creating a docking site for Axin (Mao et al, 2001; Tamai et al, 2004; Tolwinski et al, 2003). The C-terminal of Fz interacts with a cytoplasmic protein called Dishevelled (Dsh) (Wong et al, 2003; Yanagawa et al, 2002). Dsh and Axin both have amino acid sequences called DIX domains that can bind each other, facilitating recruitment by Dsh of Axin to the cell membrane upon Wnt activation to create a signalosome (Cliffe et al, 2003; Fiedler et al, 2011).

1.3 β-catenin is the central effector of the Wnt pathway

β-catenin plays a pivotal role in canonical Wnt signalling. In the absence of Wnt ligands and pathway activation, cytoplasmic β-catenin is taken into a destruction complex including APC, the Axins, CK1α and GSK3β. Understanding of the Wnt signalling model terms of the destruction complex and receptor has recently changed dramatically (Clevers & Nusse, 2012; Li et al, 2012). It was previously thought that when the Wnt pathway was not activated Axin in the destruction complex bound any free β-catenin and its N terminal was phosphorylated by CK1α and GSK3β. CK1α and GSK3β phosphorylate critical N-terminal serines and threonines (Ser33, Ser37 and Thr41) and β-catenin not phosphorylated at these sites has higher transcriptional activity (Guger & Gumbiner, 2000; Staal et al, 2002). The phosphorylated β-catenin, now dissociated from the destruction complex, was ubiquitinated by β-transducin repeat-containing protein (β-TrCP, an E3 ubiquitin ligase) prior to proteasomal degradation (Aberle et al, 1997). However, a model published in June 2012 showed that in the absence of Wnt activation β-catenin is bound by the cytoplasmic destruction complex and all whilst in this complex it is phosphorylated and then ubiquitinated by β-TrCP before being recycled by the proteasome (Figure 2) (Li et al, 2012). When the Wnt pathway is activated, the destruction complex binds to LDL receptor-related protein (LRP) through Axin, where phosphorylation of free β-catenin can still take place, but ubiquitination is blocked. The destruction complex becomes saturated with phosphorylated β-catenin, leaving free cytoplasmic β-catenin to translocate to the nucleus. Thus, instead of phosphorylation of β-catenin being impaired upon Wnt activation, ubiquitination is the critical step that cannot be completed.

The actual mechanism of transport of β-catenin to the nucleus is unclear, but may be via active transport by microtubules (Sugioka et al, 2011). Groucho usually interacts with histone deacetylases (HDAC), making DNA refractive to transcriptional activation (Chen et al, 1999). However, β-catenin can displace Groucho, forming a complex with lymphoid enhancer-binding factor/transcription factors (LEF-TCF) and coactivators to activate transcription of target genes. TCFs bind specific DNA sequences through high mobility group (HMG) domains (Laudet et al, 1993). Co-activators include legless/B-cell lymphoma 9 (BCL9), Pygopus, CREB binding protein (CBP), and Hyrax, (Daniels & Weis, 2005; Thompson et al, 2002). TCF forms a bridge between

Pygopus and the N-terminal of β-catenin and this complex has a role in the nuclear stabilization of β-catenin and may also have a direct role in the transcriptional activation carried out by β-catenin (Hoffmans et al, 2005; Townsley et al, 2004). TCF can be modulated through phosphorylation by the mitogen activate protein kinase-related NEMO-like kinase (after activation by TAK1) leading to decreased binding and transcriptional activation by the β-catenin/TCF complex (Ishitani et al, 1999). A number of other key proteins in the Wnt pathway such as APC, Axin and Dsh are also able to localize to the nucleus where it is thought they may have a role in modulating β-catenin transcriptional activity, potentially by buffering TCF-β-catenin interactions such that they only complex and activate transcription when a critical threshold of β-catenin is achieved (Cadigan & Peifer, 2009; Willert & Jones, 2006).

A broad range of Wnt target genes can subsequently be transcriptionally modulated, with functions including proliferation, cell signalling, differentiation and adhesion. Whilst transcriptional activation is most common, the TCF-β-catenin complex can repress transcription of some genes including *Cdh1* (Jamora et al, 2003). Any mutational event that stabilises nuclear β-catenin has the potential to influence proliferation and tumour progression in the intestinal epithelium through the persistent activation of the Wnt pathway. Multiple mechanisms can control the transcription of β-catenin (Jin et al, 2008). With such diverse transcriptional outputs, it is often the cell rather than the signal that dictates the response to Wnt signalling. Autoregulatory mechanisms are important with a number of components of the pathway being target genes. The discovery of known proto-oncogenes such as *C-Myc* as direct Wnt targets gave research into the role of the Wnt pathway in cancer momentum (He et al, 1998).

In addition to its function as a Wnt effector, β-catenin forms part of the adhesion complex through binding to E-cadherin. β-catenin has an amino and C-terminal terminal domain of 149 and 108 amino acids respectively that flank a central domain of 515 residues with 12 armadillo (arm) repeats that is essential for binding to cadherins, APC, Axin and TCF (Behrens et al, 1998; Behrens et al, 1996; Hulsken et al, 1994). Each arm repeat has three α helices; together these form a superhelix with a long groove that is positively charged (Huber et al, 1997). The cadherin cytoplasmic domain is unstructured in its unbound state and binds to β-catenin over a large

interface including all arm repeats (Huber et al, 2001). The lack of a rigid structure means the binding interaction can be regulated in a graded manner by posttranslational modifications. Differences exist in the binding of β-catenin to different molecules, for example, TCF binding only spans arm repeats 3-10 (Graham et al, 2000).

Given its important roles in development and tumourigenesis, there has been much interest in targeting the Wnt pathway using small molecule inhibitors, but with limited success. Two targets currently show promise. A large screen identified tankyrase inhibitors as capable of downregulating Wnt signalling (Huang et al, 2009). Tankyrase regulates Axin through ADP ribosylation: tankyrase inhibition increases the levels of Axin, decreasing the free cytoplasmic β-catenin able to translocate to the nucleus. However, a recent study highlighted potential problems targeting tankyrase by revealing that, instead of negatively regulating the Wnt pathway, Axin2 could promote metastasis in CRC by upregulating Snail1 and inducing an epithelial-mesenchymal transition (Wu et al, 2012). The other potentially promising target is Porcupine, an acyltransferase that adds vital lipid groups to Wnt proteins. A Porcupine inhibitor entered a phase I clinical trial earlier this year (Lum & Clevers, 2012).

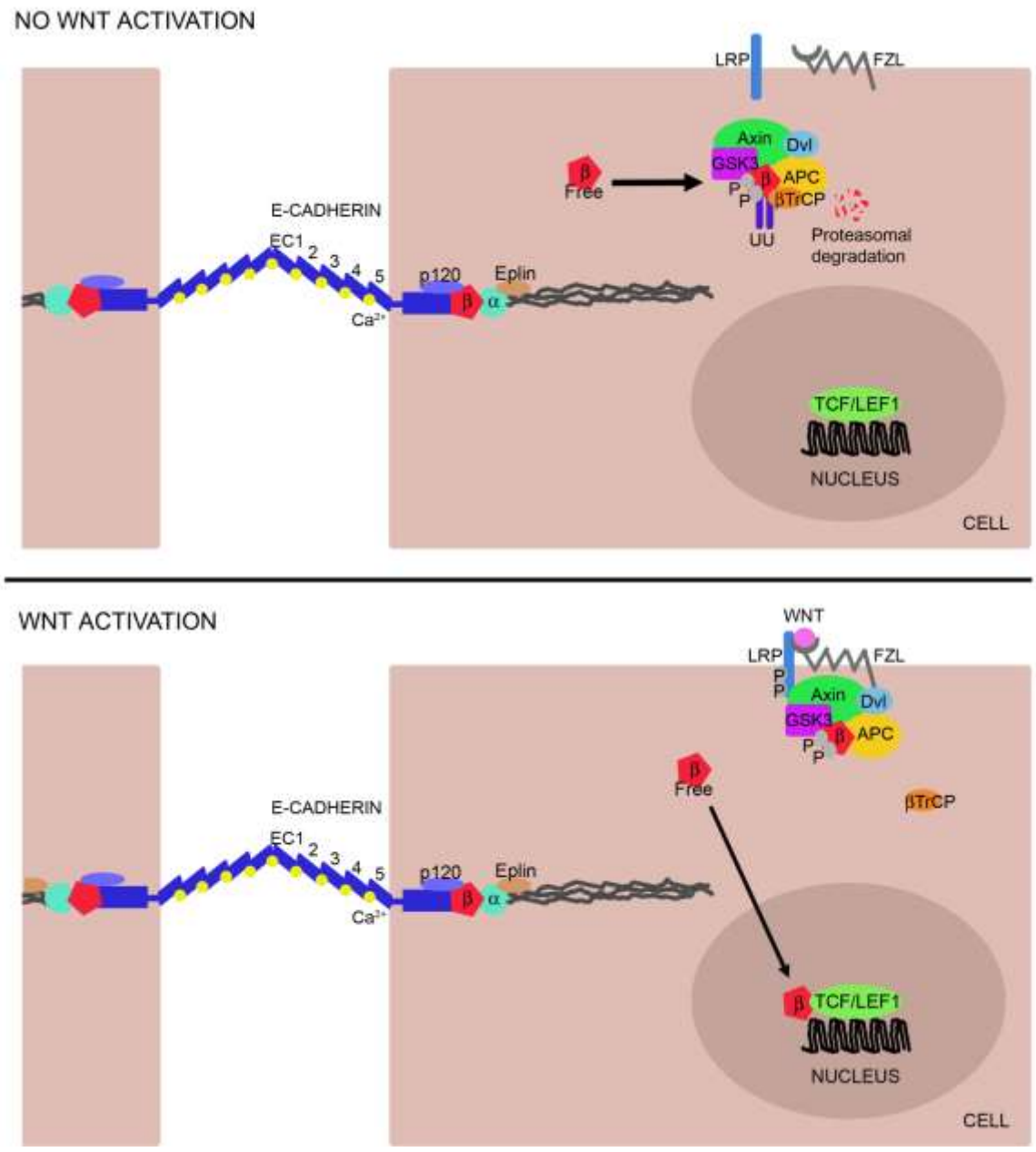

Figure 2. The Wnt pathway

The top panel shows signalling when the Wnt pathway is not activated: free β-catenin (β) is taken up by a destruction complex that includes adenomatous polyposis coli (APC), Axin, glycogen synthase kinase 3 beta (GSK3), dishevelled (Dvl) and beta-transducin repeat containing protein (βTrCP). β-catenin is phosphorylated by GSK3, then ubiquitinated by βTrCP, marking it for proteasomal degradation. The lower panel shows signalling when the Wnt pathway is active: LRP binds to Axin, tethering the destruction complex to the membrane, phosphorylation of β-catenin can still take place, however ubiquitination by βTrCP is blocked. The destruction complex becomes saturated with phosphorylated β-catenin. Free, unphosphorylated β-catenin can translocate to the nucleus, bind TCF/LEF1 and activate transcription of Wnt-regulated genes. Both panels show E-cadherin, with 5 extracellular domains (ECs) interacting through Ca^{2+} and the N-terminal EC1 domain binding to an EC1 domain on a neighbouring cell. The cytoplasmic domain of E-cadherin interacts with p120, β-catenin, α-catenin (α) and Eplin, anchoring it to actin filaments. For further detail on E-cadherin structure, see Figure 5. Diagram adapted from Li et al, 2012 and Clevers and Nusse, 2012.

1.4 The role of APC in the Wnt pathway

About 15% of CRCs appear to be dominantly inherited (Cannon-Albright et al, 1988; Houlston et al, 1992). The best defined forms are familial adenomatous polyposis (FAP, population incidence 1 in 7000) and hereditary nonpolyposis colorectal cancer (HNPCC, population incidence 1 in 500) (Kinzler & Vogelstein, 1996). Understanding the genetics of these two rare syndromes has provided insight into the pathogenesis of sporadic CRC and the importance of the Wnt pathway. Patients with FAP typically develop hundreds to thousands of colorectal polyps in their 20s and 30s. Whilst these are benign, if left untreated some will invariably develop into invasive carcinomas.

The hereditary nature of adenomatous polyposis had been described for over a century before an association with deletions in chromosome 5 was described in 1987 and then truncating mutations of APC were identified two years later (Bodmer et al, 1987; Kinzler & Vogelstein, 1996). A somatic mutation or loss of heterozygosity (LOH) of the wildtype *APC* allele was identified as the rate-limiting event in adenoma initiation (Ichii et al, 1992; Levy et al, 1994; Luongo et al, 1994). This, combined with the observation that *APC* was mutated in about 85% of sporadic CRCs, and a very early mutation, supported Knudson's "two-hit" hypothesis, which was initially applied to the difference in incidence of inherited and non-inherited childhood cancers (Ashton-Rickardt et al, 1989; Jen et al, 1994; Knudson, 1993; Knudson, 1971; Miyoshi et al, 1992; Powell et al, 1992; Smith et al, 1993). Whilst APC was a known tumour suppressor, the mechanism by which it conferred this function was unknown until an association with β-catenin and thus the Wnt pathway was discovered (Rubinfeld et al, 1993). The association of β-catenin independently with both APC and E-cadherin highlighted a possible link between tumour initiation and cell adhesion.

The role of APC in the destruction complex is not well understood. Proposed roles of APC include acting as a derepressor of Axin to allow it to be part of the destruction complex, helping localize the destruction complex correctly, acting as a cytoplasmic anchor for β-catenin, and chaperoning movement in and out of the nucleus (Bienz, 1999; Bienz, 2002; Cadigan & Peifer, 2009; Hart et al, 1998). APC interacts with β-catenin through a series of 15 and 20 amino acid repeats in the central part of the protein. Scattered through these are three Axin-binding

motifs. Axin is known to be the scaffold for assembly of the destruction complex, with Axin supply the rate-limiting step. Increasing the Axin supply in APC deficient cancer cells, restores activity of the β-catenin destruction complex and reduces β-catenin levels to normal (Hart et al, 1998; Lee et al, 2003). Mice without wildtype APC, but who have a truncated mutant form that still has a single Axin binding site are viable and do not develop intestinal neoplasia (Smits et al, 1999).

Many 'second hit' mutations occur in a region commonly referred to as the mutation cluster region (MCR). This lies in the area of codons 1250-1500, before the SAMP repeats that usually mediate the interaction of APC with the Axins in the β-catenin destruction complex, but after the β-catenin binding sites (Behrens et al, 1998; Hart et al, 1998). These SAMP repeats are vital for β-catenin interactions and also correspond to the binding sites on β-catenin where E-cadherin competes for binding (Hulsken et al, 1994). There appears to be selective pressure for a mutation in the MCR. CRC patients with a germline mutation in the MCR frequently had the remaining APC allele inactivated through a loss of heterozygosity mutation, whereas those lacking a germline mutation in the MCR had frequent somatic MCR mutations (Lamlum et al, 1999). Mouse mutants that give rise to intestinal neoplasia and the effect of mutations in different regions of APC will be discussed in Section 1.6.

1.5 Colorectal cancer and the adenoma to carcinoma transition

It is now well-established that colorectal cancer develops in a multistep process, requiring at least seven key genetic events (Kinzler & Vogelstein, 1996). Whilst *APC* mutation (or β-catenin or axin mutations with the same functional effect) is a key initiation mutation, and mutations in *K-ras*, *Smad4*, and *p53* are well-defined in promoting early progression, the role of other mutations is less clear, particularly those leading to invasion and metastasis (Figure 3). Improved understanding of these late genetic changes could offer the potential to reverse metastatic disease, making curative surgery feasible.

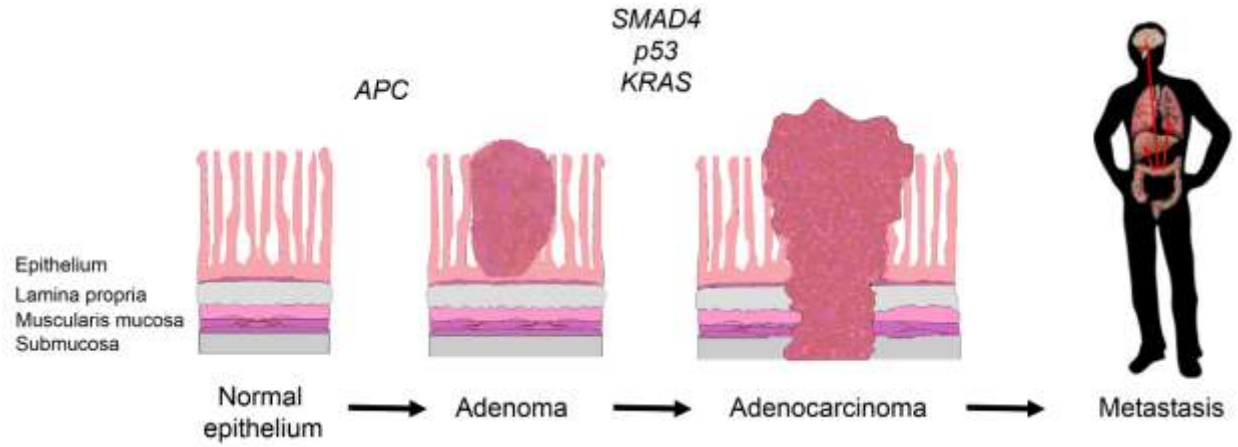

Figure 3. The adenoma to carcinoma transition
Simplified schematic outlining the histological and common genetic changes occurring during the adenoma to carcinoma transition. Loss of function of Apc (or gain of function of β-catenin) leads to the transformation from normal epithelium to an aberrant crypt focus and then an adenoma. Further genetic changes including loss of function of Smad4, p53 and Kras contribute to the progression to an adenocarcinoma that with penetration of the muscularis mucosa has the ability to metastasise to distant sites including the liver, lungs and brain. Diagram adapted from (Markowitz & Bertagnolli, 2009)

Genomic changes in 276 CRC (and matched normal) samples have recently been profiled in the most comprehensive molecular analysis of CRC to date (Cancer Genome Atlas Network, 2012). Exome sequence, DNA copy number, promoter methylation, messenger RNA expression and microRNA expression were all assessed. Tumours were divided into two groups based on their mutation rate. 16% were found to be hypermutated (a median number of 728 mutations per sample). Hypermutated tumours had microsatellite instability, due to MutL homolog 1 (*MLH1*) silencing by hypermethylation in 75% of cases, and somatic mutations in mismatch-repair and polymerase ε genes in the other 25%. Non-hypermutated samples shared very similar genomic changes. The most commonly mutated genes were *APC*, *TP53*, *KRAS*, *PIK3CA*, *FBXW7*, *SMAD4*, *TCF7L2* and *NRAS*, followed by *CTNNB1*, *SMAD2*, *FAM123B* (*WTX)* and *SOX9*. Somatic copy number alterations showed deletion of chromosome arms 18p and q (including *SMAD4*) in 66% of cases, chromosome arms 17p and q (including *TP53*) in 56% of cases and focal deletions including *APC, SMAD4*, *PTEN* and *SMAD3*. Focal amplifications included *ERBB2*, a potential drug target using the anti-ERBB2 antibody trastuzumab, and *IGF2*. A range of changes were identified in genes encoding TCF/LEF factors. Analysis of pathway regulation revealed 93% of tumours had alterations in the Wnt pathway. Over half of non-hypermutated tumours had *KRAS*, *NRAS* or *BRAF* mutations. PI3K and RAS-MAPK, TGFβ, and p53 pathway alterations were

common and almost all tumours had alterations in *MYC* transcription targets, confirming a key role for *MYC* in CRC.

Given a single tumour may have hundreds of mutations, much effort has gone into distinguishing driver mutations from passenger mutations. Statistical analysis has illustrated that in an individual tumour less than 15 mutations are likely to be 'drivers' (Sjöblom et al, 2006; Wood et al, 2007). A number of transposon based screens in mice have also been used to help identify candidate driver genes and pathways in CRC pathogenesis (March et al, 2011; Starr et al, 2009; Starr et al, 2011).

1.6 Mouse models of CRC and intestinal polyposis

Mouse models of CRC and intestinal polyposis have greatly improved our understanding of the disease. It is however important to be aware from the outset of the characteristics of the different models, key differences with human phenotypes and their limitations. Mouse models for colorectal cancer can be divided broadly into four groups: models based on *Apc* (or functionally equivalent) mutations, models for HNPCC, inflammatory models that give rise to tumours, and models for histologically distinct tumour types such as intestinal hamartomatous polyps and gastrointestinal stromal tumours. As mutation in *Apc* is the initiating event in the majority of human CRCs, it will be the focus of this work.

The *Apc* mutants that have been published to date are listed in Table 1. I include also β-catenin mutant models that confer the same functional effect as *Apc* loss of function. In human CRCs, β-catenin mutations are frequently present in *Apc* wildtype tumours and the mutations are always mutually exclusive (Sparks et al, 1998). The Apc^{Min} model, generated through N-ethyl-N-nitrosourea (ENU) mutagenesis, was the first to be discovered and is the most widely characterized (Moser et al, 1990). The adenoma phenotypes for the different mutants range from a few to hundreds of adenomas per mouse. Some of the phenotypic differences can be explained by the site of the *Apc* mutation and the extent of truncation of the protein. The capacity of the resulting truncated protein to bind critical partners such as Axin and β-catenin are proposed to correlate with the phenotype. A schematic of APC protein structure is shown in Figure 4 with important functional domains and the positions of truncation mutations produced

by the more common mutants. A 'just-right' signalling model has been proposed for *Apc* as there appears to be selection pressure on the 'second hit' event that favours preservation of some β-catenin binding domains and thus some ability to downregulate aberrant Wnt signalling (Albuquerque et al, 2002; Smits et al, 2000a). Most of the models are based on germline or conditional loss of a single *Apc* allele and rely on sporadic LOH of the second *Apc* allele for aberrant crypt formation and progression to adenoma formation.

There are some obvious differences between tumours that arise from *Apc* mutations in mice and those in humans. Firstly, whilst intestinal adenomas occur rarely in the small intestine in humans, this is the most common site for tumours in mouse models. Secondly, mice rarely develop invasive or metastatic disease. The short lifespan of mice and frequently large adenoma burdens leading to early anaemia and cachexia, preclude tumours from accumulating either subsequent mutations or epigenetic modifications required to drive invasion and metastasis. Mice with *Apc* mutations that have developed metastatic disease include Apc^{Min} hybrids who develop only a few adenomas and frequently survive over one year of age and invasive disease has been observed when *Apc* loss has been combined with *Smad* or *Pten* mutations (Halberg et al, 2009; Hamamoto et al, 2002; Marsh et al, 2008; Sodir et al, 2006; Takaku et al, 1998). The long-lived Apc^{Min} hybrids developed frequent invasive adenocarcinomas (24-87%) and occasional metastasis to regional lymph nodes (3%) (Halberg et al, 2009). As metastatic disease is the major treatment barrier for CRC, a mouse model that reliably mimics human CRC invasion and metastasis would be an important asset to the field and much superior to the orthotopic models currently used to study metastasis.

Genetic background can have a dramatic effect on the phenotype observed with a single gene mutation. The effect of strain dependent modifiers has been particularly well studied in the Apc^{Min} model, with a substantial body of literature dedicated to MOM (modifiers of Min). Soon after the discovery of the Apc^{Min} mouse it was noted that strain had a marked effect on the tumour burden. For example $Apc^{+/Min}$ F1 animals from an $Apc^{+/Min}$ C57BL/6J x AKR/J cross had an average of only six tumours per animals compared with 29 in the $Apc^{+/Min}$ C57BL/6J congenic line. Early backcross analysis suggested this could be due to a single modifier locus (Moser et al, 1992). A number of F1 hybrids were created ($Apc^{+/Min}$ C57BL/6J x AKR/J or MA/MyJ or CAST/EIJ),

each backcrossed to C57BL/6 or AKR and linkage analysis revealed a quantitative trait loci (QTL) on distal chromosome 4 that had a profound effect on tumour number which they called Modifier of Min-1 (*Mom-1*) (Dietrich et al, 1993). *Mom1* is a semi-dominant modifier and includes the secretory phospholipase A2 gene that confers a moderate resistance to tumour formation in the small intestine and strong effect in the colon, and a distal region (now called *Mom6*) that only has an effect in the small intestine (Cormier et al, 2000; Gould et al, 1996; MacPhee et al, 1995). A second modifier, *Mom2*, was identified that acts in a dominant fashion, suppressing 88-95% of adenomas in $Apc^{+/Min}$ mice, mapping to distal chromosome 18 at the site of alpha subunit of the ATP synthase gene (*Atp5a1*) (Baran et al, 2007; Silverman et al, 2002).

Mom3 was identified when a colony of $Apc^{+/Min}$ mice thought to be on a C57BL/6J background had wide variation in adenoma numbers and a novel region on distal chromosome 18 was identified that did not map to any known mouse strain. Crosses were established to achieve homozygosity of the identified markers on distal chromosome 18, close to the *Apc* gene and one line was found to have a particularly high adenoma burden and increased loss of the wildtype *Apc* allele suggesting that this modifier may have an effect on LOH frequency (Haines et al, 2005). *Mom3* has been shown to have an effect on tumourigenesis during pregnancy, but the mechanism is unclear (Suraweera et al, 2006). *Mom5* was discovered when a candidate gene on a 129P2 background was being backcrossed onto B6 in preparation for a cross with $Apc^{Min/+}$ and a test cross carried out midway through this process identified a locus on chromosome 5 that halved tumour numbers and likely involves Rad50-interacting protein 1 (*Rint-1*) (Oikarinen et al, 2009). *Mom7* maps to the pericentromeric region of chromosome 18, very close to *Apc*, with recessive alleles identified in BTBR/Pas, AKR/J and A/J lines that enhance tumourigenesis, and a dominant C57BL/6J allele that suppresses tumourigenesis (Kwong et al, 2007).

Mom12 and *Mom13* were both identified when a difference in adenoma phenotype did not correlate with the status of a knockout allele of interest in an $Apc^{+/Min}$ model, highlighting the problem of residual heterozygosity in congenic lines (Nnadi et al, 2012). Recently *Mom14-18* have been described and the finding that certain combinations of these *Moms* increased the protective effect on polyposis led the authors to analyse known gene-gene interactions or

shared pathways (Nnadi et al, 2012). Whilst genetic variation is a feature of FAP, loci syntenous to the *Moms* in the human genome to date have not been convincingly shown to be associated with variations in tumourigenesis in humans. It is possible that genetic modifiers individually may have an undetectable effect, but in combination and/or with environmental factors may impact disease.

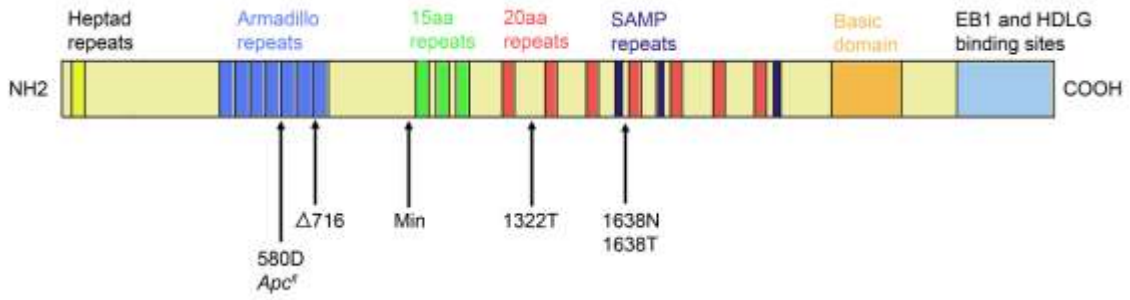

Figure 4. APC protein structure
Representation of APC showing mutation sites in mouse models detailed in Table 1. 15-aa repeats have roles in β-catenin binding. 20-aa repeats have roles in β-catenin binding and degradation. SAMP repeats are axin binding sites. The basic domain is the site of microtubule binding. EB1=end binding 1. HDLG=human disc large. Figure adapted from (Fodde et al, 2001; McCart et al, 2008; Pollard et al, 2009)

Table 1. *Apc* mutants

Mutation	*Apc* mutation	Number of adenomas: SI/colon; strain (if known)	Reference
***Apc*^{Min}**	ENU mutagenesis induced truncation at aa850	30/3; C57BL/6J x AKR/J	(Moser et al, 1990)
***Apc*^{1638N}**	Truncation at aa1638, but only 1-2% of the expected truncated protein expressed	4/0; 129/J x C57BL/6	(Fodde et al, 1994)
***Apc*$^{\Delta 716}$**	Truncation at aa716	250/3; C57BL/6J x 129/Sv	(Oshima et al, 1995)
580D/*Apc*^{fl}	Exon 14 flanked by loxP sites, truncated protein at aa580 upon Cre-recombination	*AxCANCre*: 6.7, *Vil-Cre*: 37; 129/Sv x C57BL/6J	(Hinoi et al, 2007; Shibata et al, 1997)
***Apc*$^{\Delta 1309}$**	Frameshift mutation introduced at aa1309	34	(Quesada et al, 1998)
***Apc*^{1638T}**	Truncation at aa1638, truncated protein expected 1:1 ratio with wildtype	0/0; 129/J x C57BL/6	(Smits et al, 1999)
***Catnb*$^{+/fl(ex3)}$**	Exon 3 flanked by loxP sites, resulting in dominant stable β-catenin	*Krt1-19-Cre*: 3000/0, *Fabp1-Cre:* 200-700/0; C57BL/6 x RW4	(Harada et al, 1999)
***Apc*$^{\Delta 474}$**	Truncation at aa474	120/2; C57BL/6	(Sasai et al, 2000)
***Apc*$^{\Delta 14}$**	Exon 14 flanked by loxP sites, Cre recombinase used to generate germline deletion	Conventional housing: 35/10. SPF: 65/3; C57BL/6 x 129/Ola	(Colnot et al, 2004)
***Apc*^{neoR}**, ***Apc*^{neoF}**	Insertion of a neo cassette into intron 13 in the direction of transcription (F) or the opposite direction (R)	F:1, R:0.25 (Hypomorphic alleles); C57BL/6 x 129	(Li et al, 2005)
***Apc*^{1322T}**	Truncation at aa1322	200/2; C57BL/6J	(Pollard et al, 2009)
***Apc*$^{\Delta 1\text{-}15}$**	Exons 1-15 flanked by loxP sites, recombination leads to whole protein deletion	Cre-dependent. *Vil-Cre:*160/3; C57BL/6 x FVB	(Cheung et al, 2010)
***Apc*$^{\Delta 15}$**	Exon 15 flanked by loxP sites, truncated 74kDa protein upon Cre-recombination	*EIIa-Cre* to generate germline knockout mice: 180/10. *Fabp1Cre:* 15/25; C57BL/6	(Robanus-Maandag et al, 2010)
***Apc*$^{\Delta SAMP}$**	Deletion of aa1322 to aa2006 (*Apc*^{1322T} but with an intact C-terminus)	200/2 (identical to *Apc*^{1322T}); C57BL/6	(Lewis et al, 2012)

1.7 E-cadherin

The appropriate regulation of cell adhesion is vital to morphogenesis and the maintenance of tissue architecture. The cadherin family of cell adhesion molecules play a key role in this process. During embryogenesis the temporo-spatial pattern of expression of cadherins is tightly regulated to ensure correct cell sorting and tissue development (Gumbiner, 1996; Takeichi, 1995). Cadherins retain a vital role in the maintenance of tissue integrity through the coordination of cell adhesion and correct signal processing throughout life. E-cadherin is one of the most widely studied cadherins and a compelling example this. E-cadherin null knockout mice showed embryonic lethality (Larue et al, 1994). Most epithelial tumours show an alteration in E-cadherin function during the progression to malignancy, sometimes through a process known as epithelial mesenchymal transition or the cadherin switch, whereby loss of E-cadherin expression is accompanied by a gain in mesenchymal cadherin expression with the induction of signalling cascades that promote cell migration and invasion (Cavallaro & Christofori, 2004).

1.7.1 E-cadherin structure: extracellular domain

Cadherins were first identified as single-span transmembrane-domain glycoproteins involved in calcium dependent homophilic cell adhesion in the early 1980s (Yoshida & Takeichi, 1982). We now know that the cadherin superfamily contains many members with a wide range of protein structures; all share an extracellular domain consisting of a variable number of repeated motifs (Nollet et al, 2000). The superfamily can be divided into two main groups: classical and non-classical. Classical cadherins have five extracellular domains (conventionally called EC1-5 from the amino terminus) and a conserved cytoplasmic tail that interacts with catenins to link to the actin cytoskeleton (Takeichi, 1995). Classical cadherins can be further divided into types I and II. Information to hand is superior for type I classical cadherins (simply referred to as cadherins hence) that include Epithelial (E)-, Neural (N)- and Placental (P)-cadherins. They share a conserved histidine-alanine-valine (HAV) tripeptide motif in their first extracellular domain and significant sequence homology and structural elements (Angst et al, 2001). Non-classical cadherins include desmosomal cadherins and protocadherins.

Adhesive specificity between different cell types was first displayed in the 1960s when it was shown that thymidine-labelled liver and neural retina cells in suspension preferentially associated with cell aggregates and individual cells of their respective types (Roth & Weston, 1967). Subsequent aggregation studies established there were at least two mechanisms for cell adhesion: calcium dependent and calcium independent, and that a cell surface protein with a molecular weight of about 150 kilodaltons (kDa) underwent conformational changes on reaction with calcium, suggesting a specific role in adhesion (Takeichi, 1977). Other studies confirmed the role of a cell surface protein of molecular weight of about 124 kDa required for calcium-dependent cell adhesion and termed this protein cadherin (Yoshida-Noro et al, 1984). Monoclonal antibody recognition by different tissues suggested that multiple types of cadherins exist (Hatta et al, 1985).

Whilst investigating the role of the cell surface in embryological development, an antiserum to surface antigen F9 that blocked morula compaction and blastocyte formation in mouse embryos was found (Kemler et al, 1977). This effect was reversible and was noted to be similar to the effect on compaction of embryos at low calcium concentrations (Ducibella et al, 1975). Trypsin treatment of cell membranes revealed an 84 kDa protein that interacted with calcium. The authors called this protein uvomorulin because of its role in the transition between grape-like (*uva* in latin) and mulberry-like (*morum* in latin) structures of cleavage stage embryos (Hyafil et al, 1981; Hyafil et al, 1980). Immunoprecipitation of uvomorulin revealed a 120 kDa hydrophobic molecule, suggesting the earlier size estimates of the protein were based on fragments only (Peyriéras et al, 1983). cDNA of uvomorulin was subsequently isolated. Sequencing showed significant homology with sequence reported previously for L-CAM (liver cell adhesion molecule) suggesting a common origin of these molecules (Ringwald et al, 1987; Schuh et al, 1986). Once sequenced it became apparent that uvomorulin and E-cadherin were synonymous. As its role clearly encompassed more than cell adhesion and sorting during embryological development, the name E-cadherin became widely adopted.

Whilst some rudimentary predictions could be made about cadherin structure based on sequence analysis, insights into cadherin-mediated adhesion have come from four main experimental methods: structural studies (such as xray crystallography and nuclear magnetic

resonance), observations of the effects of site-directed mutagenesis (point or domain deletions), coimmunoprecipitation of epitope-tagged cadherin molecules in adhesion complexes between cells, and physical studies (for example measurement of intermolecular forces between cadherin molecules) (Harrison et al, 2005).

Monoclonal antibodies to the HAV sequence of the first extracellular cadherin domain were shown to inhibit cadherin-mediated adhesion, suggesting it was the site of a cell adhesion recognition sequence (Blaschuk et al, 1990). Early site-directed mutagenesis studies confirmed that the binding specificity of cadherins was conferred by the region of the amino terminal 113 amino acids (Nose et al, 1990). The importance of the amino terminal region was also shown through the lack of adhesive function, despite normal cell surface cadherin expression, when the proteolytic processing of this region was obstructed (Ozawa & Kemler, 1990). Structural studies have confirmed that correct processing of this region initiates an important step in cadherin-mediated adhesion (Häussinger et al, 2004).

Initial structural studies were confined to the first cadherin domain, known to confer binding specificity. A solution structure of the amino terminal domain of mouse E-cadherin established through heteronuclear magnetic resonance spectroscopy showed a barrel shaped structure consisting of seven beta strands and two short alpha helices (Overduin et al, 1995). It was thought that a negatively charged pocket formed by an α helix and β loops at one end of the barrel was responsible for calcium ligation and a concave surface on the amino terminal extracellular repeat contributed to homophilic binding specificity.

At a similar time, the structure of the amino-terminal domain of mouse N-cadherin was described, based on x-ray crystallography (Shapiro et al, 1995). It also showed seven beta strands arranged in two sheets. Two distinct interfaces were described that formed an attractive basis for understanding cadherin interactions. The first, called the “strand dimer”, involved a strand from one amino terminal domain linking to the body of another amino terminal domain through the interaction of a tryptophan residue at position 2 (Trp-2) with a hydrophobic pocket in parallel alignment (cis interactions). The second interaction consisted of elements of four of the β strands forming an interface between opposing cells in an antiparallel

alignment (trans interactions), called the “adhesion dimer”. It was proposed that the strand and adhesion dimers together would form a ribbon of promoters and, when each amino terminal domain linked to the four other domains via calcium interactions, this would result in a ‘cell adhesion zipper’.

The third high resolution structural study examined the first two extracellular domains of E-cadherin showing two molecules, each consisting of seven-stranded β-barrel domains, connected by a ten residue linker and three calcium ions (Nagar et al, 1996). The calcium interaction was responsible for rigidifying the molecule; it was assumed similar calcium interactions occurred between successive cadherin domains, with a total of 12 calcium ions per cadherin molecule. The structure again showed dimer formation, but in contrast to N-cadherin described by Shapiro, calcium binding was integral to this dimer formation and no antiparallel interactions between molecules were evident.

Electron microscopy of ECADCOMP, in which the E-cadherin ectodomain was artificially clustered through recombinant fusion to the assembly domain of cartilage oligomeric matrix protein (COMP), provided further information about cadherin interactions (Pertz et al, 1999). It revealed that cadherins must undergo cis interactions prior to being capable of forming trans interactions, and furthermore, that trans interactions would only occur under physiological calcium concentrations, whereas cis interactions could be initiated at much lower concentrations.

Boggon and colleagues used xray crystallography to describe the structure of C-cadherin (Boggon et al, 2002). Like other classical cadherins, it consisted of five extracellular cadherin-like domains. There were shown to be arranged in a linear fashion with three calcium ions linking each domain and rigidifying the molecule in a curved structure. Whilst Boggon also described a strand dimer interface of a Trp-2 side chain interacting with a hydrophobic pocket on a neighbouring first cadherin domain, the details of this described interaction differed in two respects. Firstly, each adjoining first domain donated a Trp-2 side chain to a hydrophobic pocket on its partner molecule (‘a twofold symmetric, or reciprocated, ball-and-socket joint’). Secondly, the domains were in antiparallel alignment, as if protruding from opposing cell

surfaces and thus forming trans (or juxtaposed) cell interactions rather than the cis (or same) cell interactions postulated by his group in Shapiro's original paper. Interactions between dimers did not conform to the previously described "linear zipper model", but rather a front beta-sheet on the first cadherin domain interacted with the convex bottom of a neighbouring second cadherin domain forming cis interactions.

Boggon's postulated structure was particularly convincing because it was based on the whole cadherin ectodomain instead of one or two of the five domains, and it correlated with site-directed mutagenesis studies. The importance of Trp-2 for trans but not cis interactions has been confirmed by other electron microscopy and chemical cross-linking studies (Ahrens et al, 2002; Parisini et al, 2007). Whilst the 'linear zipper model' had initially been an attractive model for cadherin interactions, these later imaging studies combined with evidence from site-directed mutagenesis show that it was likely flawed and a product of nonphysiological crystal packing.

Given the challenges involved in high resolution structural imaging of the cadherins, site-directed mutagenesis has been a useful tool to elucidate the role of specific areas of the molecule in cell adhesion. The importance of the "strand dimer" interaction was demonstrated when site-directed mutagenesis of the region abolished the ability of both N-cadherin and E-cadherin to aggregate, despite maintenance of the structural integrity and localization of the adhesion molecules (Tamura et al, 1998).

The importance of Trp-2 for dimer formation has repeatedly been shown by site-directed mutagenesis (Kitagawa et al, 2000; Shan et al, 2000). The role of Trp-2 docking in trans, rather than cis interactions, was supported by mutagenesis of the hydrophobic docking site that disrupted trans adhesion only (Pertz et al, 1999). Harrison and colleagues have since used site-directed mutagenesis to investigate whether the strand exchange model shown in structural studies was physiological (Harrison et al, 2005). Cysteine point mutations were constructed near Trp-2 and its hydrophobic pocket so that they would form a reporter disulphide bond if strand exchange occurred during adhesion. The formation of the disulphide bond provided convincing support for the role of strand exchange. The driving force for strand

expulsion and swapping is provided by the conserved Trp-2 at one end of the strand, and a Ca^{2+}-Glu11 interaction at the opposite end (Vendome et al, 2011).

Whilst there had been much focus on the first extracellular cadherin domain and its role in dimer formation and adhesive specificity, less was known about the role of other domains. Equilibrium sedimentation analysis showed that a minimum of three C-cadherin domains were required for effective aggregation and that these must include domains one and two (Chappuis-Flament et al, 2001). Domains four and five were not essential for, but could enhance, aggregation. The authors postulated that multiple low affinity interactions between cadherin domains contributed to the net strength of the homophilic cadherin bond. Force profiles of C-cadherin adhesion were shown also to provide support for the role of multiple domains in adhesion, in a more complicated system than had originally been postulated (Leckband & Sivasankar, 2000). Subsequent serial constructs of the extracellular domains of N-cadherin demonstrated that the first two domains formed the minimal essential unit for cell adhesion (Shan et al, 2004). Whilst longer domains led to larger cell aggregates, they did not appear to confer additional adhesive strength.

The fundamental role of calcium binding in cadherin-mediated adhesion was established with early site-directed mutagenesis studies (Ozawa et al, 1990). These demonstrated that a single amino acid substitution in a calcium binding domain abolished cell adhesion. NMR spectroscopy of the first two ectodomains of E-cadherin in solution over a range of calcium and protein concentrations identified several cadherin states: a calcium free monomeric form with a kinked conformation that obscured the dimer interface, a straight non-flexible calcium bound monomer with an accessible dimer interface at low protein concentrations, and a predominantly dimeric species at intermediate protein concentrations (Häussinger et al, 2002). Oligomerization was associated with chemical shift changes centered around the integral Trp-2. This was consistent with the observed need for physiological calcium concentrations for effective cell adhesion and subsequent evidence that calcium is important in maintaining the stability of the first extracellular cadherin domain and has a role in modulating Trp-2 docking (Harrison et al, 2005).

1.7.2 E-cadherin structure: intracellular domain

Much work has focused on the role of the intracellular cadherin domain in cell adhesion. Early studies highlighted the importance of this region when the aggregation of cultured cells was abolished by cadherin mutants lacking the cytoplasmic tail or with mutations in the catenin binding site). The cytoplasmic cadherin tail interacts with catenins to form links with the actin cytoskeleton. A cytoplasmic cell adhesion complex is formed by the interaction of the carboxyl-terminal end of the cytoplasmic tail with β-catenin or plakoglobin (also known as γ-catenin) and p120 catenin (Aberle et al, 1994; Funayama et al, 1995; Hoschuetzky et al, 1994; Hülsken et al, 1994; Jou et al, 1995; Oyama et al, 1994; Reynolds et al, 1994). β-catenin binds via its amino-terminus to α-catenin and α-catenin binds to bundles of actin filaments in an interaction mediated by epithelial protein lost in neoplasm (Eplin), linking the cadherin complex to the actin cytoskeleton (Abe & Takeichi, 2008; Funayama et al, 1995; Hülsken et al, 1994; Rimm et al, 1995). α-catenin's central role in adhesive function was displayed by the observation that cultured lung carcinoma cells deficient in α-catenin adhered poorly despite normal cadherin localization, but regained normal adhesion when α-catenin was reexpressed (Hirano et al, 1992; Watabe et al, 1994).

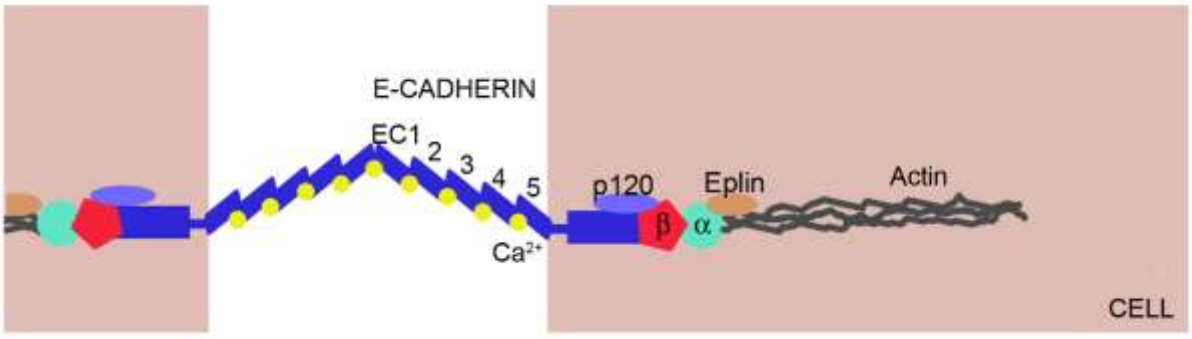

Figure 5. E-cadherin structure
Schematic representing the basic structure of E-cadherin and its association with key binding partners. E-cadherin has 5 extracellular domains (EC1-5) that rely on Ca^{2+} (shown as yellow circles) for binding interactions. The N-terminal EC1 domains on neighbouring cells bind through a strand-swapping mechanism. The cytoplasmic domain of E-cadherin is linked to the actin cytoskeleton through interactions with catenins. The C-terminal domain of E-cadherin binds to β-catenin (β) or plakoglobin (γ-catenin), and p120. β-catenin binds to α-catenin (α) and α-catenin to actin filament bundles, in an interaction mediated by epithelial protein lost in neoplasm (Eplin).

Whilst some studies have shown C-cadherin mutants in which the extracellular component was able to mediate cell adhesion independently, aggregation was enhanced in the presence of a cytoplasmic tail (Brieher et al, 1996). Forced clustering of these mutants increased adhesive strength without any observable change in the actin cytoskeleton structure, leading the authors to suggest the distribution of binding sites on the cell surface (usually mediated by the cytoplasmic tail) influences adhesion independent of cytoskeletal alterations or signalling (Yap et al, 1997). The forced clustering of cytoplasmic domains of cadherins soon after was shown to increase both cadherin and β-catenin immunofluorescence staining, supporting a clustering influence on signalling pathways (Katz et al, 1998). More recent work has revealed a complex cytoplasmic environment governed by multiple protein interactions and cell signalling pathways (Angst et al, 2001; Cavallaro & Christofori, 2004; Perez-Moreno et al, 2003).

1.7.3 E-cadherin function

Cadherins have a number of important functions, including roles in cell adhesion, cell sorting, coordinated cell movement and tissue polarity. At the cellular level, E-cadherin function can be divided into two key areas: adhesion and signalling. It is the interaction and cross-talk between these functions, much of which remains poorly understood, that makes E-cadherin such an interesting and important entity in development and tumourigenesis.

1.7.4 E-cadherin function: cell adhesion

Mammalian cells have three main types of adhesive junction: tight junctions, adherens junctions and desmosomes (Perez-Moreno et al, 2003). Together these form the Intercellular Junctional Complex. Tight junctions have a role in maintaining apical-basolateral polarity, forming a physical barrier between the apical and basolateral cell border through transmembrane proteins that link to the actin cytoskeleton. Desmosomes are formed by desmosomal cadherins from neighbouring cells that are linked to cytoskeletal intermediate filaments. Homophilic interactions between cadherins linked to the actin cytoskeleton form adherens junctions. There is increasing evidence that different junctions influence the function of one another, seen specifically in the functional interplay between tight and adherens junctions (Yap et al, 2007).

The formation of an intact epithelial sheet is a carefully coordinated process. Videofluoroscopy of cells with fluorescent protein-labeled actin and cadherin has shown that calcium leads to the stimulation of filopodia that penetrate and embed into neighbouring cells. Adherens junctions are formed by the E-cadherin that clusters at these tips, creating a zipper of embedded puncta. Through an α-catenin dependent mechanism, proteins including vinculin and Vasp are recruited. Actin reorganizes and polymerizes to create a single row of puncta, seal the cell borders and through cables linked between cells by adherens junctions create an integrated epithelial sheet (Vasioukhin et al, 2000).

The maintenance and morphogenesis of this epithelial sheet is controlled by actin dynamics. The Rho family of small GTPases that act as molecular switches to control a range of signal transduction pathways have an important role in this (Etienne-Manneville & Hall, 2002). GTPases exist in two states: an active state in which they are bound to GTP, and an inactive state in which they are bound to GDP. The switch can be regulated by over 60 activators and 70 inactivators. Over 60 targets have been identified for the three best-known GTPases, Rho, Rac and Cdc42, displaying their widespread and complex actions in eukaryotic cells. Rho, Rac and Cdc42 all have roles in the construction of actin networks. Rho induces the assembly of actin and myosin filaments into stress fibres. Rac is responsible for the induction of lamellipodia, actin-rich cell surface projections; Cdc42 encourages the formation of filopodia, longer actin-rich membrane extensions. Cdc42 has an important role, with the PAR complex, in initiating correct cell polarity. In combination with Rac, Cdc42 coordinates cadherin-cadherin interactions, leading to the formation of adherens junctions that are a necessary precursor to tight junction formation and, hence, the apical-basolateral asymmetry of an epithelial sheet. Cell migration is largely controlled by changes in the actin cytoskeleton. Rac is highly active at the leading edge during cell migration; it is believed Cdc42 has a role in stabilisation of this edge. When cells move as groups of coordinated sheets Rho has an additional role in modifying the contractility of the actin-myosin cable joining cells along the leading edge.

1.7.5 E-cadherin function: cell signalling

Given the interactions E-cadherin has with other molecules, there are a number of signalling pathways that could be functionally important. The best known of these is the Wnt pathway, through E-cadherin's interaction with β-catenin. Other potentially vital pathways include signalling through receptor tyrosine kinases and Rho GTPases. Whilst E-cadherin function can be modulated by receptor tyrosine kinases, such as EGFR and hepatocyte growth-factor receptor, there is also evidence that E-cadherin can repress or induce EGFR action and downstream signalling cascades, such as the phosphatidylinositol 3-kinase (PI3K) and mitogen-activated protein kinase (MAPK) pathways depending on the environmental context (Kovacs et al, 2002; Pece & Gutkind, 2000; Takahashi & Suzuki, 1996). In all likelihood, the tumour microenvironment impacts Wnt signalling and E-cadherin expression through growth factor modulation. For example, increased EGFR expression has been associated with increased invasion, nodal spread and less favourable prognosis in a variety of cancers (Beavon, 2000).

As discussed previously, RHO GTPases are important modulators of the interaction between adherens junctions and the actin cytoskeleton. E-cadherin adhesion can influence RHO GTPase activity, most prominently through inducing the tyrosine phosphorylation by SRC kinases of p190 RHO-GAP, thus suppressing RHO protein activity (Noren et al, 2003).

1.7.6 E-cadherin regulation

E-cadherin expression can be regulated at a number of levels, including protein turnover and recycling, post-translational modification, CpG island methylation, mutation, LOH, and by transacting factors such as miRNAs (Berx & van Roy, 2009). E-cadherin and β-catenin bind in the endoplasmic reticulum and are transported together to the cell membrane. Phosphorylation of key serine residues by CK2 and GSK3β on a C-terminal core region of E-cadherin greatly increases the affinity of binding to the armadillo repeats (Hinck et al, 1994). α-catenin and p120ctn bind at a later stage after cleavage of the prodomain. E-cadherin is transported from the Golgi via recycling endosomes and tubulovesicular carriers to the cell membrane. Endocytic

recycling is a complex system of levels of sorting that is only gradually being understood (Maxfield & McGraw, 2004).

A very broad overview of this intricate system is that cell surface molecules are taken up by receptor-mediated endocytosis, usually through clathrin-coated pits. The clathrin coats are shed and the endosomes fuse with each other and acidic sorting endosomes that contain tubular-vesicular structures. The sorting endosomes undergo a maturation process; the contents may be targeted to lysosomes for degradation, for example by ubiquitination, or through recycling pathways back to the cell membrane. Golgin-97 and Rab11-positive endosomes are essential components of this E-cadherin transport system (Lock et al, 2005; Lock & Stow, 2005). Ankyrin-G and β-2-spectrin bind to the cytoplasmic domain of E-cadherin, connecting it directly to the actin cytoskeleton. They have a role in stabilising E-cadherin and are also necessary to coordinate E-cadherin's transition from the trans-golgi network to assembly in the membrane (Kizhatil et al, 2007). Correct cleavage of the prodomain is essential to E-cadherin function; α-catenin and p120-catenin bind following this (Hinck et al, 1994; Ozawa & Kemler, 1990). Whilst incorrect cleavage has no effect on integration of E-cadherin into the cell membrane, such molecules are unable to form adhesive junctions (Ozawa & Kemler, 1990).

If cell-cell adhesion is disrupted, for example, through lowered calcium concentrations, E-cadherin endocytosis and recycling are upregulated. This suggests cell-cell contact has a direct effect on the recycling of E-cadherin (Le et al, 1999). O-glycosylation of the cytoplasmic domain of newly synthesized E-cadherin is one mechanism of rapidly regulating the destruction of E-cadherin and thus cell adhesion in some apoptotic pathways (Zhu et al, 2001). ARF6 is necessary for the disassembly of adherens junctions and internalization of E-cadherin. Activation of ARF-6 recruits Nm23-H1, a nucleoside diphosphate kinase to the cell membrane, facilitating dynamin-dependent vesicle fission at the basolateral cell surface and downregulating Rac1 activation at cellular junctions (Palacios et al, 2002).

Once E-cadherin has been endocytosed, it is transported to an early sorting endosome. From there it can either be recycled back to the cell membrane via a recycling endosome, or directed

to the late endosome and on to lysosomal degradation (van Roy & Berx, 2008). Lysosomal targeting can be promoted by a number of substances including hepatocyte growth factor-regulated tyrosine substrate kinase, the GTPases Rab5 and Rab7, and the E3 ubiquitin-ligase Hakai (Japanese for “destruction”) (Fujita et al, 2002; Palacios et al, 2005). The disruption of cell-cell adhesion through lysosomal targeting is likely to be an important mechanism in oncogenesis and epithelial to mesenchymal transition.

Disordered proteolytic cleavage of the E-cadherin ectodomain by matrix metalloproteinases and cathepsins, or the cytoplasmic domain by molecules such as caspases, can have dramatic effects of E-cadherin function (van Roy & Berx, 2008). Presenilin-1 (PS1), a protein originally found to be associated with Alzheimer’s disease, is recruited to sites of cell adhesion and forms a stabilizing complex with E-cadherin and β-catenin, promoting cytoskeletal links and cell aggregation (Baki et al, 2001). However, upon stimulation by apoptosis or increases in calcium concentrations, PS1 controls a gamma-secretase-like cleavage of E-cadherin, causing dissociation of the cadherin-catenin complex. This increases levels of cytosolic E-cadherin and soluble α and β-catenins, the latter which could potentially impact Wnt signalling (Marambaud et al, 2002).

ADAM 10 can cleave the extracellular domain of E-cadherin close to the cell membrane; the resulting free extracellular fragment has the potential to disrupt cell adhesion by competing for binding with other E-cadherin molecules (Maretzky et al, 2005). The matrix metalloproteases stromelysin-1 and matrilysin can also cleave E-cadherin to release a soluble fragment that leads to decreased cadherin aggregation and increased invasive potential (Masterson & O'Dea, 2007). The protease calpain can make a truncated form of E-cadherin and has been associated with more aggressive forms of prostate cancer (Rashid et al, 2001; Rios-Doria et al, 2003). A number of other post-translational modifications can influence E-cadherin function, for example, the protein IQGAP can modulate the cadherin-catenin interactions by competing for binding sites (Kuroda et al, 1998)

p120 has a role not only in the stabilization of E-cadherin at the cell membrane, but also in controlling cadherin turnover (Davis et al, 2003). A dileucine motif on the cytoplasmic tail of E-cadherin is involved in E-cadherin endocytosis, and p120 has a role in masking it to prevent internalization (Miyashita & Ozawa, 2007). Cell lines in which p120 is deficient or knocked down have decreased levels of E-cadherin and disrupted adhesion. p120 is downregulated in a range of epithelial cancers, suggesting it has a tumour suppressor role (Ireton et al, 2002; Thoreson & Reynolds, 2002). However p120 may also have a role as a metastasis promoter depending on when it is lost in relation to E-cadherin. If E-cadherin is lost first, p120 may accumulate in the cytoplasm, modulating Rho-GTPases and thus actin dynamics, and through increased motility and invasiveness impact metastatic potential. If p120 is lost first, upregulated degradation of the cadherin-catenin complex would be expected.

E-cadherin expression can be downregulated by a number of transcriptional repressors that bind to E2 boxes in the promoter of the E-cadherin gene. These include zinc-finger-containing proteins Snail, Slug and Smad-Interacting Protein (SIP1), and the helix-loop-helix transcription factor E12/E47 (Batlle et al, 2000; Cano et al, 2000; Hajra et al, 2002; Perez-Moreno et al, 2001). The mechanism of transcriptional inactivation is through hypermethylation, causing epigenetic silencing. Hypermethylation of the E-cadherin promoter has been shown in a number of cancers (Fujita et al, 2003). Transcriptional repressors may in fact be Wnt target genes. For example, Slug may be a target of the TCF/β-catenin complex and thus by repressing cadherin function and cell-cell adhesion Slug may increase the free cytoplasmic β-catenin and lower the threshold required for Wnt activations (Conacci-Sorrell et al, 2003; Jamora et al, 2003).

1.8 E-cadherin genetic analysis

1.8.1 E-cadherin human genetic analysis: HDGC

Compelling evidence for E-cadherin being an important tumour suppressor gene comes from hereditary diffuse gastric cancer (HDGC). Gastric Cancer (GC) can be divided into two subtypes: Diffuse Gastric Cancer (DGC), characterized histologically by poor differentiation and diffuse spread, and intestinal gastric cancer which is well differentiated and thought to arise from gastritis and metaplasia. Most gastric cancers are sporadic, with only 1-3% of gastric cancers

occurring due to familial syndromes, and *CDH1* mutations have only been implicated in the diffuse form.

In 1998, Guilford and colleagues identified an E-cadherin mutation in a large Maori kindred with early onset, poorly differentiated, high grade, diffuse gastric cancer (Guilford et al, 1998). The mutation was a G to T substitution at the donor splice consensus sequence, resulting in a truncated product. In two other families, they identified a frameshift mutation in exon 15 and a premature stop codon interrupting exon 13. Over 120 *CDH1* mutations have now been described in families with HDGC (Corso et al, 2012). Whilst some mutations have been identified in multiple unrelated families, there are no mutational hotspots. The types of mutation also vary widely, with small insertions or deletions most common (35% of cases), followed by missense (28%), nonsense (16%), splice site (16%) and large exonic deletions (5%) (Guilford et al, 2010). There does not seem to be a correlation between mutation type and phenotype and not all mutations cause complete inactivation, suggesting reduced E-cadherin function may be adequate for disease initiation (Guilford et al, 2007).

CDH1 is a classic tumour suppressor gene: tumourigenesis in HDGC requires a second hit with inactivation or loss of the second allele most commonly through hypermethylation of the promoter, but sometimes also through LOH (Grady et al, 2000; Oliveira et al, 2009). LOH is more common in metastasis and more than one second hit mechanism can be observed in the same patient (Oliveira et al, 2009). Gastric pathogens such as *Helicobacter Pylori* may have a role in promoting methylation (Yamamoto et al, 2011). Not all genetic events lead to complete inactivation of both alleles, suggesting that the second hit may be selected to maintain some residual E-cadherin function, for example, to avoid cell death by anoikis (Guilford et al, 2007). There has been no clear association between gastric cancer risk and *CDH1* polymorphisms, nor have particular haplotypes been associated with histological severity. However there may be an increased risk of GC in smokers with a particular combination of *CDH1* polymorphisms (Jenab et al, 2008). Interestingly, in countries with high incidence of GC (East Asia, Eastern Europe, parts of Central and South America), *CDH1* mutations are rare, suggesting environmental factors may be important (Corso et al, 2012).

The inheritance of *CDH1* mutation in HDGC is autosomal dominant with incomplete penetrance; carriers have a 70% lifetime risk of developing gastric cancer (mean age at diagnosis 40 years) (Guilford et al, 2007). Lobular breast cancers occur at higher frequencies in HDGC families, with penetrance reported between 39-54% for females (Kaurah et al, 2007; Pharoah et al, 2001). Additionally, two families have been described where HDGC and *CDH1* mutation are associated with cleft lip (Frebourg et al, 2006). Histologically HDGC is indistinguishable from sporadic diffuse gastric cancer, with characteristic signet ring cells and linitis plastica. Signet ring cell carcinoma foci often cluster in the transition region between the fundus and antrum of the stomach, an area thought to be enriched for gastric stem cells. The diffuse pattern of spread and submucosal location of carcinoma foci make diagnosis and surveillance challenging.

The molecular changes occurring during tumourigenesis are incompletely understood. Current hypotheses include loss of E-cadherin affecting cell polarity and mitotic spindle function, particularly in stem cells in the region where lesions are most common. Despite usually being located in the proliferative transition zone, early HDGCs show low rates of proliferation. Early HDGCs do not show invasive markers, but are located in the lamina propria, which according to classifications based on transgressing the basement membrane class them as malignant. A possible explanation for this location is that the cells in this region mature to become pepsinogen-secreting chief cells. Whilst secretion is usually directed into the gastric lumen, in cells that have lost polarity it may be secreted inappropriately into surrounding tissue, causing breakdown of tissue and facilitating inappropriate movement of cells (Guilford et al, 2007).

Current guidelines for genetic testing are at least two cases of DGC in first or second degree relatives, with at least one of these diagnosed before the age or 50, or three or more cases of DGC independent of age of onset, or age of diagnosis less than 40 (Fitzgerald et al, 2010). Some groups advocate a younger cut-off age (35 years) and additional indications such as combined diagnoses of DGC and lobular breast cancer (Dixon et al, 2012). Using these criteria, about half of families tested are found to have a *CDH1* mutation (Brooks-Wilson et al, 2004). *CDH1* mutations are uncommon in sporadic cases of DGC (about 7%) (Corso et al, 2011). Prophylactic gastrectomy is recommended for people with confirmed *CDH1* mutation and annual

mammography is recommended for females from age 35 (Fitzgerald et al, 2010). Surveillance endoscopy is controversial, because it often fails to detect even advanced stage lesions. However, it is necessary in patients who decline gastrectomy, patients under 20 and those awaiting gastrectomy. In families with known HDGC, genetic testing is usually carried out around the age of consent, but prophylactic gastrectomy rarely undertaken until the age of 20 when the mortality rate of the surgery (1%) is equal to the estimated mortality rate from HDGC at that age.

1.8.2 E-cadherin human genetic analysis: colorectal cancer

A meta-analysis of genome-wide association data identified *CDH1* (16q22.1) as a susceptibility loci for CRC (Houlston et al, 2008). Nevertheless, *CDH1* mutations are rare in CRC, for example in the recent genome scale analysis of 276 CRC samples, only 9 mutations in *CDH1* were identified (Cancer Genome Atlas Network, 2012; Ilyas et al, 1997). CDH1 is frequently downregulated in CRC, particularly at the invasive edge as part of EMT (Berx & van Roy, 2009; Buda & Pignatelli, 2011).

1.8.3 E-cadherin human genetic analysis: other cancers

As discussed, lobular breast cancer is more common in patients with HDGC. E-cadherin mutations have been identified in over 50% of cases of sporadic lobular breast cancer, usually causing truncated proteins and accompanied by inactivation of E-cadherin on the other allele by hypermethylation or LOH (Berx et al, 1998; Berx et al, 1996; Qureshi et al, 2006). Somatic E-cadherin mutations have been identified in pancreatic cancers (Berx et al, 1998). *CDH1* mutations are rare in other cancers, including lung, endometrium, ovary, bladder, oesophagus, thyroid and cholangiocarcinoma. However, as for CRC, LOH and promoter methylation are common in many tumour types, often as part of an EMT (Berx & van Roy, 2009).

1.8.4 E-cadherin mouse model genetic analysis

All published experiments with murine *Cdh1* mutants are outlined in Tables 2-9. Whilst detailed explanation of all mutants is beyond the scope of this thesis, relevant experiments will be highlighted. Table 2 documents germline models, notably no discernible abnormalities with *Cdh1* heterozygosity, but failure of trophectoderm formation and implantation with *Cdh1*

homozygosity. Experiments assessing conditional loss of *Cdh1* alone are described in Table 3, and those where *Cdh1* loss has been combined with one or more mutations are divided by organ system and outlined in Tables 4-9.

When this work was initiated, three mouse models investigating the role of *Cdh1* in the gastrointestinal system had been published. Smits and colleagues showed that $Apc^{1638N/+}$ $Cdh1^{+/-}$ animals had a 9-fold increase intestinal tumour numbers and a 5-fold increase in gastric tumours compared with $Apc^{1638N/+}$ $Cdh1^{+/+}$ littermates, but that there was no difference in tumour grade or stage (Smits et al, 2000b). Hermiston and Gordon produced indirect evidence for *Cdh1* exercising an important role in intestinal homeostasis using mouse models where E-cadherin was disrupted with a dominant negative form of N-cadherin (Hermiston & Gordon, 1995a; Hermiston & Gordon, 1995b). These models will be described in detail in Chapter 3. Briefly, they revealed changes in cell adhesion, migration, polarity and apoptosis producing an inflammatory phenotype with progression to intestinal adenomas. Kan and colleagues used a $Cdh1^{fl/Ncad}$ *Vil-Cre* model to show that N-cadherin could structurally replace E-cadherin and establish normal trophectoderm and embryonic organ development. However, following birth animals developed progressive intestinal and colonic hyperproliferation and dysplasia with Wnt activation and could not survive past 3 weeks of age (Kan et al, 2007).

In the past two years, a number of studies have been published that investigate the role of *Cdh1* loss in the gastrointestinal system, alone or in combination with other gene loss. $Cdh1^{+/-}$ mice treated with N-Nitroso-N-methylurea (NMU) had an 11-fold increase in signet-ring cell carcinomas compared with wildtype NMU-treated mice (Humar et al, 2009). Homozygous *Cdh1* loss in gastric parietal cells resulted in hyperplastic mucosa and signet ring carcinoma cells by 12 months, but animals only developed metastatic carcinomas phenocopying HDGC when combined with homozygous *p53* mutation (Mimata et al, 2011; Shimada et al, 2012). *Cdh1* homozygosity in oesophageal basal cells resulted in increased junctional permeability but no evidence of tumourigenesis (Jovov et al, 2011). Conditional homozygous intestinal loss of *Cdh1* using $Villin\text{-}CreER^{T2}$ resulted in an inflammatory phenotype with altered Paneth cell placement and differentiation (Schneider et al, 2010). This will be discussed further in Chapter 3.

Table 5 outlines three models with features of human invasive lobular breast cancer have been described when *Cdh1* homozygosity is combined with *p53* loss (Derksen et al, 2006; Derksen et al, 2011; Kotb et al, 2011). Importantly, in these studies *Cdh1* loss induced resistance to anoikis. Two other important cancer models must be mentioned. Rip1Tag2 mice that maintained E-cadherin expression in pancreatic β-islet tumour cells only developed adenomas, yet expression of a dominant-negative form of E-cadherin in those adenomas resulted in invasion and metastasis, suggesting E-cadherin has a vital role in adenoma to carcinoma transition (Perl et al, 1998). In a C-RAF driven model of non-small-cell lung cancer, homozygous loss of *Cdh1* or expression of a dominant negative form of E-cadherin in adenoma cells resulted in separation of cells and disrupted morphology, followed by increased vascularisation (Ceteci et al, 2007). The highly vascularised tumours grew rapidly with invasion and micrometastasis. E-cadherin downregulation was associated with upregulation of β-catenin, which was identified as a critical effector of vascular endothelial growth factors A and C.

Table 2. Germline *Cdh1* mouse mutants

Targeted allele; MGI identifier Mutation; strain	Phenotype and strain	Reference
Cdh1^{tm1Kem} 1857282 LacZ cDNA and a neomycin resistance cassette inserted into exon 1 of *Cdh1*, just upstream of the translation start site. 129S2/SvPas x C57BL/6.	*Cdh1*$^{+/-}$ mice healthy and normal. *Cdh1*$^{-/-}$ embryos failed to form a trophectoderm epithelium.	(Larue et al, 1994)
Cdh1^{tm1Cbm} 2182564 Targeted deletion of part of exon 7 and all of exon 8 (nucleotides 957-1211 of the cDNA), this includes an essential calcium-binding site. 129/J/C57BL/6.	*Cdh1*$^{+/-}$: healthy, fertile. *Cdh1*$^{-/-}$: morula cells initially adherent and polarised however polarisation unsustainable and blastocyst formation and implantation fail.	(Riethmacher et al, 1995)
B6 ↔129/Sv-ECAD 129/SV embryonic stem cells transfected with recombinant DNA containing the fatty acid-binding protein (*Fabp1*) gene promoter linked to mouse E-cadherin, introduced into C57BL/6 blastocysts. 129/C57BL/6.	Forced expression of E-cadherin along the crypt-villus axis suppresses proliferation and induces apoptosis in the crypt and slows cell migration up the villus. No changes in cellular differentiation and no neoplastic changes.	(Hermiston et al, 1996)
Cdh1^{tm1Mlec} 3822550 Targeted substitution within exon 4 of the glutamic acid at position 16 to a proline (E16P). This 'humanized'protein has enhanced affinity for the InlA surface protein expressed by *Listeria monocytogenes.* 129S2/SvPas.	InlA and InlB together have a role in the fetoplacental invasion of *Listeria monocytogenes*.	(Disson et al, 2008)
Cdh1$^{tm1.1Mpst}$ 4821988 Targeted insertion of cDNA coding for a C-terminally HA-tagged version of *Cdh1* into the *Cdh1* start codon. C57BL/6.	*Cdh1*$^{HA/HA}$ embryos: normal trophectoderm formation, implantation, gastrulation and neurulation, but at E10.5 are small, pale with inadequate nutrient supply due to labyrinth-specific CDH1 loss and impaired intermingling of placental embryonic and maternal blood vessels.	(Stemmler & Bedzhov, 2010)
Cdh1$^{tm2.1Mpst}$ 5426968 Expression vector encoding the N-terminal extracellular domain of Cdh2 (N-cadherin, aa 1-724) fused to the C-terminal domain of Cdh1(aa 711-884) with a HA tag was inserted downstream of the translation initiation site. C57BL/6.	*NcEc* homozygotes: do not form a trophectoderm, with cells undergoing apoptosis. This phenotype can however be rescued by restoring *Igf1r* signalling (which had been blocked by absence of the extracellular domain of *Cdh1*).	(Bedzhov et al, 2012)
Cdh1$^{tm3.1Mpst}$ 5426969 Expression vector encoding the N-terminal extracellular domain of Cdh1 (aa 1-710) fused to the C-terminal domain of Cdh2 (aa 725-906) with a HA tag was inserted downstream of the translation initiation site. C57BL/6.	*EcNc* homozygote mice have normal trophectoderm development.	(Bedzhov et al, 2012)

Table 3. Conditional *Cdh1* mouse mutants

Targeted allele MGI identifier Mutation	Cre recombinase	Phenotype and strain (if documented)	Reference
Cdh1^{tm1Jjon} 3693661 Targeted insertion of loxP sites in introns 3 and 15	*K14Cre* (human keratin 14 promoter, active in skin salivary gland and mammary gland epithelium).	*Cdh1$^{F/F}$K14Cre* animals: developmental defects in skin epithelium with abnormal hair follicle development, epidermal hyperplasia and frequent inflammation; progressive hair loss and disturbed sebaceous gland development. No abnormal mammary gland development. No skin or mammary epithelium tumours. 129P2/OlaHsd x FVB/N.	(Derksen et al, 2006)
	Lyz2$^{tm1(cre)Ifo}$ (M lysozyme promoter, active in mature macrophages and granulocytes).	E-cadherin shown to have a role as an effector molecule of alternatively activated macrophages, increasing their fusion capacity and ability to interact with other haematopoetic cells. CD1 x C57BL/6.	(Clausen et al, 1999; Van den Bossche et al, 2009)
	Rip1/Cre (promoter is a fragment of rat insulin 2, active in pancreatic β cells).	Pancreatic islet cells that had lost E-cadherin expression had higher cell surface levels of NCAM. 129P2/OlaHsd x C57BL/6.	(Ahlgren et al, 1998; Lehembre et al, 2008)
Cdh1^{tm2Kem} 2389020 Targeted insertion of loxP sites in introns 5 and 10	*Tbx18^{cre}* (T-box transcription factor 18 promoter, active in epicardium, interventricular septum, left ventricular wall and periotic mesenchyme).	*Cdh1$^{fl/fl}$ Tbx18$^{cre/+}$* mice had normal epithelial basal cell development but impaired stria vascularis integrity. The stria vascularis epithelium is vital for maintaining the endocochlear potential and endolymph composition that are essential for sensory transduction in the cochlea. NMRI.	(Christoffels et al, 2009; Trowe et al, 2011)
	CD4-Cre (Cd4 promoter, expressed in CD4+ and CD8+ memory T cells).	E-cadherin expression by CD8 T cells in the submandibular gland promotes accumulation of these lymphocytes in the tissue (without a requirement of local antigen presentation).	(Boussadia et al, 2002; Hofmann & Pircher, 2011; Lee et al, 2001)
	Zp3-Cre (Mouse zona pellucida 3 promoter, expressed in oocytes).	Preimplantation mouse embryos completely lacking maternal and zygotic *Cdh1* have disrupted epithelial polarity and a greater proportion than normal express trophectoderm markers. ICR.	(Lewandoski et al, 1997; Stephenson et al, 2010)
	Vil-CreER^{T2} (Villin promoter, active in intestinal and colonic epithelial cells, including progenitor cells).	*Cdh1$^{+/fl}$ Vil-CreER^{T2+}* mice: normal. *Cdh1$^{fl/fl}$ Vil-CreER^{T2+}* mice: ill within 6 days of recombination with weight loss, haemorrhagic diarrhoea, disrupted crypt-villus architecture in the small intestine and colon, increased apoptosis, decreased goblet cells and mislocalised Paneth cells. With attenuated levels of recombination mice remained well but had disorganised crypts, decreased goblet cells, mislocalised Paneth cells, disrupted secretory cell maturation, disturbed cell migration, decreased Wnt signalling (decreased Axin2 at crypt base) and impaired bacterial defense. C57BL/6. Discussed in detail in Chapter 3.	(Boussadia et al, 2002; el Marjou et al, 2004; Schneider et al, 2010)

Table 3. Conditional *Cdh1* mouse mutants (continued)

Targeted allele MGI identifier Mutation	Cre recombinase	Phenotype and strain (if documented)	Reference
Cdh1^{tm2Kem} 2389020 Targeted insertion of loxP sites in introns 5 and 10	*Nestin-Cre* (nestin promoter, active in neuronal and glial cell precursors by E11).	*Cdh1$^{fl/fl}$Nes-Cre+* mice: defects in self-renewal of neural stem cells. CD1 x B57.	(Boussadia et al, 2002; Karpowicz et al, 2009; Tronche et al, 1999)
	Recombinant Cre-expressing adenovirus (*in vitro*).	Ablation of *Cdh1* in spermatogonial stem cells did not impair homing or spermatogenesis. C57BL/6.	(Boussadia et al, 2002; Kanatsu-Shinohara et al, 2008)
	Alfp-Cre (albumin promoter and alpha fetoprotein enhancer, active in the developing liver).	*Cdh1$^{fl/fl}$ Alfp-Cre* mice: viable, fertile and had no signs of illness or obvious structural changes in the hepatic epithelium.	(Battle et al, 2006; Boussadia et al, 2002; Parviz et al, 2002)
	K14-Cre (human keratin 14 promoter, active in basal layer of epidermis, outer root sheath of hair follicle and oral epithelium).	*Cdh1$^{fl/fl}$ K14-Cre:* newborn mice smaller than usual, less active and had fewer and smaller whiskers but only minor changes in epidermal architecture. In the adult animals there was progressive epidermal hyperproliferation but progressive loss of hair follicles.	(Tinkle et al, 2004; Vasioukhin et al, 1999)
	Atp4b-Cre (Atp4b promoter, active in progenitors of parietal cells).	*Cdh1$^{fl/fl}$ Atp4b-Cre+*: Cdh1 negative rounded parietal cells pushed from the glands into stroma. Hyperplastic gastric mucosa from 3 months age, Cdh1 negative cells from the parietal lineage clustered from 6 months and signet ring carcinoma cells present in these clusters by 12 months. No invasive carcinomas.	(Mimata et al, 2011)
	KRT5-CreERT2 (keratin5 promoter, active in oesophageal basal cells).	*Cdh1$^{fl/fl}$ KRT5-CreERT2+* mice had oesophageal epithelium with increased junctional permeability. C57BL/6.	(Jovov et al, 2011)
	Vil-Cre (Tg(*Vil-Cre*)997Gum, active in intestinal epithelium but not in visceral endoderm .	*Cdh1$^{fl/fl}$ Vil-Cre:* died within 24 hours of birth. Severe disruption of intestinal morphogenesis with compromised barrier function, decreased epithelial cells, increased proliferation, increased activation of Wnt target genes but decreased cytoplasmic and nuclear β-catenin.	(Bondow et al, 2012; Madison et al, 2002)
Cdh1$^{tm3.1Kem}$ 3574479 Targeted insertion of loxP sites to flank intron 2	*CMV-Cre* (human cytomegalovirus promoter, active in most cells/tissues). *K14-Cre* (human keratin 14 promoter, expressed in epidermis, hair follicles and tongue epithelium). *K19-Cre* (cytokeratin 19 promoter, expression in trophectoderm, gut endoderm and endoderm-derived epithelia and at later stages in surface ectoderm)	Intron 2 deletion: E-cadherin locus inactive in embryonic stem cells and during early embryonic development. From E11.5 onwards: weak activation of the locus in the absence of intron 2. E-cadherin expression in the yolk sac is independent of intron 2 whereas expression in the lens and salivary gland relies on intron 2. Intron 2 has important roles both in initiation of E-cadherin transcription and maintaining E-cadherin expression.	(Hafner et al, 2004; Harada et al, 1999; Schwenk et al, 1995; Stemmler et al, 2005)

Table 4. Compound *Cdh1* mouse mutants: gastrointestinal system

Targeted allele MGI identifier Mutation	Targeted allele MGI identifier Mutation	Cre recombinase	Phenotype and strain (if documented)	Reference
Cdh1^{tm1Cbm} 2182564 Targeted deletion of part of exon 7 and all of exon 8 (nt 957-1211 of cDNA), includes an essential Ca^{2+}-binding site.	Apc^{tm1Rak} (Apc1638N) 1857951 Targeted mutation at codon 1638 resulting in a truncated protein.	-	*Apc$^{+/-}$Cdh1$^{+/-}$* : 9-fold increase in intestinal tumour numbers and 5 fold increase in gastric tumour numbers compared with *Apc$^{+/-}$Cdh1$^{+/+}$* animals. No difference in tumour stage or grade. C57BL/6JIco(B6) x Ola129/129J.	(Smits et al, 2000b)
	Treatment with drinking water supplemented with 120ppm *N*-methyl-*N*-nitrosourea (MNU), a known gastric carcinogen.	-	MNU-treated *Cdh1$^{+/-}$* mice: 11 fold increase in murine signet-ring cell carcinomas compared with MNU-treated *Cdh1$^{+/+}$* animals. C57BL6.	(Humar et al, 2009)
Cdh1^{tm2Kem} 2389020 Targeted insertion of loxP sites in introns 5 and 10.	Cdh1$^{tm4(Cdn2)Kem}$ 3696711 Targeted insertion of N-cadherin into the E-cadherin genomic locus at the ATG start codon.	*Vil-Cre* (Villin promoter, active in intestinal and colonic epithelial cells, including progenitor cells).	*Cdh1$^{fl/Ncad}$ Vil-Cre* mice: viable, showing that N-cadherin can structurally replace E-cadherin and establish normal organ architecture. However following birth a progressive mutant phenotype developed with increased epithelial cell proliferation, nuclear localisation of β -catenin and activation of Wnt target genes, BMP pathway suppression, severe intestinal and colonic dysplasia, death at 2-3weeks of age. C57BL/6.	(Boussadia et al, 2002; el Marjou et al, 2004; Kan et al, 2007)
	Trp53^{tm1Brn} 1931011 Targeted insertion of loxP sites in introns 1 and 10.	*Atp4b-Cre* (At p4b promoter, active in progenitors of parietal cells).	*Cdh1$^{fl/fl}$ Trp53$^{fl/fl}$ Atp4b-Cre+*: intramucosal cancers from 6 months and invasive cancers from 9 months of age with 100% penetrance of fatal diffuse-type gastric cancer by one year of age and frequent lymph node metastasis. Tumours composed of poorly differentiated carcinoma and signet ring cells. First mouse model of diffuse-type gastric cancer.	(Jonkers et al, 2001; Shimada et al, 2012; Syder et al, 2004)

Table 5. Compound *Cdh1* mouse mutants: mammary system

Targeted allele MGI identifier Mutation	Targeted allele MGI identifier Mutation	Cre recombinase	Phenotype and strain (if documented)	Reference
Cdh1^{tm1Jjon} 3693661 Targeted insertion of loxP sites in introns 3 and 15	Trp53^{tm1Brn} 1931011 Targeted insertion of loxP sites in introns 1 and 10.	*K14Cre* (human keratin 14 promoter, expressed in epidermis, hair follicles and tongue epithelium).	*Cdh1*$^{F/F}$*Trp53*$^{F/F}$ *K14Cre* females: accelerated skin and mammary tumour development compared with *Trp53*$^{F/F}$ *K14Cre*. *Cdh1* loss in *Cdh1*$^{F/F}$*Trp53*$^{F/F}$ *K14Cre* and *Cdh1*$^{F/F}$*Trp53*$^{F/+}$ *K14Cre* females led to shift from expansive to invasive mammary carcinomas with distal metastasis phenocopying human invasive lobular carcinoma. *Cdh1* loss induced anoikis resistance and facilitated angiogenesis. *Trp53*$^{F/F}$ *K14Cre* and *Cdh1*$^{F/+}$ *Trp53*$^{F/F}$ *K14Cre:* pilomatricomas or squamous cell carcinomas without invasion. *Cdh1*$^{F/F}$*Trp53*$^{F/F}$ *K14cre* and *Cdh1*$^{F/F}$*Trp53*$^{F/+}$ *K14Cre* mice: invasive skin tumours.	(Derksen et al, 2006; Marino et al, 2000)
	Trp53^{tm1Brn} 1931011 Targeted insertion of loxP sites in introns 1 and 10.	*WCre* (whey acidic protein promoter, active in the luminal compartment of mammary epithelium).	*Trp53*$^{fl/fl}$ *Cdh1*$^{fl/fl}$ *WCre+*: impaired mammary gland function during pregnancy with disorganised epithelium due to anoikis resistance. Developed lactation-independent invasive and metastatic mammary carcinomas with features resembling human pleotrophic invasive lobular carcinoma.	(Derksen et al, 2011)
Cdh1^{tm1Kem} 1857282 LacZ cDNA and a neomycin resistance cassette inserted into exon 1 of *Cdh1*, just upstream of the translation start site	Cdh1^{tm2Kem} 2389020 Targeted insertion of loxP sites in introns 5 and 10.	*MMTV-Cre* (Mouse mammary tumour virus promoter, expressed in mammary gland cells, hormone responsive acting on differentiating epithelial cells).	*MMTV-Cre;Cdh1*$^{fl/-}$: normal mammary glands until 16-18 days of pregnancy but developed a severe phenotype at the time of parturition with a dramatic reduction in milk proteins prohibiting suckling of offspring due to extensive cell death and a mammary gland resembling an involuted gland usually seen post weaning.	(Boussadia et al, 2002; Larue et al, 1994)
Cdh1$^{tm4(Cdn2)Kem}$ 3696711 Targeted insertion of N-cadherin into the E-cadherin genomic locus at the ATG start codon	Cdh1^{tm1Jjon} 3693661 Targeted insertion of loxP sites in introns 3 and 15. Trp53^{tm1Brn} 1931011 Targeted insertion of loxP sites in introns 1 and 10.	*WCre* (whey acidic protein promoter, active in the luminal compartment of mammary epithelium).	*Ecad*$^{Ncad/fl}$ *WCre* females: impaired lactation with pups dying 2-3 days postnatally. *Ecad*$^{fl/fl}$ *WCre* females: impaired lactation however pups gained weight for 10 days postnatally before this became apparent. *Ecad*$^{Ncad/fl}$ *WCre+* and *Ecad*$^{fl/fl}$ *WCre+* lactating females: small mammary glands with collapsed alveolar structures. *Ecad*$^{Ncad/fl}$ *WCre+* mammary glands had activated p-Stat3, p53 and cleaved caspase 3. *Ecad*$^{fl/fl}$ *WCre+* mammary glands only had activated p53. The addition of *P53*$^{fl/+}$ rescued the *Ecad*$^{Ncad/fl}$ *WCre* lactation capacity, but did not alter the *Ecad*$^{fl/fl}$ *WCre* capacity. *Ecad*$^{Ncad/fl}$ *WCre* and *Ecad*$^{Ncad/fl}$ *p53*$^{fl/+}$ *WCre* mice developed progressive fibrosis and cyst formation with increasing age and lactation cycles and 55% of *p53* heterozygotes developed malignant and invasive tumours.	(Kan et al, 2007; Kotb et al, 2011)

Table 6. Compound *Cdh1* mouse mutants: skin

Targeted allele MGI identifier Mutation	Targeted allele MGI identifier Mutation	Cre recombinase	Phenotype and strain (if documented)	Reference
Cdh1^{tm1Kem} 1857282 LacZ cDNA and neomycin resistance cassette in exon 1 of *Cdh1*, just upstream of the translation start site.	Cdh1^{tm2Kem} 2389020 Targeted insertion of loxP sites in introns 5 and 10.	*Krox20^{Cre}* (Egr2 promoter, expression in epidermis, hair follicles of murine back skin and whisker follicles).	*Cdh1$^{-/fl}$ Krox$^{+/Cre}$*: normal until age of 30 days, then showed progressive back hair loss, dermal fibrosis and whisker hairs that were curled and shorter than control *Cdh1$^{+/fl}$ Krox$^{+/Cre}$* mice. C57BL/6/129.	(Boussadia et al, 2002; Larue et al, 1994; Voiculescu et al, 2000; Young et al, 2003)
		K14-Cre (human keratin 14 promoter, expressed in epidermis, hair follicles and tongue epithelium).	*Cdh1$^{fl/fl}$ K14-Cre* and *Cdh1$^{fl/-}$ K14-Cre:* died within 7-12 hours of birth due to an impaired epidermal water barrier. Absence of E-cadherin resulted in mislocalisation of tight junction proteins causing increased permeability. There was no change in desmosome formation.	(Boussadia et al, 2002; Hafner et al, 2004; Larue et al, 1994; Tunggal et al, 2005)
Cdh1^{tm2Kem} 2389020 Targeted insertion of loxP sites in introns 5 and 10.	Braf^{tm1Mmcm} 3711771 Targeted insertion of loxP-flanked human *BRAF* cDNA (exons 15-18) with *BRaf^{V600E}* mutation and mouse *BRaf* polyadenylation sequence into intron 14. Mice express normal *BRaf* but recombination leads to *BRaf^{VE}* expression. Ctnnb1^{tm1Mmt} 1858008 Targeted insertion of loxP sites in introns 2 and 3. Exon 3 contains important phosphorylation targets and excision of exon 3 leads to a degradation-resistant form of β -catenin. Pten$^{tm2.1Ppp}$ 2679886 Targeted insertion of loxP sites in introns 3 and 5.	*Tyr-CreER^{T2}* (Tyrosinase promoter, expressed in melanocytes).	*Cdh1* inactivation had no effect on primary tumour growth or metastasis in *Pten/Braf/Bcat-STA* melanomas. Mixed C57BL/6, FVB, 129.	(Bosenberg et al, 2006; Boussadia et al, 2002; Damsky et al, 2011; Dankort et al, 2007; Harada et al, 1999; Trotman et al, 2003)
	Tg(Krt14-RNAi:Cdh3)1Efu 3830534 Targeted insertion of short hairpin RNA directed against Cdh3 (P-Cadherin), under the keratin 14 promoter.	*K14-Cre* (human keratin 14 promoter, active in basal layer of epidermis, outer root sheath of hair follicle and oral epithelium).	*K14-Cre Cdh1$^{fl/fl}$ K14-PcadRNAi* mice small and died 1-2 hours following birth. They had shiny, inflexible skin with ventral flaking, and blistering. There was epidermal hyperthickening, loss of polarity, increased apoptosis, compromised epithelial barrier and tight junction defects.	(Tinkle et al, 2008; Vasioukhin et al, 1999)

Table 7. Compound *Cdh1* mouse mutants: embryogenesis

Targeted allele MGI identifier Mutation	Targeted allele MGI identifier Mutation	Cre recombinase	Phenotype and strain (if documented)	Reference
Cdh1^{tm2Kem} 2389020 Targeted insertion of loxP sites in introns 5 and 10	Cdh1$^{tm4(Cdn2)Kem}$ 3696711 Targeted insertion of N-cadherin into the E-cadherin genomic locus at the ATG start codon.	*Zp3-Cre* (Mouse zona pellucida 3 promoter, expressed in oocytes).	*Cdh1*$^{Ncad/Ncad}$ mice phenocopy *Cdh1*$^{-/-}$ embryos with failure to form intact trophectoderm. When maternal E-cadherin was removed (*Cdh1*$^{fl/fl}$ *Zp3-Cre+* mothers) N-cadherin could provide adequate cellular adhesion to mediate morula compaction, but was unable to continue to formation of a polarized, functional trophectoderm. C57BL/6.	(Boussadia et al, 2002; de Vries et al, 2000; Kan et al, 2007)
	Ctnnb1^{tm2Kem} 2148567 Targeted insertion of loxP sites in introns 1 and 6.	*Zp3-Cre* (Mouse zona pellucida 3 promoter, expressed in oocytes).	Generated oocytes lacking either maternal *Cdh1* or β-catenin, or both. Embryos lacking maternal *Cdh1* had failed blastomere adhesion and increased nuclear translocation of β-catenin. Embryos expressing truncated β-catenin also had failed adhesion. In both, blastomere adhesion was restored after expression of the protein from the paternal allele. Absence of β-catenin decreased developmental success rates, however this was restored when they also lacked maternal *Cdh1*. This suggests nuclear translocation of β-catenin is vital, and the balance between free β-catenin and that sequestered by E-cadherin at the membrane is important. C57BL/6J.	(Boussadia et al, 2002; Brault et al, 2001; De Vries et al, 2004; Lewandoski et al, 1997)

Table 8. Compound *Cdh1* mouse mutants: endocrine system

Targeted allele MGI identifier Mutation	Targeted allele MGI identifier Mutation	Cre recombinase	Phenotype and strain (if documented)	Reference
$Cdh1^{tm1Kem}$ 1857282 LacZ cDNA and a neomycin resistance cassette inserted into exon 1 of *Cdh1*, just upstream of the translation start site.	$Cdh1^{tm2Kem}$ 2389020 Targeted insertion of loxP sites in introns 5 and 10.	Tg^{Cre} (thyroglobulin promoter, expressed in thyrocytes from E14.5).	At postnatal day 7 thyroid follicle lumens in the *TgCre Cdh1*$^{-/fl}$ mice were about 30% smaller than $Tg^{Cre}Cdh1^{+/fl}$ mice and had an irregular shape. CD1.	(Boussadia et al, 2002; Calì et al, 2007; Larue et al, 1994)
Tg(RIP1-Tag)2Dh 2429941 Targeted insertion of the upstream region of rat insulin II gene and sequences coding for the large T antigen of simian virus 40. This results in expression of large T antigen in the β-cells of the endocrine pancreas and development of β-cell tumours.	Tg(Rip1-Cdh1*)3Semb 5435912 As for RIP1Tag but includes dominant mutant mouse E-cadherin (contains a 10 amino acid epitope from C-Myc). Tg(Rip1-Cdh1)3Gcr 5435916 As for RIP1TAG but includes cDNA encoding mouse E-cadherin.	–	Rip1Tag2 mice that maintain expression of E-cadherin in β-tumour cells have tumours that do not develop past the adenoma stage. Rip1Tag2 mice expressing a dominant-negative form of E-cadherin develop tumours with early invasion and metastasis.	(Dahl et al, 1996; Hanahan, 1985; Perl et al, 1998)

Table 9. Compound *Cdh1* mouse mutants: other systems

Targeted allele MGI identifier Mutation	Targeted allele MGI identifier Mutation	Cre recombinase	Phenotype and strain (if documented)	Reference
Cdh1^{tm1Kem} 1857282 LacZ cDNA and neomycin resistance cassette inserted into exon 1 just upstream of the translation start site.	Msh2^{tm1Rak} 2151801 *Msh2* exon 7 replaced by neomycin selection cassette.	-	*Msh2*$^{-/-}$ *Cdh1*$^{+/-}$: decreased survival due to development of more aggressive lymphomas compared with *Msh2*$^{-/-}$ *Cdh1*$^{+/+}$ animals. *Msh2*$^{-/-}$*Cdh1*$^{+/-}$: increased incidence of endometriod cancers (20% versus 0%). C57BL/6	(Kovtun et al, 2011; Smits et al, 2000a)
	Cdh1^{tm2Kem} 2389020 Targeted insertion of loxP sites in introns 5 and 10.	*Krox-20-Cre* (Egr2 promoter, active in hindbrain, bones, peripheral nervous system, and germline)	*Cdh1*$^{fl/-}$ *Krox-20-Cre* mice with absent E-cadherin in peripheral nerves had widened outer mesaxons however this had no long-term effect on the functional integrity of the myelin sheath. C57BL/6/129	(Boussadia et al, 2002; Voiculescu et al, 2000; Young et al, 2002)
Cdh1^{tm2Kem} 2389020 Targeted insertion of loxP sites in introns 5 and 10.	Cdh2^{tm1Glr} 3522469 Targeted insertion of loxP sites to flank exon 1.	*Le-Cre* (Pax6 promoter, Cre and GFP expression in the surface ectoderm, developing lens, cornea and pancreas)	*Cdh1*$^{fl/fl}$*Le-Cre+*: eye development defects at 3 weeks of age with microphthalmia, iris hyperplasia, absent pupils, small lenses lacking distinct epithelial layer. *Cdh2*$^{fl/fl}$*Le-Cre+*: more severe phenotype with defects in lens fibre cell integrity. *Cdh1*$^{fl/fl}$ *Cdh2*$^{fl/fl}$ *LeCre+*: more severe phenotype including defects in lens vesicle separation.	(Ashery-Padan et al, 2000; Boussadia et al, 2002; Kostetskii et al, 2005; Pontoriero et al, 2009)
	Tg(SFTPC-RAF1-BxB)1Urr 2447567 Targeted insertion of human SFTPC promoter and a human mutant RAF1 cDNA. Tg(SFTPC-rtTA)5Jaw 2445716 Targeted insertion of a reverse tetracycline responsive transactivator gene under the SFTPC promoter (active in respiratory epithelial cells).	*Tet-O-Cre* (human cytomegalovirus promoter, transcription of Cre recombinase activated by rtTA in the presence of doxycycline).	*SP-C rtTA/Tet-O-Cre/Cdh1*$^{fl/fl}$ mice treated with DOX developed diffuse hyperplastic lesions with scattered unpolarized cells and increased proliferation. *SP-C C-RAF BXB/SP-C rtTA/Tet-O-Cre/Cdh1*$^{fl/fl}$ mice (or animals expressing a dominant negative E-cadherin) with tumours at 6 weeks of age, then treated with DOX, had tumours with cell separation and partial loss of cuboidal morphology, increased vascularisation. These vascularised tumours grew rapidly, had invasive fronts and produced micrometastasis. β-catenin was upregulated and identified as a critical effector of VEGF-A and VEGF-C.	(Boussadia et al, 2002; Ceteci et al, 2007; Kerkhoff et al, 2000; Schönig et al, 2002; Tichelaar et al, 2000)
Cdh1^{tm1Jjon} 3693661 Targeted insertion of loxP sites in introns 3 and 15.	Trp53^{tm1Brn} 1931011 Targeted insertion of loxP sites in introns 1 and 10.	*Pgr-Cre* (progesterone receptor promoter, active in uterus, mammary gland, oviduct/ovary).	*Cdh1*$^{fl/fl}$ *Pgr-Cre+:* severe defects of neonatal uterus with disorganized epithelium, endometrial gland ablation, loss of adherens and tight junctions, abnormal proliferation and apoptosis. *Cdh1*$^{fl/fl}$ *p53*$^{fl/fl}$ *Pgr-Cre+*: endometrial carcinomas with myometrial invasion.	(Reardon et al, 2012)

1.9 Epithelial-mesenchymal transition

Epithelial-mesenchymal transition (EMT) is a fundamental process in embryonic development, with critical roles in mesoderm formation, the development of the neural crest, heart and craniofacial system (Thiery, 2002). It is also a vital process in the invasive and metastatic stages of carcinomas (Yang & Weinberg, 2008). During EMT, tightly adherent, polarized epithelial cells lose E-cadherin, become more motile and gain characteristics and markers of mesenchymal cells. EMT can be induced by the loss of E-cadherin or the activation of the Wnt signalling pathway, with β-catenin the key intermediary in both processes. In addition to increasing cell motility and invasiveness, EMT has other effects that promote tumour survival such as resistance to apoptosis and anoikis, cellular senescence and oncogene addiction (Tiwari, 2012).

EMT has been shown in a number of tumour types (Li & Herlyn, 2000; Thiery, 2003; Tomita et al, 2000). Gain of mesenchymal cadherins confers increased cell motility and migration. It is crucial for some morphological events in development, however can contribute to tumour progression when disordered (Hazan et al, 2000; Li et al, 2001; Nieman et al, 1999). It is thought that gain of mesenchymal cadherins may not only result in decreased epithelial cell adherence, but may also enhance the interaction of cells with mesenchymal components, thus encouraging invasion and metastasis. The reverse process, mesenchymal-to-epithelial transition may encourage growth of secondary tumours following dissemination (Chaffer et al, 2007).

β-catenin is likely to have an important role in EMT. Immunohistochemical analysis of colorectal cancers has shown that cells in the central part of the tumour have membranous β-catenin localization as is seen in normal epithelium, whereas tumour cells at the invasive front display nuclear β-catenin (Brabletz et al, 1998). The accumulation of nuclear β-catenin is associated with cell-cycle arrest, the progressive loss of E-cadherin expression and EMT (Brabletz et al, 2001; Jung et al, 2001). Such cells at the invasive front have been labeled “migrating cancer stem cells”. They have stem-cell like qualities, such as the ability to self-renew, and are able to transiently differentiate into mesenchymal cells, increasing their invasive potential, and ultimately resulting in distant metastases when they undergo mesenchymal-epithelial transition (Brabletz et al, 2005).

The heterogenous distribution of β-catenin within tumours suggests that Wnt signalling is modulated by the tumour microenvironment. An initial mutation in APC or β-catenin is necessary but insufficient for full Wnt signalling activation. Tumour cells at the invasive front may be exposed to metabolites that increase Wnt pathway activation and enhance β-catenin nuclear translocation (Gaspar & Fodde, 2004; Reya et al, 2001). A combination of intrinsic (tumour cell-autonomous) and extrinsic (tumour microenvironment) factors are likely to be responsible for modulation of Wnt/β-catenin signalling and tumour invasion and spread (Fodde & Brabletz, 2007).

The microenvironment at the invasive front of tumours modulates Wnt signalling through paracrine secretion by myofibroblasts and other stromal cells (Gregorieff et al, 2005). Growth factors with effects on Wnt signalling include hepatocyte growth factor, which leads to tyrosine phosphorylation of β-catenin, nuclear accumulation and increased invasive potential and platelet-derived growth factor which enhances β-catenin nuclear translocation and Wnt activation through the activation of tyrosine kinase receptors and the tyrosine phosphorylation of p68 (Heldin & Westermark, 1999; Rasola et al, 2007; Yang et al, 2006). The mesenchymal forkhead transcription factors *Foxf1* and *Foxf2* usually limit paracrine Wnt signalling and promote the production of intestinal extracellular matrix (Ormestad et al, 2006). Mice with mutations in *Foxf1* and *Foxf2* have altered epithelial proliferation and survival, and express increased levels of Wnt5a, possibly through alterations in BMP Hedgehog signalling.

Inflammation is known to promote oncogenesis, at least partially through Wnt modulation. Colorectal cancers are associated with increased inflammation and in particular macrophage expression, which through paracrine effects can increase Wnt ligand expression and advance tumour progression (Smith et al, 1999). Non-steroidal anti-inflammatory drugs decrease the number and size of polyps in patients with FAP, through altered prostaglandin E2 levels (PGE2). PGE2 has been shown to stimulate the growth of colorectal cancer cells through activation of Wnt signalling via the release of GSKβ from the β-catenin destruction complex (Castellone et al, 2005).

1.10 Evidence for an association between β-catenin in the adhesion complex and β-catenin mediating Wnt signalling

There is much contention within the field about whether β-catenin initially bound to E-cadherin can contribute to Wnt signalling when it dissociates from the adhesion complex, or if the adhesion and Wnt pools of β-catenin are completely independent. Skeptics of any overlap cite the very short half-life of cytoplasmic β-catenin and *C. Elegans* having distinct β-catenin homologues for adhesion and signalling functions to support their argument (Clevers & Nusse, 2012; Korswagen et al, 2000). Moreover, human breast cancer cell lines with E-cadherin mutations or transcriptional silencing of the gene do not show Wnt pathway activation assessed using a TCF reporter (van de Wetering et al, 2001).

There is a body of work, comprised mostly of experiments employing overexpression of E-cadherin, that supports E-cadherin being capable of titrating the amount of cytoplasmic β-catenin, altering Wnt signalling and influencing cell growth. Whether this ability depends only on the cytoplasmic domain of E-cadherin, or also on adhesion is however even more controversial. In *Xenopus* embryos, overexpression of cadherins results in a phenotype with reduced dorsal axial structures identical to that seen with depletion of maternal β-catenin (Heasman et al, 1994). In experiments in *Drosophila,* Sanson and colleagues used wildtype E-cadherin (*shotgun*) or a dominant-negative truncated form (lacking the extracellular domain) to show both constructs were capable of titrating *armadillo* from a signalling to a junctional pool, and that overexpression of either construct phenocopied *wingless* or *armadillo* mutants (Sanson et al, 1996). They concluded cadherins may be able to buffer the signalling pool of *armadillo,* but that this function is not linked to the adhesion function of the cadherin. Stockinger and colleagues showed that overexpression of E-cadherin in epithelial or fibroblastoid cells suppressed cell proliferation through E-cadherin's ability to negatively regulate β-catenin mediated Wnt activation, and this effect did not require a functional extracellular adhesion domain (Stockinger et al, 2001).

Gottardi and colleagues demonstrated that E-cadherin could suppress growth in a CRC cell line (Gottardi et al, 2001). By using wildtype E-cadherin, or constructs lacking the cytoplasmic β-catenin binding domain (an E-cadherin-α-catenin chimera or an E-cadherin Δ β-catenin mutant), or lacking the adhesive activity of E-cadherin (the E-cadherin cytoplasmic domain fused to the interleukin-2 receptor α subunit), they showed that the

growth suppression was independent of adhesive function but relied on a functional β-catenin binding domain. Growth suppression was associated with decreased β-catenin transcriptional activity. They also showed that in these cells there was a large pool of β-catenin that was not active in adhesion or Wnt signalling. The same group showed that Wnt signalling may result in a molecular form of β-catenin with a COOH terminus conformational change that preferentially binds to TCF rather than E-cadherin, thus enhancing Wnt signalling, and that E-cadherin preferentially binds β-catenin-α-catenin dimers rather than β-catenin monomers (Gottardi & Gumbiner, 2004). Phosphorylation of E-cadherin however enabled binding of the monomeric form of β-catenin: the authors postulated that regulation of the different adhesive or signalling functions of β-catenin may depend on the cell type and circumstances.

More recently, the same authors investigated whether changes in cell adhesion could alter β-catenin signalling, showing that cadherins were capable of indirectly promoting N-terminal phosphorylation of β-catenin by the destruction complex at the cell membrane and that β-catenin turnover was increased with cell adhesion (Maher et al, 2009). These experiments included using normal human epidermal keratinocytes (NHEKs), which have cadherin-based adhesion that responds sensitively to Ca^{2+} concentrations. The results revealed that when these cells were stimulated with Lithium Chloride, mimicking Wnt activation, loss of cadherin-based adhesion (low Ca^{2+} conditions) led to increased cytosolic β-catenin, including the active unphosphorylated form. Importantly, this happened despite no change in the levels of E-cadherin protein or the amount of β-catenin associated with E-cadherin. The increased free β-catenin was accompanied by increased *Axin2* expression. Such results suggest cell adhesion may have a role in limiting Wnt activation.

In other situations where the Wnt pathway is already active, E-cadherin has also been shown to influence Wnt signalling. Orsulic and colleagues established that E-cadherin null embryonic stem (ES) cells (genetically targeted) had free β-catenin that could translocate to the nucleus, bind to LEF and mimic Wnt signalling, and that overexpression of E-cadherin could reverse this Wnt activation through direct binding of the E-cadherin cytoplasmic domain with β-catenin (Orsulic et al, 1999). Kuphal and Behrens examined a CRC cell line with constitutive Wnt activation, illustrating that siRNA-mediated knock-down of E-cadherin resulted in increased Wnt activation as measured by nuclear β-catenin expression and the

Wnt TOP-flash reporter system (Kuphal & Behrens, 2006). Conversely, in a fibroblast cell line which had neither Wnt activation nor E-cadherin expression, expression of ectopic E-cadherin resulted in morphological changes and stabilization of β-catenin at the cell membrane but no alteration in Wnt activity.

As discussed previously, a causal role for E-cadherin was shown in the transition from adenoma to carcinoma in a Rip1Tag2 model of β-islet cell carcinogenesis (Perl et al, 1998). However, E-cadherin loss was not shown to contribute to tumourigenesis through Wnt activation in this model (Herzig et al, 2007). Herzig and colleagues revealed that in β-islet tumour cell lines lacking E-cadherin expression, β-catenin levels correlated with E-cadherin levels. When they stimulated Wnt signalling by Wnt-1 overexpression, or stabilization of β-catenin with a proteasome inhibitor or GSK3β inhibitor, in the presence of E-cadherin β-catenin levels were high and resistant to Wnt stimuli suggesting E-cadherin had a role in sequestration of β-catenin. In the absence of E-cadherin high β-catenin levels were only detectable with Wnt activation. Using a TOP-flash reporter, β-catenin/TCF transcriptional activity was high with transient expression of a wildtype β-catenin or expression of a constitutively-active β-catenin when E-cadherin was not present, but absent when E-cadherin was expressed.

Despite much contention within the Wnt field about the potential for E-cadherin to influence Wnt signalling, clearly it may have a role. Many of the experiments discussed have relied on overexpression systems with non-physiological concentrations of E-cadherin; the constructs lacking adhesion function have usually lacked the whole extracellular domain and sometimes resulted in dominant negative effects. The work has predominantly been *in vitro* or non-mammalian systems. Further work is required to investigate a possible association between E-cadherin and the Wnt pathway, and to assess the relative roles of the cytoplasmic (β-catenin-binding) versus extracellular (adhesive) domains of E-cadherin.

1.11 Aims of this work

This project uses mouse models to assess the effect of E-cadherin loss of function in the intestine, including in the setting of Wnt pathway activation.

1. The embryonic lethality of germline mutants has ensured the tissue specific effects of normal E-cadherin function in the intestine remain unknown. What is the effect of E-cadherin loss on the intestine, in particular the stem cell compartment, cellular differentiation and anoikis?
2. What are the consequences of E-cadherin loss during *Apc* loss of function adenoma formation?
3. Do the above *in vivo* models contribute any additional information to the existing knowledge of additive or synergistic effects of E-cadherin loss on the Wnt pathway?
4. Can an *in vitro* model be utilized to define the cell adhesion versus Wnt regulatory functions of E-cadherin?
5. Do E-cadherin regulatory pathways also modify *Apc* loss of function models? In this case *Smad4* loss of function will be investigated.

2 Materials and Methods

2.1 Mice

2.1.1 Home office and ethical approval

All procedures were approved under Project licence 20 2245 from the United Kingdom Home Office in accordance with the Animals (Scientific Procedures) Act 1986. The project was also approved by a University of Oxford Research Ethics Committee.

2.1.2 Animal husbandry

Germline experiments were carried out in a conventional animal facility. Conditional breeding and experiments were conducted in a specific pathogen free (SPF) facility following rederivation of animals to achieve the required health status. *Villin-Cre* (*Vil-Cre*) and *Villin-CreER^{T2} (Vil-CreER^{T2}*) animals were known to have positive *Helicobacter hepaticus* infection status. In both facilities there was a 12 hour light/dark cycle, temperature 19-23°C, normal chow and water were available *ad-libitum* and cages contained environmental enrichment. Animals were ear clipped at approximately postnatal day 10 (P10) for identification and the ear tissue was used for genotyping. If identification was required before P10 a number was drawn on the animal's abdomen using a surgical marker pen. Experimental animals were sacrificed using Schedule 1 approved methods.

2.1.3 Humane experimental endpoints

Apc$^{+/Min}$ animals were initially culled at 120 days. For extended survival analysis of the *Apc$^{+/Min}$* animals and for other experiments with adult mice, animals were monitored closely and culled using the Schedule 1 method of cervical dislocation when they reached a defined humane endpoint as detailed in Table 10.

Table 10. Defined humane endpoint score sheet

Sign		Score
Body condition	Well-conditioned	0
	Underconditioned: *Segmentation of vertebrae evident. Dorsal pelvic bones palpable.*	2
	Emaciated: *Skeletal structure extremely prominent. Little or no flesh cover, vertebrae distinctly segmented*	3
Weight	Normal	0
	Reduced by <5%	1
	Reduced by 10-15%	2
	Reduced by >15%	3
Respiratory rate	Normal	0
	Increased by <5%	1
	Increased by 10-20%	2
	Increased by >20% or 10-20% accompanied by nasal discharge	3
Evoked response	Normal	0
	Less alert	2
	Violent, very weak, very still or hunched	3
Tumour and intestinal features	No abnormality	0
	Distended abdomen, tumour lump 0.5-1.5cm, anaemia (pale/translucent hind paws)	2
	Tumour >1.5cm, any ulceration, any abdominal distension affecting normal movement, rectal bleeding or fresh blood in cage, diarrhoea	3
Total		

Interpretation: 3 in any category: animal is distressed and should be humanely killed. Total score >5: the animal should be monitored closely (at least twice daily) and humane killing considered if no improvement within 24 hours.

2.1.4 Mouse strains

The animals used in this study have all been reported previously. In the tables MGI identifier refers to a unique identifier available on the Mouse Genome Informatics (MGI) database (http://www.informatics.jax.org/). They are detailed in the below tables and for ease of reference have been divided into four groups:

- Germline alleles (Table 11)
- Conditional alleles (Table 12)
- Reporter alleles (Table 13)
- Cre-transgenes (Table 14)

Table 11. Germline alleles

Gene	Targeted construct	Nomenclature	MGI identifier	Reference	Strain
Apc	Chemically induced transversion point mutation changing nucleotide 2549 from T to A	Apc^{Min}	1856318	(Su et al, 1992)	C57BL6/J
Cdh1	LacZ gene and neomycin resistance cassette inserted into exon 1, immediately upstream of the initiation codon of the gene	$Cdh1^{tm1Kem}$	1857282	(Larue et al, 1994)	C57BL6/J

Table 12. Conditional alleles

Gene	Targeted construct	Nomenclature	MGI identifier	Reference	Strain
Apc	Exon 14 flanked by loxP sites	Apc^{tm1Tno}	3764940	(Shibata et al, 1997)	C57BL6/J
Cdh1	Exons 4 to 15 flanked by loxP sites	$Cdh1^{tm1Jjon}$	3693661	(Derksen et al, 2006)	C57BL6/J
Smad4	Exon 1 of *Smad4* flanked by loxP sites	$Smad4^{tm1Rob}$	3624262	(Chu et al, 2004)	129/C57BL6/J

Table 13. Reporter alleles

Gene	Targeted construct	Nomenclature	MGI identifier	Reference	Strain
Rosa-LacZ	Targeted insertion of a splice acceptor site, neo expression cassette flanked by loxP sites and LacZ gene into Rosa26 locus	$Gt(ROSA)26Sor^{tm1Sor}$	1861932	(Soriano, 1999)	129S4/SvJaeSor
Rosa26YFP	Targeted insertion of EYFP, preceded by loxP-flanked strong transcriptional termination sequence, into Rosa26 locus	$Gt(ROSA)26Sor^{tm1(EYFP)Cos}$	2449038	(Srinivas et al, 2001)	C57BL/6J

Table 14. Cre-transgenes

Gene	Targeted construct	Nomenclature	MGI identifier	Reference	Strain
AhCreER^{T}	Tamoxifen-dependent Cre recombinase driven by Cyp1a1	Tg(Cyp1a1-Cre/ERT)1Dwi	3829429	(Sansom et al, 2004)	C57BL/6J
Lgr5-IRES-EGFP-CreER^{T2}	Tamoxifen-dependent Cre recombinase driven by Lgr5 promoter (EGFP-IRES-CreER^{T2} cassette inserted into exon 1 of Lgr5)	Lgr5$^{tm1(cre/ERT2)Cle}$	3764660	(Barker et al, 2007)	129P2/ OlaHsd
Villin-Cre	Constitutively active Cre recombinase driven by 9kb region of the villin promoter	Tg(Vil-cre)20Syr	3053819	(el Marjou et al, 2004)	B6D2 (C57BL6 x DBA/2)
Villin-CreER^{T2}	Tamoxifen-dependent Cre recombinase (Cre recombinase fused to mutated ligand binding domain of the human oestrogen receptor) driven by 9kb region of the villin promoter	Tg(Vil-cre/ERT2)23Syr	3053826	(el Marjou et al, 2004)	B6D2 (C57BL6 x DBA/2)

2.1.5 Mouse breeding

Breeding strategies are outlined at the start of each chapter.

2.1.6 Embryonic dissections

Timed matings were performed by placing one or two female mice with a male. Females were checked for seminal plugs at 9am. Conception was considered to be within 12 hours of plug detection. Before cervical dislocation at the predetermined time-point, females were examined carefully to confirm pregnancy. A midline abdominal incision was made, uterine horns dissected from the vagina and placed in PBS on ice. Embryos were removed from the uterine horns, cooled on ice or decapitated (depending on embryonic age), and dissected using a Nikon SMZ800 dissecting microscope. Samples were fixed in neutral buffered formalin (NBF, 100ml 37% Formaldehyde, 40mM Na_2HPO_4, 29mM $NaH_2PO_4.H_2O$ in 900ml ddH_2O, pH7.6). A tail sample was taken for genotyping.

2.1.7 Adult necropsy protocol

Animals were sacrificed at the defined endpoint using the Schedule 1 method of cervical dislocation and weighed. A midline abdominal incision was made. After a rapid survey of the internal abdominal organs, an excision was made at the oesophageal junction, and the stomach, small intestine (SI) and colon systematically dissected from mesentery and anchoring ligaments. The stomach, small intestine and colon were removed en bloc,

weighed and placed in ice cold phosphate buffered saline (PBS, calcium free). The colon was divided from the small intestine and the small intestine was then divided into equal length thirds. The stomach, intestine segments and colon were placed on the absorptive side of Benchkote (Whatman) and opened longitudinally to expose the inner epithelium. Digestive contents were removed through gentle washing in PBS and manual removal using a gloved finger. Length and width of intestinal sections were recorded.

If intestinal samples were being collected for adenoma counts and histology only, the Benchkote was rolled and placed in a falcon tube in NBF. If samples were being collected for other applications those samples were collected and stored as detailed in Table 15.

Finally, the abdomen was surveyed carefully for evidence of lymphadenopathy and the liver, spleen and kidneys were inspected for macroscopic changes. If metastatic disease was suspected (lymphadenopathy, advanced tumour features or macroscopic hepatic changes) the liver, spleen, kidneys, enlarged lymph nodes, lungs, heart and brain were each dissected en bloc and collected in NFB. An ear clip or splenic sample was taken to confirm genotyping. Photos of dissection findings were taken using a Canon Powershot digital camera.

Table 15. Necropsy protocol

Tissue	Application	Dissection	Storage
Stomach/Intestine/Colon	Histology Immunolabelling	Dissected from mesentery and removed en bloc. Divided longitudinally on Benchkote	NBF for 24 hours
Stomach/Intestine/Colon, brain, heart, lungs, kidney	*LacZ* staining	Dissected from mesentery and removed en bloc. Divided longitudinally on Benchkote	2% paraformaldehyde, full details in Section 2.7.2.2
Intestine	RNA extraction	1cm length section of proximal SI 10cm from gastroesophageal junction excised	RNAlater or snap frozen on dry ice, -80°C
Caecum	RNA extraction	$1cm^2$ area of caecum excised	RNAlater or snap frozen on dry ice, -80°C
Colon	RNA extraction	1cm length sections of mid colon excised	RNAlater or snap frozen on dry ice, -80°C
Intestinal/colonic adenomas/tumours	RNA extraction	Adenoma/tumour excised from underlying epithelium using scissors	RNAlater or snap frozen on dry ice, -80°C
Adenoma/tumour	Adenoma culture	See specific protocol Chapter 5	
Spleen	Genotyping	$0.5cm^2$ area excised	-20°C
Spleen	RNA extraction	$1cm^2$ area excised	RNAlater or snap frozen on dry ice, -80°C
Brain, heart, lung, liver, kidney	Histology (if invasive disease queried)	Excised en bloc, dissected to segments ≤1.5cm width	NBF for 24 hours

2.2 Tissue storage

2.2.1 Formalin fixation and storage

Samples were fixed in 10% NBF overnight at room temperature. They were then washed in 70% ethanol (30% water) and stored in 70% ethanol at 4°C in sealed falcon tubes.

2.2.2 Samples for RNA analysis

Samples for RNA analysis were either snap frozen and then stored at -80°C or stored in RNAlater overnight at 4°C to allow tissue permeabilisation and then stored at -80°C.

2.3 Adenoma counting

Intestinal specimens were laid flat and viewed under a dissecting microscope (Nikon SMZ800). Using specially designed sizing loops (1mm-6mm diameter) the number and size of adenomas were recorded for each third of the small intestine and the colon. Adenoma counting was performed by a single investigator (JM) twice for each specimen and a further count was performed if there was any discrepancy. JM was blinded to genotype at the time of counting.

2.4 Histopathology

2.4.1 Sample preparation

The intestinal segments and colon were prepared as swiss rolls (Figure 6). Caecal tumours were bisected longitudinally. Other organs were dissected into 1cm width segments.

Figure 6. Swiss roll
Photo shows small intestine (SI) and colon assembled in a swiss roll. P: proximal third SI. M: middle third SI. D: distal third SI. C: colon (with or without caecum). Scale bar 1cm.

2.4.2 Tissue processing and sectioning

Samples were processed by Richard Stillion (RS) at the Dunn School Tissue and Molecular Pathology Service. Prepared formalin-fixed samples were processed by an automated system and embedded by RS and JM. Tissue blocks were sectioned using a Leica microtome by RS.

2.4.3 Haematoxylin and eosin staining

Every fifth section was stained for haematoxylin and eosin (H&E) by RS.

2.5 DNA extraction

DNA was extracted from ear clip or splenic samples using either high-salt/ethanol precipitation (Hassan & Howell, 2000) or hot sodium hydroxide and Tris ('HotSHOT'

protocol) (Truett et al, 2000) as detailed below. DNA was stored initially at 4°C whilst genotyping was conducted and then long-term at -20°C.

2.5.1 High-salt/ethanol precipitation

Tissue samples were incubated at 55°C for at least 3 hours (often overnight) in 250µl of lysis buffer (50mM Tris (pH 8.0), 100mM EDTA, 100mM NaCl, 1% SDS) with 0.5µg/ml proteinase K (Roche). 2µg/ml RNase (Sigma) was then added and incubated at 37°C for 30 minutes. Subsequently 150µl of 5M sodium chloride was added, the samples were shaken vigorously for 30 seconds and then centrifuged at 10,000xg for 15 minutes. The supernatant was transferred to a fresh tube containing 400µl of ice cold 100% ethanol. Samples were shaken gently, then centrifuged for 15 minutes at room temperature. The supernatant was removed, the pellet washed with 150µl 70% ethanol and centrifuged for 5 minutes. The ethanol was removed by pipetting and residual ethanol evaporated by placing samples in a 70°C incubator. The DNA was resuspended in 100µl TRIS-EDTA buffer.

2.5.2 'HotSHOT' protocol

75µl of alkaline lysis buffer (25 mM NaOH, 0.2 mM EDTA, pH 12) was added to tissue samples and incubated for 1 hour at 95°C. 75µl of neutralization buffer (40 mM Tris-HCl) was then added, samples were vortexed, centrifuged at 13,000xg for 5 minutes and the supernatant was transferred to a clean tube.

2.6 Genotyping

2.6.1 Polymerase chain reaction

Genotyping was performed by polymerase chain reaction (PCR) using the Qiagen HotStar Plus Taq kit (Qiagen) and the relevant primers (Sigma) and cycling conditions as documented in Appendix 1. Reactions were run on a Bio-Rad MyCycler Thermal Cycler, Bio-Rad MJMini Personal Thermal Cycler, or MJ Research Dyad Thermal Cycler.

2.6.2 Gel electrophoresis

1.6%-2% agarose was dissolved in 0.5M TBE (Tris-borate-EDTA) by heating in a microwave for 2 minutes. The solution was cooled, mixed with 2µg/ml of ethidium bromide and set in a gel plate with 2mm combs. When set, the gel was covered in TBE buffer. 5µl of PCR marker (Bio-Rad) was loaded and 10µl of each PCR sample. The gel was run at 80V for 25-30

minutes then transilluminated with ultraviolet light (302nm wavelength) using a Syngene Gene Genius.

2.6.3 Extraction of PCR products from agarose gels

PCR products that needed to be sequenced were cut from agarose gels whilst being visualised with ultraviolet light. They were then extracted using Zymoclean Gel DNA Recovery Kit as per manufacturer's instructions.

2.7 Cre recombination

2.7.1 Activation of Cre recombination in vivo

For inducible conditional experiments Cre recombination was activated in adult mice at 8-12 weeks of age by intraperitoneal (IP) injection of tamoxifen in corn oil. Tamoxifen solution was prepared by dissolving tamoxifen (Sigma) in 100% ethanol to make a 10mg/ml solution. 300uL aliquots of corn oil (Sigma) were placed in microcentrifuge tubes and the required dose of tamoxifen in ethanol added to each aliquot. The tubes were vortexed, centrifuged at low speed briefly to remove any liquid from the cap and then placed in a vacuum centrifuge for 20 minutes to evaporate the ethanol. The solution was checked for crystals or residual ethanol before injection.

Only animals weighing over 20g were included for injection. Details of the doses used are provided in the relevant chapters. BD insulin syringes (28 gauge, 0.5ml volume) were used for injection. Any air bubbles were removed prior to injection. Animals were scruffed, the needle inserted in the left or right lower abdomen (alternating between sides), aspirated to check correct positioning and then the solution injected. Animals were monitored closely following injection, including daily weighs, and sacrificed when they reached a defined endpoint.

2.7.2 Detection of Cre recombination

Activation of Cre recombination was detected using a reporter gene (*Rosa-YFP* or *Rosa-LacZ*) as detailed below and by genotyping for the recombined product (Appendix 1).

2.7.2.1 Rosa-YFP detection

Initial attempts to detect YFP in formalin fixed paraffin embedded (FFPE) tissue sections or frozen sections were unsuccessful. An anti-GFP antibody (Abcam) was thus used successfully for detection using the immunolabelling protocol outlined in Section 2.8. *Rosa-YFP* was the preferred reporter gene because samples could be processed normally and labelling for multiple markers carried out.

Figure 7. *Rosa-YFP* detection
Confocal microscopy images of small intestine, labelling for the nuclear marker DAPI (blue) and the *Rosa-YFP* reporter (yellow, detected using an anti-GFP antibody and yellow secondary fluorochrome). Samples from animals that were *Vil-CreER^{T2}-* or *YFP$^{+/+}$* did not express the YFP reporter (left and middle panels). Samples from animals that were *YFP$^{+/fl}$* or *YFP$^{fl/fl}$* and *Vil-CreER^{T2}+* did express YFP (right panel). Scale bar 50µm.

2.7.2.2 β-galactosidase detection

For β-galactosidase detection intestines (and other organs if appropriate) were dissected as usual but samples were fixed in 2% paraformaldehyde on ice immediately. The intestines were pinned onto wax blocks and fixation continued for one hour at room temperature. They were then washed in PBS three times (5 minutes each wash) before incubation for 45 minutes in a solution of 20mM DL-Dithiothreitol (DTT), 20% ethanol in 150mM Tris-HCl, pH8. The samples were washed again three times in PBS and then incubated overnight at 4°C in staining solution: 2mM X-gal, 4mM potassium ferricyanide, 4mM potassium ferrocyanide and 2mM magnesium chloride at pH7.6. The following morning samples were washed three times in PBS and staining assessed. *RosaLacZ* was used to verify *RosaYFP* results and to assess recombination rates in organs other than the intestine, but it was not used routinely as it limited the use of samples for other purposes.

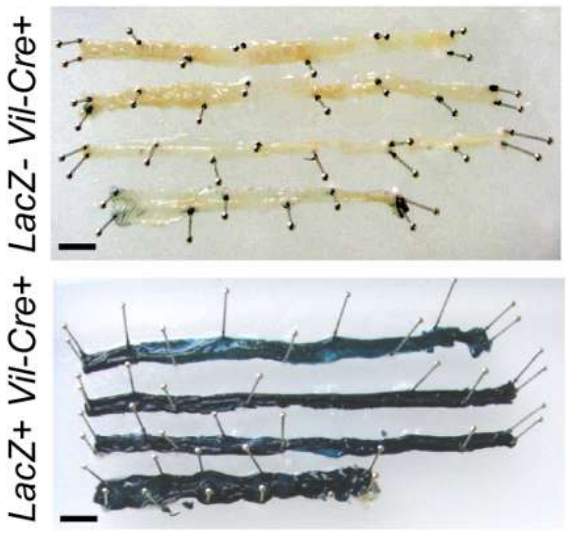

Figure 8. β-galactosidase detection
Negative staining of whole intestinal mount from *LacZ* negative mouse (top panel). Positive staining of intestinal mounts from *LacZ+ Vil-Cre+* animal (bottom panel). Scale bars 1cm.

2.8 Immunolabelling

Formalin fixed, paraffin-embedded sections were deparaffinised in xylene (Fisher, 2x 5 minutes), then rehydrated in an ethanol series (100% x2, 95%, 80%, 70%, 50% for 3 minutes each). After rinsing twice in deionised water, slides were incubated in deionised water with 0.5% tween for 30 minutes. Antigen retrieval was carried out in citrate buffer (1.92g citric acid in 1000ml distilled water, pH6) using a decloaking chamber (Biocare Medical, DC2008US) at 125°C for 2 minutes and 85°C for 10 minutes. Slides were cooled in the retrieval solution and washed in 1% Tris-buffered saline (TBS: 8.8g NaCl, 0.2g KCl, 3g Tris base, 1000ml distilled water, pH 7.4, 3x 3minutes) before blocking for one hour with 10% serum (same source as secondary antibody, Vector laboratories), and 0.5% Tween© in TBS. An Immedge pen (Vector Laboratories) was used to mark the area of slide to be blocked and stained.

Slides were incubated with the primary antibody in 3% serum, 0.3% Tween© and TBS overnight in a humidified chamber at 4°C. The following day slides were washed in TBS (3x 3 minutes) and incubated with secondary antibody in TBS for 2 hours. Details of antibodies used are in Tables 16-18 including optimized concentrations. During the secondary labelling and subsequent steps the samples were protected from bright light. The slides were washed in TBS (3x 3 minutes), incubated with 4',6-diamidino-2-phenylindole (DAPI, 1:5,000 in TBS, 10 minutes), washed again in TBS and mounted with ProLong Gold antifade reagent (Invitrogen). Labelling was visualised using an Olympus BX60 fluorescent microscope and images were taken using a Nuance multi-spectral camera and software or using an Olympus FluoView FV1000 confocal microscope.

Table 16. Primary antibodies

Antibody	Epitope	Species raised in	Manufacturer (catalogue)	Optimised dilution
Axin-2	Within 800 aa of C-terminus	Rabbit polyclonal	Abcam (ab32197)	1:100
β-catenin	aa 571-781	Mouse IgG1	BD laboratories (610154)	1:200
β-catenin	Residues around Ser37 of human β-catenin	Rabbit polyclonal	Cell signaling (#9562)	1:200
Chromogranin A	Residues at N-terminal of human Chromogranin A	Rabbit polyclonal	Epitomics (1773-1)	1:300
Cleaved caspase 3	Large fragment of cleaved caspase 3	Rabbit polyclonal	Cell signaling (#9664L)	1:200
Cre recombinase	aa 77-343	Mouse IgG1	Millipore (3120)	1:500
E-cadherin	Cytoplasmic domain human E-cadherin	Mouse IgG2a	BD Laboratories (610182)	1:200
Fibronectin	Murine fibronectin	Rabbit polyclonal	Abcam (ab23750)	1:200
GFP	EGFP	Chicken polyclonal	Abcam (Ab13970)	1:500
Ki-67	C-terminus	Rabbit IgG	Thermo Scientific (RM9106)	1:300
Lysozyme	Human lysozyme	Rabbit polyclonal	Dako (A0099)	1:500
Mucin 2	aa 4880-5179	Rabbit polyclonal	Santa cruz (sc-15334)	1:500
Smad4	aa 1-552 of human Smad4	Mouse IgG1	Santa cruz (sc-7966)	1:200
Twist	aas 146-195 of human twist	Rabbit polyclonal	Abcam (ab49254)	1:100
Villin	Chicken villin	Mouse IgG1	Santa cruz (sc-58897)	1:50
Vimentin	Residues within 400 aa of C-terminus	Rabbit polyclonal	Abcam (ab45939)	1:200

Table 17. Secondary antibodies

Antibody	Species raised in	Manufacturer	Dilution
Alexa-488 IgG1	Goat (anti-mouse)	Invitrogen (A21121)	1:300
Alexa-488 IgG	Goat (anti-rabbit)	Invitrogen (A11034)	1:300
Alexa-555 IgG1	Goat (anti-mouse)	Invitrogen (A21127)	1:300
Alexa-555 IgG2a	Goat (anti-mouse)	Invitrogen (A21137)	1:300
Alexa-555 IgG	Goat (anti-rabbit)	Invitrogen (A21429)	1:300
Alexa-594 IgG1	Goat (anti-mouse)	Invitrogen (A21135)	1:300
Alexa-594 IgG2a	Goat (anti-mouse)	Invitrogen (A21125)	1:300
Alexa-594 IgG	Goat (anti-rabbit)	Invitrogen (A11037)	1:300
Alexa-647 IgG1	Goat (anti-mouse)	Invitrogen (A21240)	1:300
Alexa-647 IgG2a	Goat (anti-mouse)	Invitrogen (A21241)	1:300
Alexa-647 IgG	Goat (anti-rabbit)	Invitrogen (A21245)	1:300
Dylight-550 IgG	Goat (anti-chicken)	Abcam (ab96948)	1:200

Table 18. Primary conjugated antibodies

Antibody	Epitope	Species raised in	Manufacturer	Dilution
β-catenin Alexa-488	Mouse β-Catenin aa. 571-781	Mouse	BD (562605)	1:10
Cleaved caspase-3 Alexa-488	Large fragment of cleaved caspase 3	Rabbit	Cell signaling (#9669S)	1:50
E-cadherin Alexa-647	Cytoplasmic domain human E-cadherin	Mouse	BD (560062)	1:10
Mouse IgG1 (isotype control) Alexa-488	IgG1	Mouse	BD (557782)	1:13
Mouse IgG2a (isotype control) Alexa-647	IgG2a	Mouse	BD (557715)	1:40
Rabbit IgG1 (isotype control) Alexa-488	IgG1	Rabbit	Cell signaling (#2975S)	1:267

Antibodies for immunolabelling were selected by performing a literature search to find products that had successfully and specifically detected the epitope of interest through immunolabelling (particularly published articles using fluorescent secondary antibodies), or on the recommendation of other researchers. In the event that an appropriate antibody could not be identified using these methods, an antibody was chosen based on manufacturer's datasheets that showed specificity for the protein of interest (usually by Western blot).

2.9 Image capture

For consistency images were taken from the middle third of the small intestine. Brightfield images were obtained using a Nuance camera and software (CRI, Massachussets). Fluorescent images were obtained using an Olympus BX60 fluorescent microscope and Nuance camera and software or Olympus confocal microscope. Nuance, ImageJ (NIH) or Olympus Fluoview software was used for image analysis. Figures were constructed using Photoshop (Abode). Further details of image analysis are given in relevant chapters.

2.10 Quantification of nuclear β-catenin

High power confocal images of immunolabelled intestinal tissue sections were used to quantify nuclear β-catenin expression. Colocalisation of the nuclear marker DAPI and β-catenin was judged for each cell using Olympus Fluoview software by a single assessor (JM) who was blinded to genotype. For each genotype at least 3000 epithelial cells in the area of interest (crypt, villus, or adenoma) were assessed from at least three animals (>1000 cells per animal).

2.11 Statistical analysis

Data was stored in Microsoft Access or Excel databases and analysed using Excel or Graphpad Prism. The specific tests used are documented with results. For Mendelian ratio analysis, the number of progeny or embryos of each genotype obtained was compared with the number expected using the χ^2 test and the level of significance assessed according to the appropriate degrees of freedom. Survival curves were plotted using the Kaplan-Meier method and comparisons between genotypes were made using the log-rank test. Serial weights were compared using an ANOVA with Bonferroni post test for each timepoint. Comparisons between two groups were made using a student's t-test. Comparisons

between more than two groups were made using a one-way ANOVA with Bonferroni post-test. All p values are 2-sided and significance was accepted at <0.05. For bar charts, means are shown and error bars represent the standard error of the mean. Non-significant results have usually not been shown on graphs.

2.12 RNA extraction, reverse transcription and quantitative real-time PCR

2.12.1 RNA extraction

Samples for RNA extraction were either snap frozen or stored in RNAlater at -80°C as documented in Section 2.2.2). Other measures to minimize the effect of RNases at the time of RNA extraction included cleaning equipment and surfaces with RNaseZAP (Sigma-Aldrich), the use of RNase free plasticware and diethylpyrocarbonate (DEPC) treated water.

RNA was extracted from tissue samples using TRI reagent (Sigma-Aldrich) according to the manufacturer's instructions. Tissue samples were defrosted on ice. Each tissue sample was added to 500µl of TRIreagent, homogenized using a 21 gauge needle (Terumo) and 1ml syringe, incubated at room temperature for 5 minutes and then centrifuged at 12,000xg for 10 minutes at 4°C. The supernatant was added to a new tube, mixed with 100µl 1-bromo-3-chloropropane (BCP, Sigma-Aldrich), incubated at room temperature for 15 minutes and centrifuged at 12,000g for 15 minutes at 4°C. The aqueous phase was carefully transferred to a fresh tube, 250µl isopropanol was added, the solution vortexed for 5 seconds, incubated at room temperature for 10 minutes and centrifuged at 12,000xg for 8 minutes at 4-25°C. The supernatant was discarded, 500µl of 75% ethanol (with ddH_2O) was added to the pellet and it was centrifuged at 7,500xg for 5 minutes. The ethanol was removed completely, the pellet briefly air dried and resuspended in 50µl DEPC-treated water. The interphase and organic phase were stored at 4°C in case protein or DNA were required.

2.12.2 DNase inactivation

A DNase inactivation step was carried out to remove any contaminating genomic DNA before RNA was reverse transcribed to cDNA. The TURBO DNA-*free* Kit (Ambion) was used as per manufacturer's instructions: 0.1 volume of 10X TURBO DNase buffer and 1µl of TURBO DNase were added to each RNA sample and mixed gently, the samples were incubated at 37° C for 20-30 minutes, 0.1 volume DNase Inactivation Reagent was added

and mixed well, the sample was incubated for a further 5 minutes at room temperature with occasional mixing, and finally centrifuged at 10,000xg for 1.5 minutes and the RNA transferred to a fresh tube.

2.12.3 RNA quantity and quality assessment

Intestinal samples are particularly susceptible to RNA degradation. At the outset of this work protocols from dissection to reverse transcription were assessed and modified to optimize RNA yield and quality. A Nanodrop 2000 spectrophotometer (Thermo Fisher) was used to quantify extracted RNA. The Nanodrop measures absorbance of a sample at 260 and 280 nm. The concentration of nucleic acid in a sample is calculated according to the Beer-Lambert law that predicts a linear change in absorbance with concentration. 40µg/ml of RNA is known to give an A260 measurement of 1.0. Sample absorbance is adjusted for absorbance of a 'blank' RNase free water sample. RNA purity was assessed by the A260/A280 ratio, with a value of 1.8-2.1 considered suitable for downstream applications.

The Agilent RNA 6000 Nano kit (Agilent Technologies) and a bioanalyzer were used to assess RNA integrity of selected samples, particularly when optimizing the dissection protocol and method of homogenization, working with small tissue samples, obtaining low RNA yields or when the A260/A280 ratio was below 1.8. Figure 9 shows examples of high quality RNA that would be included in analysis and heavily degraded RNA that would be excluded. Unfortunately the software available did not calculate an objective RNA integrity number (RIN).

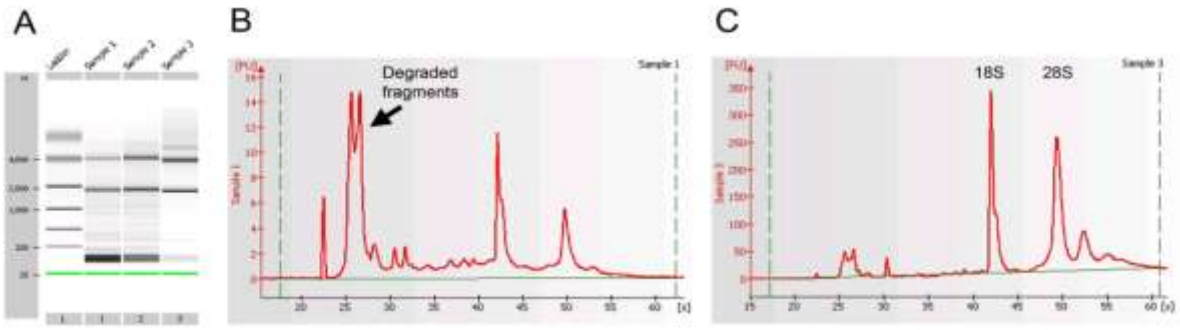

Figure 9. Bioanalyzer example
Highly degraded RNA sample in B and lane 1 of A. Intact, high quality sample with large 18S and 28S ribosomal RNA peaks in C and lane 3 of A.

2.12.4 RNA storage

Extracted RNA was stored at -80°C. Reverse transcription was carried out immediately following extraction when possible, and usually within one month of extraction.

2.12.4 Reverse transcription of RNA

A random priming approach was used to reverse transcribe RNA to cDNA (Feinberg & Vogelstein, 1983). The Applied Biosystems High Capacity cDNA kit with RNase inhibitor was used as per manufacturer's instructions. Reagents and RNA samples were defrosted on ice. For each sample two reactions were performed: one with reverse transcriptase (RT) and a control without reverse transcriptase (noRT). For each reaction 10µl of 0.2µg/µl RNA solution was added to a PCR tube. 10µl of the relevant mastermix (RT or no-RT) as detailed in Table 19 was then added to the RNA and carefully mixed by pipetting. Samples were spun down using a microfuge and then run on a Bio-Rad MyCycler Thermal Cycler, Bio-Rad MJMini Personal Thermal Cycler, or MJ Research Dyad Thermal Cycler using the following conditions: 25°C for 10 minutes; 37°C for 120 minutes; 85°C for 5 minutes. At completion of the reaction 180µl of RNase-free water was added to each sample and mixed carefully. Assuming 100% reverse transcription this gives a final concentration of 10ng/µl cDNA. The cDNA was stored at -20°C.

Table 19. Reverse transcription mastermix

Reagent	Volume per reaction: RT	Volume per reaction: noRT
RNase free water	3.2	4.2
10x RT buffer	2.0	2.0
25x dNTP mix (100mM)	0.8	0.8
10x RT random primers	2.0	2.0
Multiscribe reverse transcriptase	1.0	0
RNase inhibitor	1.0	1.0
Total	10	10

2.12.5 Quantitative real-time PCR

Quantitative real-time PCR (RT-QPCR) was carried out using SensiMix NoRef kit reagents (Bioline), primers and probes designed using the Roche website (except for previously published primers and Sybr green for bacterial rRNA RT-QPCR), and a Rotor Gene Q (Qiagen) machine.

2.12.5.1 RT-QPCR mastermix and sample preparation

The SensiMix NoRef kit reagents were used for mastermix preparation as detailed in Table 20. A Corbett liquid handling robot was used to pipette samples for RT-QPCR, combining 15µl of mastermix and 10µl of cDNA in a 0.2 µl tube.

Table 20. RT-QPCR mastermix

Reagent	Roche primer/probe: volume per reaction (µl)	Sybr green: volume per reaction (µl)	Final concentration
Sensimix QPCR solution	12.5	12.5	
ddH20	0.25		
10mM primer	2	2	800nM
Roche universal probe	0.25	-	100nM
Sybr green mix	-	0.5	
Total volume	15	15	

2.12.5.2 RT-QPCR primers and probes

The Roche Universal Probe Library (UPL) system and ProbeFinder software (found at https://www.roche-applied-science.com/sis/rtpcr/upl/index.jsp) were used to determine optimal RT-QPCR primer and probe combinations. UPL probes are short (8-9 nucleotide) hydrolysis probes with a fluorescein (FAM) label at the 5' end and a dark quencher dye at the 3' end. Locked Nucleic Acids (LNA), DNA nucleotide analogues with increased binding strength compared to standard nucleotides, are incorporated into the UPLs to optimize binding specificity and conserve melting temperature. 165 UPL probes are available, achieving 99% coverage of the mouse transcriptome. For each gene of interest ProbeFinder software was used to design a set of specific primers and identify a suitable UPL. ProbeFinder is based on Primer3 software and uses optimized default settings including a melting temperature of 59-61°C for both primers, a primer length of 18-27 nucleotides, an amplicon length 60-150 base-pairs and intron-spanning assays if possible to minimize the risk of amplification of contaminant genomic DNA. Primer and probe combinations are detailed in Table 21.

Table 21. RT-QPCR primers and probes

Gene	MGI identifier	UPL	Forward (F) primer sequence	F primer position	Reverse (R) primer sequence	R primer position	Amplicon length	Intron spanning?
Axin-2 (*Axin2*)	1270862	51	AGGAACCACTCGGCTGCT	Exon 2	CAGTTTCTTTGGCTCTTTGTGA	Exon 3	90	Yes
β-actin (*Actb*)	87904	56	AAGGCCAACCGTGAAAAGAT	Exon 3	GTGGTACGACCAGAGGCATAC	Exon 4	110	Yes
CD44 (*Cd44*)	88338	49	CTCCTTCTTTATCCGGAGCAC	Exon 5	TGGCTTTTTGAGTGCACAGT	Exon 6	60	Yes
Myc proto-oncogene (*C-Myc*)	97250	77	CCTAGTGCTGCATGAGGAGAC	Exon 2	TCTTCCTCATCTTCTTGCTCTTC	Exon 3	67	Yes
E-cadherin (*Cdh1*)	88354	102	GTTGCAGAAGGCGCTGTT	Exon 5	GTGTTGACGTCATCGTCTGC	Exon 6	74	Yes
Ephrin type-B receptor 2 (*EphB2)*	99611	103	GAGCTGGGCTGGATGGTA	Exon 2	GTTCATGTTCTCGTCGTAGCC	Exon3	69	Yes
Ephrin type-B receptor 3 (*EphB3)*	104770	42	CCCTGGACTCCTTTCTACGG	Exon 11	GCAATGCCTCGTAACATGC	Exon 12	76	Yes
Glyceraldehyde-3-phosphate dehydrogenase (*Gapdh*)	95640	77	CAATGAATACGGCTACAGCAAC	Exon 6	TTACTCCTTGGAGGCCATGT	Exon 6	64	No
Beta glucuronidase (*Gusb*)	95872	42	CCGATTATCCAGAGCGAGTATG	Exon 11	CTCAGCGGTGACTGGTTCG	Exon 12	197	Yes
Hypoxanthine guanine phosphoribosyl transferase (*Hprt*)	96217	95	TCCTCCTCAGACCGCTTTT	Exon 1	CCTGGTTCATCATCGCTAATC	Exon 2	90	Yes
Leucine rich repeat containing G protein coupled receptor 5 (*Lgr5)*	1341817	60	CTTCACTCGGTGCAGTGCT	Exon 5	CAGCCAGCTACCAAATAGGTG	Exon 6	72	Yes
TATA box binding protein (*Tbp*)	101838	107	CAAACCCAGAATTGTTCTCCTT	Exon 7	ATGTGGTCTTCCTGAATCCCT	Exon 8	131	Yes

2.12.5.3 Bacterial 16S rRNA RT-QPCR

Quantification of bacterial 16S rRNA (a component of the 30S small subunit of prokaryotic ribosomes) was performed on reverse transcribed splenic RNA to look for presence of systemic bacteraemia. A stool sample was used as a positive control. Primers used were 5'-AGAGTTTGATCCTGGCTCAG-3' (forward) and 5'-CTGCTGCCTYCCGTA-3' (reverse) (Hill et al, 2010) with Sybr mastermix as per Table 20.

2.12.5.4 QPCR reactions

QPCR reactions were carried out on a Rotor Gene Q (Qiagen) using the following cycling conditions:

Step	Temp (°C)	Time
1	95	15 min
2	60	60 sec
3	95	15 sec
4		Repeat steps 2-3 further 39 cycles

RT reactions were performed in duplicate and a no-RT control reaction was performed for each sample.

2.12.5.5 Reaction efficiency

A standard curve was created for each gene to check reaction efficiency and calculate a Ct threshold. cDNA samples we pooled and 5 serial 5-fold dilutions performed. Rotorgene software was used to calculate the threshold and create a standard curve as per Figure 10.

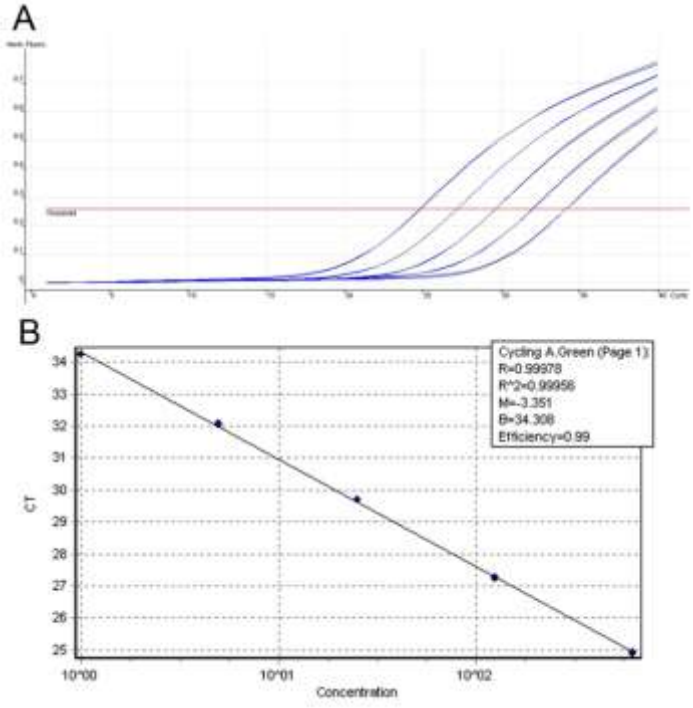

Figure 10. Standard curve example

Example of a standard curve (**B**) for *Hprt* generated using CT values from 5 serial 5-fold dilutions shown in (**A**).

2.12.5.6 Reference gene selection

RT-QPCR analysis relies on normalization to reference genes that are stably expressed in the samples being analysed. Historically a single reference gene has been used however this can produce considerable errors and normalisation to the geometric mean of multiple carefully selected reference genes is now best practice (Vandesompele et al, 2002). Three common reference genes (*Actb*, *Gapdh, Hprt*) and two reference genes that had been reported to be stably expressed in murine intestinal tissue (*Gusb* and *Tbp*) were chosen for evaluation (Wang et al, 2010). Genorm^{PLUS} (Biogazelle) was used to validate the choice of reference genes. It uses the methodology described in the 2002 Vandesompele paper: an internal control gene stability measure (*M*) is calculated that represents the average variation of a particular control gene with all other control genes. Genes with lower *M* values have more stable expression. The optimum number of reference genes for normalization is then calculated by comparing the pairwise variation (V) between two sequential normalization factors.

GeNorm analysis was carried out separately for three groups of tissue:

1. 24 wildtype, *Cdh1$^{fl/fl}$Vil-CreERT2* or *Apc$^{fl/fl}$Cdh1$^{fl/fl}$Vil-CreERT2* small intestinal samples: best reference gene combination *Hprt* and *Actb* as shown in Figure 11.
2. 26 normal intestine or tumour samples from *Apc$^{fl/fl}$Lgr5-CreERT2* or *Apc$^{fl/fl}$Cdh1$^{fl/fl}$Lgr5-CreERT2* animals: best reference gene combination *Hprt* and *Gapdh*.
3. 8 splenic samples from wildtype or *Cdh1$^{fl/fl}$Vil-CreERT2* animals: best reference gene combination *Hprt* and *Actb*.

The geometric mean of the best reference gene combination for the specific type of tissue was used for subsequent analysis.

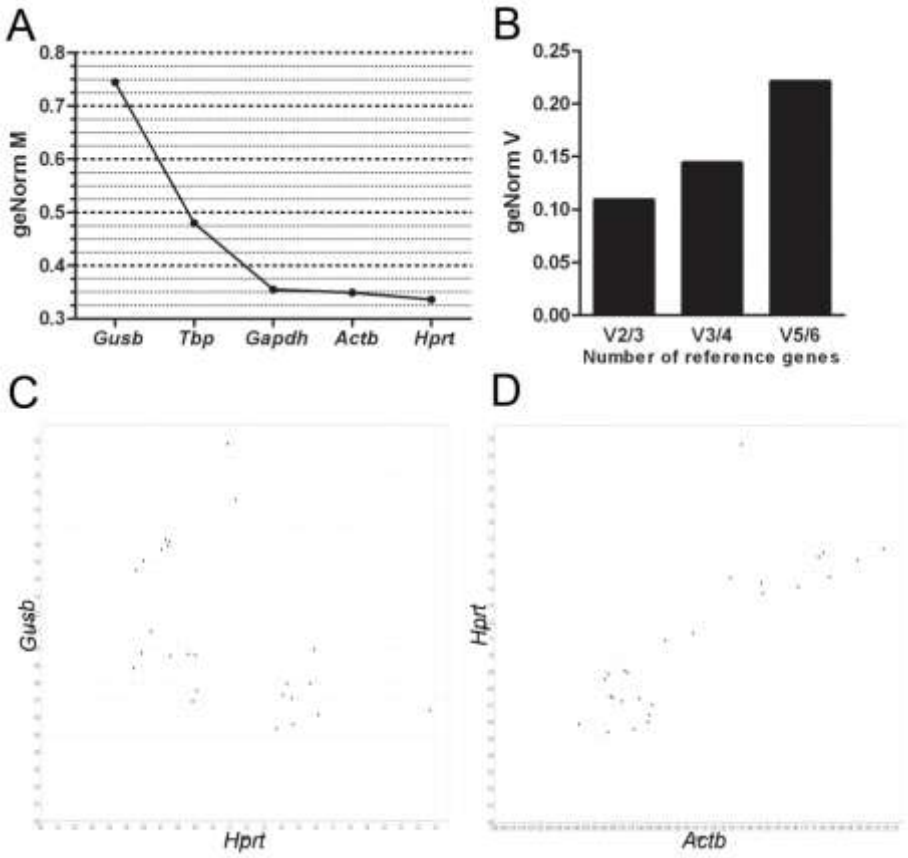

Figure 11. GeNorm analysis to determine best reference gene combination
Small intestinal samples from *wildtype, Cdh1$^{fl/fl}$ Vil-CreER^{T2} and Apc$^{fl/fl}$ Cdh1$^{fl/fl}$ Vil-CreER^{T2}* animals. (**A**) GeNorm *M* calculated for each candidate reference gene. (**B**) Optimum number of reference genes determined to be 2. (**C**) Poor correlation between *Gusb* and *Hprt* expression. (**D**) Good correlation between *Hprt* and *Actb* expression.

2.12.5.7 RT-QPCR analysis

The average of the two Ct values for duplicates of each sample for each gene was taken. The average Ct for the gene of interest (GOI) was normalized to the geometric mean of two reference genes (GMRG) as identified in section 2.11.6.6 and then samples were normalized to wildtype results using the ΔΔCt method as per this equation:

$$\Delta\Delta Ct = [(Ct_{Sample.GOI} - Ct_{Sample.GMRG})] - [(Ct_{Wildtype.GOI} - Ct_{Wildtype.GMRG})]$$

Results were calculated using Microsoft Excel, then graphed and analysed using Graphpad Prism.

3 The effect of *Cdh1* homozygosity

3.1 Introduction

At the time this study was initiated, it was known that germline E-cadherin homozygosity was embryonic lethal due to failure to form a trophectoderm (Larue et al, 1994) and that germline E-cadherin heterozygosity alone had no detectable phenotype, either in the developing embryo or the adult intestine (Smits et al, 2000b).

Hermiston and Gordon produced indirect evidence of E-cadherin having an important role in intestinal function. Using mouse intestinal models they disrupted E-cadherin using a dominant negative form of N-cadherin (Hermiston & Gordon, 1995a). In this model 129/Sv embryonic stem cells transfected with a dominant negative N-cadherin mutant (NCADΔ, lacking an extracellular domain) under a specific intestinal promoter (fatty acid binding protein, *Fabp*) were introduced into C57BL/6 mouse blastocysts to create chimeras. Only 129/Sv derived cells bind *Ulex europeaus* agglutinin type 1, facilitating identification of ribbons of crypt-villus units with expression of the mutant gene and C57BL/6 ribbons as internal controls within the same microenvironment.

NCADΔ expression resulted in disrupted cellular adhesion, increased migration of cells up the crypt-villus axis, loss of polarity and increased cell death (Hermiston & Gordon, 1995a). NCADΔ was expressed in both crypt progenitor cells and differentiated cells of all four lineages and resulted in a phenotype resembling inflammatory bowel disease (Hermiston & Gordon, 1995b). Early disruption of the epithelial barrier, large lymphoid aggregates, increased proliferation and apoptosis progressed to histopathological features of Crohn's disease by three months of age and the mice developed intestinal adenomas by six months of age. The same promoter was used to increase expression of E-cadherin, and this resulted in decreased migration of cells up the crypt-villus axis and increased apoptosis in the crypt, but no changes in cellular differentiation (Hermiston et al, 1996).

Given the evidence from the dominant negative and overexpression models, it was highly likely E-cadherin had a vital role in the intestine. As germline loss of function models could not assess the effect of E-cadherin on the intestine due to embryonic lethality, a conditional genetic approach was necessary. Conditional mouse models facilitate functional assessment of embryonic lethal genes in the adult mouse. In addition to bypassing embryonic lethality,

major advantages of the conditional system are the ability to control for time of recombination and tissue specificity. Promoter choice determines tissue specificity and temporal control. However additional temporal control can be achieved, for example if the Cre construct is fused to a mutant ligand-binding domain of the oestrogen receptor (ER^T) the Cre recombinase will only be able to enter the nucleus and activate recombination upon the administration of exogenous tamoxifen.

One of the earliest genes studied in the mouse intestine using a conditional genetic approach was the tumour suppressor *Apc*. The effect of acute homozygous conditional loss of *Apc* on the adult mouse intestinal epithelium was established using loxP flanked *Apc* alleles and *AhCreER^T*, where Cre expression is controlled by a cytochrome P450 promoter that can be upregulated by lipophilic xenobiotics including β-napthoflavone (Ireland et al, 2004; Sansom et al, 2004). *Apc* homozygosity resulted in acute activation of Wnt signaling, and marked changes in cellular differentiation, migration, proliferation and apoptosis with cells adopting a ''crypt progenitor-like'' phenotype (Sansom et al, 2004). An almost identical phenotype was seen with *Apc* homozygosity achieved using *Villin-CreER^{T2}* (Andreu et al, 2005). Sansom and colleagues found that Wnt activation was marked by nuclear translocation of β-catenin and microarray data confirmed upregulation of multiple Wnt regulated genes previously identified *in vitro* including *C-Myc*, *CD44, Axin2, EphB2* and *EphB3*. This *Apc* homozygous phenotype was completely dependent on *C-Myc*, with homozygous deletion of both *Apc* and *C-Myc* rescuing the phenotype, even in the presence of nuclear β-catenin. *C-Myc* was also required to mediate activation of most of the Wnt target genes identified (Sansom et al, 2007).

The aim of the work presented in this chapter was to elucidate the effect of conditional E-cadherin loss of function on the adult intestine, and further, to examine the effect in combination with acute homozygous *Apc* loss. Given the potential interaction between *Cdh1* and *Apc* through the Wnt effector β-catenin discussed in the main introduction, of particular interest was the effect of E-cadherin loss on Wnt signalling in both settings.

3.2 Methods

General methods are described in Chapter 2. Methods specific to this chapter are described below.

3.2.1 Breeding

Initially these experiments were to be conducted using *AhCreER^{T}*. As will be discussed further in Chapter 4, experimental planning included having all animals on a C57BL/6J background to guard against the effect of strain-dependent modifiers. Pilot experiments using *AhCreER^{T}* however showed unreliable recombination rates and discussion with other groups using the construct revealed that silencing of the transgene could be a problem with increased generations of breeding. The decision was made to switch to a *Villin-Cre* (*Vil-Cre*) and *Villin-CreER^{T2}* (*Vil-CreER^{T2}*) strategy. *Vil-CreER^{T2}* animals were obtained from Professor Elizabeth Robertson (University of Oxford) and were on a B6D2 (C57BL6 x DBA/2) background. Whilst it would have been preferable to have the animals on a C57BL/6J background, the backcrossing required was not feasible within the timeline for these experiments.

The breeding for the crosses described in this chapter is explained in Figures 12-15. The figures outline the optimal breeding strategies. Genotyping PCR was unable to differentiate between heterozygotes and homozygotes for *Vil-Cre*, *Villin-CreERT^{T2}* or *LacZ*. The figures reflect the often unknown expected proportion of animals that would be Cre or *LacZ* negative. Controls included animals that were wildtype for *Cdh1* but positive for *Vil-CreER^{T2}*. However the nature of the *Apc Cdh1 YFP Villin-CreER^{T2}* cross meant a breeding strategy including littermate controls that were wildtype for *Apc* and *Cdh1* but *Vil-CreER^{T2}* positive was not feasible. In this instance animals negative for *Villin-CreER^{T2}* were used as controls.

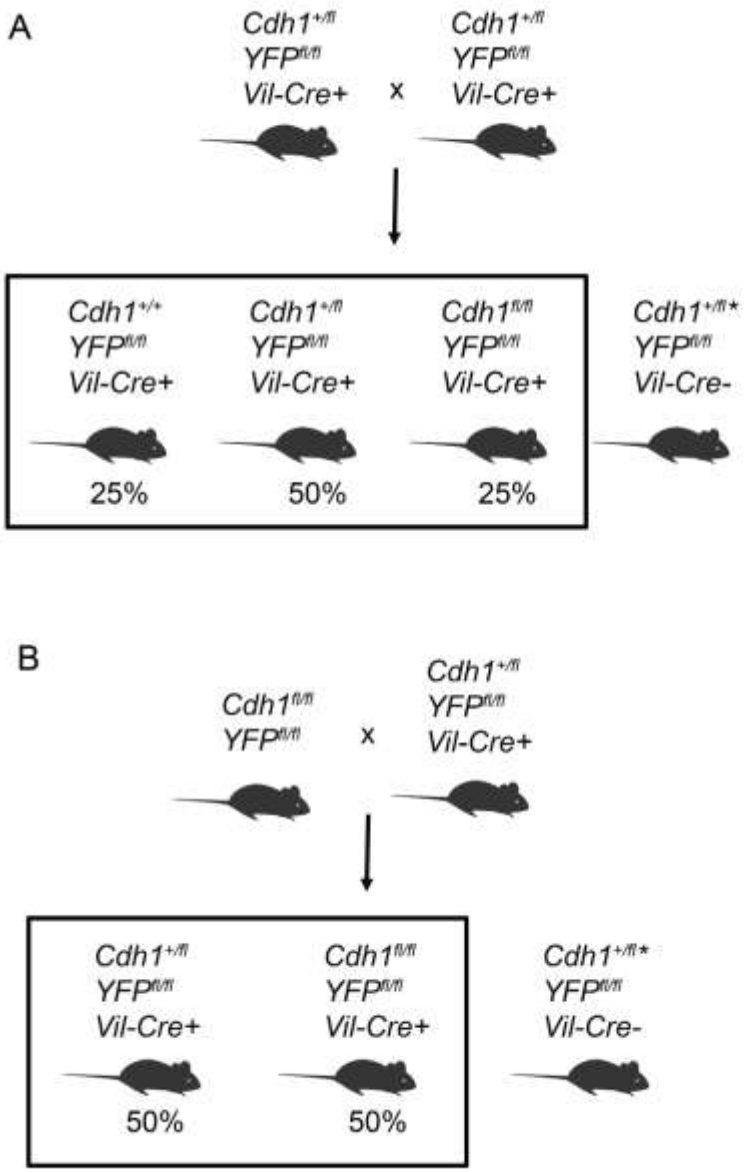

Figure 12. *Cdh1 Vil-Cre* breeding
Cdh1$^{fl/fl}$ *Vil-Cre+* embryos were generated using one of two breeding strategies. The breeding depicted in (**A**) was preferred and generated *Cdh1* wildtype, heterozygote and homozygote embryos. The strategy in (**B**) was also used to generate more *Cdh1*$^{fl/fl}$ animals. Numbers below mice represent the expected Mendelian ratio of that genotype. * following *Cdh1* in *Vil-Cre-* animals indicates that only heterozygous animals have been depicted in the diagram but *Cdh1* wildtype and homozygote animals that were *Vil-Cre* negative were also generated. Boxes outline experimental animals. The proportion of *Vil-Cre+* animals could not be predicted as the genotyping PCR does not differentiate between heterozygosity and homozygosity.

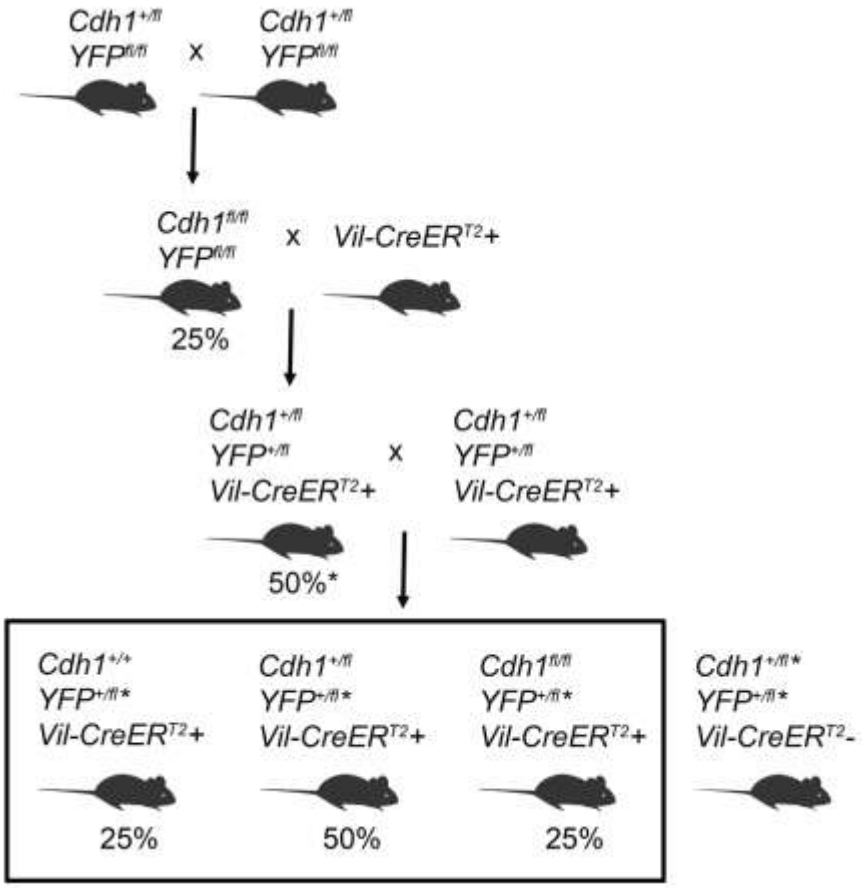

Figure 13. *Cdh1 RosaYFP Vil-CreER^{T2}* breeding
Numbers below mice represent the expected Mendelian ratio of that genotype. *following a number signifies this number depends on the parent's *Vil-CreER^{T2}* status (heterozygous or homozygous) which could not be differentiated by genotyping PCR. *following a genotype (*Cdh1* in *Vil-CreER^{T2}*- animals, or *YFP*) indicates that for simplicity only the most common heterozygous genotype has been represented in the figure, however wildtype or homozygous alleles were also generated. The box outlines experimental animals.

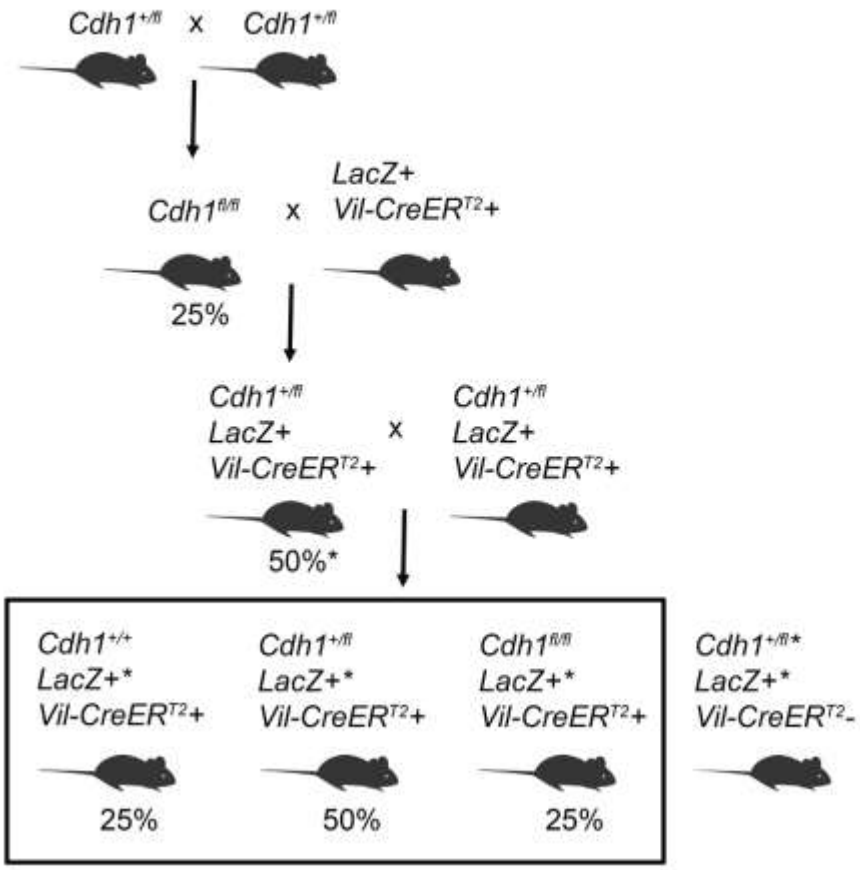

Figure 14.*Cdh1 LacZ Vil-CreER^{T2}* **breeding**
Numbers below mice represent the expected Mendelian ratio of that genotype. *following a number signifies this number depends on the parent's *Vil-CreER^{T2}* status (heterozygous or homozygous) which could not be differentiated by genotyping PCR. *following a genotype (*Cdh1* in *Vil-CreER^{T2}*- animals, or *LacZ*) indicates that for simplicity only the most common heterozygous genotype has been represented in the figure, however wildtype or homozygous alleles were also generated. The box outlines experimental animals.

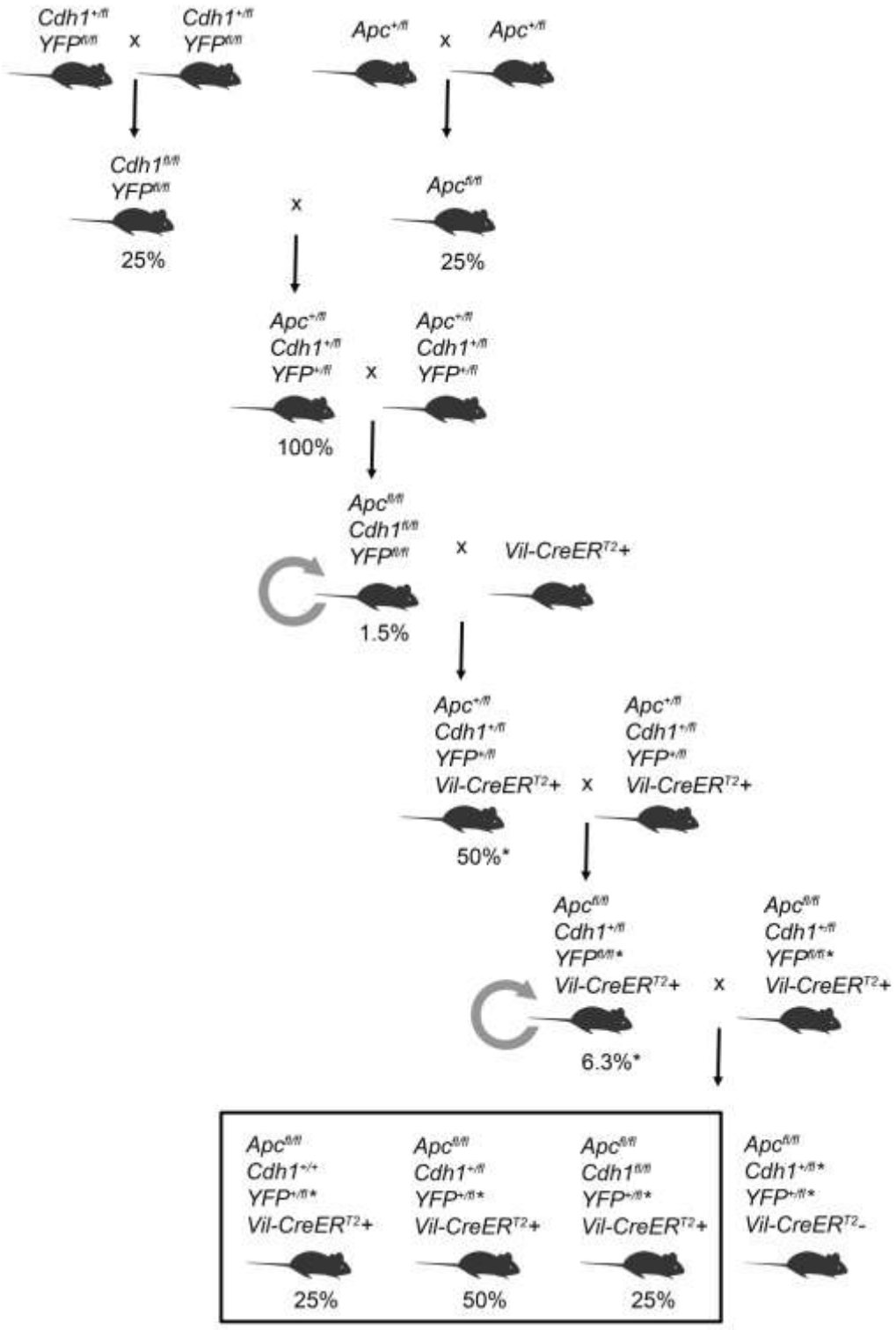

Figure 15. *Apc Cdh1 Rosa-YFP Vil-CreER^{T2}* breeding
Numbers below mice represent the expected Mendelian ratio of that genotype. *following a number signifies this number depends on the parent's *Vil-CreER^{T2}* status (heterozygous or homozygous) which could not be differentiated by genotyping PCR. *following a genotype (*Cdh1* in *Vil-CreER^{T2}* animals, or *YFP*) indicates that for simplicity only the most common heterozygous genotype has been represented in the figure, however wildtype or homozygous alleles were also generated. The box outlines experimental animals, however *Vil-CreER^{T2}* negative animals were also used as controls. The circular arrows represent steps at which an intercross was undertaken to generate more animals of the required genotype.

3.2.2 BrdU labelling

Experiments to assess proliferation were conducted using the synthetic thymidine analogue 5-bromo-2'deoxyuridine (BrdU). BrdU is incorporated into newly synthesized DNA of replicating cells during the S phase of the cell cycle. Animals received a single IP injection of 100mg/kg BrdU (Roche) either 2 hours or 24 hours before they were expected to become unwell. At least 2 animals of each genotype were included for each timepoint.

Intestinal samples were collected and processed routinely however the immunolabelling protocol was adjusted to incorporate a step to denature the DNA so that the BrdU-labelled DNA was accessible to the antibody. The Roche BrdU labelling and detection kit was used with a modified version of the immunolabelling protocol described in Chapter 2, section 2.8. After the permeabilisation and blocking step slides were incubated with anti-BrdU working solution overnight at 4°C in a humidified chamber. The next day the slides were washed three times in TBS before incubation with anti-mouse-Ig-fluorescein (Roche, dilution 1:10) for 2 hours at 37°C in a humidified chamber.

For BrdU analysis, the cumulative frequency of BrdU positive nuclei counted from the crypt base to the villus tip was recorded. For each genotype at each timepoint at least 40 crypt-villus units were assessed from at least 2 animals.

3.2.3 Image analysis for markers of differentiation and apoptosis

Immunolabelling to detect lysozyme identified Paneth cells. The position of Paneth cells for different genotypes was ascertained. This analysis included at least 3 animals of each genotype and for each animal lysozyme positive cells were assayed from at least 20 crypt-villus units. The distance from the crypt base to a given cell was measured in µm using ImageJ software, the results were plotted in GraphPad Prism and genotypes compared using the student's t-test.

Immunolabelling for mucin 2 and chromogranin identified goblet cells and enteroendocrine cells respectively. Cleaved caspase 3 (CC3) Immunolabelling identified apoptotic cells. For each marker, positive stained cells per crypt-villus unit were counted to generate an average number of positive cells per crypt-villus unit per animal. Analysis included at least 3 animals of each genotype and at least 20 crypt-villus were assessed per animal. Results were plotted using Graphpad Prism and genotypes compared using student's t-test.

3.3 Results

3.3.1 Cdh1 *homozygosity with* Vil-Cre *is embryonic lethal*

Vil-Cre is expressed from embryonic day (E) 9 in the visceral endoderm of the yolk sac and by E12.5 in the developing intestinal epithelium (el Marjou et al, 2004). Assessment of genotypes from breeding of *Cdh1*$^{+/fl}$ *Vil-Cre+* x *Cdh1*$^{+/fl}$ *Vil-Cre+,* or *Cdh1*$^{fl/fl}$ *Vil-Cre+* x *Cdh1*$^{+/fl}$ *Vil-Cre+* animals showed a highly significant deviation from the expected Mendelian ratios at birth (P0, Table 22). Embryonic dissections showed expected ratios and normal morphology of embryos at E10.5. At E11.5-E12.5 an increased number of embryonic resorptions were observed (Figure 16). *Cdh1*$^{fl/fl}$ *Vil-Cre* embryos were often smaller than their *Cdh1*$^{+/fl}$ or *Cdh1*$^{+/+}$ littermates (Figure 17A), did not have a yolk sac at dissection, or were both small and lacking a yolk sac (Figure 17B). Immunolabelling of visceral endoderm from a small embryo with an intact yolk sac at E12.5 showed decreased Cdh1 expression (Figure 17C). As the embryonic gut is in its very early stages of development at this timepoint and the embryo does not yet rely on a functioning intestine for nutritional support, it is likely the loss of *Cdh1* in the embryonic membranes was responsible for the demise of *Cdh1*$^{fl/fl}$ embryos. As intestinal-related lethality was unlikely, this approach using *Vil-Cre* was not pursued. Instead an approach using *Vil-CreER*^{T2}, that can be activated by administration of exogenous tamoxifen was used.

Table 22. Mendelian segregation of *Cdh1 Vil-Cre* embryos and neonates

Timepoint		**Genotype** *Cdh1*$^{+/+}$ *Vil-Cre*	*Cdh1*$^{+/fl}$ *Vil-Cre*	*Cdh1*$^{fl/fl}$ *Vil-Cre*	Total
E10.5	Observed	4	6	8	18
	Expected	*4.5*	*9*	*4.5*	
E11.5	Observed	2	13	5	20
	Expected	*3.5*	*10*	*6.5*	
E12.5	Observed	4	12	1	17
	Expected	*4.25*	*8.5*	*4.25*	
E15.5+	Observed	8	13	0*	21
	Expected	*5.25*	*10.5*	*6.25*	
P0	Observed	8	39	0***	47
	Expected	*8.5*	*23.5*	*15*	

*=p<0.05, **=p<0.001, Chi-square test

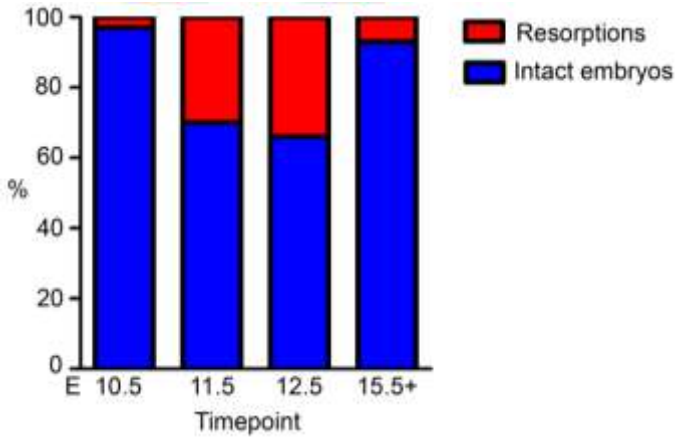

Figure 16. Embryonic resorptions at different timepoints
Embryonic resorptions found at dissection at the specified timepoint as a percentage of the total number of intact embryos and resorptions. p=0.011, one-way ANOVA, Bonferroni post-test not significant for individual comparisons.

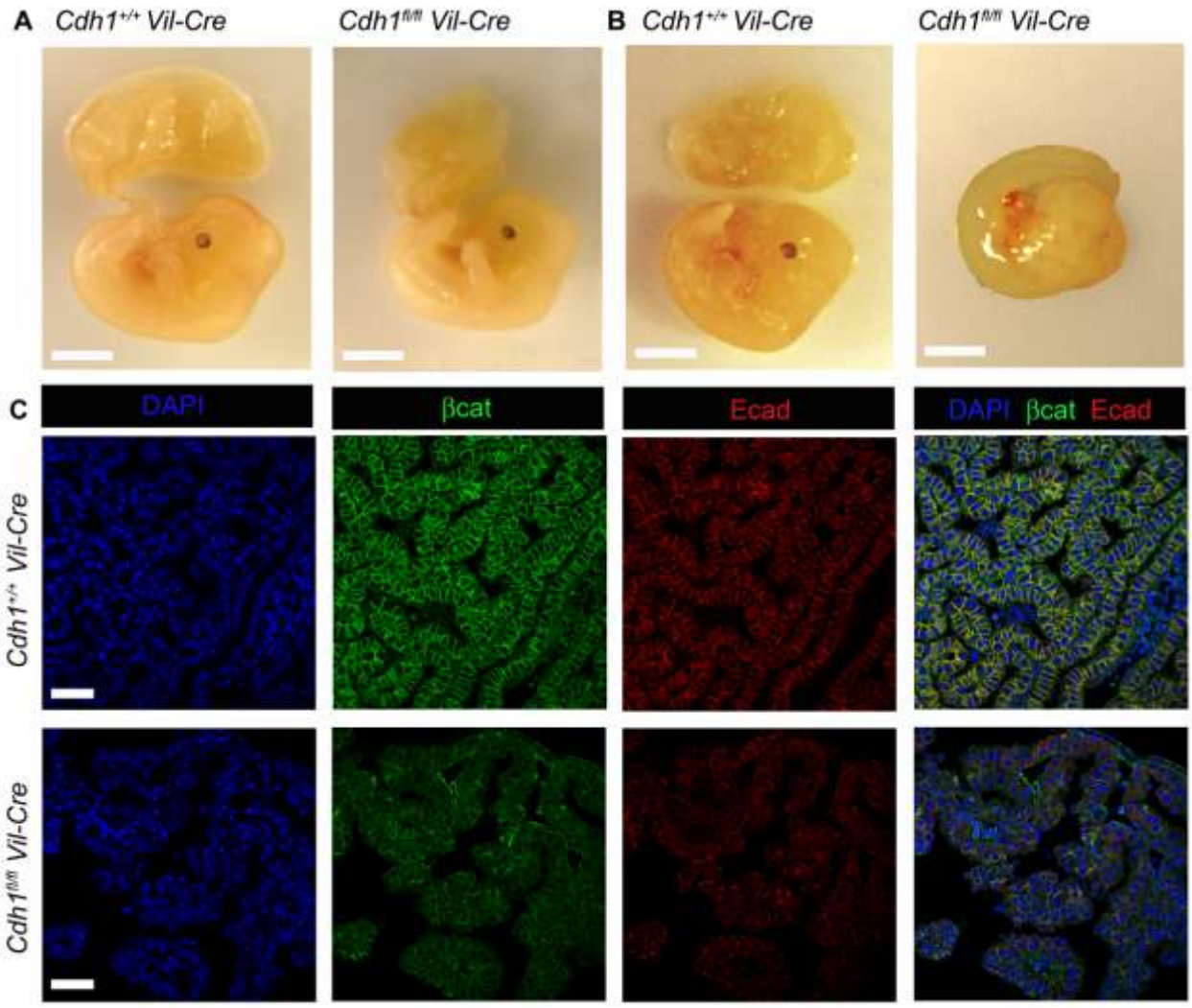

Figure 17. Embryo morphology and immunolabelling of visceral endoderm at E11.5-12.5
(**A**) An example of the appearance of embryos at E12.5 showing a *Cdh1*$^{fl/fl}$ *Vil-Cre* embryo that is smaller but has extraembryonic membranes which appear intact. (**B**) An example of the appearance of embryos at E11.5 showing a *Cdh1*$^{fl/fl}$ *Vil-Cre* embryo that is smaller, deformed and has absent extraembryonic membranes. Scale bars in (**A**) and (**B**) 2mm. (**C**) Immunolabelling of extraembryonic membranes from the embryos pictured in (**A**) showing loss of membrane bound E-cadherin (red) and β-catenin (green) with *Cdh1* homozygosity. Scale bars 50μm.

3.3.2 Cdh1 homozygosity using Vil-CreER^{T2}

Cdh1$^{fl/fl}$, *Cdh1$^{+/fl}$* and *Cdh1$^{+/+}$ Vil-CreER^{T2}+* animals were treated with a total dose of 200mg/kg tamoxifen IP (40mg/kg each day for 5 days, 5mg total for a 25g mouse). Wildtype and heterozygote animals remained well with no significant weight loss. Homozygous animals either remained well ('not sick') or became sick ('sick') with weight loss, dehydration and diarrhoea 4-5 days following injection (Figure 18). *Cdh1$^{+/+}$*, *Cdh1$^{fl/fl}$* 'not sick' and *Cdh1$^{fl/fl}$* 'sick' animals were censored when the *Cdh1$^{fl/fl}$* 'sick' animals reached the defined humane endpoint as detailed in Table 10 (Chapter 2, Materials and Methods). Genotyping of intestinal samples for the recombined *Cdh1* allele, immunolabelling for *RosaYFP* and E-cadherin, and RT-QPCR confirmed efficient recombination in *Cdh1$^{fl/fl}$* 'sick' animals with less than 50% *Cdh1* mRNA expression and patchy protein loss, but incomplete recombination and/or recovery from *Cdh1* loss in 'not sick' animals. When treated with a total dose of 400mg/kg tamoxifen IP (200mg/kg for 2 days, 10mg total for a 25g mouse), wildtype and heterozygote animals had no significant weight loss, however all homozygote animals developed the 'sick' phenotype by day 4 following injection as defined by the humane endpoint score sheet (Figure 18). This injection regime was used for subsequent experiments and analysis.

At dissection 'sick' *Cdh1$^{fl/fl}$ Vil-CreER^{T2}* animals had grossly dilated small intestines and colons that were significantly shortened and hyperaemic with prominent vasculature (Figure 18). Intestinal contents consisted of loose yellow stool with occasional blood. There was no gross evidence of intestinal perforation. 'Not sick' *Cdh1$^{fl/fl}$ Vil-CreER^{T2}*, *Cdh1$^{+/fl}$ Vil-CreER^{T2}* and *Cdh1$^{+/+}$ Vil-CreER^{T2}* animals had no obvious abnormal findings at dissection.

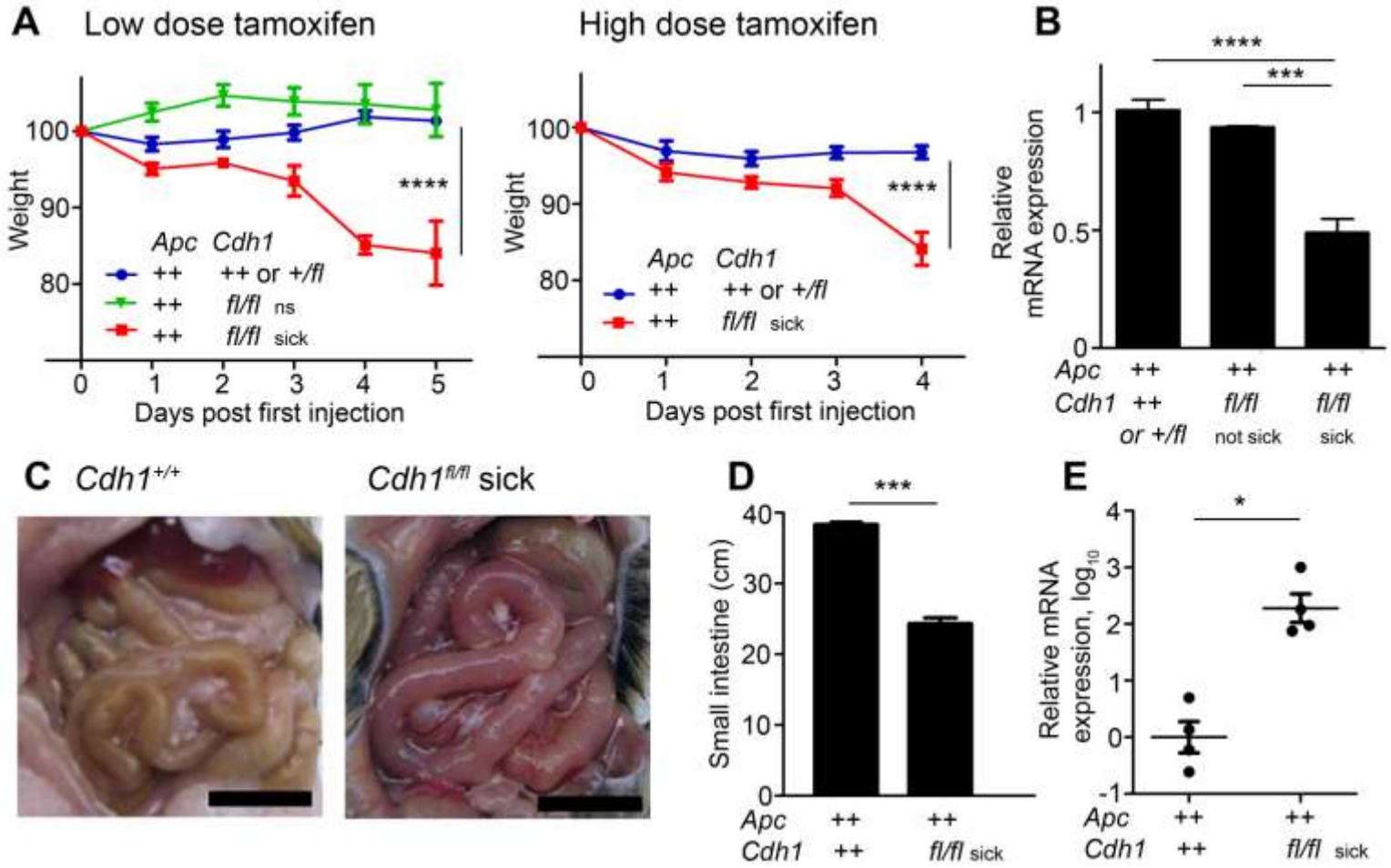

Figure 18. ***Cdh1*** **homozygous phenotype with** ***Vil-CreER^{T2}***

(**A**) Whole animal weights (represented as % of pre-injection weight) following intra-peritoneal injection with low or high dose tamoxifen. For low dose tamoxifen *Apc*$^{+/+}$*Cdh1*$^{+/+ \text{ or } +/fl}$ n=12, *Apc*$^{+/+}$*Cdh1*$^{fl/fl}$ not sick n=4, *Apc*$^{+/+}$*Cdh1*$^{fl/fl}$ sick n=2. For high dose tamoxifen *Apc*$^{+/+}$*Cdh1*$^{+/+ \text{ or } +/fl}$ n=10, *Apc*$^{+/+}$*Cdh1*$^{fl/fl}$ sick n=8. ANOVA with Bonferroni post test for each time point. (**B**) *Cdh1* mRNA expression. *Apc*$^{+/+}$*Cdh1*$^{+/+ \text{ or } +/fl}$ n=6, *Apc*$^{+/+}$*Cdh1*$^{fl/fl}$ not sick n=4, *Apc*$^{+/+}$*Cdh1*$^{fl/fl}$ sick n=4. One way ANOVA with Bonferroni post test. (**C**) Intestinal appearance at dissection. Scale bar 1 cm. (**D**) Small intestinal length. Student's t- test. (**E**) Splenic S16 mRNA expression, $\log_{10}$ scale, showing systemic bacteraemia with *Cdh1* homozygosity. Student's t-test. For bar charts the mean is shown and whiskers represent standard error of the mean. * p<0.05. *** p<0.001. **** p<0.0001.

3.3.3 Cdh1 *homozygosity leads to an inflammatory intestinal phenotype*

'Sick' E-cadherin homozygotes had severe changes in small intestinal histology with distorted crypt-villus architecture, loss of the normally well-defined crypt-villus boundary, changes in cell polarity with loss of uniform cell stacking up the crypt-villus axis, mucous pooling, villus tufting, epithelial cell shedding and inflammatory infiltrates (Figure 19). 'Not sick' E-cadherin homozygotes had no obvious histological changes. RT-QPCR for bacterial ribosomal S16 RNA (a component of the 30S small subunit of prokaryotic ribosomes) indicated 'sick' homozygotes had systemic bacteraemia, suggesting associated breakdown of the intestinal barrier and permeability to bacteria (Figure 18F). Disruption of the crypt-villus boundary was demonstrated by immunolabelling for villin. Villin is normally expressed by mature enterocytes throughout the length of the villus, however in $Cdh1^{fl/fl}$ 'sick' animals villin labelling was more prominent in the upper villi and there was patchy loss of the protein as for E-cadherin (Figure 23).

3.3.4 E-cadherin loss does not alter localization of β-catenin

To assay for Wnt pathway activation intestinal sections were immunolabelled to assess for increased cytoplasmic β-catenin expression and in particular nuclear translocation of β-catenin. RT-QPCR of small intestinal samples was also undertaken to assess expression of mRNA of Wnt target genes. E-cadherin loss resulted in areas of colocalised loss of membrane-bound β-catenin and E-cadherin in both the crypt and the villus but no convincing increase in cytoplasmic β-catenin and no nuclear β-catenin consistent with no Wnt pathway activation (Figure 20). RT-QPCR for Wnt target gene expression gave inconsistent results showing significant downregulation of *Axin2*, but significant upregulation of the Wnt target genes *C-Myc*, *CD44* and *EphB3* (Figure 20). *Axin2* is considered to be a reliable Wnt reporter (http://www.stanford.edu/group/nusselab/cgi-bin/wnt/main). Immunolabelling confirmed normal cytoplasmic Axin2 expression in the crypts of wildtype animals but decreased expression with E-cadherin loss (Figure 21). Immunolabelling did not show upregulation of C-Myc or EphB2 with *Cdh1* loss (Figure 34).

$Cdh1^{fl/fl}$ animals that did not become sick had β-catenin and Axin2 immunolabelling and RT-QPCR results for Wnt target genes that were indistinguishable from wildtype animals.

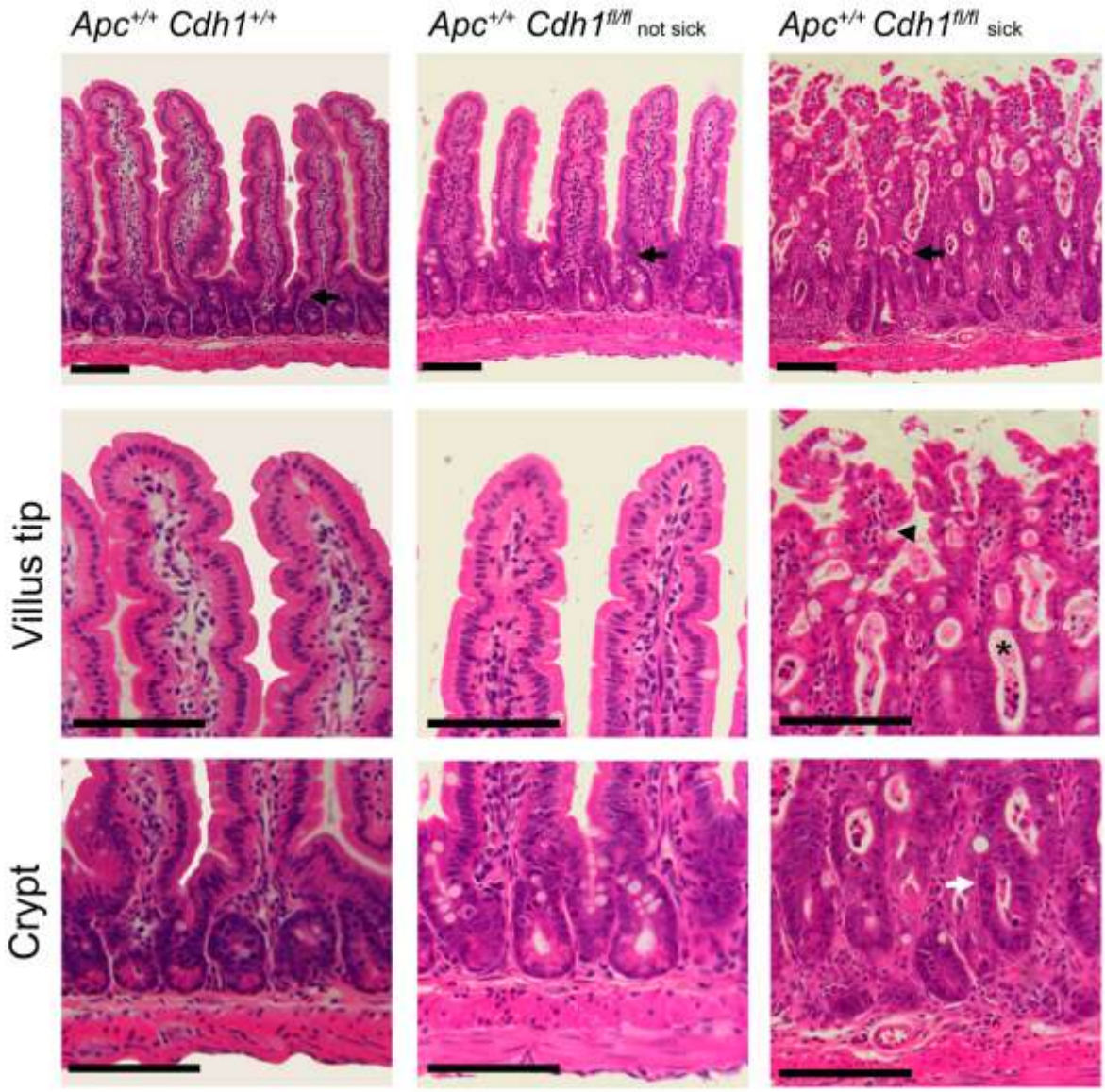

Figure 19. The effect of *Cdh1* homozygosity on intestinal architecture
H&E staining of small intestine, with high power views of crypt and villus, from animals culled 4-5 days following tamoxifen injection (when the *Cdh1*$^{fl/fl}$ 'sick' animals reached the defined humane endpoint). Black arrows show crypt-villus boundary (disrupted in *Cdh1*$^{fl/fl}$). Black arrowhead shows villus tufting. Black * shows mucus pooling. White arrow shows loss of uniform cell stacking and cell polarity. Scale bars 50µm.

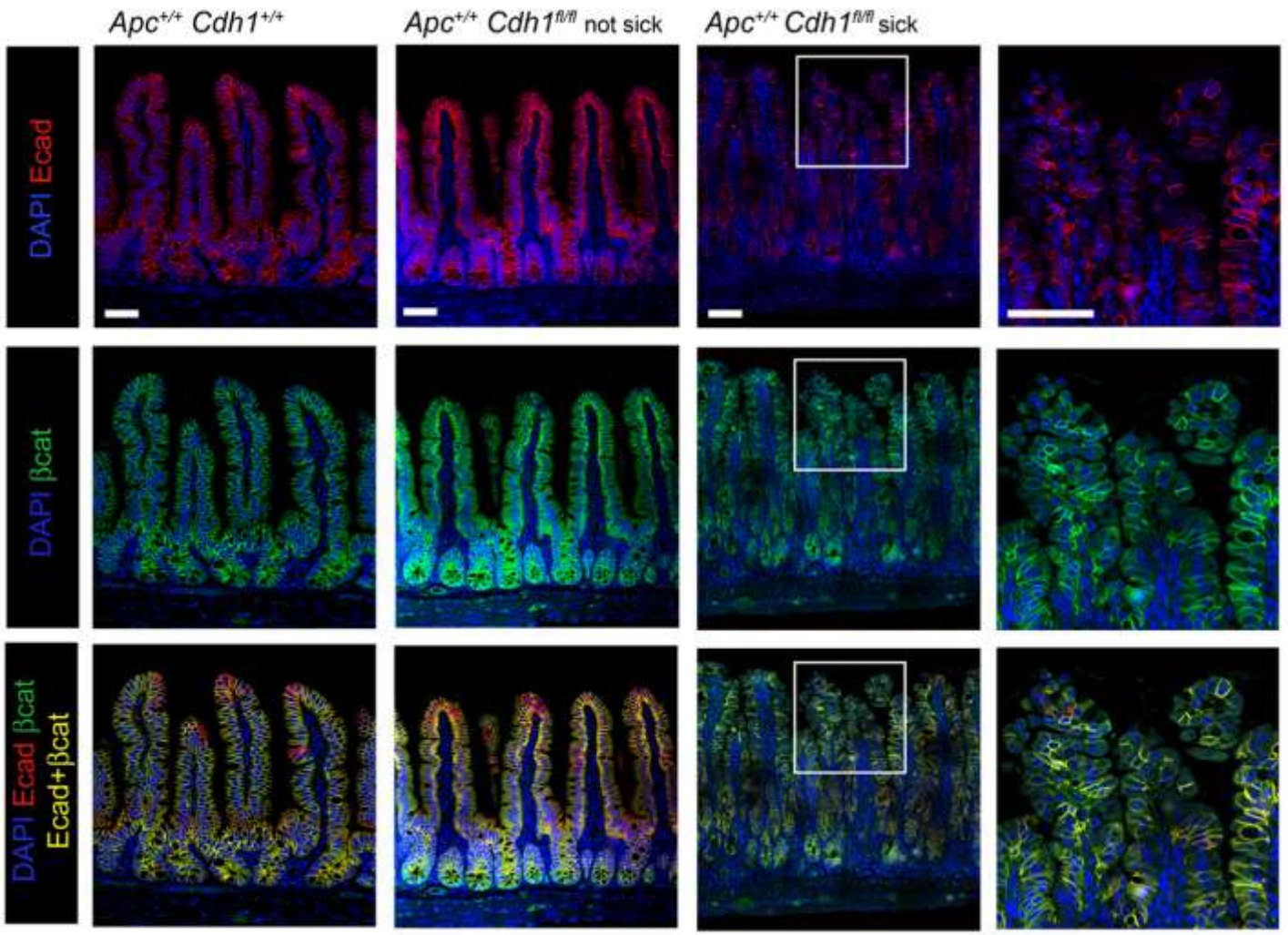

Figure 20. The effect of *Cdh1* homozygosity on E-cadherin and β-catenin expression

Immunolabelling for DAPI, E-cadherin and β-catenin in small intestine from *Cdh1*$^{+/+}$ *Vil-CreER*^{T2}, *Cdh1*$^{fl/fl}$ *Vil-CreER*^{T2} not sick and *Cdh1*$^{fl/fl}$ *Vil-CreER*^{T2} sick animals. The far right panels show high power views of the crypt-villus transition zone of *Cdh1*$^{fl/fl}$ *Vil-CreER*^{T2} animals marked with white boxes. Patchy colocalised loss of membrane-bound E-cadherin and β-catenin can be seen in *Cdh1*$^{fl/fl}$ *Vil-CreER*^{T2} sick animals but there is no apparent increase in cytoplasmic or nuclear β-catenin. Scale bars 50μm.

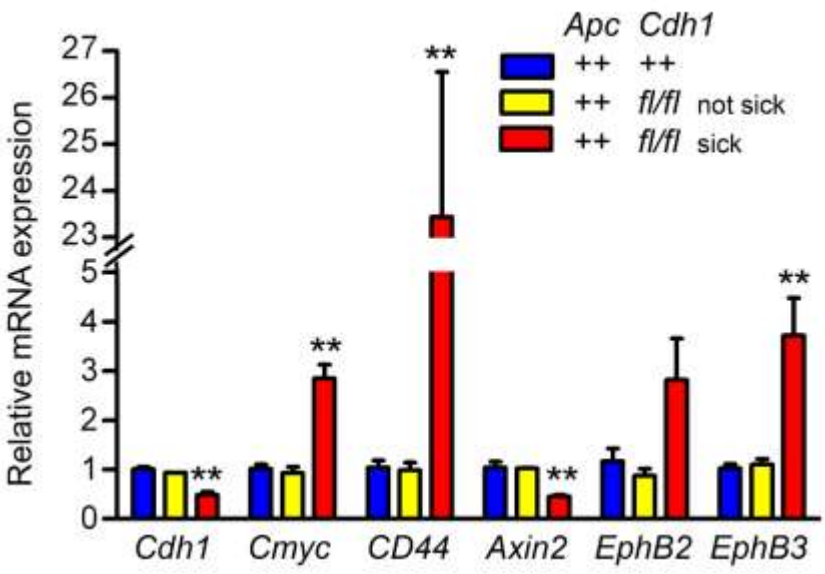

Figure 21. Effect of *Cdh1* homozygosity on *Cdh1* and Wnt target gene expression: RT-QPCR
RT-QPCR of *Cdh1* and Wnt target genes. n≥3 mice for each genotype. Reference genes *Actb* and *Hprt*. Expression relative to wildtype small intestine. Student's t-test for comparison with wildtype samples. Bars represent means and whiskers show standard error of the mean. ** p<0.01.

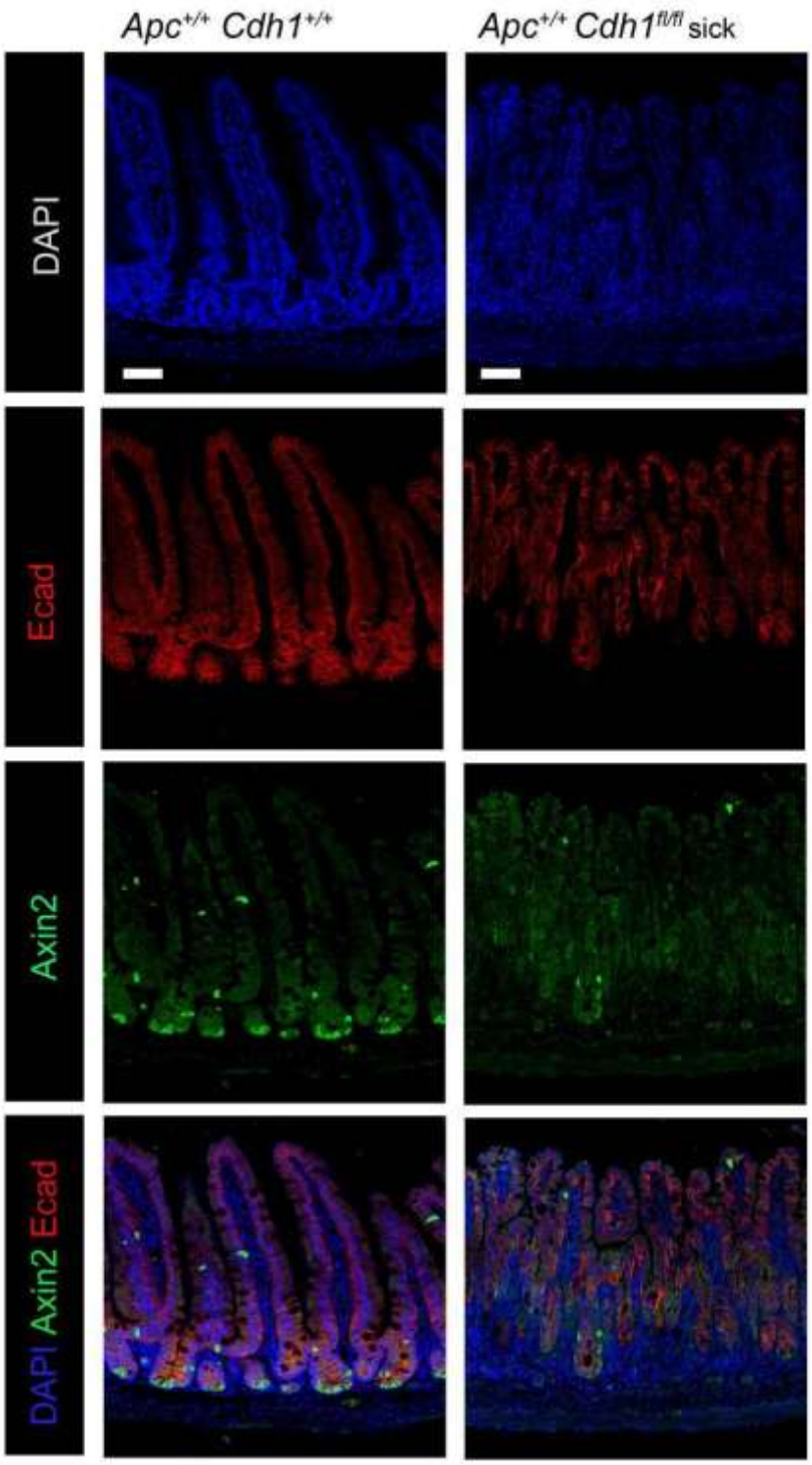

Figure 22. The effect of *Cdh1* homozygosity on Axin2 expression: immunolabelling
Immunolabelling for DAPI, E-cadherin and Axin2 in small intestine from *Cdh1*$^{+/+}$ *Vil-CreER*^{T2} and *Cdh1*$^{fl/fl}$ *Vil-CreER*^{T2} animals. Axin2 labelling is decreased with *Cdh1* loss. Scale bars 50µm.

3.3.5 E-cadherin loss has a dramatic effect on secretory cell lineages

'Sick' *Cdh1*$^{fl/fl}$ animals had dramatic alterations in features of secretory cell lineages, particularly Paneth cell positioning. Paneth cells, usually localized to the crypt base where they have a role in maintaining the stem cell niche, were scattered along the crypt-villus gradient (labelled green using anti-lysozyme antibody in Figure 24). Mature Paneth cells are usually Wnt activated however there was no evidence of cytoplasmic or nuclear β-catenin in the mispositioned cells suggesting that they were not completely differentiated (Figure 25). Unfortunately the lack of an effective antibody against *Lgr5* meant we were unable to assess if progenitor cells were also mispositioned with Paneth cells. Goblet cells and enteroendocrine cells were significantly reduced in number and predominant in the upper villus compared with wildtype animals (labelled with yellow for Muc2 and grey for Chromogranin A respectively, Figure 24).

3.3.6 E-cadherin loss results in increased proliferation and apoptosis

BrdU labelling showed dramatic changes in the position of proliferating cells in animals with homozygous *Cdh1* loss (Figure 26). Within 2 hours of labelling, BrdU labelled cells were present half way up the villus and at 24 hours they were also seen at the villus tip. This was confirmed by Ki-67 immunolabelling that showed proliferating cells confined to the crypt in wildtype animals but in the villus in *Cdh1*$^{fl/fl}$ animals (Figure 27). With *Cdh1* loss cells were less densely packed (Figure 26, grey bars depicting the distance for 10 cells). Apoptosis, assessed by cleaved caspase-3 immunolabelling, was also significantly increased in animals with homozygous E-cadherin loss (Figure 28).

3.3.7 Inefficient recombination of **Cdh1** *resulted in no detectable phenotype*

Animals treated with low dose tamoxifen that did not become unwell had no detectable changes compared with wildtype animals in histology, immunolabelling for *Cdh1*, β-catenin or markers of secretory cell lineages, or mRNA expression of *Cdh1* and Wnt target genes. This combined with no detectable changes in *Cdh1*$^{+/fl}$ animals suggests the phenotype only becomes apparent with near complete loss of *Cdh1.*

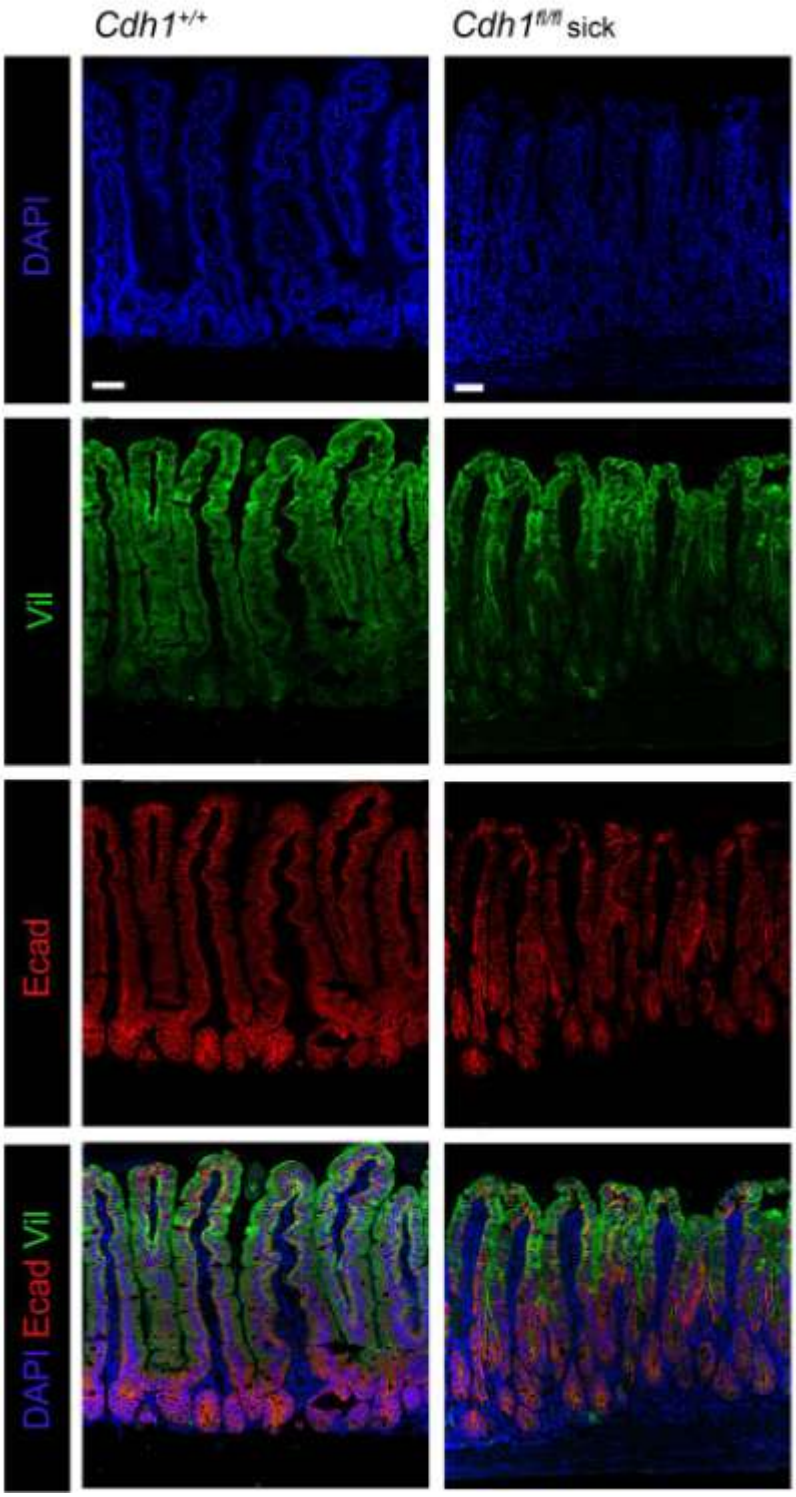

Figure 23. The effect of *Cdh1* homozygosity on differentiated enterocytes
Immunolabelling for DAPI, E-cadherin and villin. Villin immuno-labelling shows differentiated enterocytes and the crypt-villus junction. The crypt-villus junction is disrupted with *Cdh1* homozygosity. Scale bars 50µm

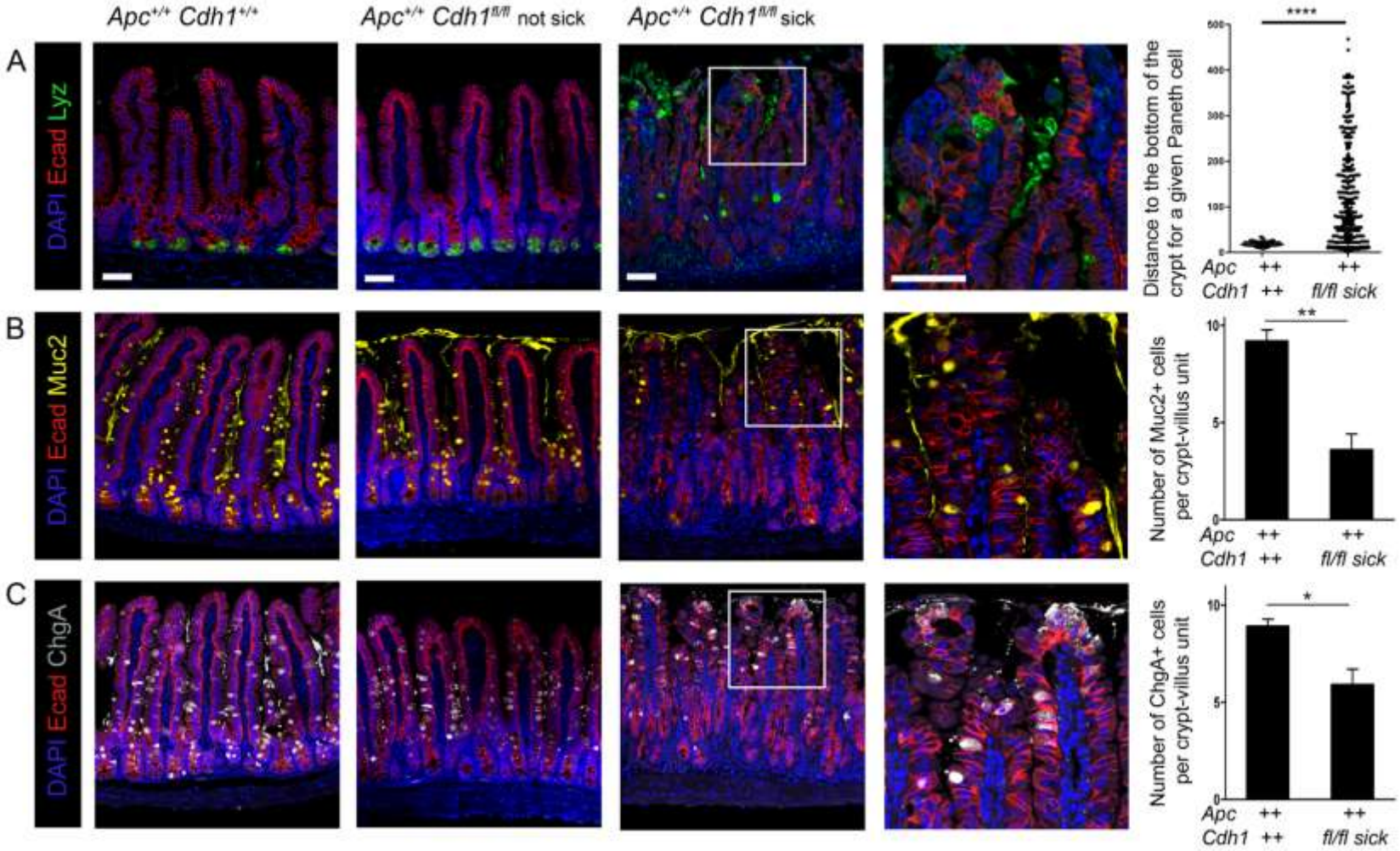

Figure 24. The effect of *Cdh1* homozygosity on secretory cell lineages

Immunolabelling for DAPI, E-cadherin and lysozyme (to detect Paneth cells (**A**)), Mucin 2 (to detect goblet cells (**B**)), or Chromogranin A (to detect enteroendocrine cells (**C**)). Quantification of mislocalisation of Paneth cells by measurement of distance in µm of each cell from the crypt base (**A**). Quantification of the average number of goblet or enteroendocrine cells per crypt-villus unit (**B-C**). For each genotype and marker ≥3 mice and ≥20 crypt-villus units assessed per animal. Student's t-test to compare *Cdh1*$^{fl/fl}$ *Vil-CreER*^{T2} with wildtype, only significant differences shown. Bars show means and whiskers standard error of mean. Scale bars 100µm. * p<0.05. ** p<0.01. **** p<0.0001.

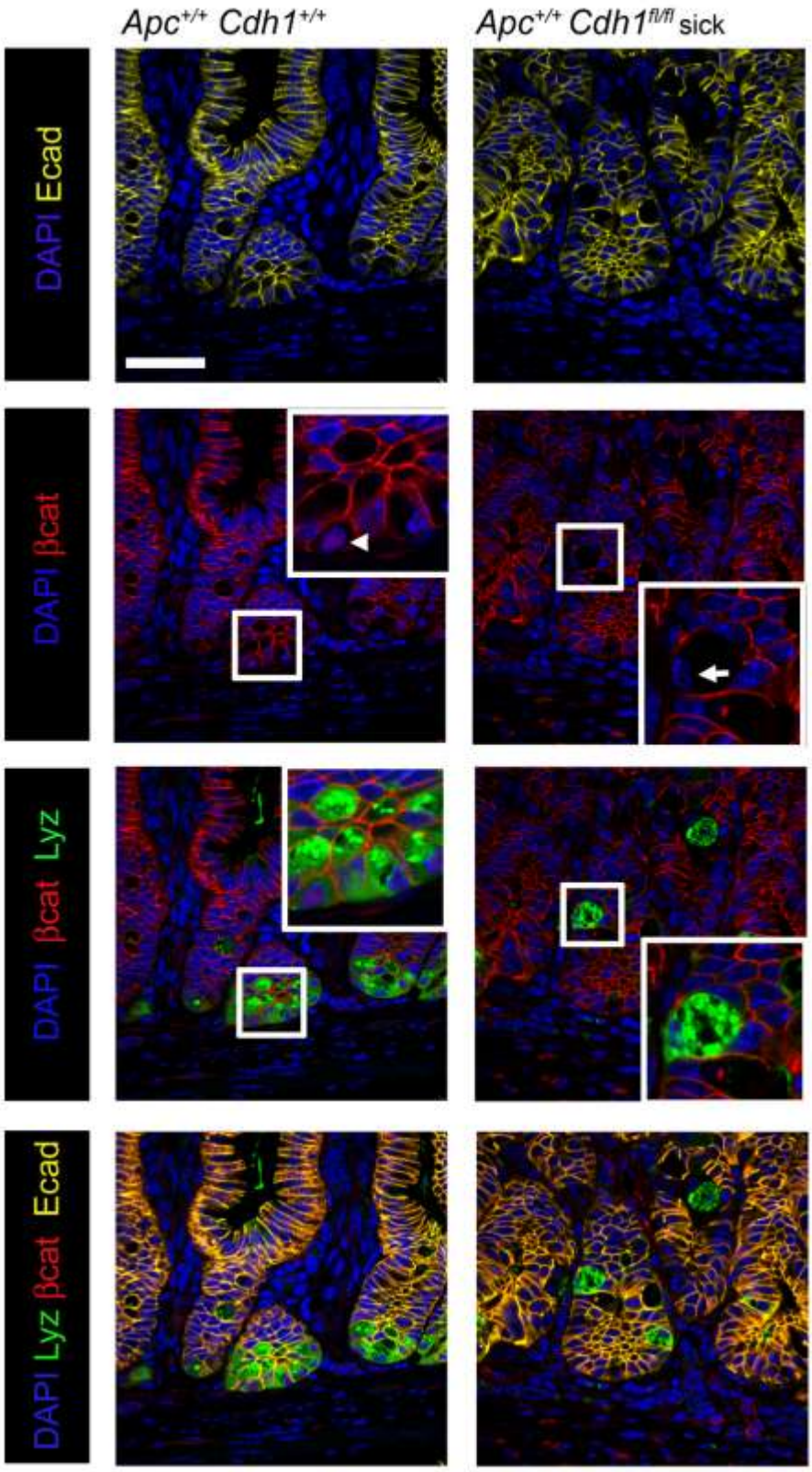

Figure 25. The effect of *Cdh1* homozygosity on Wnt activation in lysozyme labelled cells
Immunolabelling for DAPI, lysozyme, β-catenin and E-cadherin in small intestine from *Cdh1*$^{+/+}$ *VilCreER*^{T2} and *Cdh1*$^{fl/fl}$ *VilCreER*^{T2} animals. Arrowhead shows an example of nuclear β-catenin in lysozyme-labelled Paneth cells at the crypt base of wildtype animals. Arrow shows absence of nuclear β-catenin in a lysozyme-labelled cell in *Cdh1* homozygote animal suggesting this incomplete Paneth cell differentiation. Scale bar 50μm.

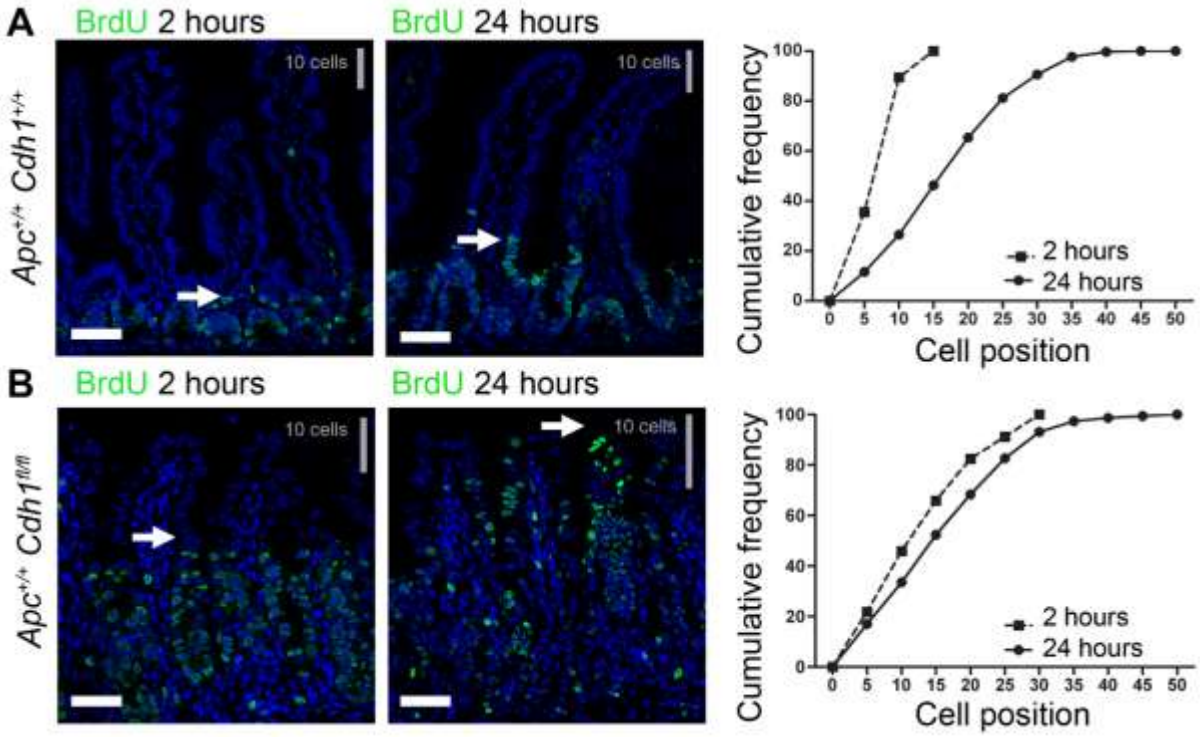

Figure 26. The effect of *Cdh1* homozygosity on proliferation (BrdU)
DAPI and BrdU immunolabelling of wildtype and *Cdh1* homozygote animals 2 or 24 hours prior to dissection. White arrows show the leading edge of BrdU labelling. Grey bars indicate the distance spanned by 10 cells. Scale bars 50µm. Cumulative frequency plots quantifying BrdU labelling. Cell position is the number of cells up the crypt-villus axis from the crypt base.

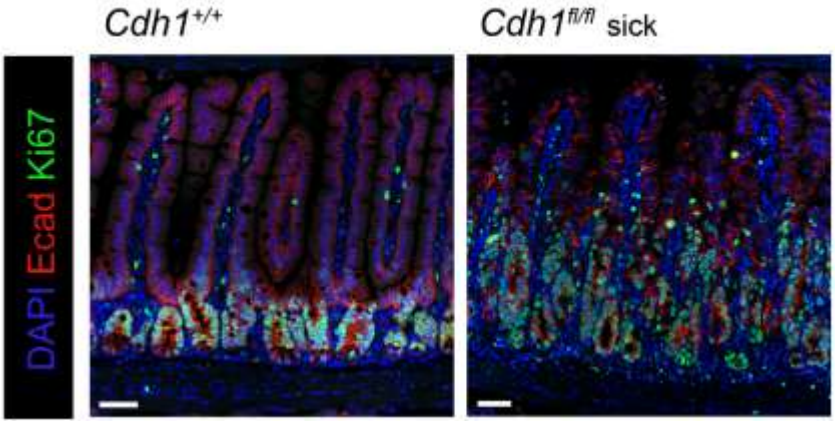

Figure 27. The effect of *Cdh1* homozygosity on proliferation (Ki-67)
DAPI, E-cadherin and Ki-67 immunolabelling of wildtype and *Cdh1* homozygote animals showing proliferating epithelial cells confined to the crypt in $Cdh1^{+/+}$ animals but mispositioned up the crypt-villus axis in $Cdh1^{fl/fl}$ animals. Scale bars 50µm.

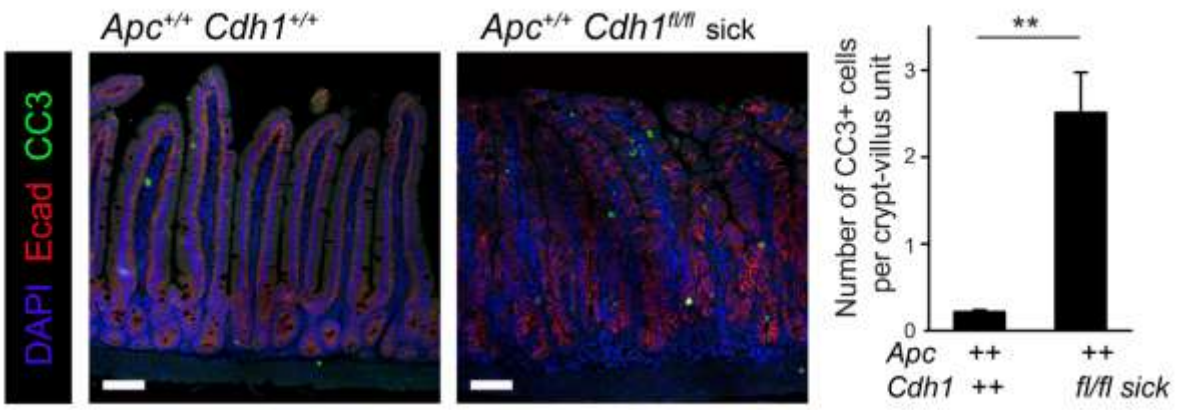

Figure 28. The effect of *Cdh1* homozygosity on apoptosis
Immunolabelling of small intestine from wildtype and *Cdh1* homozygote animals for DAPI. E-cadherin and cleaved caspase 3 (CC3) and quantification of the number of positive cells per crypt-villus unit. ≥3 animals per genotype and ≥20 crypt-villus units analysed per animal. Student's t- test. Bars represent means and whiskers standard error of mean. ** $p<0.01$.

3.3.8 Conditional Apc *homozygosity in the intestine*

Apc homozygosity using *Vil-CreER*^{T2} and an induction protocol of 2 doses of 200mg/kg tamoxifen on successive days results in the *Apc* homozygosity phenotype characterized using *AhCreER*^{T} and *Vil-CreER*^{T2} previously (Andreu et al, 2005; Sansom et al, 2004). *Apc* homozygote animals became unwell with weight loss and diarrhoea five days following initiation of tamoxifen treatment. Unlike *Cdh1*$^{fl/fl}$ animals there was no evidence of intestinal shortening or dilatation at dissection (Figure 29B). Histology showed expanded crypt zones with densely stacked, organized cells but increased apoptotic nuclei and a clear boundary between the proliferative zone and the villus (Figure 30). This clear boundary was confirmed by immunolabelling for villin showing a defined border between cells in the expanded crypt zone and the villus in *Apc*$^{fl/fl}$ *Cdh1*$^{+/+}$ animals but a less well defined border at a higher level in *Apc*$^{fl/fl}$ *Cdh1*$^{fl/fl}$ animals (Figure 35). Immunolabelling showed increased proliferation and apoptosis in the expanded crypt zone (Figures 37-39).

E-cadherin immunolabelling appeared localized to the cell membrane (Figure 30), however there was increased cytoplasmic β-catenin, C-Myc and EphB2 expression in the expanded crypt compartment indicating Wnt activation in this area (Figures 31, 32 and 34). RT-QPCR showed expected upregulation of Wnt target genes including *C-Myc, CD44* and *Axin2* (Figure 33). Paneth cells, labelled with lysozyme, were often mispositioned away from the crypt base but were still confined to the expanded proliferative zone where Wnt activation was present (Figure 36).

3.3.9 Combined Apc *and* Cdh1 *homozygosity results in a more severe phenotype than* Apc *or* Cdh1 *loss alone*

Double homozygous animals, as *Cdh1* homozygotes, became unwell with weight loss, diarrhoea, intestinal dilatation and shortening within 5 days of the first tamoxifen injection (Figure 28). Histology showed phenotypic features attributable to both *Apc* and *Cdh1* homozygosity: an expanded crypt zone, but disorganized crypt structure and crypt-villus boundary, and shedding of cells from the villus tip (Figure 29). Immunolabelling showed E-cadherin loss was particularly marked in the villus region, with patchy loss in the expanded crypt zone (Figure 30). This was confirmed by RT-QPCR showing less than 50% *Cdh1* mRNA expression in *Apc*$^{fl/fl}$ *Cdh1*$^{fl/fl}$ small intestine compared to *Apc*$^{fl/fl}$ *Cdh1*$^{+/+}$ (Figure 32).

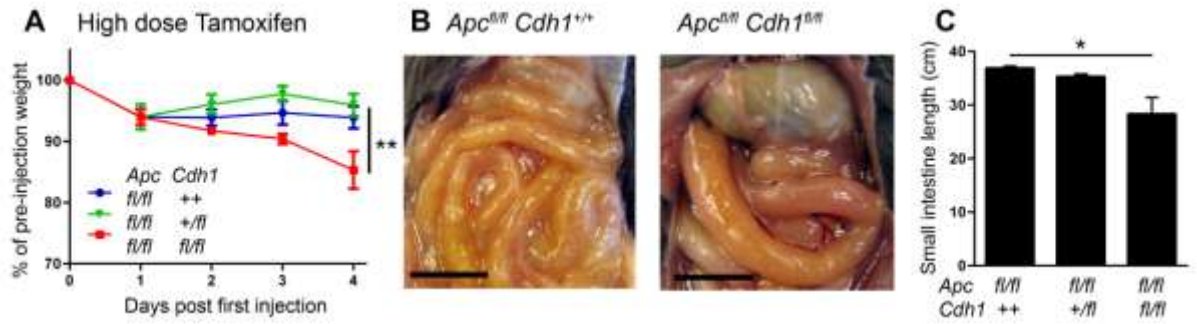

Figure 29. Combined *Apc* and *Cdh1* homozygosity phenotype
(**A**) Whole animal weights (represented as % of pre-injection weight) following intraperitoneal injection with high dose tamoxifen. n≥4 for each group. ANOVA with Bonferroni post test for each timepoint. (**B**) Intestinal appearance at dissection. Scale bars 1 cm. (**C**) Small intestinal length. One-way ANOVA with Bonferroni post test. Whiskers standard error of mean. * p<0.05. ** p<0.01.

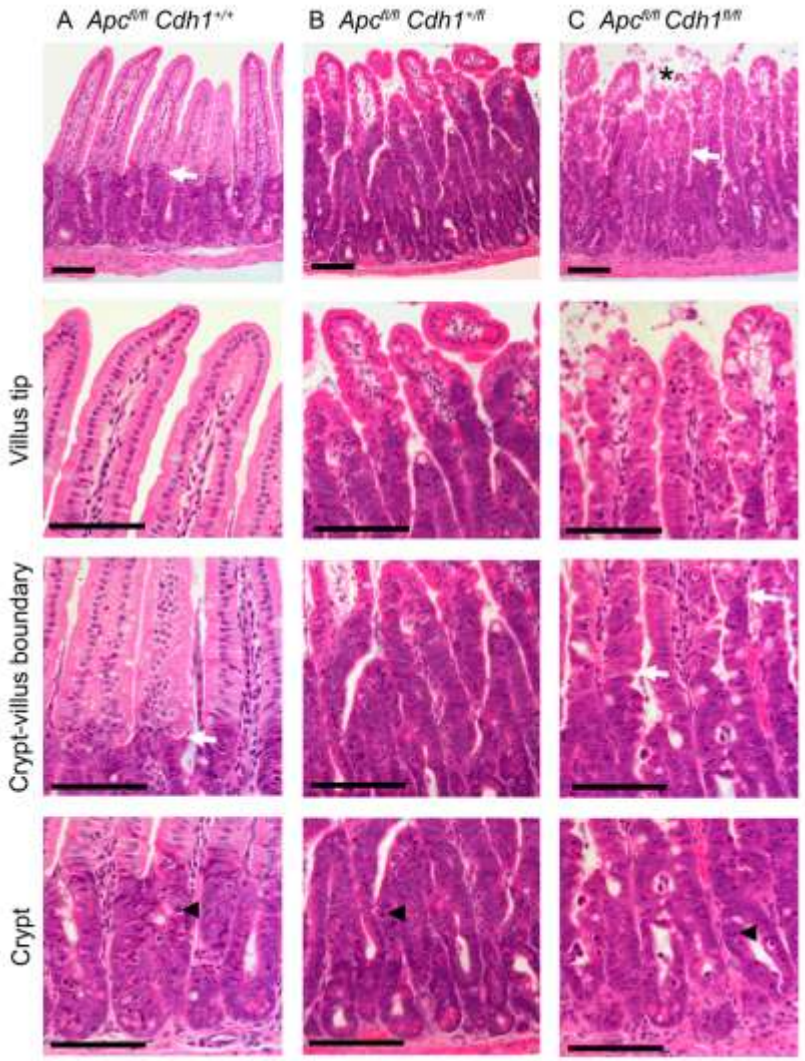

Figure 30. The effect of combined *Apc* and *Cdh1* homozygosity on intestinal architecture
H&E staining of small intestine, with high power views of crypt, crypt-villus boundary and villus. White arrows show crypt-villus junction. Black arrowheads show apoptotic nuclei. * shows cell shedding. Scale bars 50µm.

3.3.10 The effect of combined Apc *and* Cdh1 *homozygosity on Wnt signalling*

Immunolabelling of intestines from double homozygote animals for β-catenin showed a striking increase in cytoplasmic and nuclear β-catenin (Figures 31-32). Nuclear β-catenin was quantified to assess Wnt pathway activation. Images from at least three animals of each genotype were assessed and for each region (crypt or villus) over 1000 cells were assessed for colocalisation of DAPI and nuclear β-catenin. In $Apc^{fl/fl}$ $Cdh1^{+/+}$ animals nuclear β-catenin was visible in the expanded proliferative zone (mean 26.6% cells) but rare in the villus (mean 1.4% cells). In $Apc^{fl/fl}$ $Cdh1^{+/+}$ animals nuclear β-catenin was present in a high percentage of cells in both the crypt and the villus (mean 84.7% and 84.9% respectively). The differences in nuclear β-catenin localization between genotypes were highly significant (Figure 32). Immunolabelling for the Wnt markers C-Myc and EphB2 showed upregulation not only in the expanded crypt zone but also in the villus with combined *Apc* and *Cdh1* homozygosity (Figure 34).

RT-QPCR results were again not consistent with immunolabelling findings. $Apc^{fl/fl}$ $Cdh1^{fl/fl}$ small intestine showed increased *Axin2* compared to wildtype, but less overall *Axin2* expression than $Apc^{fl/fl}$ $Cdh1^{+/+}$ (student's t-test, p=0.007, Figure 33). Expression of *C-Myc* and *CD44* was significantly higher in $Apc^{fl/fl}$ $Cdh1^{fl/fl}$ intestines compared with $Apc^{fl/fl}$ $Cdh1^{+/+}$ (student's t-test, p=0.02 and 0.0007 respectively), but there was not a significant difference in *EphB2* or *EphB3* expression. It is unclear from the RT-QPCR data if *Cdh1* loss has an additive effect on overall Wnt signaling in the intestine but the immunolabelling is consistent with high Wnt pathway upregulation with combined homozygous *Apc* and *Cdh1* loss (Figures 31-34).

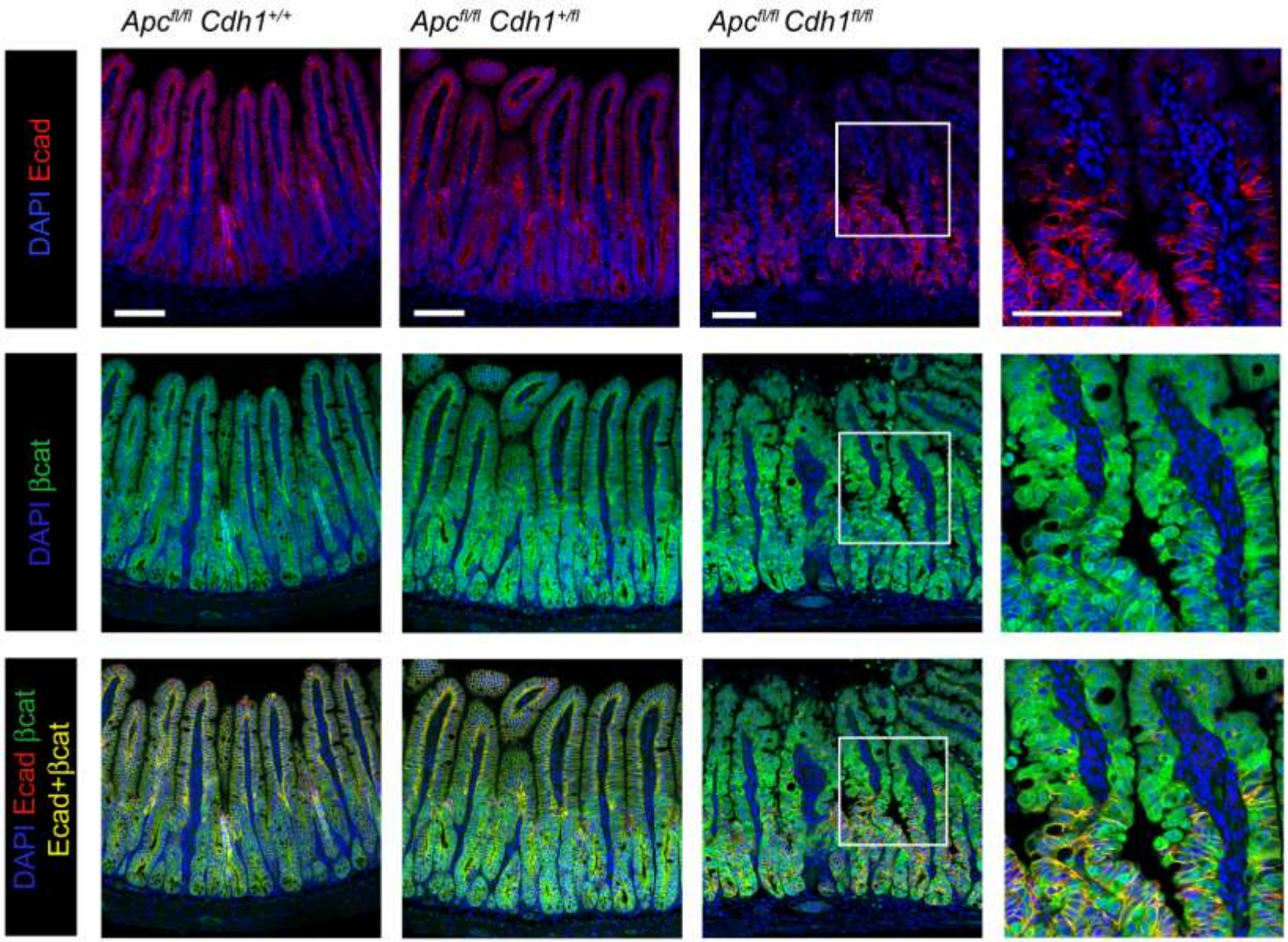

Figure 31. The effect of combined *Apc* and *Cdh1* homozygosity on E-cadherin and β-catenin expression
Immunolabelling for DAPI, E-cadherin and β-catenin in small intestine from *Apc*$^{fl/fl}$ *Cdh1*$^{+/+}$ *Vil-CreER*^{T2}, *Apc*$^{fl/fl}$ *Cdh1*$^{+/fl}$ *Vil-CreER*^{T2} and *Apc*$^{fl/fl}$ *Cdh1*$^{fl/fl}$ *Vil-CreER*^{T2} animals. The far right panels show high power views of the crypt-villus transition zone of *Apc*$^{fl/fl}$ *Cdh1*$^{fl/fl}$ *Vil-CreER*^{T2} animals. Scale bar 100µm.

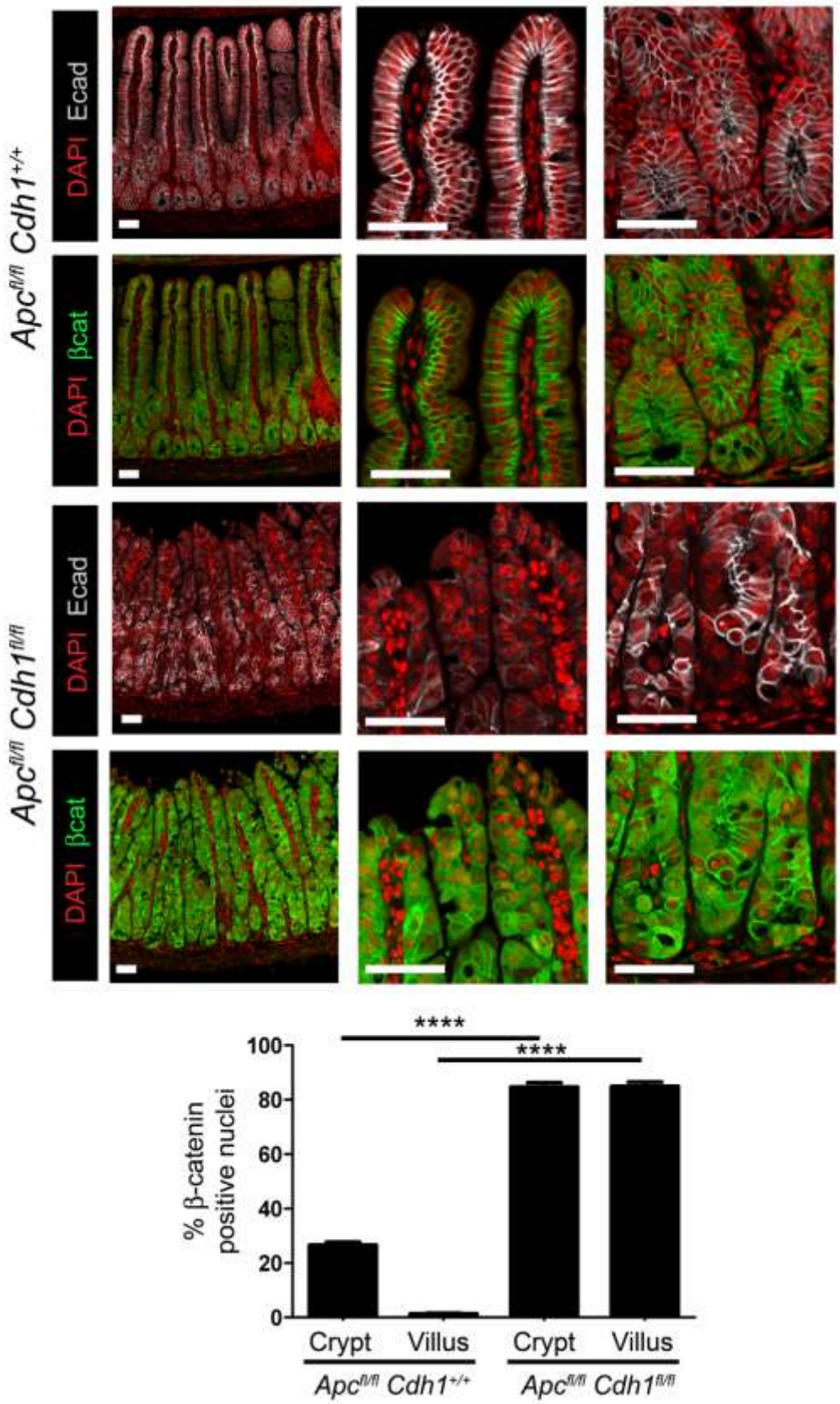

Figure 32. The effect of combined *Apc* and *Cdh1* homozygosity on β-catenin localisation
Immunolabelling for E-cadherin and DAPI, and β-catenin and DAPI in small intestine from *Apc*$^{fl/fl}$ *Cdh1*$^{+/+}$ *Vil-CreER*^{T2} and *Apc*$^{fl/fl}$ *Cdh1*$^{fl/fl}$ *Vil-CreER*^{T2} animals. Scale bars 50µm. Quantification of nuclear β-catenin in crypt or villus from each genotype (3 animals/genotype, >1000cells counted per area for each genotype). Unpaired t-test. Bars represent means and whiskers standard error of mean. ** p<0.01. **** p<0.0001.

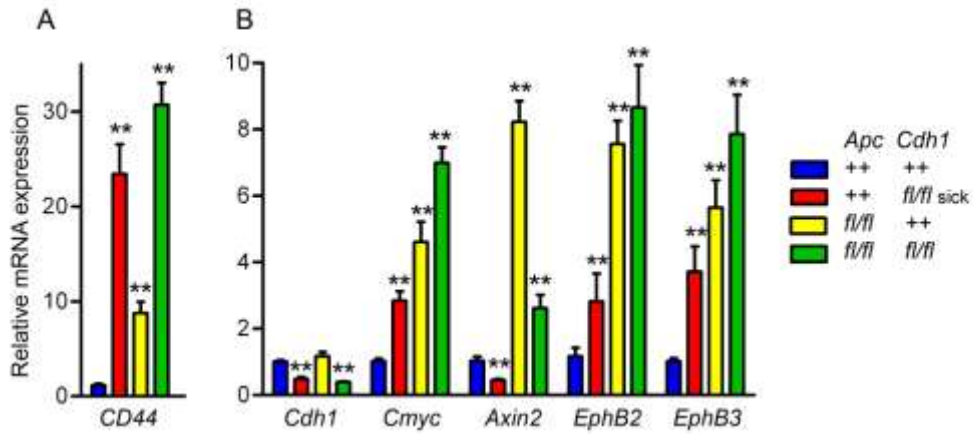

Figure 33. Combined *Apc* and *Cdh1* homozygosity: RT-QPCR

RT-QPCR for *Cdh1* and Wnt target gene mRNA expression. There is decreased *Cdh1* expression with *Cdh1* homozygosity. With *Apc* homozygosity there is Wnt target gene upregulation. With combined *Apc* and *Cdh1* homozygosity the effect on some Wnt target genes is additive. n≥3 mice for each genotype. Reference genes *Actb* and *Hprt.* ** denotes p<0.01 using student's t-test for comparison with wildtype samples. Bars represent means and whiskers standard error of mean.

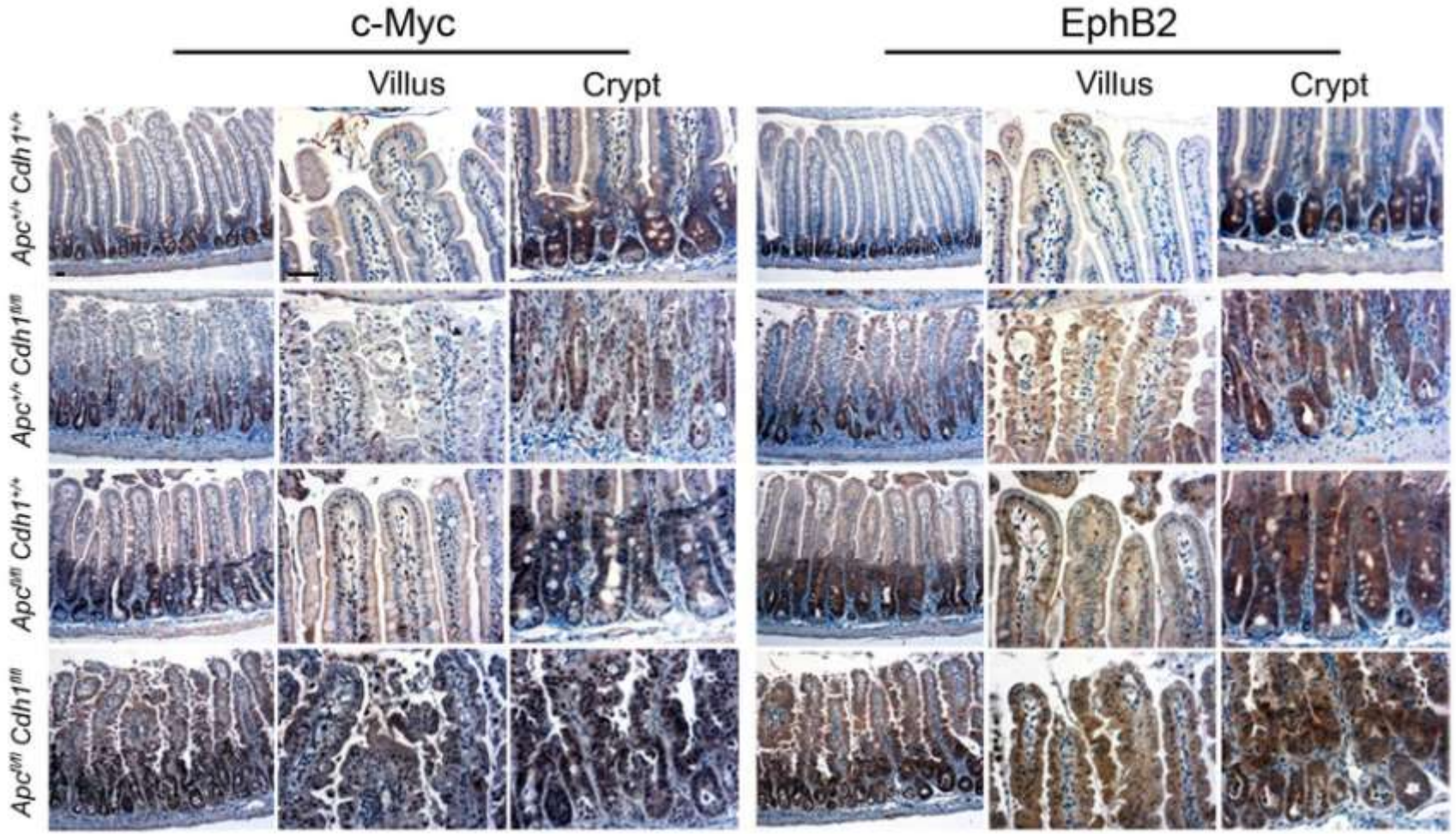

Figure 34. The effect of *Cdh1* homozygosity or combined *Cdh1* and *Apc* homozygosity on Wnt target gene expression: Immunolabelling
Immunolabelling of small intestine from *Apc*$^{+/+}$ *Cdh1*$^{+/+}$ *Vil-CreER*^{T2}, *Apc*$^{+/+}$ *Cdh1*$^{fl/fl}$ *Vil-CreER*^{T2}, *Apc*$^{fl/fl}$ *Cdh1*$^{+/+}$ *Vil-CreER*^{T2} and *Apc*$^{fl/fl}$ *Cdh1*$^{fl/fl}$ *Vil-CreER*^{T2} animals for the Wnt target genes C-Myc and EphB2. Sections have been counterstained with haematoxylin. C-Myc and EphB2 expression are high in the crypt regions of all genotypes as expected, but also increased in the villus region of *Apc*$^{fl/fl}$ *Cdh1*$^{fl/fl}$ animals consistent with aberrant Wnt signalling in this region with combined *Apc* and *Cdh1* loss. Scale bars 100µm.

3.3.11 Effect of combined **Apc** *and* **Cdh1** *homozygosity on secretory cell lineages*

Combined *Apc* and *Cdh1* loss showed Paneth cell mislocalisation similar to *Cdh1* loss alone, including the presence of lysozyme labelled cells in the villus structures, and more severe than that seen in $Apc^{fl/fl}$ $Cdh1^{+/+}$ animals. Goblet and enteroendocrine cell numbers were decreased in $Apc^{fl/fl}$ $Cdh1^{fl/fl}$ intestines compared with $Apc^{fl/fl}$ $Cdh1^{+/+}$ intestines (Figure 36).

3.3.12 Effect of combined Apc and Cdh1 homozygosity on proliferation and apoptosis

BrdU labelling showed proliferating cells present in the crypt and the villus at both 2 and 24 hours with combined *Apc* and *Cdh1* homozygosity, compared with BrdU labelled cells just exiting the expanded proliferative zone at 2 hours and present about 25% of the distance up the villus by 24 hours in $Apc^{fl/fl}$ $Cdh1^{+/+}$ animals (Figure 37). The mislocalisation of proliferating cells in the villus compartment with *Cdh1* loss was confirmed by Ki-67 immmunolabelling (Figure 38). Cumulative frequency graphs of BrdU labelled cells showed $Apc^{fl/fl}$ $Cdh1^{fl/fl}$ intestinal cells migrating at a similar rate to the $Apc^{fl/fl}$ $Cdh1^{+/+}$ cells, despite the marked difference in the appearance of the BrdU labelling between genotypes. This can be explained by the observation that $Apc^{fl/fl}$ $Cdh1^{fl/fl}$ intestines had cells that were less densely packed in the expanded proliferative zone than $Apc^{fl/fl}$ $Cdh1^{+/+}$ intestines and fewer total number of cells along the crypt-villus axis. The proliferative changes with *Cdh1* loss could represent attempted epithelial regeneration.

Apoptosis was markedly increased in the expanded proliferative zone of *Apc* homozygote animals, with or without concomitant *Cdh1* loss. Additionally in some sections a large number of non-adherent cleaved caspase 3 cells were present in the intestinal lumen in $Cdh1^{fl/fl}$ animals (Figure 39). As this was not a consistent finding between animals (possibly due to these loose cells being lost during sample preparation), this change could not be quantified, but suggested increased cell shedding by anoikis.

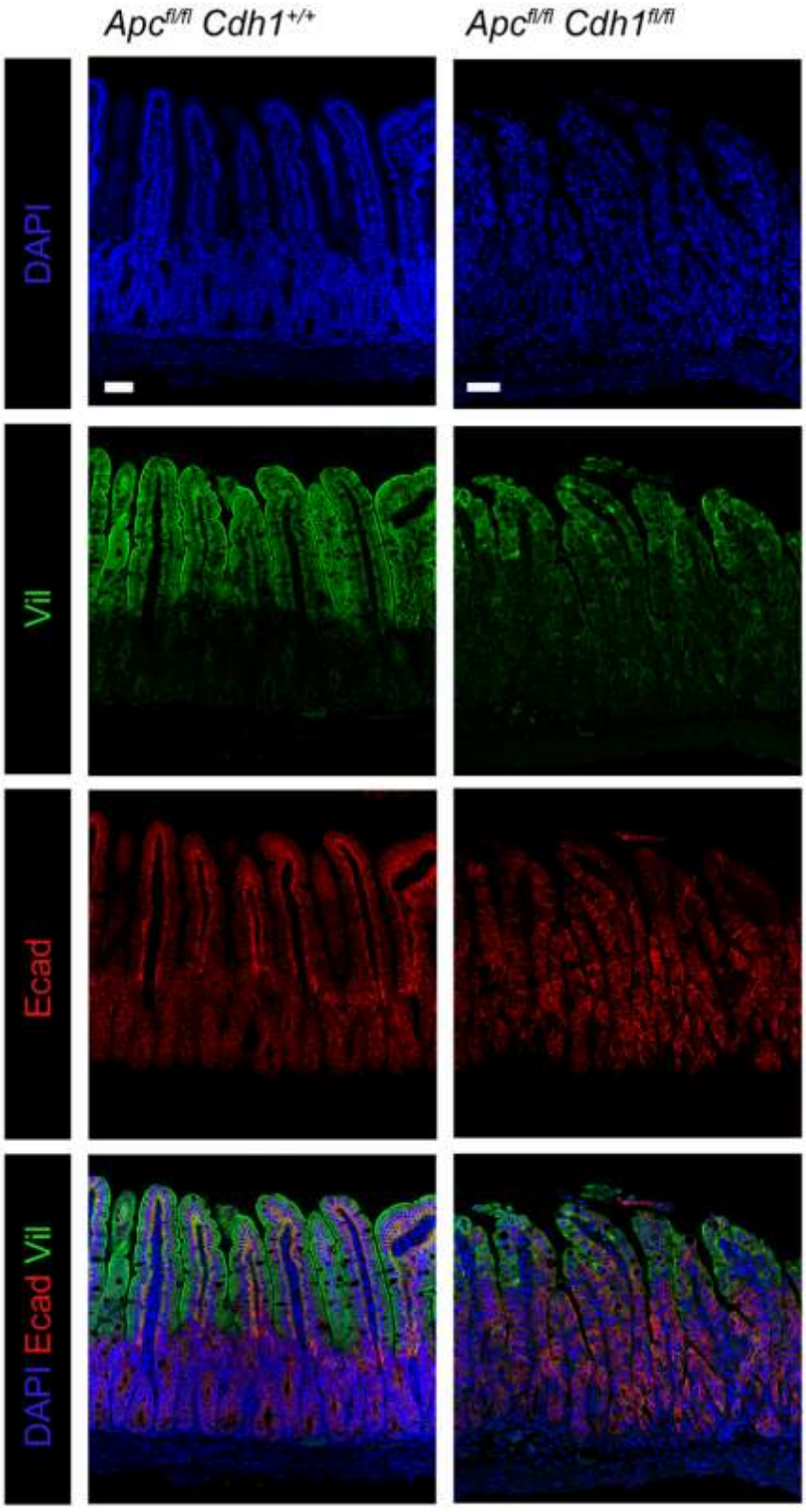

Figure 35. The effect of combined *Apc* and *Cdh1* homozygosity on differentiated enterocytes
Immunolabelling for DAPI, E-cadherin and villin in small intestine from *Apc*$^{fl/fl}$ *Cdh1*$^{+/+}$ *Vil-CreER*^{T2} and *Apc*$^{fl/fl}$ *Cdh1*$^{fl/fl}$ *Vil-CreER*^{T2} animals. Villin immunolabelling shows differentiated enterocytes and the crypt-villus junction. The crypt zone is expanded in *Apc*$^{fl/fl}$ *Cdh1*$^{+/+}$ *Vil-CreER*^{T2} animals but the crypt-villus junction is intact. With combined *Apc* and *Cdh1* homozygosity there is disruption of the crypt-villus junction and decreased differentiated enterocytes. Scale bars 50µm.

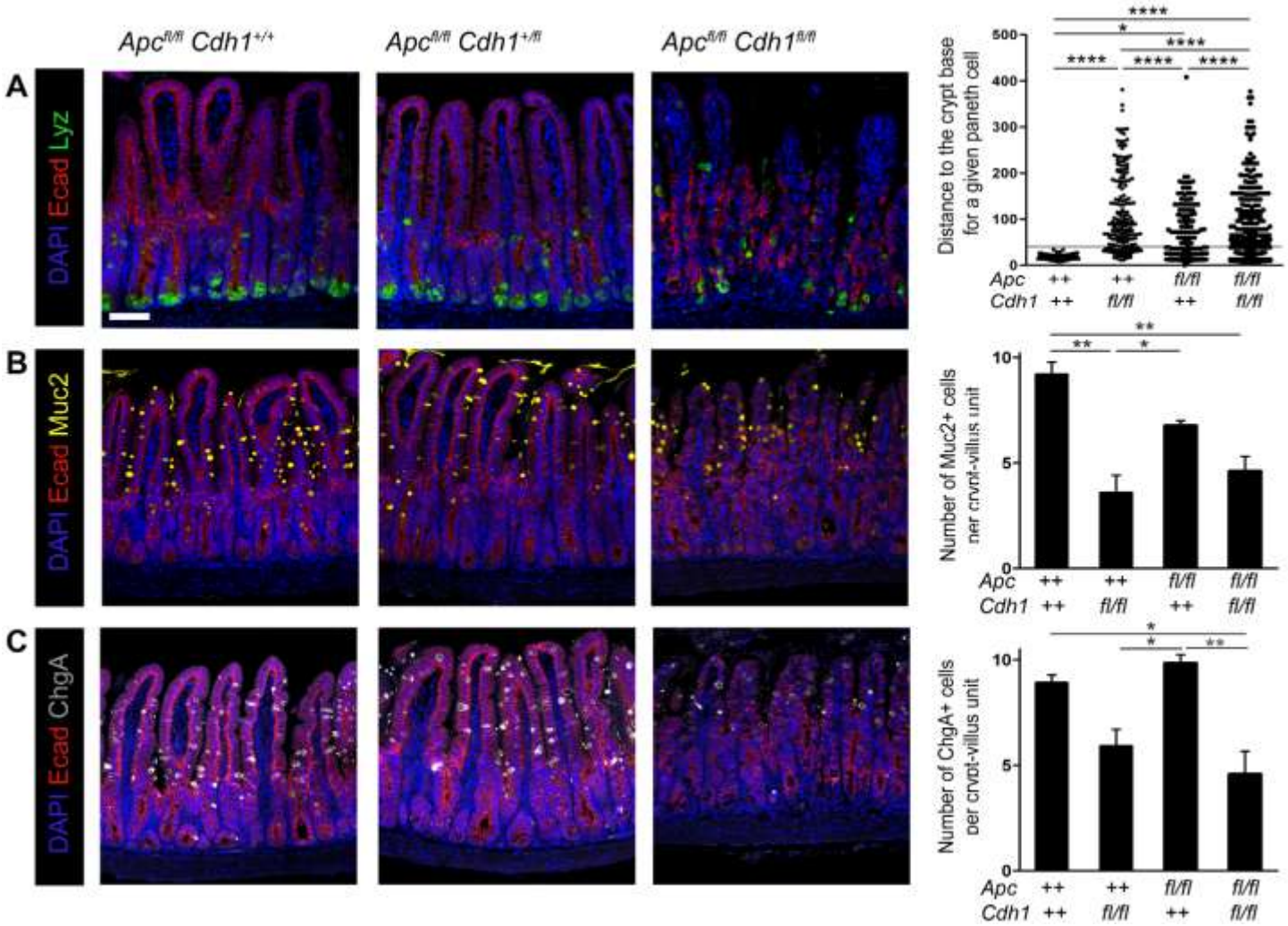

Figure 36. The effect of combined *Apc* and *Cdh1* homozygosity on secretory cell lineages

Immunolabelling for DAPI, E-cadherin and lysozyme (to detect Paneth cells (**A**)), Mucin 2 (to detect goblet cells (**B**)), or Chromogranin A (to detect enteroendocrine cells (**C**)). All $Apc^{+/+}$ $Cdh1^{fl/fl}$ animals analyzed were the sick phenotype. Quantification of mislocalisation of Paneth cells by measurement of distance in µm of each cell from the crypt base (**A**). Quantification of the average number of goblet or enteroendocrine cells per crypt-villus unit (**B-C**). For each genotype and marker ≥3 mice and ≥20 crypt-villus units assessed per animal. One way ANOVA with Bonferroni post-test to compare between genotypes, only significant differences shown. Bars show means and whiskers standard error of mean. Scale bars 100µm. * p<0.05. ** p<0.01. **** p<0.0001.

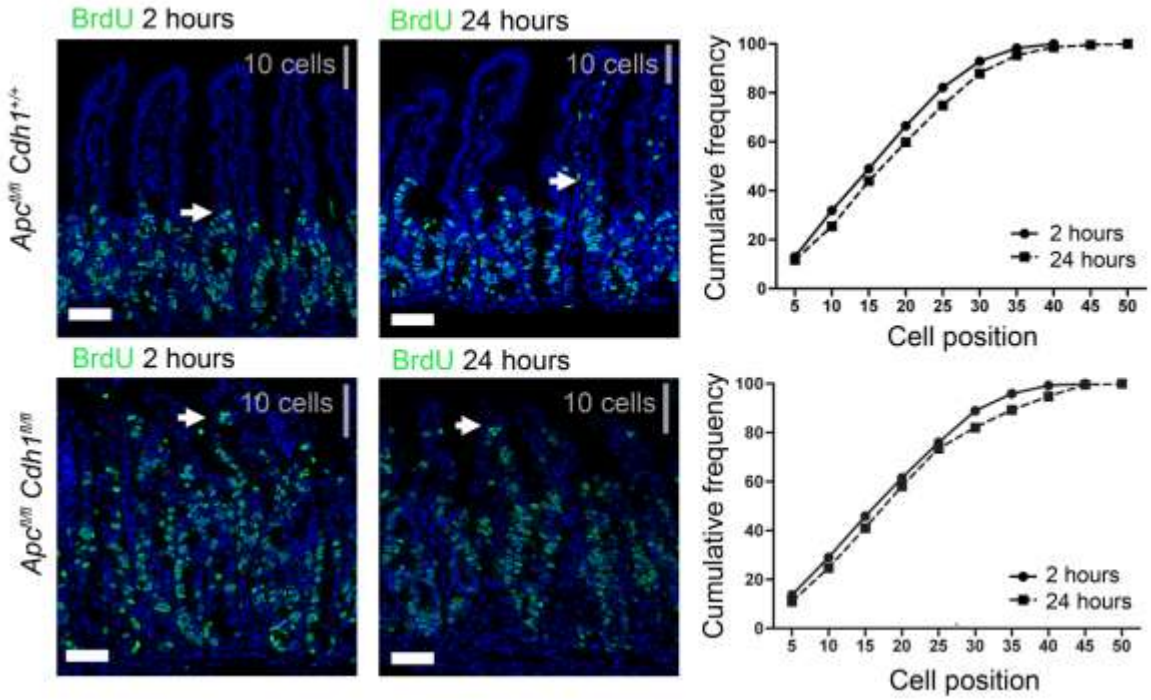

Figure 37. The effect of combined *Apc* and *Cdh1* homozygosity on proliferation (BrdU)
DAPI and BrdU immunolabelling of small intestine from *Apc*$^{fl/fl}$ *Cdh1*$^{+/+}$ *Vil-CreER*^{T2} and *Apc*$^{fl/fl}$ *Cdh1*$^{fl/fl}$ *Vil-CreER*^{T2} animals 2 or 24 hours prior to dissection. White arrows show the leading edge of BrdU labelling. Grey bars indicate the distance spanned by 10 cells. Scale bars 50µm. Cumulative frequency plots quantifying BrdU labelling. Cell position is the number of cells up the crypt-villus axis from the crypt base.

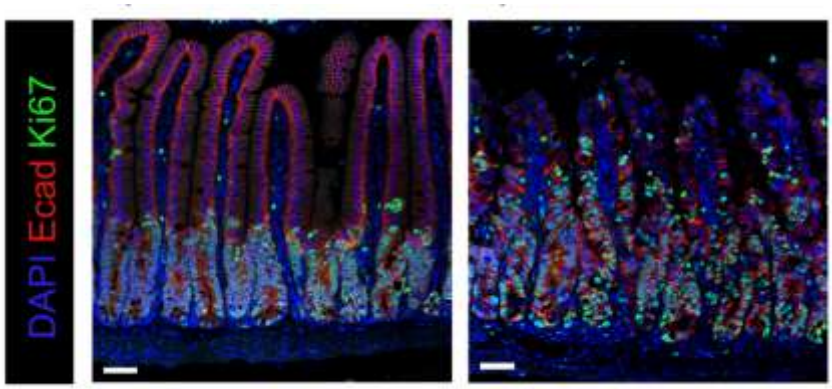

Figure 38. The effect of combined *Apc* and *Cdh1* homozygosity on proliferation (Ki-67)
DAPI, E-cadherin and Ki-67 immunolabelling of small intestine from *Apc*$^{fl/fl}$ *Cdh1*$^{+/+}$ *Vil-CreER*^{T2} and *Apc*$^{fl/fl}$ *Cdh1*$^{fl/fl}$ *Vil-CreER*^{T2} animals showing proliferating epithelial cells confined to the expanded crypt zone in *Apc*$^{fl/fl}$ *Cdh1*$^{+/+}$ *Vil-CreER*^{T2} animals but mispositioned up the crypt-villus axis in *Apc*$^{fl/fl}$ *Cdh1*$^{fl/fl}$ *Vil-CreER*^{T2} animals. Scale bars 50µm.

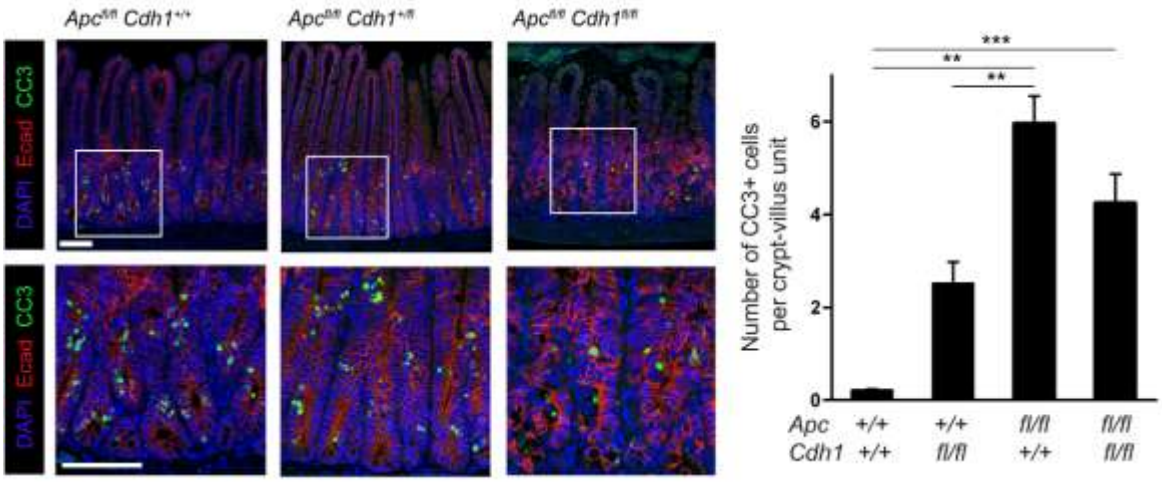

Figure 39. The effect of combined *Apc* and *Cdh1* homozygosity on apoptosis
Immunolabelling of small intestine from *Apc*$^{fl/fl}$ *Cdh1*$^{+/+}$ *Vil-CreER*^{T2} and *Apc*$^{fl/fl}$ *Cdh1*$^{fl/fl}$ *Vil-CreER*^{T2} animals for DAPI, E-cadherin and cleaved caspase 3 (CC3). Lower panel shows high power views of the areas marked in the top panel. Graph shows quantification of the number of CC3 positive cells per crypt-villus unit. ≥3 animals per genotype and ≥20 crypt-villus units analysed per animal. One way ANOVA with Bonferroni post-test. Bars represent means and whiskers standard error of mean. ** $p<0.01$, *** $p<0.001$. Scale bars 100µm.

3.4 Discussion

3.4.1 Cdh1 homozygosity with Vil-Cre is embryonic lethal

Germline *Cdh1* homozygosity is embryonic lethal due to failure to form trophectoderm epithelium at E2.5-E3.5 (Larue et al, 1994). *Vil-Cre* is active in the visceral endoderm from E9 and detectable in the developing intestinal epithelium at E10.5 (el Marjou et al, 2004). Thus, *Cdh1* homozygosity activated using *Vil-Cre* would be expected to bypass the gastrulation defect seen with germline *Cdh1* loss. A detailed explanation of embryonic development of the gastrointestinal system is beyond the scope of this thesis, however the important stages are formation from the endoderm of a gut tube at E8.5, organ budding from E10.5, and the presence of organ specific cells by E14.5 (Wells & Melton, 1999). The visceral endoderm, which has the same origin as the gut, contributes to the yolk sac from E6. The gut is sterile during embryogenesis and first relied upon for nutrition at birth, thus a defect in the gastrointestinal epithelium only would not be expected to manifest until birth.

The absence of any $Cdh1^{fl/fl}$ *Vil-Cre* animals at birth suggested embryonic lethality or very early postnatal lethality. Dissections in late embryogenesis (E15.5+) showed absence of any *Cdh1* homozygotes, excluding early postnatal lethality. The knowledge that embryos do not rely on the gastrointestinal tract for nutrition and that *Vil-Cre* is expressed in the visceral endoderm made a yolk sac defect due to *Cdh1* homozygosity the most likely cause of embryonic demise. The increased incidence of embryonic resorptions at E11.5-E12.5, and observation of smaller embryos, often lacking extraembryonic membranes, at these timepoints strengthened this hypothesis. Immunolabelling confirmed loss of Cdh1 in the yolk sac. Given the aim of this work was to investigate the effect of *Cdh1* loss on the intestine, as the embryonic demise was most likely related to yolk sac function this work was not pursued further. Instead a conditional approach using *Villin-CreER*^{T2} in the adult intestine was taken.

Recently Bondow and colleagues showed that E-cadherin is necessary for intestinal morphogenesis (Bondow et al, 2012). They used the same approach as us but a different *Vil-Cre* transgene (Tg(*Vil-Cre*)997Gum) that uses a 12.4kb fragment of the villin gene as a promoter and is active in the intestine but not the yolk sac (Madison et al, 2002). They found that *Cdh1* homozygotes died within the first 24 hours of birth (Bondow et al, 2012; Madison et al, 2005). *Vil-Cre* was active in the intestine from E14.5, but there was only

efficient loss of Cdh1 by E17.5-E18.5. *Cdh1* homozygote pups had dilated, shortened intestines with very disrupted intestinal architecture notable for absent or blunted villi, epithelial cells that were rounded rather than columnar and reduced in number, and compromised barrier function. The adherent cells did not have increased apoptosis as assessed by immunolabelling for cleaved caspase 3, however apoptosis was increased in cells shed into the lumen. There were increased proliferating cells, no change in the proportion of goblet cells, a slight decrease in enteroendocrine cells and Paneth cells could not be assessed as these do not mature until birth. Despite RT-QPCR showing increased expression of a number of Wnt target genes including *CD44, C-Myc* and *Axin2* with *Cdh1* loss, there was no change in β-catenin mRNA expression and decreased cytoplasmic and nuclear β-catenin were observed with immunolabelling. The authors concluded that *Cdh1* homozygote pups likely died from hypoglycaemia due to malabsorption and that the increased proliferation likely occurred as a response to attempt to repair the disrupted epithelium. To explain the paradoxical results regarding Wnt activation, namely that β-catenin expression was reduced but expression of Wnt target genes increased, they suggested that in the mutant epithelium Wnt target gene expression may occur through β-catenin-independent mechanisms, such as signaling by other catenins.

3.4.2 Cdh1 homozygosity in the adult intestine results in an inflammatory phenotype with changes in secretory cell lineages

This work shows that *Cdh1* homozygosity in the intestine with high levels of recombination is lethal due to an inflammatory phenotype with disrupted intestinal architecture, breakdown of the intestinal barrier and systemic bacteraemia. *Cdh1* loss is accompanied by increased apoptosis, but also increased cellular proliferation (including proliferating cells in the villus compartment) suggesting that in response to the inflammation the intestine is attempting to regenerate and recover. Even sick animals with severely distorted crypt-villus structure, still had some crypts with intact CDH1. The animals treated with low dose tamoxifen who did not become unwell may represent animals with incomplete recombination where regeneration has been successful. *Cdh1* homozygosity led to abnormalities in secretory cell lineages in particular Paneth cell placement, and the abundance of goblet and enteroendocrine cells. Impaired function of these cells that have

important roles in maintaining crypt sterility and forming a protective mucous layer for the epithelium may have contributed to the inflammatory phenotype.

During this study a paper was published using the same model of *Cdh1*$^{fl/fl}$ *Vil-CreER*^{T2}+ with very similar findings to this work (Schneider et al, 2010). Schneider and colleagues described a *Cdh1* homozygosity phenotype with altered differentiation of goblet and Paneth cells, misplacement of Paneth cells, enhanced epithelial cell shedding and apoptosis, increased cell migration along the crypt-villus axis and impaired clearance of enteropathogenic bacteria. They used two 4-hydroxytamoxifen (4OHT) injection regimes: a total dose of 5mg 4OHT over 5 days gave a phenotype similar to our high dose regime; however they used a more severe experimental endpoint with animals often losing 25% of their bodyweight and having severely distorted tissue architecture. In the second regime they gave a total dose of 4mg 4OHT over 8 days and found the animals had mild histological changes 12 days following the first injection despite appearing well. The studies had somewhat different objectives in that Schneider and colleagues were primarily interested in loss of E-cadherin and immune function, whereas I was particularly interested in Wnt signalling, but the findings were very similar. One that differed between the two studies is that Schneider and colleagues did not observe an alteration in enteroendocrine cell numbers, however they used synaptophysin as a marker for these cells, whereas we used Chromogranin A. Chromogranin A is used widely as a pan enteroendocrine cell marker and thought to be superior to synaptophysin in the intestine (Portela-Gomes et al, 1999).

Both studies show E-cadherin has an important role in intestinal homeostasis through maintenance of barrier function and roles in cellular differentiation, migration and survival. Whilst Hermiston and Gordon's work had shown E-cadherin was likely to affect barrier function, cell migration and cell death, the influence on cellular differentiation was surprising. The phenotype I observed immediately drew comparison with other phenotypes, in particular *p120*, *EphB3* and *ADAM10* knock-out models. Homozygous loss of *p120* in the intestine using *Villin-Cre* resulted in mice that appeared normal at birth but became unwell postnatally, dying within three weeks due to widespread intestinal barrier defects and inflammation (Smalley-Freed et al, 2010). A mechanism was suggested by which p120 disrupts the neonatal intestinal barrier, increasing neutrophil engagement in the gut just as it is being colonized with a microbiome, leading to a massive inflammatory response. Low

levels of *p120* ablation using *Villin-CreER*^{T2} (limited to 10% of the intestinal epithelium) led to animals that remained well but had areas of *p120* null epithelium with inflammation from 2 months following injection. 45% of these animals developed intestinal tumours within 18 months, however all tumours retained *p120* expression (Smalley-Freed et al, 2011). I aged a small cohort of 'not sick' *Cdh1* homozygotes treated with the low dose tamoxifen regime (and controls) to one year following injection but saw no evidence of macroscopic tumours (*Cdh1*$^{fl/fl}$ n=4, *Cdh1*$^{+/fl}$ n=6, *Cdh1*$^{+/+}$ or *Vil-CreER*^{T2}- n=3).

EphB3 null mice have mispositioned Paneth cells scattered along the crypt-villus axis (Batlle et al, 2002). This Paneth cell misplacement is phenocopied by *ephrin-B* conditional intestinal knockout mice and transgenic mice expressing ADAM10$^{\Delta MP}$ (a dominant negative form of ADAM10 lacking the metalloproteinase domain) in the Paneth cells (Cortina et al, 2007; Solanas et al, 2011). E-cadherin mediates EphB-Ephrin interactions: activation of EphB leads to ADAM10 mediated shedding of E-cadherin extracellular domains at boundaries with cells expressing ephrin-B1. The resulting asymmetric localization of E-cadherin maintains boundaries between cellular compartments by creating different affinities between EphB and ephrin-B expressing cells. The effects of mislocalised Paneth cells with E-cadherin loss may be a result of E-cadherin being unable to mediate these Eph-Ephrin interactions.

Paneth cells have an important role in the secretion of anti-microbial peptides to protect against enteropathogens and maintain a sterile crypt environment. The mispositioning and incomplete maturation of these cells may compound the inflammation caused by impaired barrier function with E-cadherin loss. Decreased secretion of mucin by goblet cells may also contribute. E-cadherin loss has previously been implicated in inflammatory bowel disease. 16q22, which contains *CDH1*, has been identified as a susceptibility locus for ulcerative colitis in a large genome-wide association study (Barrett et al, 2009). Decreased E-cadherin expression has been observed in areas of colitis in patients with ulcerative colitis and Crohn's disease (Karayiannakis et al, 1998). A large genome-wide association meta-analysis for Crohn's disease did not identify E-cadherin as a susceptibility locus, however a candidate gene approach showed an association with Crohn's disease and patients with a specific risk haplotype had increased cytoplasmic E-cadherin expression due to a truncated protein (Barrett et al, 2008; Muise et al, 2009).

The transcription factor Math1 and the Notch signaling pathway control differentiation of intestinal stem cells to a secretory lineage. *Math1* null neonates fail to develop Paneth, goblet or enteroendocrine cells and intestinal specific mosaic deletion of *Math1* in the adult intestine results in *Math1* null crypts with decreased secretory cells (Shroyer et al, 2007; Yang et al, 2001). Notch signaling inhibition leads to decreased crypt cell proliferation and directs cells to a goblet cell fate and Notch activation increases proliferation but impairs differentiation of crypt stem cells (Fre et al, 2005; van Es et al, 2005). No direct link has been described between Math1 and E-cadherin. As both the Wnt and Notch pathways have key roles in intestinal development and homeostasis it is not surprising cross-talk exists between them, with some authors coining the term 'Wntch' because they are so intertwined (Fre et al, 2009; Muñoz Descalzo & Martinez Arias, 2012). Wnt pathway downregulation with E-cadherin loss and distortion of the normal crypt and transition amplifying region niche for cellular differentiation and maturation may influence Notch signalling, affecting cellular differentiation.

3.4.3 Cdh1 homozygosity does not appear to activate the Wnt pathway

The central role of β-catenin as a key element of E-cadherin mediated adhesion and an effector of the Wnt pathway makes an interaction between the two attractive; however the ability of β-catenin originally bound by E-cadherin to contribute to the transcriptional pool is contentious. The results demonstrate challenges assaying the Wnt pathway reliably. Immunolabelling for β-catenin showed colocalised loss of membrane bound E-cadherin and β-catenin. There was no evidence of nuclear localization of β-catenin in CDH1 null cells and no obvious increase in cytoplasmic β-catenin. These findings suggest *Cdh1* loss does not activate Wnt signaling. RT-QPCR results show downregulation of *Axin2*, but upregulation of other Wnt target genes including *CD44*, *EphB3* and the critical mediator *C-Myc*. Upregulation of these Wnt target genes is inconsistent with the absence of nuclear or cytoplasmic β-catenin, so a true effect on the Wnt pathway is not convincing. These findings are similar to those seen by Bondow and colleagues who postulated the observed Wnt target gene activation may be real but due to a mechanism independent of β-catenin, for example through signalling by other catenins (Bondow et al, 2012). E-cadherin mediates the effect of *EphB* receptors so upregulation of *EphB2* and *EphB3* may reflect an attempt to compensate for impaired cell sorting and compartmentalization in the absence of

E-cadherin. *C-Myc* and *CD44* can both be upregulated during inflammation, so this may explain their increased expression with *Cdh1* loss (Johnson & Ruffell, 2009).

3.4.4 Combined Apc and Cdh1 homozygosity results in a phenotype more severe than loss of either gene alone and with Wnt pathway derangement

Combined *Apc* and *Cdh1* homozygosity with *Vil-CreER*^{T2} results in a phenotype with features of both *Apc* and *Cdh1* loss: an expanded crypt zone, Wnt activation, increased proliferation and apoptosis, but poorly demarcated crypt-villus boundary and disorganised cellular architecture. Immunolabelling shows marked upregulation of β-catenin and significantly increased nuclear localization of β-catenin in animals with *Cdh1* loss in addition to *Apc* loss. This supports the hypothesis that in the setting of Wnt activation, upon loss of E-cadherin, β-catenin originally sequestered by E-cadherin can contribute to cytoplasmic and nuclear pools of the protein. RT-QPCR results for Wnt target gene expression are again inconsistent with immunolabelling. In the double homozygote animals all Wnt target genes are elevated compared with wildtype intestine as expected. However when double homozygote results are compared with *Apc* homozygosity alone, mRNA expression of *C-Myc* and *CD44* is significantly increased but *Axin2* expression is decreased. Given the marked changes seen with immunolabelling for β-catenin, and the widespread use of *Axin2* as a reliable Wnt reporter, the *Axin2* RT-QPCR results were surprising. One possible method of resolving this would be to repeat the experiment including a Wnt reporter mouse (Aoki & Taketo, 2008). Flow cytometry analysis could also add additional information about the correlation between *Cdh1* loss and Wnt target gene upregulation for populations of cells. Another possible explanation is that *Axin2* regulation is more complex than previously thought; indeed a recent paper showed that instead of functioning as a tumour suppressor in CRCs by inhibiting the Wnt pathway, *Axin2* could promote tumour progression through upregulation of *Snail1* (Wu et al, 2012).

This chapter aimed to determine the effect of conditional *Cdh1* homozygosity on the adult mouse intestine, including in the setting of acute homozygous *Apc* loss and in particular whether *Cdh1* loss contributed to Wnt signaling. The results show that E-cadherin has a vital role in maintenance of the barrier function in the intestine and that loss of function results in increased proliferation and apoptosis and changes in the secretory cell lineages, particularly Paneth cell misplacement. There is no convincing evidence that *Cdh1* loss alone

activates the Wnt pathway, however immunolabelling strongly suggests that in the setting of Wnt pathway activation conferred by *Apc* loss, additional loss of *Cdh1* can increase Wnt activity. Whilst this model provides useful information about the effect of *Cdh1* loss *in vivo*, the complex phenotype including acute inflammation, regeneration and apoptosis means it is not an ideal system in which to assess the effect of *Cdh1* loss on Wnt signaling. However, knowing *Cdh1* has a vital role in the intestine and that it may be able to influence Wnt signaling in the setting of *Apc* loss provides a good rationale for investigating this further in tumour models. The following two chapters explore the effect of *Cdh1* loss in the setting of intestinal adenomatosis conferred by *Apc* loss of function.

4 The effect of *Cdh1* heterozygosity on intestinal tumourigenesis

4.1 Introduction

The main introduction outlined a number of mouse models of colorectal cancer and adenomatosis that have contributed to our knowledge of the disease and some of the challenges using these models including the impact of genetic background on the phenotype. The results presented in Chapter 3 showing *Cdh1* has a vital role in intestinal function, and that *Cdh1* loss may result in increased Wnt-signalling competent β-catenin in the setting of *Apc* loss of function, provided a good rationale for investigating the effect of *Cdh1* loss in the setting of intestinal adenomatosis.

Smits and colleagues had previously shown that *Cdh1* heterozygosity conferred a nine-fold increase in intestinal adenoma numbers in an *Apc*1638N model (Smits et al, 2000b). Tumour numbers are relatively low in the *Apc*1638N model, with $Apc^{+/1638N}$ $Cdh1^{+/+}$ animals having 1.24 tumours per animals and $Apc^{+/1638N}$ $Cdh1^{+/-}$ animals having an average of 11.3 tumours per animal. There was also a five-fold increase in gastric tumour numbers with *Cdh1* loss. In this cross $Cdh1^{+/-}$ animals were on a mixed Ola129/129J background and *Apc*1638N animals on a C57BL/6JIco background. There were no differences in the grade or stage of tumours and no evidence of metastatic disease. Tumours from double heterozygote animals showed a tendency towards being smaller, leading the authors to postulate *Cdh1* loss has an effect on adenoma initiation rather than progression. Whereas LOH of *Apc* was common, LOH of *Cdh1* was not observed.

James Harper, a previous PhD student in our group, has shown that *Cdh1* heterozygosity conferred a fourfold increase in adenoma burden on the Apc^{Min} phenotype on a mixed C57BL/6J and 129Ola background. Additionally there was good evidence from mouse models of lobular breast cancer and pancreatic β-islet cell tumourigenesis that *Cdh1* could have an important role in the invasive stage of epithelial tumours (Derksen et al, 2006; Perl et al, 1998).

The aim of the work presented in this chapter was to repeat this germline cross on a C57BL/6J background and characterize any differences attributed to *Cdh1* loss, in particular in relation to Wnt activation. I also aimed to validate the effect of combined *Apc* and *Cdh1* heterozygosity using a conditional approach with *AhCreER*^{T}.

4.2 Methods

General methods are described in Chapter 2. Methods specific to this chapter are described below.

4.2.1 Breeding

In planning for the experiments in this chapter, I aimed to minimize the effect of strain dependent modifiers by aiming for coisogenic strains to produce experimental animals, where ideally animals were all on a C57BL/6J background, differing only at the sites of the relevant mutant alleles.

4.2.1.1 Breeding for $Apc^{+/Min}$ $Cdh1^{+/-}$ cross

In order to restrict strain-specific modifying effects on the Apc^{Min} phenotype, mice from an inbred C57BL6J Apc^{Min} line (line 1) with a specific adenoma number phenotype originally obtained from Professor Andrew Silver (Queen Mary College, University of London) were used. Apc^{Min} line 1 was maintained by brother-sister mating, animals from each generation were culled at 120 days and adenomas scored to ensure a consistent adenoma number and phenotype between successive generations.

$Cdh1^{+/-}$ animals obtained from Professor Alan Clarke (Cardiff University) were originally on a mixed C57BL/6J/129Ola background. They were backcrossed onto a C57BL/6J background for more than 10 generations to create a congenic strain before the breeding strategy used for this experiment was started (Figure 40). This experiment was carried out in a conventional non-SPF animal facility. A similar experimental cross had previously been carried out in our group by James Harper, however the $Cdh1^{+/-}$ animals used for breeding in that instance were still on a mixed background (less than 5 generations of backcrossing to C57BL/6J).

4.2.1.2 Breeding for $Apc^{+/fl}$ $Cdh1^{+/fl}$ Vil-Cre cross

Pilot experiments using $AhCreER^{T}$ (on C57BL/6J background) showed unreliable recombination rates using *Rosa-LacZ* reporter (not shown, carried out by Jennifer Hughes). As a result I decided to switch to a *Vil-Cre* and $Vil\text{-}CreER^{T2}$ strategy. *Vil-Cre* animals were obtained from Professor Elizabeth Robertson (University of Oxford) and were on a B6D2 (C57BL6 x DBA/2) background. Whilst backcrossing the *Vil-Cre* animals onto a C57BL/6J background to create a congenic or speed congenic strain would have been preferable, it

was not feasible within the timeline for these experiments as the animals moved from a conventional to a SPF facility immediately prior to this, requiring a lengthy rederivation period. The *Vil-Cre* animals were backcrossed one generation to generate more *Vil-Cre+* breeding animals (outlined by dashed black box in Figure 41) before being crossed with animals with the conditional alleles of interest. I accepted the experimental animals (outlined by the black box in Figure 41) would be on a mixed C57BL/6J/DBA/2 background, and that modifiers of Min may be present. In particular there was the chance a *Mom-1* modifier may be introduced as C57BL/6 is known to carry the *Mom-1* susceptible allele and DBA/2 carries the *Mom-1* resistance allele (http://www.informatics.jax.org/). I also produced a cohort of animals where the *Villin-Cre* was backcrossed onto C57BL/6J for 2 generations for comparison. This additional step is outlined in Figure 42.

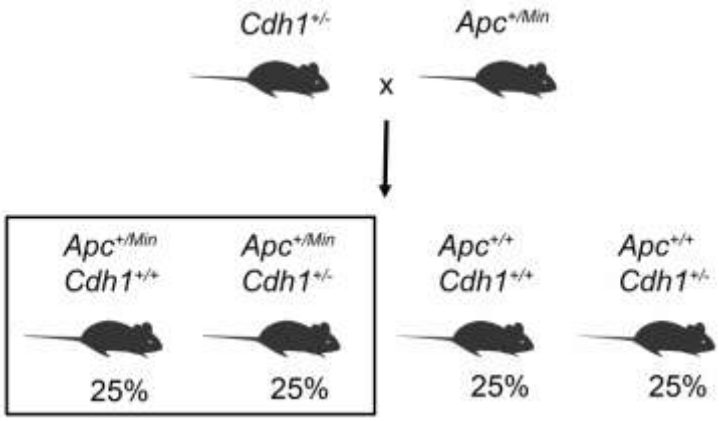

Figure 40. *Apc*$^{+/Min}$ *Cdh1*$^{+/-}$ breeding
Breeding to produce *Apc*$^{+/Min}$ *Cdh1*$^{+/-}$ and *Apc*$^{+/Min}$ *Cdh1*$^{+/+}$ animals (experimental animals shown in black box). Numbers show the percentage of each genotype produced by breeding. *Apc*$^{+/+}$ animals were culled at weaning. C57BL/6J background, backcrossed >10 generations.

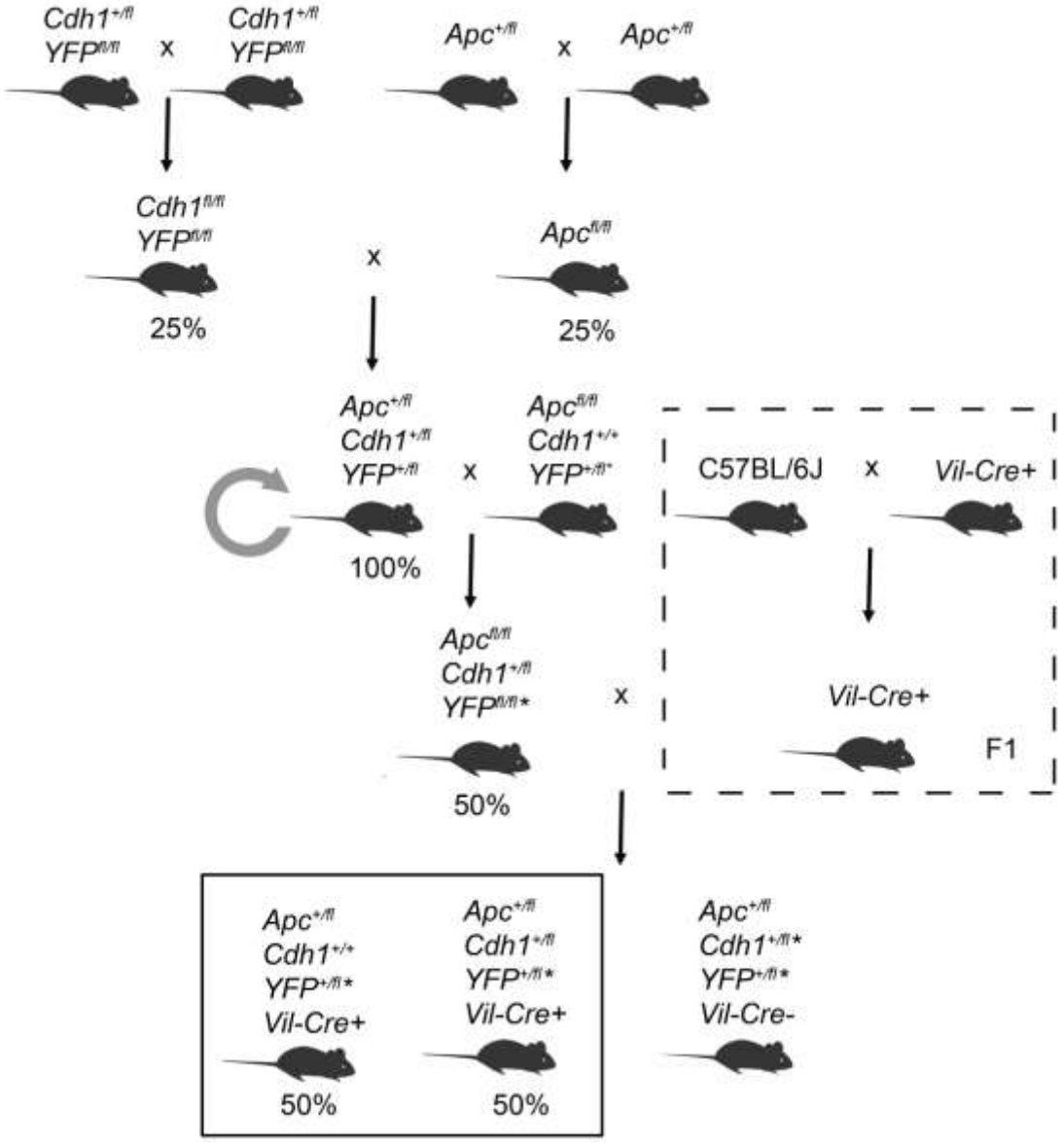

Figure 41. *Apc*$^{+/fl}$ *Cdh1*$^{+/fl}$ *Vil-Cre* breeding

Numbers below mice represent the expected Mendelian ratio of that genotype. *following a genotype (*Cdh1* in *Villin-Cre*- animals, or *YFP*) indicates that for simplicity only heterozygous genotype has been represented in that part of the figure, however *Cdh1* wildtype and *YFP* wildtype and homozygous alleles were also generated. The box with the solid black line outlines experimental animals. The circular arrow represents an intercross step to generate *Apc*$^{fl/fl}$ animals required for the next breeding step. The box with the dashed black outline shows the stage at which backcrossing of *Vil-Cre* to C57BL/6J took place. Figure 42 shows how an additional back cross step could be added.

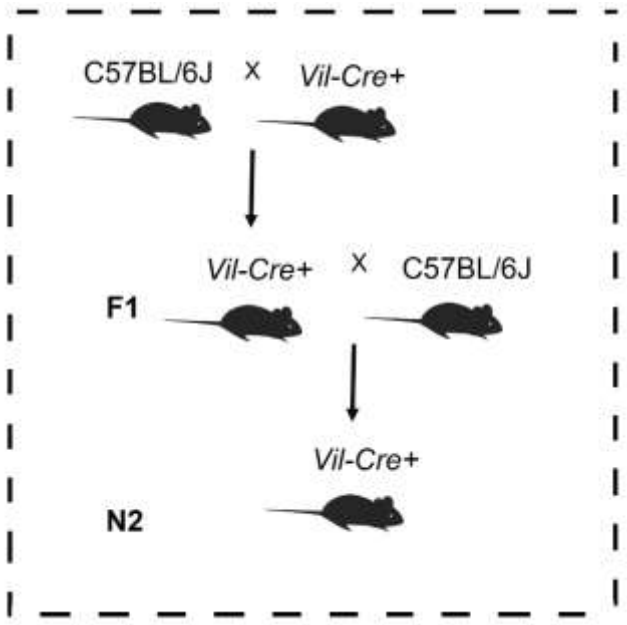

Figure 42. Increased backcrossing of *Vil-Cre* to C57BL/6J
Outline of the additional backcross step that was added for a cohort of animals before *Vil-Cre+* animals were crossed with animals with the conditional alleles of interest as per Figure 41.

4.3 Results

4.3.1 Cdh1 heterozygosity does not modify Apc^{Min} phenotype on a C57BL/6J background

On a mixed C57BL/6J/129Ola background (less than 5 generations backcrossing to C57BL/6J, C57BL/6J 12.5-50%) James Harper showed that *Cdh1* heterozygosity conferred a significant increase in small intestine adenoma burden (Figure 43A). The colonic adenoma burden was very low and was not altered by *Cdh1* status (Figure 43A). There was no significant difference in adenoma sizes or distributions with or without *Cdh1* loss (Figure 43A). It is worth noting that although the difference in small intestinal adenoma burden is highly significant (P<0.0001, student's t-test), the distribution of adenoma counts in the $Apc^{+/Min}$ $Cdh1^{+/-}$ group was very wide. These data concurred with the observations of Smits and colleagues (Smits et al, 2000b).

When I repeated this cross however on a C57BL/6J background, *Cdh1* heterozygosity had no significant effect on small intestinal adenoma burden, colonic adenoma burden, adenoma size or distribution when the animals were censored at 120 days of age (Figure 43B). Disease specific survival to 120 days was 100% for both groups, with any illness or death before 120 days unrelated to adenoma burden. The $Apc^{+/Min}$ $Cdh1^{+/+}$ small intestinal adenoma burden was very similar to that seen in the mixed C57BL/6J/129Ola cross. The colonic adenoma burden was increased with or without *Cdh1* loss on a C57BL/6J background compared with the C57BL/6J/129Ola cross. There was also a non-significant trend towards fewer colonic adenomas with *Cdh1* loss (p=0.0640, student's t-test). These data suggested that strain modified the *Apc Cdh1* interaction. Histology showed tumours of similar grades (majority had low to moderate dysplasia) regardless of *Cdh1* genotype (Figure 45).

4.3.2 Cdh1 heterozygosity does not modify Apc^{Min} survival on a C57BL/6J background

On the C57BL/6J background there was a trend towards a higher proportion of small adenomas (<2mm diameter) with *Cdh1* heterozygosity, so given the unexpected negative results for adenoma numbers I wondered if I was censoring the animals too early. An extended survival analysis of a cohort of animals revealed no significant difference between the $Apc^{+/Min}$ $Cdh1^{+/+}$ control group and the $Apc^{+/Min}$ $Cdh1^{+/-}$ combined animals (Figure 44, Log-rank test).

4.3.3 Cdh1 heterozygosity does not significantly modify Wnt activation in Apc^{Min} adenomas

RT-QPCR confirmed lower levels of *Cdh1* mRNA expression in small intestine and small intestinal adenomas from $Apc^{+/Min}$ $Cdh1^{+/-}$ animals. There was no significant difference in *C-Myc* expression between $Cdh1^{+/+}$ and $Cdh1^{+/-}$ adenomas (Figure 46). The small size of adenomas made sample collection and extraction of high quality RNA challenging. Immunolabelling showed decreased CDH1 protein expression in $Cdh1^{+/-}$ animals. Quantification of the number of adenoma cells with nuclear β-catenin did not show a difference between $Apc^{+/Min}$ $Cdh1^{+/+}$ and $Apc^{+/Min}$ $Cdh1^{+/-}$ animals (Figure 47).

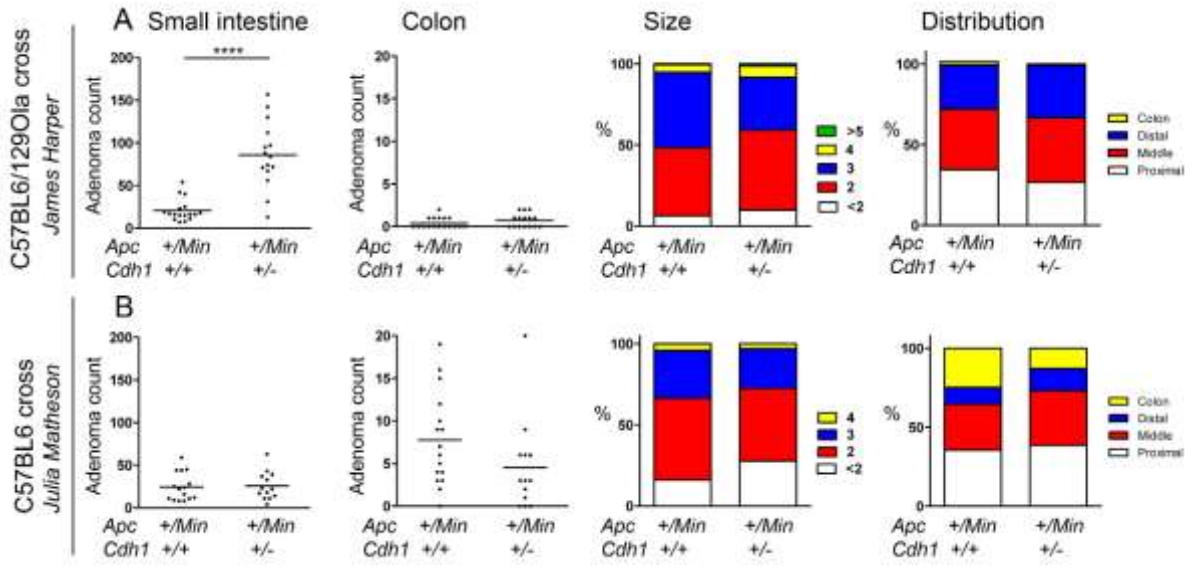

Figure 43. *Cdh1* heterozygosity does not alter *Apc*^{Min} phenotype on a C57BL/6J background
Comparison of the effect of *Cdh1* heterozygosity on the *Apc*^{Min} phenotype at 120 days of age on a mixed C57BL/6J/129Ola background in work carried out by James Harper (**A**), and on a C57BL/6J background in this study (**B**). (**A**) *Apc*$^{+/Min}$ *Cdh1*$^{+/+}$ n=17, *Apc*$^{+/Min}$ *Cdh1*$^{+/-}$ n=15. (**B**) *Apc*$^{+/Min}$ *Cdh1*$^{+/+}$ n=16, *Apc*$^{+/Min}$ *Cdh1*$^{+/-}$ n=13. Student's t-test to compare adenoma counts between genotypes. Size measured in mm. **** p<0.0001.

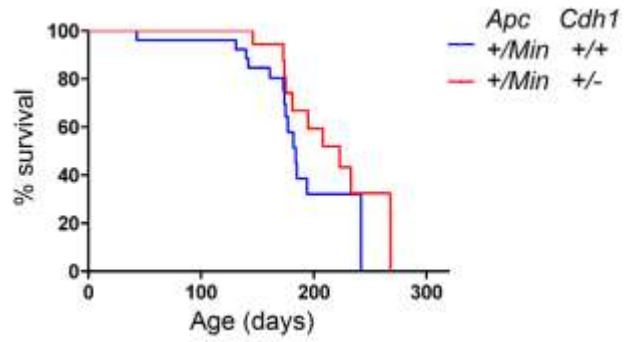

Figure 44. *Cdh1* heterozygosity does not alter survival of *Apc*^{Min} animals on a C57BL/6J background
Survival analysis of *Apc*$^{+/Min}$ animals with or without *Cdh1* heterozygosity. *Apc*$^{+/Min}$ *Cdh1*$^{+/+}$ $n_{\text{defined humane endpoint}}$ =14, $n_{\text{censored before defined humane endpoint}}$=12. *Apc*$^{+/Min}$*Cdh1*$^{+/-}$ $n_{\text{defined humane endpoint}}$=10, $n_{\text{censored before defined humane endpoint}}$ =8. Median age of animals censored: *Apc*$^{+/Min}$ *Cdh1*$^{+/+}$ = 172 days, *Apc*$^{+/Min}$*Cdh1*$^{+/-}$ = 192 days. Log-rank test, p=0.1359.

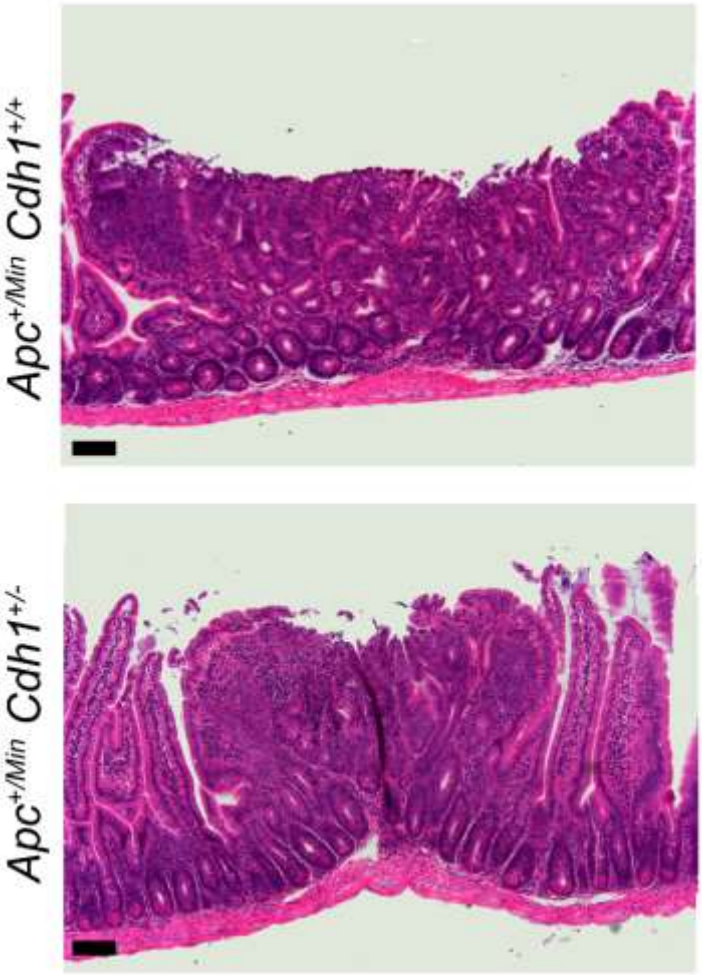

Figure 45. *Apc*$^{+/Min}$ *Cdh1*$^{+/+}$ and *Apc*$^{+/Min}$ *Cdh1*$^{+/-}$ histology
H&E staining showing examples of typical adenomas from *Apc*$^{+/Min}$ *Cdh1*$^{+/+}$ and *Apc*$^{+/Min}$ *Cdh1*$^{+/fl}$ animals. Scale bars 100µm

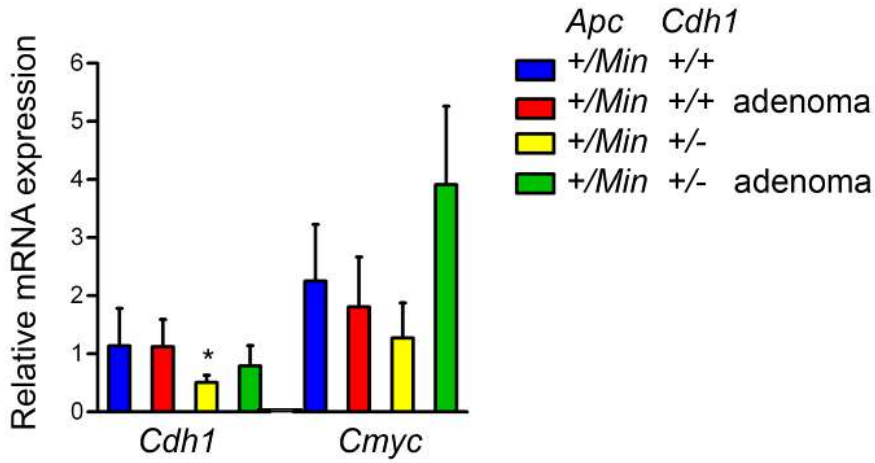

Figure 46. The effect of *Cdh1* heterozygosity on adenoma *Cdh1* expression and Wnt signaling (RT-QPCR)
RT-QPCR of *Cdh1* and *C-Myc* (a Wnt target gene). n>3 mice for each genotype. Reference genes *Gapdh* and *Hprt*. mRNA expression relative to wildtype small intestine. Student's t-test for comparison with wildtype samples. Bars represent means and whiskers standard error of mean. * p<0.05.

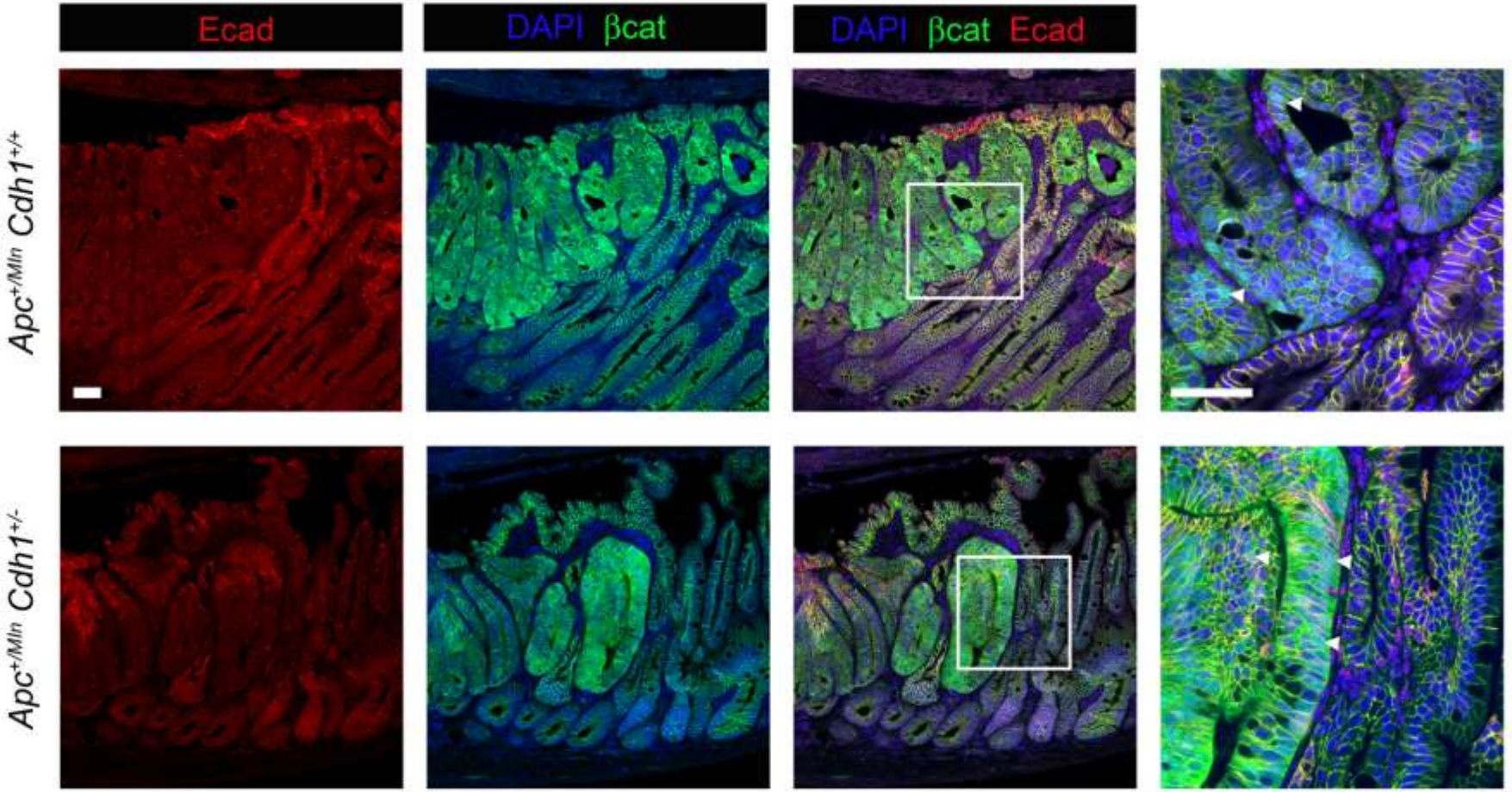

Figure 47. Effect of *Cdh1* heterozygosity on CDH1 expression and β-catenin localisation
Immunolabelling of small intestinal adenomas from $Apc^{+/Min}$ $Cdh1^{+/+}$ and $Apc^{+/Min}$ $Cdh1^{+/-}$ animals for DAPI, E-cadherin and β-catenin. Arrowheads point to examples of nuclear β-catenin. Nuclear β-catenin was assayed by looking for colocalisation of β-catenin and the nuclear marker DAPI in high-power confocal images. There was no significant difference between genotypes in the proportion of adenoma cells with nuclear β-catenin (data not shown). Far right panel shows higher power views of the areas marked with white boxes. CDH1 expression often appeared increased in the epithelium directly adjacent to adenomatous tissue, regardless of *Cdh1* genotype. This may be due to EphB signalling which is known to have a role in the compartmentalization of adenomas through enforced E-cadherin expression. Scale bars 50µm.

4.3.4 Cdh1 heterozygosity modifies Apc$^{+/fl}$ Vil-Cre+ phenotype

As discussed in the methods, two cohorts of experimental animals were established to investigate the effect of *Cdh1* heterozygosity on the *Apc$^{+/fl}$ Vil-Cre+* phenotype: one where *Vil-Cre* on a B6D2 background was backcrossed one generation onto C57BL/6J before it was combined with conditional alleles on a C57BL/6J background, and a second where *Vil-Cre* was backcrossed two generations onto C57BL/6J before combination with the conditional alleles. Animals were aged until they reached a defined humane endpoint. *Cdh1* heterozygosity significantly decreased survival in both crosses, however there were notable differences between the crosses. In the cohort with less C57BL/6J the median survival was 137 days with *Cdh1* heterozygosity or 199 days without (p=0.0019, log-rank test. Figure 48A), whereas in the group with more C57BL/6J median survivals were 97 days and 127 days respectively (p=0.0184, log-rank test. Figure 48B).

On both backgrounds there was a significant increase in adenoma burden in the small and large intestine with *Cdh1* heterozygosity (Figure 48). With *Cdh1* heterozygosity the adenoma count variance was higher, suggesting a modifier may be influencing the results. It would be interesting to investigate this further and given the background strains genotyping for *Mom-1* would be a good initial screen. *Apc$^{+/fl}$ Cdh1$^{+/+}$* animals tended to have a higher proportion of larger adenomas compared to *Apc$^{+/fl}$ Cdh1$^{+/fl}$* animals, which may be a reflection of their increased survival. Interestingly there was not an increase in adenoma number with increased age, in fact regardless of *Cdh1* status there was a negative correlation between age and adenoma count (Figure 49). In the cohort with less C57BL/6J linear regression analysis gave lines with identical slopes, showing that this effect was independent of *Cdh1* (Figure 49A). In the cohort with more C57BL/6J, linear regression analysis gave slopes that were not significantly different (Figure 49B). When the same genotypes from each cross were compared directly, there was a significant difference in survival within the same genotype (p=0.0013 for *Apc$^{+/fl}$ Cdh1$^{+/+}$* animals, p=0.0017 for *Apc$^{+/fl}$ Cdh1$^{+/fl}$* animals, log-rank tests), but no difference in adenoma count (Figure 50) showing strain differences influenced survival rather than adenoma count.

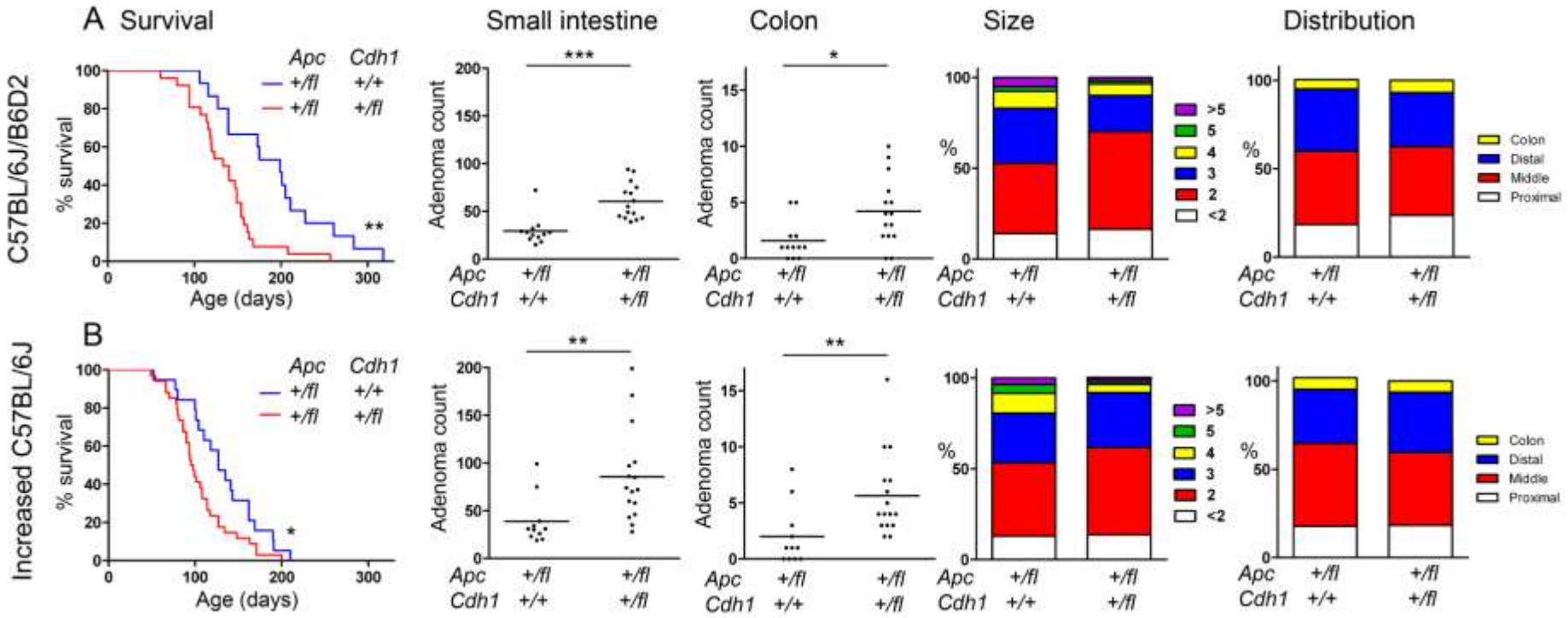

Figure 48. The effect of *Cdh1* heterozygosity on the *Apc*$^{+/fl}$ *Vil-Cre+* phenotype

(**A**) Experimental animals obtained as per breeding in Figure 40. (**B**) Experimental animals obtained with additional backcross step to C57BL/6J as per Figure 41. (**A**) Survival: *Apc*$^{+/fl}$ *Cdh1*$^{+/+}$ n=15, *Apc*$^{+/fl}$ *Cdh1*$^{+/fl}$ n=26. Adenoma phenotyping: *Apc*$^{+/fl}$ *Cdh1*$^{+/+}$ n=12, *Apc*$^{+/fl}$ *Cdh1*$^{+/fl}$ n=15. (**B**) Survival: *Apc*$^{+/fl}$ *Cdh1*$^{+/+}$ n=19, *Apc*$^{+/fl}$ *Cdh1*$^{+/fl}$ n=34. Adenoma phenotyping: *Apc*$^{+/fl}$ *Cdh1*$^{+/+}$ n=11, *Apc*$^{+/fl}$ *Cdh1*$^{+/fl}$ n=16. Macroscopic adenoma counts, adenoma size measured in mm diameter. Log-rank test for survival analysis. Student's t-test for other analysis. * p<0.05, ** p<0.01, *** p<0.001.

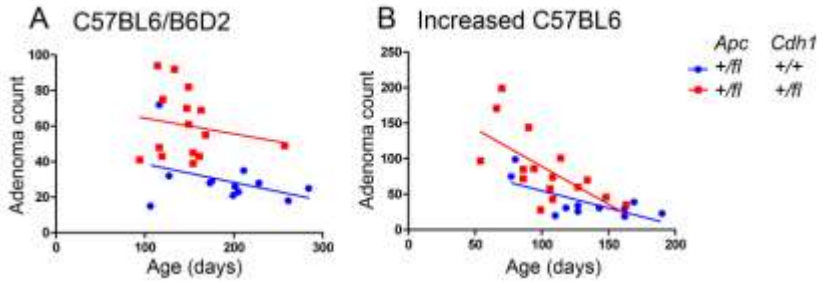

Figure 49. Negative correlation between age to survival and adenoma count, independent of *Cdh1*
Linear regression analysis of age compared with adenoma count for both cohorts of animals (the cross where C57BL6 mice were crossed with B6D2 mice and the cross where there was an additional backcross step to C57BL6). There was no significant difference between the slopes, indicating no difference in the correlation between age and adenoma count between the two strains.

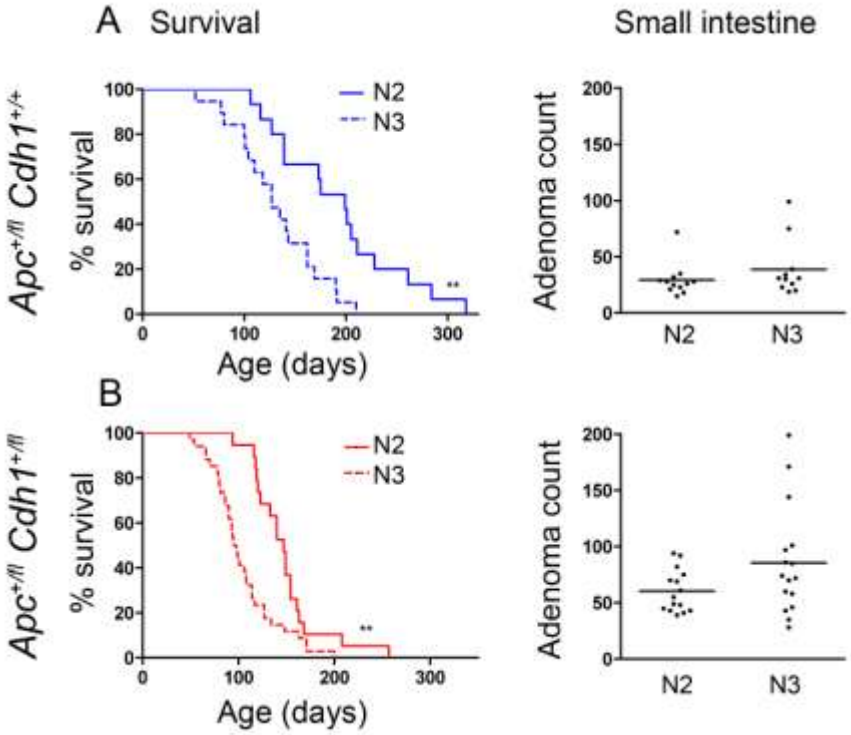

Figure 50. Comparison of survival and small intestinal counts for the same genotypes from different crosses
(**A**) compares survival and small intestinal adenoma counts for *Apc*$^{+/fl}$ *Cdh1*$^{+/+}$ animals when *Vil-Cre+* animals were backcrossed to C57BL/6J once before being crossed with conditional mice on C57BL/6J background (N2) or backcrossed to C57BL/6J twice before being crossed with conditional mice on C57BL/6J background (N3). (**B**) compares *Apc*$^{+/fl}$ *Cdh1*$^{+/fl}$ animals from the same crosses. Log-rank test for survival analysis. Student's t-test to compare adenoma counts. Only statistically significant differences shown. **=p<0.01.

4.3.5 Cdh1 heterozygosity does not appear to augment Wnt signaling in $Apc^{+/fl}$ Vil-Cre+ adenomas

$Apc^{+/fl}$ $Cdh1^{+/+}$ Vil-Cre+ animals tended to have larger adenomas that *$Apc^{+/fl}$ $Cdh1^{+/fl}$ Vil-Cre+* animals but histology showed tumours with a similar spectrum of grades. Examples of small intestinal sessile adenomas and colonic pedunculated villous adenomas are shown in Figure 51. The majority of adenomas were low to moderate grade. There was no evidence of invasive or metastatic disease. Immunolabelling showed similar CDH1 protein expression in *Cdh1* heterozygote and wildtype animals (although exact protein amounts are difficult to assess from imaging). Counting of cells with nuclei positive for β-catenin did not show a significant increase with *Cdh1* loss (mean number of β-catenin positive nuclei 12% and 26% for *$Apc^{+/fl}$ $Cdh1^{+/+}$ Vil-Cre* and *$Apc^{+/fl}$ $Cdh1^{+/fl}$ Vil-Cre* adenomas respectively, p=0.12, student's t-test, Figures 52-53).

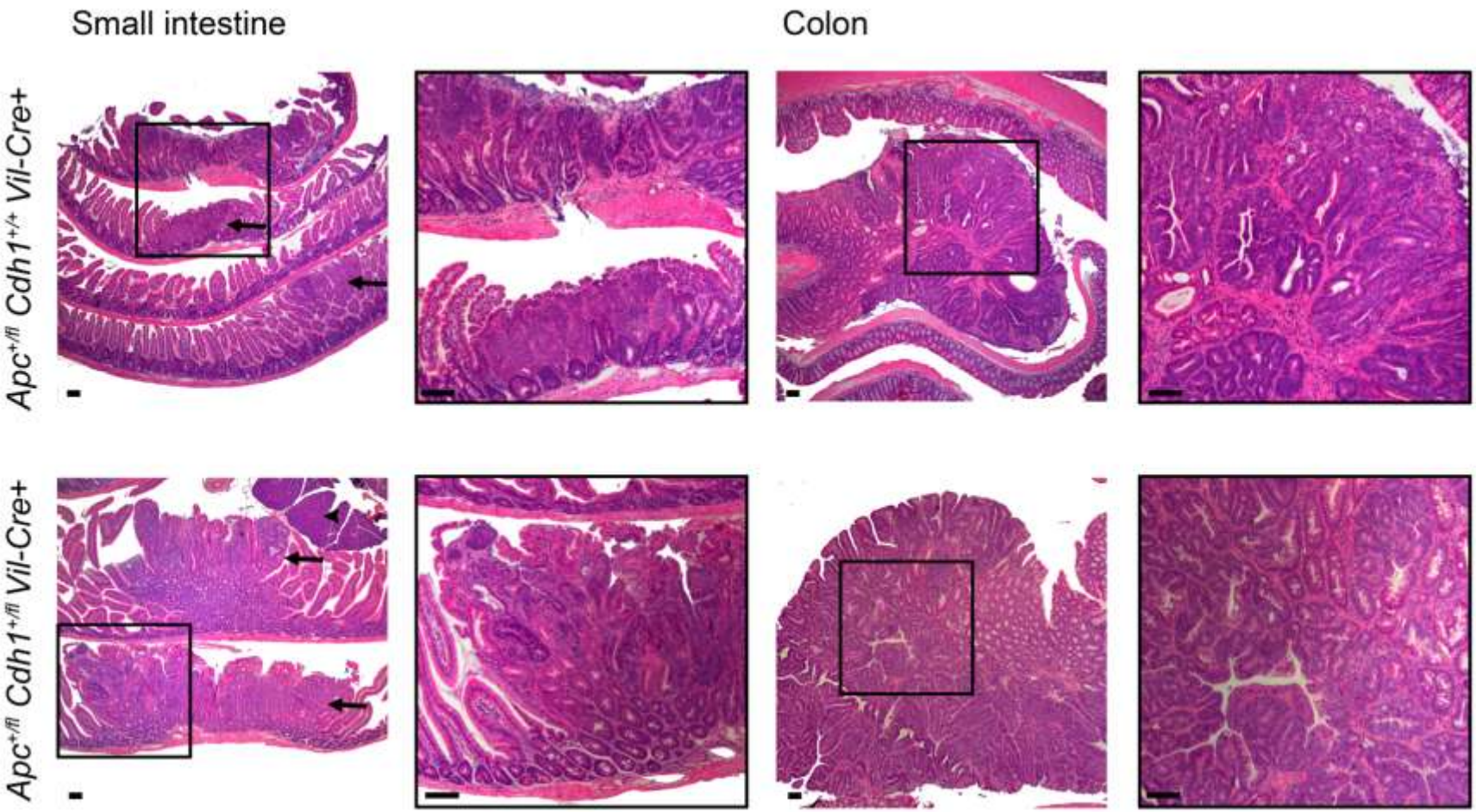

Figure 51. The effect of combined *Apc* and *Cdh1* heterozygosity with *Villin-Cre*: histology
Representative histology from the small intestine and colon of *Apc*$^{+/fl}$ *Cdh1*$^{+/+}$ *Vil-Cre+* and *Apc*$^{+/fl}$ *Cdh1*$^{+/fl}$ *Vil-Cre+* animals showing a similar spectrum of adenomas between genotypes. Arrows point to adenomas in low power views. Arrowhead points to part of a Peyer's patch. Areas marked with boxes are shown at higher power magnification in adjacent panels. Scale bars 100µm.

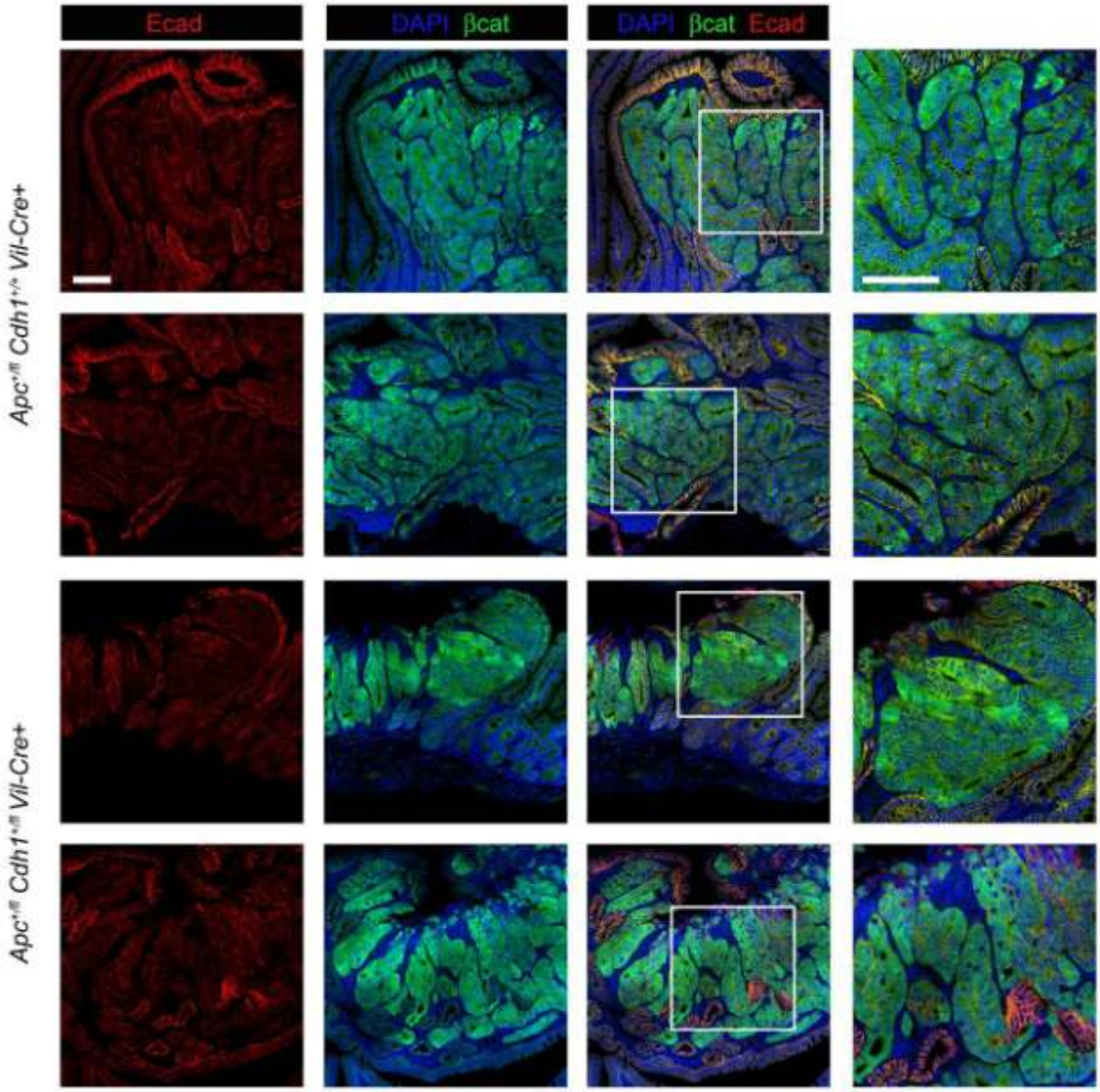

Figure 52. The effect of combined *Apc* and *Cdh1* heterozygosity on E-cadherin and β-catenin expression
Representative immunolabelling of small intestine from *Apc*$^{+/fl}$ *Cdh1*$^{+/+}$ *Vil-Cre* and *Apc*$^{+/fl}$ *Cdh1*$^{+/fl}$ *Vil-Cre* animals for DAPI, E-cadherin and β-catenin. Adenomatous tissue can be identified by morphology and the presence of cytoplasmic and/or nuclear β-catenin. The right panel shows higher power views of the areas marked with boxes. Scale bars 50μm.

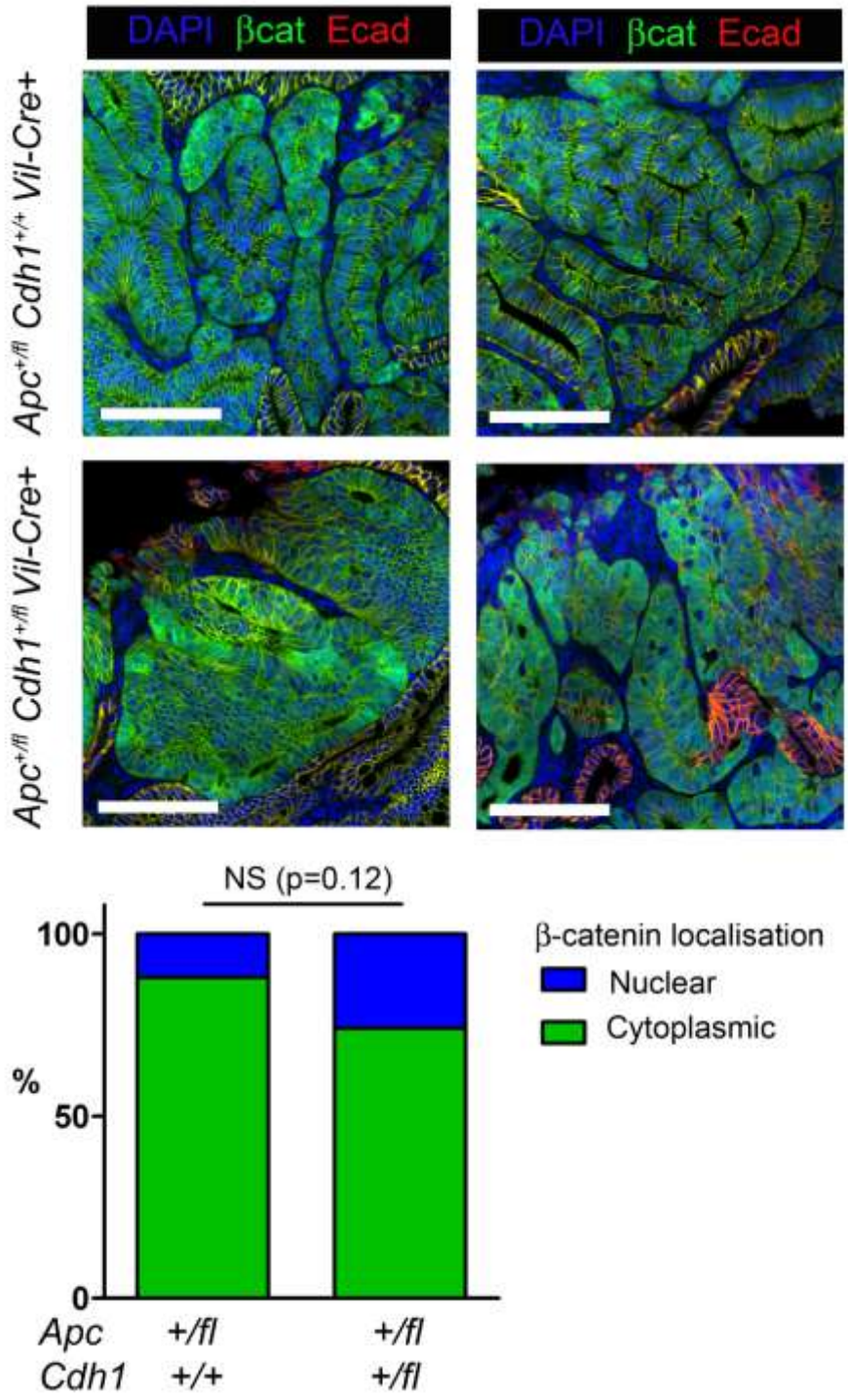

Figure 53. The effect of *Cdh1* heterozygosity on nuclear β-catenin
Immunolabelling of adenomas from *Apc*$^{+/fl}$ *Cdh1*$^{+/+}$ *Vil-Cre* and *Apc*$^{+/fl}$ *Cdh1*$^{+/fl}$ *Vil-Cre* animals for DAPI, E-cadherin and β-catenin. Quantification of the % of adenoma cells with nuclear β-catenin by counting images from at least 3 mice and >3000 cells per genotype. Student's t-test to compare the % of adenoma cells with nuclear β-catenin from at least 3 mice of each genotype showing no significant difference between genotypes. Failure to detect a significant difference may be due to high variability. Scale bar 50μm.

4.4 Discussion

4.4.1 Cdh1 heterozygosity does not modify adenoma number or survival on a C57BL/6J background

The absence of an effect on adenoma count or survival with *Cdh1* heterozygosity in the $Apc^{+/Min}$ model on a C57BL/6J background was unexpected. Given James Harper's positive results on a mixed background and the published effect of *Cdh1* heterozygosity in the *Apc*1638N model the results were highly suggestive of one or more strain dependent modifiers. It must be noted however that as the crosses were not carried out in parallel, environmental effects cannot be excluded. A literature review did not reveal any known modifiers located close to the *Cdh1* locus. We considered conducting linkage analysis but after consultation with experts decided that given the relatively low number of animals, poor quality archival DNA material, potential for confounding factors and lack of familiarity with the techniques involved we may not reach a satisfactory result. *Cdh1* heterozygosity did not have a convincing effect on Wnt signalling.

4.4.2 Cdh1 heterozygosity modifies survival and adenoma phenotype on a mixed background

As discussed in the methods, experimental planning attempted to control for genetic background in the intended conditional cross using $AhCreER^{T}$, with all animals on a C57BL/6J background. Unfortunately unreliable recombination rates with $AhCreER^{T}$ necessitated the change to a *Vil-Cre* approach and those animals were on a B6D2 (C57BL6 x DBA/2) background. Ideally we would have backcrossed these animals onto a C57BL/6 background, however we could not afford the significant time this would take and instead accepted that we would have a mixed background, an increased chance of strain modifying effects and that interpretation of results would need to take this into account. Creating two cohorts of experimental animals, one where *Villin-Cre* had a further backcross step before combination with the conditional alleles, was an approach to see if an additional backcross step had any effect on phenotype.

In both experimental cohorts $Apc^{+/fl}$ $Cdh1^{+/fl}$ *Vil-Cre* animals had significantly reduced survival and increased adenoma burdens, both in the small intestine and the colon, when compared with $Apc^{+/fl}$ $Cdh1^{+/+}$ *Vil-Cre* animals. The effect of *Cdh1* loss on adenoma number rather than adenoma size or grade suggests *Cdh1* may be having an effect on adenoma

initiation, for example by promoting *Apc* LOH. To explore this further, LOH analysis could be performed for adenomas from both genotypes. The difference in survival between the two genotypes was less significant with increased backcross to C57BL/6J. When the same genotypes from different crosses were compared there was no significant difference in adenoma burden, but there was a marked difference in survival with animals on an increased C57BL/6J background reaching the defined humane endpoint earlier. This finding after only a single additional backcross step was surprising. Whilst it provided some reassurance that the *Cdh1* effect was more likely to be a true genetic effect as it was replicated in both cases, it also highlighted the potential for strain dependent effects. As mentioned already *Mom-1* would be a possible modifier given the variability in adenoma counts observed with *Cdh1* heterozygosity. *Mom-1* is known to affect tumour multiplicity and the two background strains in this cross, C57BL/6 and DBA/2, are known to carry *Mom-1* susceptibile and resistance alleles respectively. Genotyping for these *Mom-1* alleles would be a prudent and relatively straight-forward next step to investigate the involvement of modifiers. We also considered using an Illumina GoldenGate SNP genotyping array to look for potential modifying loci, however DNA extracted using the HOTshot method could not be purified adequately to achieve the required sample quality. The HOTshot method of DNA extraction is fast, cost effective and provides reliable genotyping results, however the poor sample purity means that the use of DNA extracted using this method for other applications is limited. Thus for future experiments whilst this method is appropriate for initial genotyping, an alternative method that obtains high quality DNA samples to archive should be conducted on postmortem samples.

4.4.3 Cdh1 heterozygosity does not convincingly modify Wnt signaling in the setting of intestinal tumours initiated by Apc loss of function

The analysis to date shows that tumours from $Apc^{+/fl}$ $Cdh1^{+/fl}$ animals do not have a significantly increased incidence of cells with nuclear β-catenin compared with $Apc^{+/fl}$ $Cdh1^{+/+}$ animals. This suggests that *Cdh1* heterozygosity does not modify Wnt signalling in the setting of an impaired β-catenin destruction complex. Further work is required to confirm this definitively (such as RT-QPCR to assay Wnt target gene activation) however the finding is consistent with no effect on the Wnt pathway seen with *Cdh1* heterozygosity in the $Apc^{+/Min}$ model.

An improved model for assessing the effect of *Cdh1* loss on intestinal tumourigenesis would facilitate homozygous loss of *Cdh1* in the setting of *Apc* loss of function. Homozygous deletion of *Apc* using *Lgr5-IRES-EGFP-CreER*^{T2}, specifically in intestinal progenitor cells, leads to rapid adenoma formation and bypasses the lethality effect seen with Cre recombinases with high recombination efficiency (Barker et al, 2009). The next chapter uses this model to assess the effect of combined *Apc* and *Cdh1* homozygosity.

This chapter highlights the problem of strain dependent modifiers in mouse models of tumourigenesis. Careful experimental planning is required to minimize confounding results due to strain effects, and unfortunately this often requires lengthy and expensive backcrossing steps. Interpretation of data from mouse models must be considered in the context of the background strain. For this work, investigation for a *Mom-1* modifier would be a sensible next step.

5 The effect of combined *Cdh1* and *Apc* homozygosity using *Lgr5-Cre*

5.1 Introduction

Apc homozygosity, either in germline mutants or intestinal-specific conditional models associated with high levels of recombination, is lethal (Andreu et al, 2005; Moser et al, 1995; Sansom et al, 2004). Models of colorectal cancer based on *Apc* loss have mimicked the sequence of events common in human CRCs: mutation of one *Apc* allele, followed by LOH of the second allele leading to the formation of an aberrant crypt focus. *Cdh1* homozygosity is also lethal in the germline and as outlined in Chapter 3 lethal with high levels of recombination in the intestine.

In 2007 Nick Barker and colleagues identified the elusive intestinal stem cell (Barker et al, 2007). The Wnt target gene *Lgr5* exclusively marked cycling crypt base columnar cells that gave rise to all four cell lineages of the intestine over a 60 day period. They also created a mouse knockin expressing tamoxifen inducible Cre recombinase under the *Lgr5* promoter allowing for intestinal stem cell specific deletion of genes of interest. Activation of this Cre with a single injection of 2mg tamoxifen IP resulted in transformation of cells in about 6% of crypts, a relatively low level of recombination. Homozygous deletion of *Apc* using *Lgr5-Cre* resulted in transformation of these cells within days leading to rapid microadenoma formation and macroscopic adenomas within 3-5 weeks (Barker et al, 2009). Not only did this identify *Lgr5* positive cells as the cells of origin of adenomas, but also provided an extremely useful tumour model that could bypass the lethality effect of widespread homozygous *Apc* loss in the intestine, and generate tumours rapidly without relying on sporadic LOH events. In these tumours *Lgr5* positive cells made up about 6.5% of the tumour cell population. Recently using lineage retracing and the multicolour Cre reporter *R26R-Confetti* mouse, they have provided proof of the cancer stem cell hypothesis using this model showing *Lgr5* cells maintain the growth of adenomas (Schepers et al, 2012).

Given the strain dependent results regarding the effect of *Cdh1* heterozygosity on intestinal tumourigenesis, I decided to used *Lgr5-Cre* to activate homozygous recombination of both *Apc* and *Cdh1*. *Lgr5-Cre* has the advantage of being able to induce non-lethal homozygous

Apc loss and generate tumours more rapidly than the $Apc^{+/Min}$ and $Apc^{+/-}$ *Vil-Cre* models described in Chapter 4.

5.2 Methods

General methods are described in Chapter 2. Methods specific to this chapter are described below.

5.2.1 Breeding

The breeding to generate $Apc^{fl/fl}Cdh1^{fl/fl}$ $YFP^{fl/fl}$ *Lgr5-Cre+* animals is outlined in Figure 54. $Apc^{fl/fl}Cdh1^{fl/fl}$ $YFP^{fl/fl}$ animals were on a C57BL/6J background. *Lgr5-Cre* animals were obtained with Hans Clevers' permission from Dr David Adams (Wellcome Trust Sanger Institute) and were on a 129P2/OlaHsd background. Again whilst the preference would be to have the *Lgr5-Cre* line on a C57BL/6J background, I was limited by the strain available at the time and the time-frame for extensive backcrossing was prohibitive.

5.2.2 Activation of Cre recombination in vivo

Cre recombination was activated in adult mice at 8-12 weeks of age by intraperitoneal injection of tamoxifen in corn oil. Tamoxifen solution was prepared as described in Chapter 2, Section 2.7.1. Pilot experiments used a single dose of 2mg tamoxifen IP, however $Apc^{fl/fl}$ animals remained well without pallor or weight loss at one month, only reaching the defined endpoint 100 days following injection. With a single dose of 5mg tamoxifen, animals started becoming unwell between 34 and 78 days following injection. Previous experiments had shown that two doses of 200mg/kg tamoxifen on successive days (10mg total tamoxifen for a 25mg mouse) was tolerated, so this regime was adopted with consistent results (all animals becoming unwell within 2 months of injection). The complex breeding precluded the use littermate controls that were $Apc^{+/+}$ $Cdh1^{+/+}$ *Lgr5-Cre+*, so animals negative for *Lgr5Cre* were injected as controls. Animals were weighed at least once daily in the first five days following injection.

5.2.3 Detection of Cre recombination in vivo

Cre recombinase activation was detected using the *Rosa-YFP* reporter and genotyping for recombined *Apc* and *Cdh1* alleles (as described in Chapter 2, Section 2.7.2 and Appendix 1).

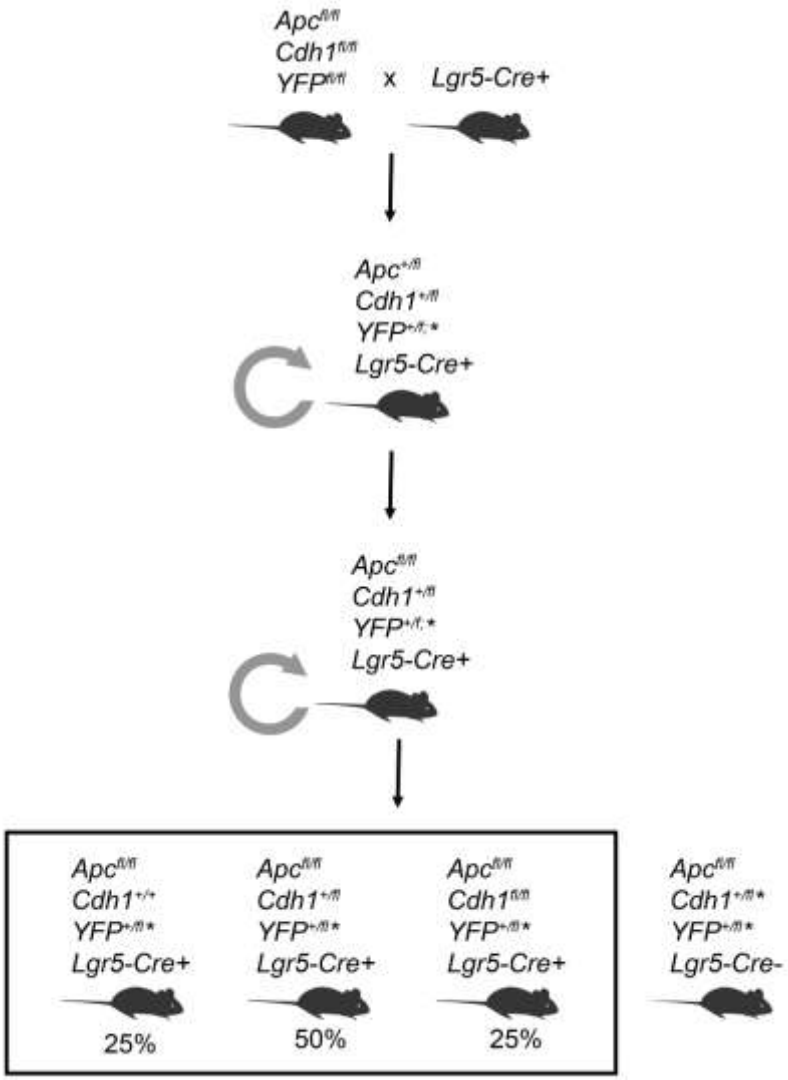

Figure 54. *Apc$^{fl/fl}$Cdh1$^{fl/fl}$ Lgr5-Cre* breeding

Numbers below mice represent the expected Mendelian ratio of that genotype. *following a genotype indicates that for simplicity only the heterozygous genotype has been represented in that part of the figure, however *Cdh1* and *YFP* wildtype and homozygous alleles were also generated. The box outlines experimental animals. The circular arrows represent an intercross step to generate *Apc$^{fl/fl}$* animals required for the next generation.

5.2.4 Adenoma culture

The adenoma culture protocol was obtained from Professor Owen Sansom (Beatson Institute, Glasgow) and is an adapted version of that published by the Clevers group (Sato et al, 2011a). Table 23 lists details of the reagents used.

When an animal was at or close to the defined humane endpoint (and thus had a significant tumour burden) necropsy was carried out. Caecal tumours were taken preferentially for culture due to their larger size. The tumour was cut from the intestine using scissors and placed in ice-cold PBS. Dissection was carried out as quickly as possible and a maximum of three mice dissected at one time for this protocol. Each adenoma was cut into small pieces using scissors in ice cold sterile PBS. The adenoma was washed 4-5 times using PBS to remove debris with slow centrifuge spins (1200rpm, 5 minutes each) between washes. The adenoma was then incubated in 5mM EDTA in PBS for 10 minutes at room temperature, shaken vigorously to deplete remaining villi and washed 2-3 times using PBS (without calcium and magnesium) to remove EDTA. Next, cells were incubated in 5ml 10x Trypsin (5mg/ml), supplemented with 100U DNase (to prevent clumping of the cells), at 37°C for 30 minutes. Subsequent wash steps used ADF medium (details in Table 23) warmed to 37°C. The cell solution was shaken vigorously, centrifuged at 1200rpm for 3 minutes and the supernatant removed. The remaining adenoma cells were then resuspended in 5ml ADF and dissociated by hard pipetting, before being centrifuged and the supernatant being collected in a separate 50ml tube. This resuspension, dissociation, centrifuge step was repeated five times, with any remaining adenoma being transferred to the new tube following the final step. The solution was filled up to 50ml with ADF, passed through a 70µm cell strainer and centrifuged at 1200rpm for 5 minutes before removing the supernatant, washing twice with ADF to remove any traces of trypsin. The cells were resuspended in 1ml ADF, and counted using a NucleoCounter (Chemotech) that assessed cell number, the proportion of single cells and viability. The NucleoCounter uses fluorescence microscopy and image analysis to assess cell number by labelling with Acridine Orange and cell viability by labelling with DAPI that can only reach the nucleus of a cell if the cell membrane is compromised.

3000 viable cells were plated per well in 24-well plates. A glass coverslip was placed in each well prior to plating of cells. For each well, 35µl matrigel was combined with 35µl cell suspension (3000 cells in ADF). Enough matrigel/cell suspension mix was made for only 12

wells at a time so that the mixture could be pipetted easily without the matrigel solidifying. The plates were incubated at 37°C for 10 minutes to solidify the matrigel, then 500µl of ADF supplemented with N2, B27, EGF and Noggin was added to each well. A similar protocol exists for the culture of intestinal and colonic crypts, however this protocol requires the addition of R-spondin to provide the Wnt drive necessary for crypt viability (Sato et al, 2009). The absence of R-spondin in adenoma culture ensures that any intestinal cells in the culture that are not adenoma cells do not survive.

Adenoma organoids could be maintained by weekly passage and plating in new matrigel. To do this the medium was removed from each well, the tip was cut off a 1000ml pipette tip (to create a larger aperture) and a 1000ml pipette was used to aspirate the matrigel and collect it in a 15ml tube. A fire-polished glass pipette with an aperture of 0.5-1mm was used to mechanically dissociate matrigel and organoids, they were washed 2-3 times with ADF, counted and plated as above. It was more difficult to obtain single cell suspensions on passage than at primary culture, so primary culture was preferred particularly when activating Cre recombination.

Table 23. Reagents for adenoma culture

Reagent (supplier)	Details	Working concentr-ation	Preparation	Final concentration
Growth factor reduced matrigel (BD)	Protein mixture secreted by Engelbreth-Holm-Swarm mouse sarcoma cells, includes collagen, laminin and entactin and is used for 3D cell culture systems	1x	Thawed on ice at 4° C overnight. Diluted 1:1 with cell suspension immediately prior to plating	0.5x
Advanced DMEM/F12 media, ADF (Invitrogen)	Advanced Dulbecco's Modified Eagle Medium/ Ham's F-12, reduced serum medium	1x	To a 500ml bottle, add 5ml Glutamine, 5ml 1M HEPES, 5ml Pen/Strep. Aliquot 48.5ml into 50ml tubes and store at -20° C	1x
N2 (Invitrogen)	Serum-free supplement used for neuronal cell applications	100x, 500µl aliquots	One aliquot added to 48.5ml ADF immediately before use	1x
B27 (Invitrogen)	Serum-free supplement used for neuronal cell applications	50x, 1ml aliquots	One aliquot added to 48.5ml ADF immediately before use	1x
EGF (Peprotech)	Epidermal growth factor	100ng/ml, 650µl aliquots	Powder resuspended in PBS/0.1% BSA to make 1µg/µl stock. 10µl of 1µg/µl stock diluted in 10ml PBS/0.1%BSA to make working stock	5ng/ml (add 50µl of working stock per ml of media)
Noggin (Peprotech)	BMP inhibitor	5µg/ml, 400µl aliquots	Powder resuspended to make 5µg/ml stock in PBS/0.1% BSA	0.1µg/ml (add 20µ of working stock to each ml of media)

5.2.5 Activation of Cre recombination in vitro

As will become apparent in the results section, *Apc*$^{fl/fl}$ *Cdh1*$^{fl/fl}$ *Lgr5-Cre* adenomas had persistent E-cadherin expression following Cre activation with tamoxifen *in vivo*. Therefore recombination of *Cdh1* was reattempted *in vitro*.

5.2.5.1 Activation of Cre recombination in vitro using 4-hydroxytamoxifen

An initial attempt was made to activate Cre recombination *in vitro* using 4-hydroxytamoxifen (Sigma) It was appreciated that recombination efficiency would rely on the number of cells expressing *Lgr5* in the adenomas and that whilst *Lgr5* is a Wnt dependent gene and would be expected to be upregulated in adenomas, the level of recombination may still be prohibitively low. Adenomas were cultured as per Section 5.2.4. On day 5 following culture 4-hydroxytamoxifen dissolved in 100% ethanol was added to selected wells to achieve a final concentration of 500nM. The same volume of 100% ethanol (5µl) was added to control wells.

5.2.5.2 Activation of Cre recombination in vitro using viral construct

An adenovirus expressing Cre recombinase under the cytomegalovirus (CMV) promoter was obtained from Vector Biolabs (Ad-Cre). This recombinant human adenovirus type 5 lacks the E1 region of the virus that encodes genes involved in viral replication and is thus replication deficient. It also has the E3 region deleted as this is not required for viral growth *in vitro*. The adenoviral vector was chosen as it was reported to have high efficiency of gene delivery and be well tolerated by mammalian cells.

A multiplicity of infection (MOI) of 500 with Ad-Cre has previously been shown to confer efficient gene delivery with minimal effects on cell viability in cultures of mouse embryonic fibroblasts (Hawley et al, 2010). MOI 500 was used for pilot experiments and well tolerated. The below calculations were used to calculate the volume of virus stock solution required:

Estimated number of cells = number of cells plated x $2^{(\text{number of days since plated/passaged})*}$
**Assumes doubling of the number of cells each day*

Viruses needed = desired MOI x number of cells
Volume of virus stock needed = viruses needed/concentration of virus stock

For example to plate 3000 cells/well and infect with MOI 500 on the day of culture:
Virus stock solution: $1x10^{10}$ plaque forming units (PFU)
Estimated number of cells = $3000 \times 2^0 = 3000$ cells
Viruses needed = 500 x 3000 = 1,500,000
Volume of virus stock needed = $1.5x10^6/1x10^{10} = 0.00015mL = 0.15\mu l$/well

In the initial experiments adenomas were transfected with Ad-Cre 2-3 days following culture and plating. A stock of virus solution was made in ADF so that 5µl would confer the correct number of viruses per well. 5µl of this stock was added to each well and mixed by gentle shaking. For subsequent experiments cells were transfected on the day of culture before being embedded in matrigel. The cell suspension was aliquoted to provide the correct number of cells for 12 wells, the appropriate number of viruses were added to the cell suspension and incubated for 10 minutes before the suspension was mixed with matrigel and plated. All experiments included four experimental arms to control for adenoma genotype (*Cdh1*$^{+/+}$ or *Cdh1*$^{fl/fl}$) and transfection with Ad-Cre (+ or -):

1) *Apc*$^{fl/fl}$ *Cdh1*$^{+/+}$ Ad-Cre-
2) *Apc*$^{fl/fl}$ *Cdh1*$^{+/+}$ Ad-Cre+
3) *Apc*$^{fl/fl}$ *Cdh1*$^{fl/fl}$ Ad-Cre-
4) *Apc*$^{fl/fl}$ *Cdh1*$^{fl/fl}$ Ad-Cre+

5.2.6 Detection of Cre recombination in vitro

Detection of Cre recombination *in vitro* was challenging. As *Lgr5-Cre* had already been activated with tamoxifen *in vivo*, the *Rosa-YFP* reporter was already being expressed and thus could not be used to identify cells when Cre recombinase was activated again *in vitro*. Immunolabelling with an anti Cre recombinase antibody to detect Cre recombinase expression and anti E-cadherin antibody to detect loss of E-cadherin expression was performed.

5.2.7 EDTA treatment

As described previously Ca^{2+} is essential for maintaining the stability of the first extracellular domain of E-cadherin and has a role in modulating the strand swapping required for adhesion (Harrison et al, 2005). The common use of EDTA in tissue culture to detach cells and create cell suspensions takes advantage of the inhibitory effect of this chelation agent on cadherin-mediated adhesion through the sequestration of Ca^{2+}. Thus a simple way of assessing the effect of loss of cadherin-mediated adhesion on adenomas in culture is treatment with EDTA. Obviously this must be interpreted with caution as restriction of Ca^{2+} supply may have effects on cells other than abrogating adhesion. Coverslips with adenomas from *Apc*$^{fl/fl}$ *Cdh1*$^{+/+}$ *Lgr5-Cre* animals on day five following culture were used. The cell culture medium was removed, the coverslip washed once with PBS (without calcium and

magnesium), treated with 500µl 2.5mM EDTA in PBS (pH7.4) for 10 minutes, washed again with PBS, then left in calcium free medium for 48 hours. The calcium free medium used was Keratinocyte Serum Free Medium with L-Glutamine and without Calcium Chloride (Gibco). Unfortunately the suppliers would not release full formulation details.

5.2.8 Live cell imaging

Time lapse microscopy of adenoma samples was conducted using a Zeiss LSM510 META confocal microscope and LSM5 software. Initial attempts to image multiple samples using a 24 well plate were unsuccessful due to movement of coverslips when the stage changed position to scan samples sequentially and suboptimal environmental control. Imaging was thus carried out for a single sample at one time. A sample on a coverslip, covered by 500µl medium, was placed in a centre well organ culture dish (Falcon) and this was enclosed within a chamber with controlled temperature (37°C), humidity and pH (through CO_2 induction). Images were taken every 2 minutes for between 24 and 72 hours using a 10x objective. Imaging was monitored regularly and the focus adjusted as needed.

.lsm files from LSM5 software were loaded into FIJI (http://fiji.sc/) and converted to a .tiff stack. This stack was then saved as an uncompressed .avi movie file with 29 frames per second.

5.2.9 Immunolabelling of adenomas

A modified version of the protocol described in Chapter 2, Section 2.8 was used to immunolabel adenomas in culture. Medium was aspirated from wells and 1ml of 4% paraformaldehyde was added to each well for 10 minutes to fix the adenomas. Fixation was carried out at room temperature and also resulted in dissolution of the matrigel. Care was taken with subsequent pipetting steps to pipette at the edge of the coverslip/well to minimize disruption and loss of adenomas and encourage adhesion of adenomas to the glass coverslip. Each sample was washed in PBS three times, blocked for one hour with 10% serum (same source as secondary antibody, Vector laboratories), 0.5% triton in TBS (20µl serum and 1µl triton in 179µl TBS). Samples were incubated with the primary antibody in 3% serum, 0.3% triton and TBS (6µl serum and 0.6µl triton in 193.4µl TBS) overnight on a rocking platform. The following day they were washed in TBS (3x 3 minutes) and incubated with secondary antibody in TBS for 2 hours (details of antibodies in Tables 16 and 17) and

protected from bright light. They were then washed in TBS (3x 3 minutes), incubated with DAPI (1:5,000 in TBS, 10 minutes), washed again in TBS and coverslips were mounted on glass slides with ProLong Gold antifade reagent (Invitrogen). Staining was checked using an Olympus BX60 fluorescent microscope and images were taken using an Olympus confocal microscope.

5.2.10 EdU labelling

To assay proliferation *in vitro* adenoma organoids were labelled with the thymidine analogue 5-ethynyl-2'-deoxyuridine (EdU). The Invitrogen Click-iT® EdU Alexa Fluor® 555 Imaging kit was used. EdU uses click chemistry rather than antibody detection of the incorporated nucleoside so does not require the DNA denaturation step needed with BrdU labelling. Organoids were labelled with EdU as per the manufacturer's instructions: a 2X working solution of EdU was prepared in ADF and 500µl of this solution was added to the 500µl of ADF already in each adenoma culture well to achieve a final EdU concentration of 10µM. Organoids were incubated with EdU for 2 hours at 37°C before fixation, washing and blocking as per Section 5.2.9. Next, 0.5ml of Click-iT® reaction cocktail was added to each sample and incubated at room temperature for 30 minutes protected from light. The reaction cocktail was then removed, the sample washed in TBS before proceeding to labelling with primary antibodies for other markers of interest as per section 5.2.9.

5.2.11 Image analysis

Tumour scoring was carried out blinded to genotype by Professor Hans Morreau (Leiden University Medical Center). Other image analysis was carried out using Olympus Fluoview and ImageJ software. The development of a method to analyse images is described in the results section. Heat maps were created using R software (*R Development Core Team*, 2008).

5.2.12 Flow cytometry

To detect expression of E-cadherin, β-catenin and cleaved caspase 3 using flow cytometry, adenoma organoids were detached from coverslips, dissociated from matrigel and disrupted into cell suspensions by careful pipetting using a 1ml tip with an enlarged aperture. Samples were then washed twice in PBS and fixed in 4% paraformaldehyde for 10 minutes. After blocking in 10% goat serum and 0.5% triton in TBS adenoma cell samples

were incubated with the appropriate fluorochrome-conjugated monoclonal antibodies or Ig isotype control antibody (Table 18) for 30 minutes. Flow cytometry analysis was performed on a FACSCalibur (BD Biosciences) and data analysed using FlowJo software.

5.3 Results

5.3.1 Cdh1$^{fl/fl}$ did not modify survival or adenoma phenotype

Apc$^{fl/fl}$ Lgr5-Cre animals reached the experimental endpoint within 2 months following injection. *Cdh1* genotype had no effect on survival with median survivals of 36, 32 and 41 days for *Cdh1$^{+/+}$*, *Cdh1$^{+/fl}$* and *Cdh1$^{fl/fl}$* respectively (Figure 55). *Cdh1* status also had no significant effect on adenoma count or adenoma size (Figure 55).

5.3.2 Apc$^{fl/fl}$ Lgr5-Cre animals develop caecal tumours

One finding was that *Apc$^{fl/fl}$ Lgr5-Cre* animals frequently had large caecal tumours at dissection. Caecal tumours were rare in *Apc* heterozygosity tumour models. Examples of the tumours and caecal weights are shown in Figure 565, with *Cdh1* status having no effect on the size of these tumours. Ileocaecal intussusceptions were often present, particularly in animals whose condition deteriorated quickly (example in Figure 57).

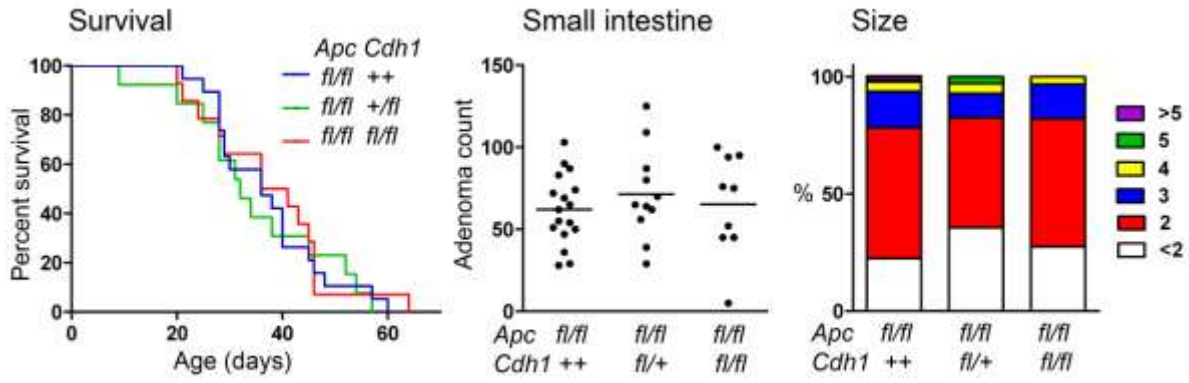

Figure 55. *Cdh1* homozygosity has no effect on *Apc*$^{fl/fl}$ *Lgr5-CreER*^{T2} survival and adenoma phenotype
Survival analysis showing no significant difference between genotypes, log rank test, *Apc*$^{fl/fl}$ *Cdh1*$^{+/+}$ n=19, *Apc*$^{fl/fl}$ *Cdh1*$^{+/fl}$ n=13, *Apc*$^{fl/fl}$ *Cdh1*$^{fl/fl}$ n=14. Small intestine adenoma counts and adenoma sizes (in mm diameter) showing no significant difference between genotypes, one-way ANOVA with Bonferroni post test, *Apc*$^{fl/fl}$ *Cdh1*$^{+/+}$ n=17, *Apc*$^{fl/fl}$ *Cdh1*$^{+/fl}$ n=11, *Apc*$^{fl/fl}$ *Cdh1*$^{fl/fl}$ n=9.

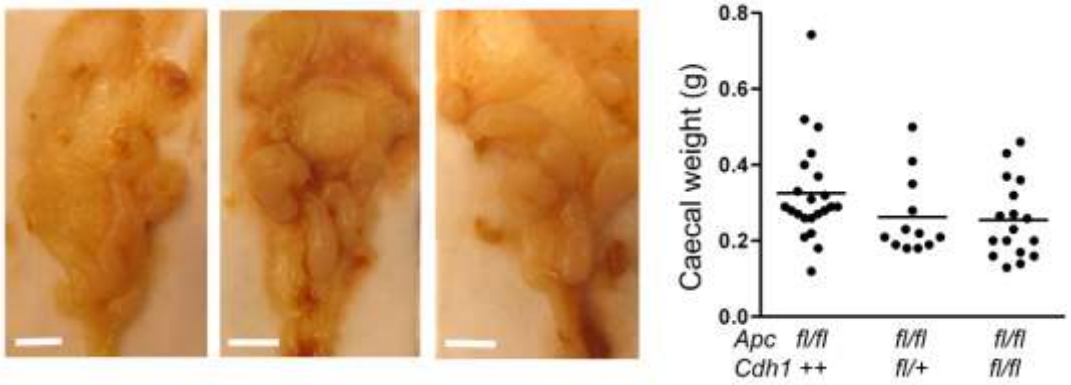

Figure 56. Caecal tumours at dissection
Examples of caecal tumours at dissection. The caecum has been opened longitudinally in each case. Caecal weights showing no significant difference between genotypes, one-way ANOVA with Bonferroni post test, *Apc*$^{fl/fl}$ *Cdh1*$^{+/+}$ n=22, *Apc*$^{fl/fl}$ *Cdh1*$^{+/fl}$ n=12, *Apc*$^{fl/fl}$ *Cdh1*$^{fl/fl}$ n=17. Scale bar 0.5cm. The large volume of caecal tumours seen in this model was an advantage for adenoma culture techniques.

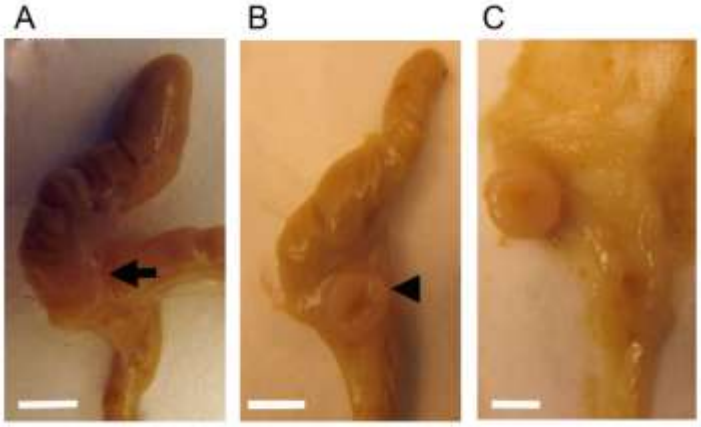

Figure 57. Ileocaecal intussusception
(**A**-**C**) show an example of an ileocaecal intussusception where part of the ileum has invaginated into the caecum. The arrow in (**A**) points to the ileocaecal junction. The ileum is dilated. The arrowhead in (**B**) points to an adenoma visible when the ileum has been opened, a possible cause for the invagination. (**C**) shows the intussusceptum when the caecum has been opened longitudinally. Scale bars 0.5cm.

5.3.3 Cdh1 status had no effect on tumour histology

H&E staining of caecal tumour samples and intestinal and colonic swiss rolls were assessed by Professor Hans Morreau who was blinded to genotype. There was a wide spectrum of disease severity. Out of 20 small intestinal swiss rolls assessed all but two (both *Apc$^{fl/fl}$ Cdh1$^{+/fl}$ Lgr5-Cre*) showed diffuse adenomatosis, including microadenomas that would not have been visible when counting intestinal whole mounts. Cystic changes were common and dirty necrosis (necrotic cellular debris in the lumen of intestinal glands) observed. Most tumours were sessile adenomas with low grade dysplasia however tumours with high grade dysplasia (HGD) or focal areas of carcinoma *in situ* (CIS) were present in all genotypes (Table 24). There was no evidence of invasive disease. The number of histology samples assessed was too small to draw definite conclusions regarding a correlation between adenoma grade and genotype, but from the samples assessed HGD and CIS were less common with *Cdh1* loss. Examples of small intestinal and caecal tumour histology are shown in Figures 58 and 59.

Table 24. Number of high grade tumours for each genotype
Number of samples showing HGD or CIS/total number of samples assessed for that genotype

Genotype	HGD	CIS
Apc$^{fl/fl}$ Cdh1$^{+/+}$ Lgr5-Cre	3/10	1/10
Apc$^{fl/fl}$ Cdh1$^{+/fl}$ Lgr5-Cre	2/15	1/15
Apc$^{fl/fl}$ Cdh1$^{fl/fl}$ Lgr5-Cre	1/14	1/14

5.3.4 CDH1 was not completely lost in Apc$^{fl/fl}$ Cdh1$^{fl/fl}$ Lgr5-Cre tumours

Genotyping of tumours revealed the presence of the recombined *Apc* allele and some residual intact loxP flanked product for adenomas regardless of *Cdh1* genotype. For *Apc$^{fl/fl}$ Cdh1$^{+/+}$* adenomas there was no evidence of a recombined *Cdh1* product, but the recombined product was present in *Apc$^{fl/fl}$ Cdh1$^{+/fl}$* and *Apc$^{fl/fl}$ Cdh1$^{fl/fl}$* tumours. Tumours with a recombined *Cdh1* product had residual intact loxP flanked product also (Figure 61). Immunolabelling showed robust expression of *RosaYFP* and cytoplasmic β-catenin in tumours. CDH1 expression was reduced in both *Apc$^{fl/fl}$ Cdh1$^{+/fl}$* and *Apc$^{fl/fl}$ Cdh1$^{fl/fl}$* tumours in areas where *RosaYFP* was expressed, but more so in the double homozygotes. In no areas however was CDH1 completely lost despite thousands of cells being viewed by confocal

microscopy (Figure 60). RT-QPCR showed *Cdh1* mRNA levels in $Apc^{fl/fl}$ $Cdh1^{fl/fl}$ tumours was no different to adjacent non-adenomatous tissue (Figure 62).

It is known that the recombination efficiency may differ between conditional alleles using *Lgr5-Cre* (Schepers et al, 2012). A possible explanation for these results was incomplete recombination of *Cdh1* in all cells where recombination had been activated. We knew however from the $Cdh1^{fl/fl}$ *Vil-CreER*^{T2} model that the $Cdh1^{fl}$ allele was not refractive to recombination. An alternative hypothesis was that the absence of any cells with *RosaYFP* activation and cytoplasmic β-catenin expression (indicating *Apc* loss of function) with complete CDH1 loss could mean that combined homozygous *Apc* and *Cdh1* loss was associated with changes in *Lgr5* cell survival.

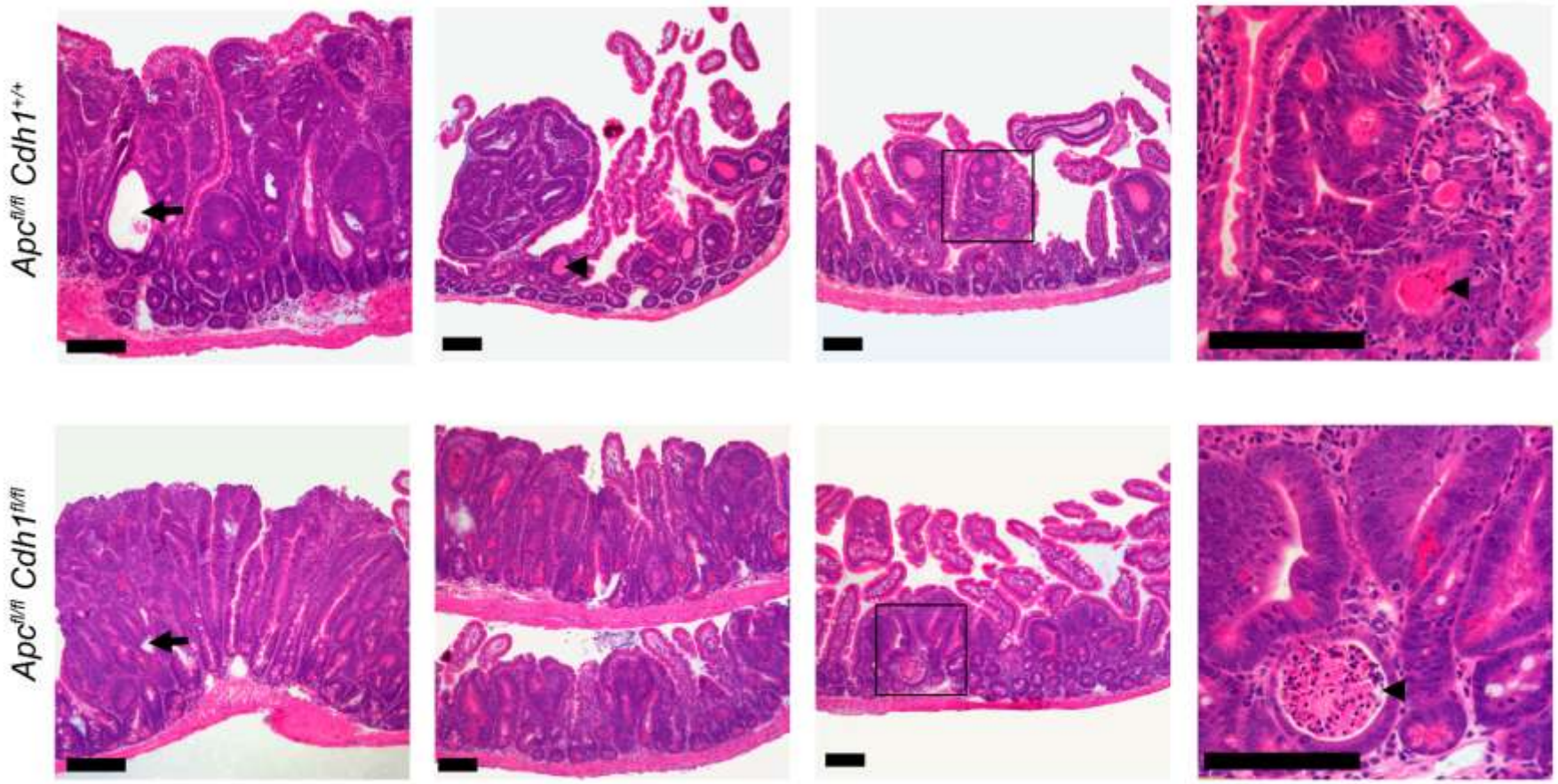

Figure 58. *Cdh1* homozygosity has no effect on *Apc*$^{fl/fl}$ *Lgr5-CreER*^{T2} small intestine histology
Representative histology (H&E) from *Apc*$^{fl/fl}$ *Cdh1*$^{+/+}$ *Lgr5-CreER*^{T2} and *Apc*$^{fl/fl}$ *Cdh1*$^{fl/fl}$ *Lgr5-CreER*^{T2} animals showing sessile adenomas, diffuse adenomatosis, dirty necrosis (arrowheads, necrotic cellular debris within the lumen of neoplastic glands) and cystic changes (arrows) in both genotypes. Far right panel shows higher power views of the areas marked with boxes. Scale bars 100µm.

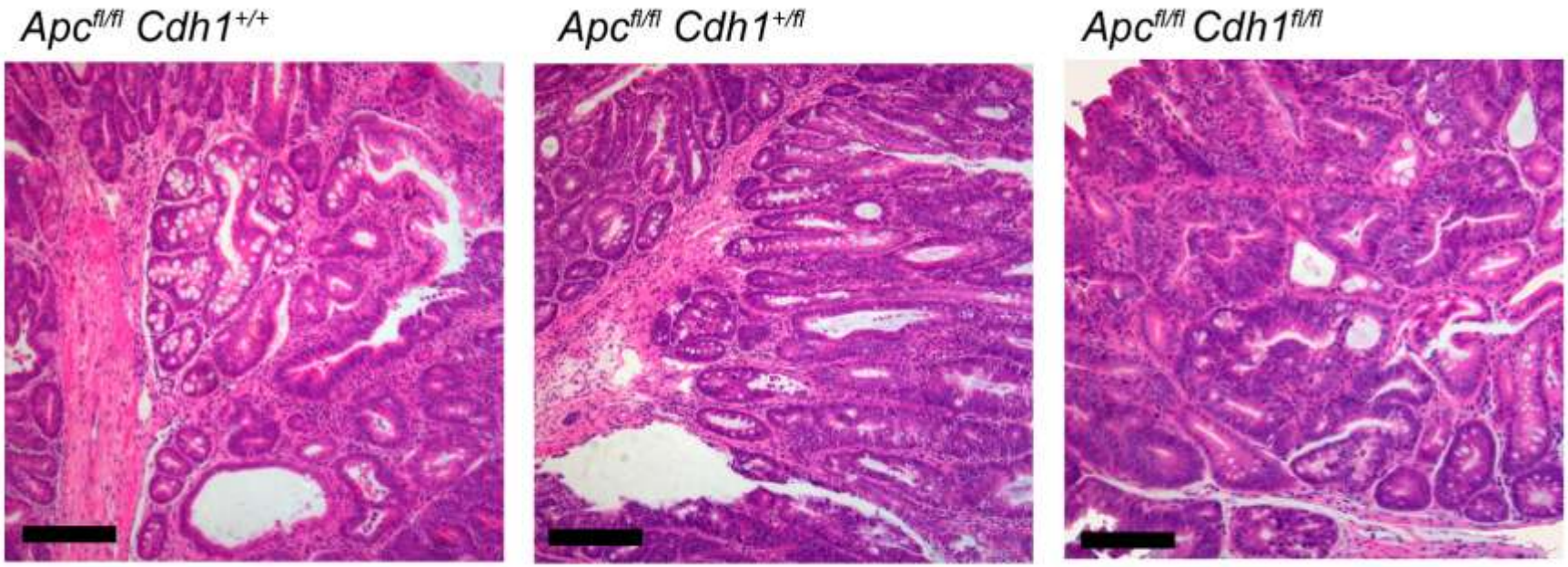

Figure 59. *Cdh1* heterozygosity or homozygosity has no effect on *Apc*$^{fl/fl}$ *Lgr5-CreER*^{T2} caecal tumour histology
Representative histology (H&E) of caecal tumours from *Apc*$^{fl/fl}$ *Cdh1*$^{+/+}$ *Lgr5-CreER*^{T2}, *Apc*$^{fl/fl}$ *Cdh1*$^{+/fl}$ *Lgr5-CreER*^{T2}and *Apc*$^{fl/fl}$ *Cdh1*$^{fl/fl}$ *Lgr5-CreER*^{T2} animals showing a similar spectrum of adenoma grades. Scale bars 100µm

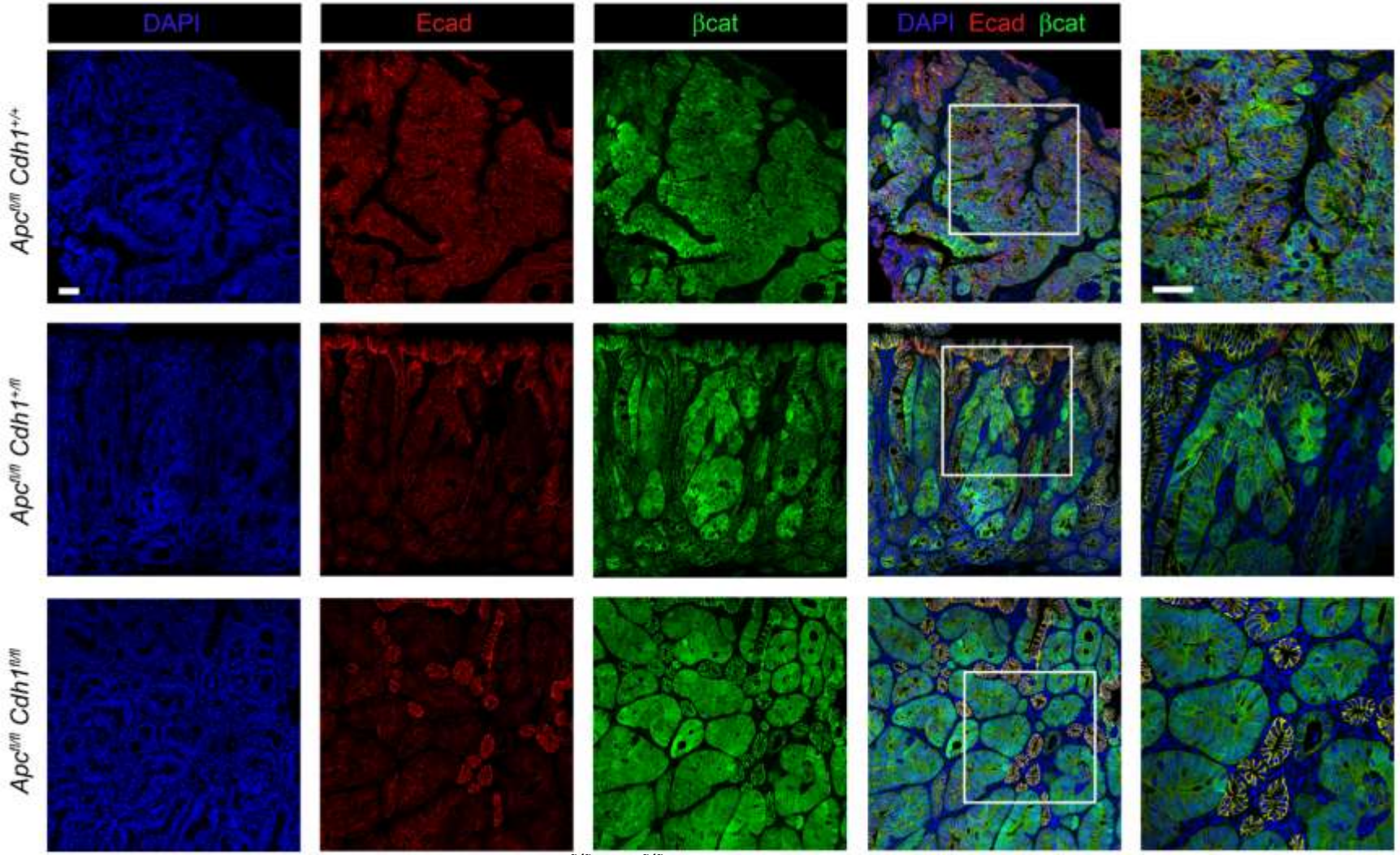

Figure 60. E-cadherin is reduced but never completely lost in *Apc$^{fl/fl}$ Cdh1$^{fl/fl}$ Lgr5-Cre* tumours

Immunolabelling of small intestinal tumours from *Apc$^{fl/fl}$ Cdh1$^{+/+}$ Lgr5-CreER^{T2}*, *Apc$^{fl/fl}$ Cdh1$^{+/fl}$ Lgr5-CreER^{T2}* and *Apc$^{fl/fl}$ Cdh1$^{fl/fl}$ Lgr5-CreER^{T2}* animals for DAPI, E-cadherin and β-catenin. E-cadherin is reduced but never completely lost in tumours from *Apc$^{fl/fl}$ Cdh1$^{+/fl}$ Lgr5-CreER^{T2}* and *Apc$^{fl/fl}$ Cdh1$^{fl/fl}$ Lgr5-CreER^{T2}* animals. Far right panel shows higher power views of the areas marked with white boxes. Scale bars 50μm.

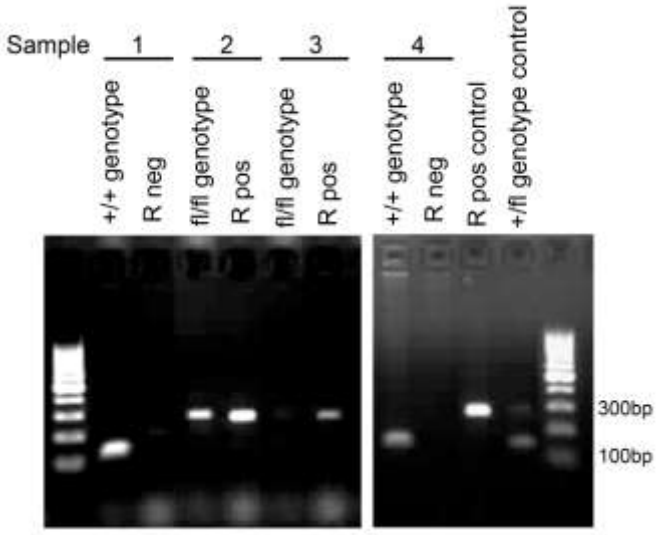

Figure 61. Genotyping for recombined *Cdh1*^{fl} allele
Genotyping of adenomas, including for presence of a recombined *Cdh1*^{fl} allele (R pos). Because the genotyping reactions for unrecombined *Cdh1*^{fl} (fl genotype) and recombined *Cdh1*^{fl} (R pos) gave products of similar sizes they were carried out separately. On the far right are two controls: a positive control for recombined *Cdh1*^{fl} (R pos control) and a control for a known *Cdh1*$^{+/fl}$ genotype showing the *Cdh1*$^{+}$ and *Cdh1*^{fl} bands. Samples 1 and 4 are examples of results for *Apc*$^{fl/fl}$ *Cdh1*$^{+/+}$*Lgr5* tumours showing the wildtype genotyping band in the left lane and no recombined *Cdh1* allele in the right lane. Samples 2 and 3 are examples of results for *Apc*$^{fl/fl}$ *Cdh1*$^{fl/fl}$ *Lgr5* tumours showing the *Cdh1*$^{fl/fl}$ genotype in the left lane (very weak in sample 3 indicating a high recombination rate in this adenoma) and positive recombined allele in the right lane.

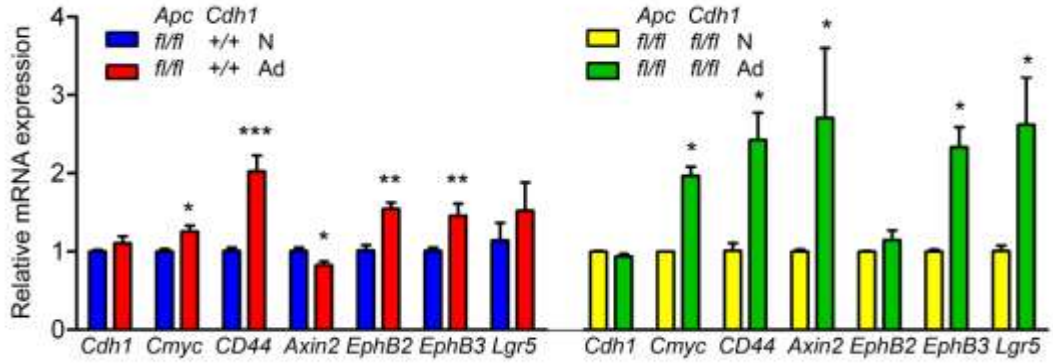

Figure 62. Persistent *Cdh1* mRNA expression in *Apc*$^{fl/fl}$ *Cdh1*$^{fl/fl}$ *Lgr5-Cre+* tumours regardless of *Cdh1* status
RT-QPCR of *Cdh1* and Wnt target genes in caecal adenoma (Ad) compared with normal caecal tissue (N) from the same animal. Reference genes *Gapdh* and *Hprt*. n>3 animals. Student's t-test to compare mRNA expression in adenoma sample compared with matched normal tissue. There is upregulation of Wnt target genes in adenomas from both genotypes. There is no significant decrease in *Cdh1* mRNA expression in adenomas from *Apc*$^{fl/fl}$ *Cdh1*$^{fl/fl}$ *Vil-CreER*^{T2} animals. Whiskers standard error of mean. *=p<0.05. **=p<0.01. ***=p<0.001.

5.3.5 Cdh1 recombination rechallenge in vivo

I attempted to reactivate recombination in *Lgr5* positive cells in $Apc^{fl/fl}Cdh1^{fl/fl}$ adenomas *in vivo*. At the outset I realized that this strategy may not be successful as the known recombination efficiency of *Lgr5-Cre* is only about 6% so detecting cells where a second recombination event had taken place could be extremely difficult, particularly as I couldn't rely on a reporter allele that was already active. I took an $Apc^{fl/fl}$ $Cdh1^{fl/fl}$ animal that had received two doses of 200mg/kg tamoxifen IP 28 days previously, so would be expected to have a significant tumour burden, but was at that time well. This animal was given another single dose of 200mg/kg tamoxifen IP and monitored carefully. Four days following the additional tamoxifen the animal was unwell with weight loss, pallor and bloody diarrhea. At dissection there were fibrotic bands in the abdominal cavity suggesting peritonitis and fresh blood in the intestine. Histology was notable for adenomas with disrupted structure and cell shedding, large Peyers patches, cystic areas and prominent dirty necrosis with large glandular cysts containing cellular debris (Figure 64). Apart from the cell shedding these features had however all been observed previously in $Apc^{fl/fl}$ *Lgr5-Cre* animals. This animal was one of the few generated from the breeding strategy that was wildtype for *Rosa-YFP*, meaning that an anti-GFP antibody could be used to label *Lgr5-Cre* cells. Careful analysis of a number of tumours identified a small number of *Lgr5* cells that may be positive for cleaved caspase 3 (Figure 65).

In a second pilot experiment three $Apc^{fl/fl}$ $Cdh1^{fl/fl}$ animals received the usual two doses of 200mg/kg tamoxifen IP and then two further doses 16 days later at a stage when they were likely to have adenomas but had not yet reached the defined humane endpoint. The animals that were rechallenged with tamoxifen had reduced survival: a median survival of 20 days compared with 41 days for double homozygote animals only receiving the initial tamoxifen doses (log-rank test, p=0.0072, Figure 63). Two of the three animals became unwell 4 days after the second round of tamoxifen, with one of these again showing evidence of peritonitis. The third became unwell two weeks later. Adenoma counts in the rechallenged group varied widely, with the animals that became unwell quickly having low or moderate adenoma numbers and the animal that became unwell later having an adenoma count higher than any other $Apc^{fl/fl}$ $Cdh1^{fl/fl}$ animals. Animals that were rechallenged with tamoxifen had a higher proportion of smaller adenomas. This may have

been due to the earlier time of death. Histology again showed some adenomas with areas of haemorrhage and unusual architecture but no invasive areas (Figure 64).

There are obvious flaws with the above pilot experiments including very small sample sizes and the lack of a control group of $Apc^{fl/fl}$ $Cdh1^{+/+}$ animals being rechallenged with tamoxifen. Whilst one must be wary of overinterpreting the observations, they did raise some interesting questions. One could postulate that the peritonitis seen with two of the animals could be due to intestinal perforation at the time of injection, however given this was a very rare complication of IP injection (about 1% of animals in my hands) it seems unlikely. Was a second hit of recombination of *Cdh1* in adenomas causing intestinal perforation, either directly or as a result of focal inflammation or apoptosis? Was it a coincidental that the animal that survived more than 4 days following the second round of injections had a very high adenoma burden? If not, was *Cdh1* loss in preexisting adenomas increasing tumourigenesis, or were naïve $Apc^{fl/fl}$ *Lgr5-Cre* cells being recombined resulting in a second wave of adenomas contributing to the burden?

Whilst these questions were intriguing it was immediately apparent that achieving satisfactory answers to any of these questions *in vivo* would be challenging. The known relatively low abundance of *Lgr5* positive cells in tumours, compounded by the low levels of recombination with *Lgr5-Cre* meant the frequency of a second recombination event would be low and the effects may be quite subtle. The lack of suitable *in vivo* imaging modalities would preclude the analysis of tumour progression in an individual mouse and given heterogeneity, a large number of animals would be required to achieve necessary experimental power even if a large effect was seen. This provided good rationale for moving to an *in vitro* adenoma culture system.

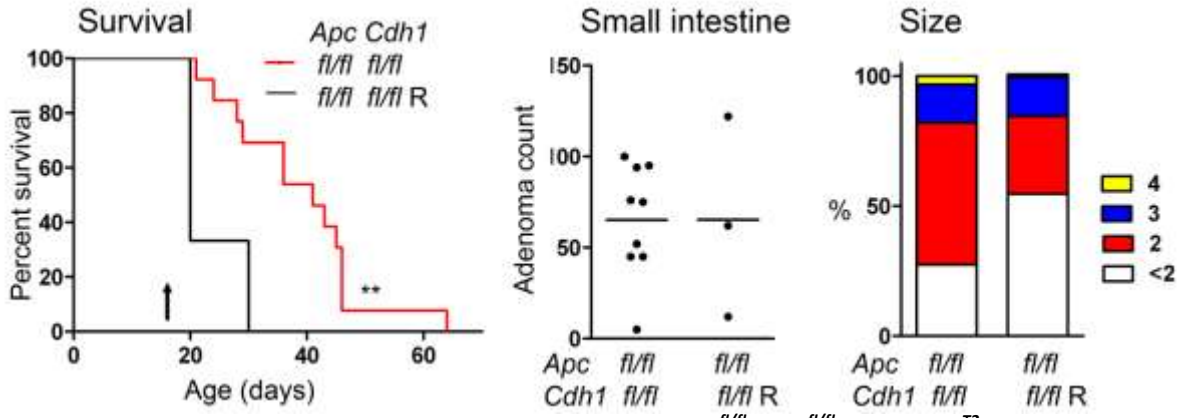

Figure 63. Survival and small intestine adenoma phenotype in *Apc$^{fl/fl}$ Cdh1$^{fl/fl}$ Lgr5-CreER^{T2}* animals with tamoxifen rechallenge

Three *Apc$^{fl/fl}$ Cdh1$^{fl/fl}$ Lgr5-CreER^{T2}* animals were treated with a second round of tamoxifen injections 16 days after the initial injections (arrow on survival graph marks second injection point). R=rechallenged. There was a significant difference in survival as analysed by log-rank test. There was no significant difference in adenoma count between the two groups however there was a significant difference in adenoma size (measured in mm diameter), with the rechallenged group having a higher proportion of smaller adenomas (student's t-test, $p<0.01$). **=$p<0.01$.

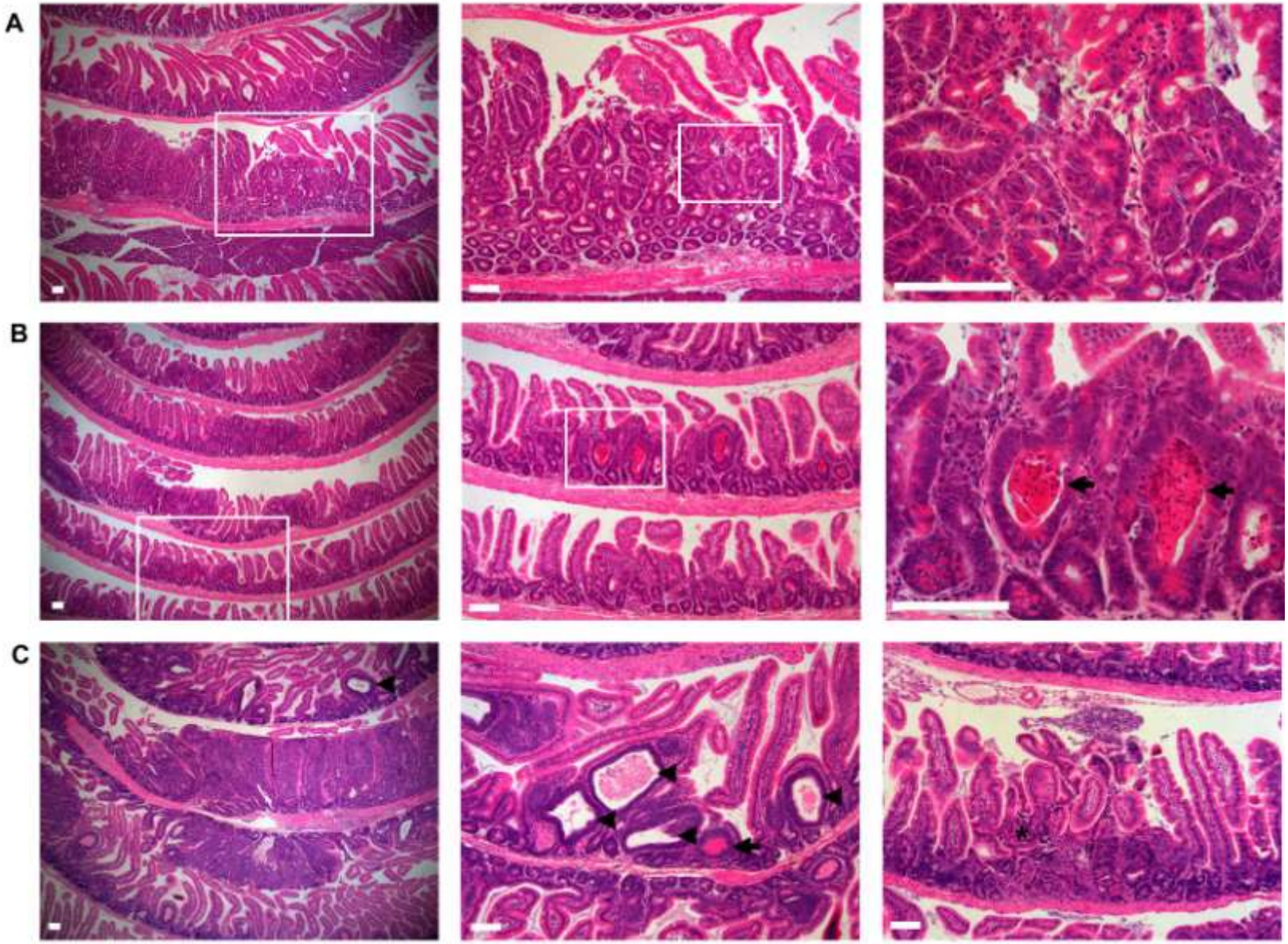

Figure 64. Representative small intestinal histology from *Apc*$^{fl/fl}$ *Cdh1*$^{fl/fl}$ *Lgr5-CreER*^{T2} animals rechallenged with tamoxifen

H&E staining. For (**A**) and (**B**) areas marked with white boxes are shown at higher power in images to the right. (**A**) example of widespread adenomatous change, and a large Peyers patch. High magnification shows adenoma with disrupted architecture and cell shedding. (**B**) Widespread adenomatous changes with multiple foci of dirty necrosis (black arrows). (**C**) Three examples of adenomas, from left to right: large sessile adenomas on a background of diffuse adenomatosis with prominent cystic changes; marked cystic change (black arrowheads) and glands with dirty necrosis (black arrows); disruption of adenoma structure (black star). Scale bars 100µm.

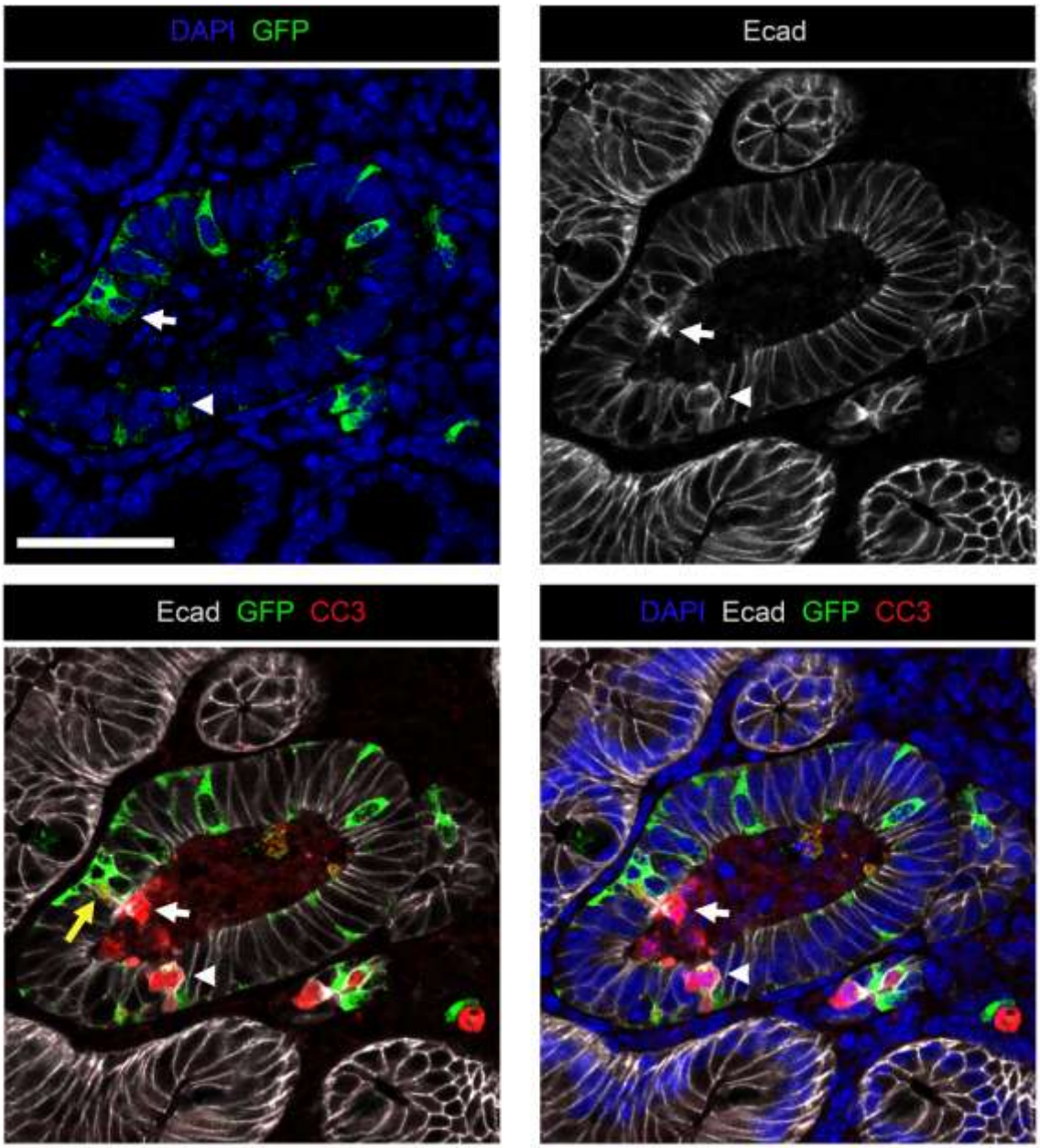

Figure 65. Colocalisation of GFP-labelled *Lgr5* positive cells and cleaved caspase 3
Immunolabelling of small intestine from an *Apc*$^{fl/fl}$ *Cdh1*$^{fl/fl}$ *Rosa-YFP*$^{+/+}$ *Lgr5-CreER*^{T2} animal for DAPI, E-cadherin, GFP and cleaved caspase 3 (CC3). White arrow points to an *Lgr5* positive cell that is also positive for CC3 (yellow arrow shows colocalisation of GFP and CC3. The white arrowhead points to a second *Lgr5* cell also expressing CC3. Scale bar 50µm

5.3.6 Adenomas can be grown in three dimensional culture

Adenomas from both *Apc*$^{fl/fl}$ *Cdh1*$^{+/+}$ *Lgr5-Cre* and *Apc*$^{fl/fl}$ *Cdh1*$^{fl/fl}$ *Lgr5-Cre* animals could be grown in three dimensional culture in matrigel using the protocol described in Section 5.2.4. Growth of adenoma spheroids immunolabelled for E-cadherin and DAPI is shown in Figure 66. Adenomas all had membrane-bound E-cadherin, including the *Cdh1*$^{fl/fl}$ genotype. They were highly proliferative as assessed by EdU labelling (Figure 74). By day 6-8 following culture adenomas reached a size where they required passage and replating in matrigel. At this stage the spheres often contained a core of necrotic cells (assessed by CC3 staining in Figure 75).

5.3.7 EDTA treatment disrupts E-cadherin and activates apoptosis

E-cadherin requires calcium to mediate its cell adhesion function. Thus an indirect way of assessing the effect of loss of E-cadherin mediated cell adhesion in adenomas is to restrict the supply of calcium. As absence of calcium may have other effects, this is an imperfect control to evaluate the effect of loss of adhesion. A better control is being developed (details in discussion) however whilst awaiting it EDTA was used to assess the possible effect of disrupted adhesion in adenoma cultures. EDTA was used to chelate calcium, followed by culture in calcium-free medium. Adenomas underwent morphological changes within minutes, becoming shrunken and losing their spherical shape. Live cell imaging showed involution of the adenoma spheroids. Immunolabelling of adenomas after EDTA treatment and 36 hours in calcium free medium revealed loss of membrane bound E-cadherin, very pyknotic nuclei and cleaved caspase 3 activity. β-catenin appeared variable with some adenoma showing prominent nuclear β-catenin, albeit in apoptotic nuclei, and others showing minimal β-catenin immunolabelling (Figure 67). EDTA treatment and calcium restriction had a dramatic effect of adenoma, however the contribution of lack of adhesion specifically is unclear.

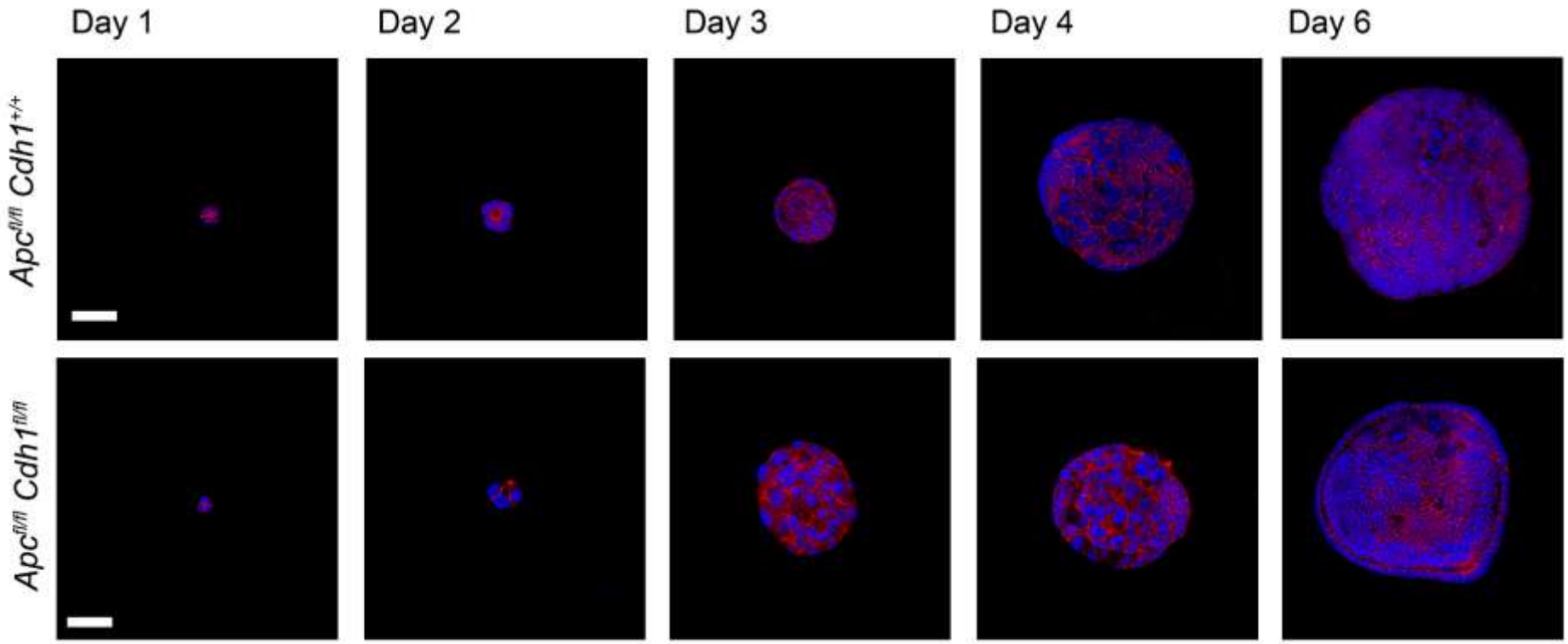

Figure 66. Culture of adenomas from *Apc*$^{fl/fl}$ *Cdh1*$^{+/+}$ and *Apc*$^{fl/fl}$ *Cdh1*$^{fl/fl}$ animals
Immunolabelling of adenomas cultured from *Apc*$^{fl/fl}$ *Cdh1*$^{+/+}$ *Lgr5-CreER*^{T2} and *Apc*$^{fl/fl}$ *Cdh1*$^{fl/fl}$ *Lgr5-CreER*^{T2} animals for DAPI and E-cadherin. Day refers to day following culture. There were no obvious differences in growth or adenoma appearance between the two genotypes. Adenomas could be cultured reproducibly (more than 6 culture experiments conducted). Scale bar 50µm.

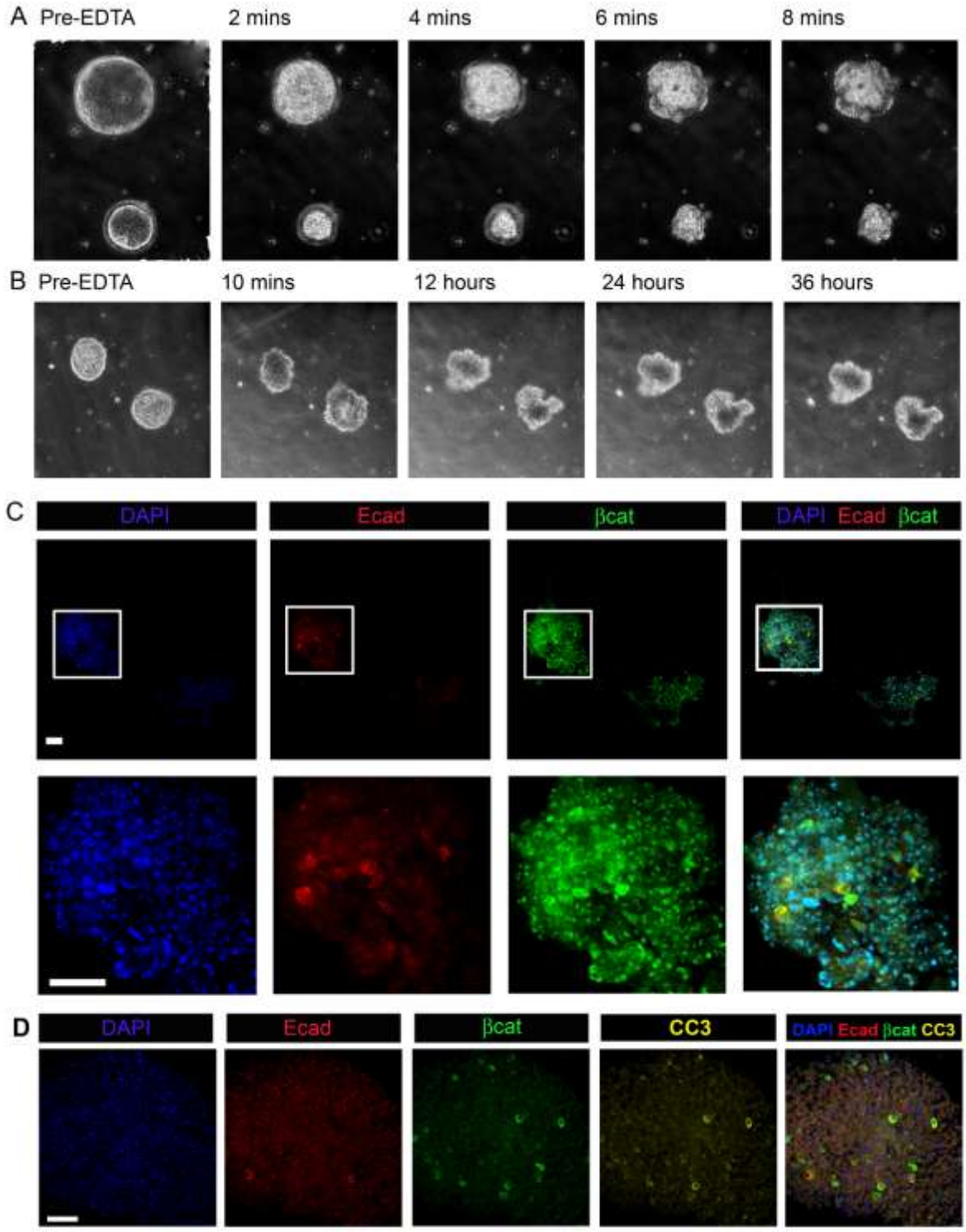

Figure 67. The effect of EDTA treatment of cultured adenomas

Phase contrast images or immunolabelling (for DAPI, E-cadherin, β-catenin and cleaved caspase 3 (CC3)) of adenomas treated with EDTA for 10 minutes followed by calcium free medium for 24 hours. (**A**) Morphological effects over minutes. (**B**) Morphological effects over hours/days. (**C**) Adenomas with pyknotic nuclei and variable changes in β-catenin. Adenoma on left (and enlarged below) with increased β-catenin. Adenoma on right (not enlarged) has minimal β-catenin. (**D**) Adenoma with some cells with increased β-catenin and CC3. Scale bars 50μm.

5.3.8 Recombination of Cdh1$^{fl/fl}$ in adenomas in vitro

When considering methods for activating recombination of *Cdh1*$^{fl/fl}$ in adenomas *in vitro* one of the major considerations was the ability to reliably detect recombination. The *in vivo* models relied on use of the *Rosa-YFP* reporter gene however this would already be expressed in the cultured adenomas. An immunolabelling approach using an anti Cre recombinase antibody was used, with positive labelling for Cre and loss of membrane bound E-cadherin indicating successful recombination. Initial attempts to activate recombination through *Lgr5-Cre* using 4-hydroxytamoxifen did not result in an observable phenotype and cells with positive immunolabelling for Cre recombinase were rare. Given the known low proportion of adenoma cells that are *Lgr5* positive, this was not surprising, particularly when Cre recombinase activity and E-cadherin loss could only be assayed at a single time point when cells were fixed for immunolabelling. One could postulate that if *Cdh1* loss in *Lgr5* cells was leading for example to cell death, the ability to detect this would be limited by the low number of cells affected and the regenerative ability of neighbouring unaffected cells.

An approach using an adenoviral construct expressing Cre recombinase under the CMV promoter was successful. The only commercially available form of *Ad-Cre* with a fluorescent reporter uses GFP. As we already had EGFP in the *Lgr5-Cre* construct and *Rosa-YFP* as our reporter gene (that required detection with an anti-GFP antibody), we could not use this so persisted with detection of Cre activity and E-cadherin loss using an immunolabelling approach. An approach using a Cre construct with a red reporter is being developed currently. Pilot studies established that recombination was most efficient in primary adenoma culture (rather than passaged cells) when *Ad-Cre* was added to cells at the time of culture, before the cells were suspended in matrigel.

5.3.9 Homozygous loss of Cdh1 *in cultured adenomas results in an EMT phenotype*

Within 2 days of treatment with Ad-Cre, cells immunolabelled for Cre recombinase could be detected in both *Apc*$^{fl/fl}$ *Cdh1*$^{+/+}$ and *Apc*$^{fl/fl}$ *Cdh1*$^{fl/fl}$ cultures (Figures 71 and 73). In cultures not treated with Ad-Cre no Cre-labelled cells were present (Figures 70 and 72). Cre-labelled cells in *Apc*$^{fl/fl}$ *Cdh1*$^{+/+}$ Ad-Cre+ cultures had intact E-cadherin, whereas E-cadherin was lost in *Apc*$^{fl/fl}$ *Cdh1*$^{fl/fl}$ Ad-Cre+ Cre-labelled cells. Within 3 days *Apc*$^{fl/fl}$ *Cdh1*$^{fl/fl}$ Ad-Cre+ adenomas had dramatically altered morphology compared with *Apc*$^{fl/fl}$ *Cdh1*$^{fl/fl}$ Ad-Cre- cultures and

Apc$^{fl/fl}$ *Cdh1*$^{+/+}$ Ad-Cre+ or Ad-Cre- cultures. Microscopy using a 4x objective of *Apc*$^{fl/fl}$ *Cdh1*$^{fl/fl}$ Ad-Cre+ adenomas immunolabelled with the nuclear marker DAPI showed some adenomas with tight spherical structures (<15% on day 6 after culture) but the majority had lost their circular shape and had dispersed cells (Figure 68). This was an interesting observation as the Drosophila homologue of E-cadherin was named *Shotgun* because zygotic mutation resulted in multiple holes in the epidermis and cuticle, that gave it a shotgun blast appearance similar to the appearance of these adenomas (Nusslein-Volhard et al, 1984; Tepass et al, 1996). Adenoma growth assessment was attempted by measuring the DAPI fluorescence of at least 4 views using a 4x objective of adenoma cultures of different genotypes with or without Ad-Cre each day. Whilst no difference in growth rate was detected using this method, a more sensitive assay would be useful (Figure 68).

Apc$^{fl/fl}$ *Cdh1*$^{fl/fl}$ Ad-Cre+ adenomas lost their uniform spherical shape and developed spindle-shaped projections with motile cells at their edges. The morphological changes are best demonstrated by videos from live cell imaging of adenomas over a 24-36 hour time period. Still frames from the start and end of two of the videos are shown in Figure 68. Video 1 shows the appearance of *Apc*$^{fl/fl}$ *Cdh1*$^{fl/fl}$ Ad-Cre- adenomas on days 4-6 following culture. Three neighbouring adenomas of uniform spherical shape and different sizes are shown that expand and then involute multiple times over a 36 hour period. The involution may be related to the adenomas reaching a critical pressure within the matrigel at a particular size or the clearance of cellular debris from the centre of the sphere. Also visible in this video are some fibroblasts at the top of the image frame. Fibroblasts were never completely removed during preparation of the adenoma culture, however Immunolabelling showed they were not expressing *RosaYFP* so had not originated from adenoma cells. *Apc*$^{fl/fl}$ *Cdh1*$^{+/+}$ cultures showed the same morphology and growth as *Apc*$^{fl/fl}$ *Cdh1*$^{fl/fl}$ Ad-Cre- adenomas regardless of Ad-Cre treatment.

Videos 2 and 3 show the appearance and growth of *Apc*$^{fl/fl}$ *Cdh1*$^{fl/fl}$ Ad-Cre+ adenomas 4-6 days following culture. Video 2 shows 4 groups of cells: two groups of spindle shaped cells in the lower left corner, an adenoma with spindle shaped projections in the centre of the frame, and an adenoma with normal spherical morphology in the upper right corner. The adenoma in the upper right corner has a growth pattern very similar to those not treated with Ad-Cre. The adenoma at the centre of the picture initially has a spherical structure but

with disruption of the right border. Over time other borders of the adenoma become disrupted with motile cells with visible filopodia, the adenoma involutes and gradually adopts a more elongated morphology. The fibroblast-like cells in the lower left corner of the image are highly motile. Video 3 shows two groups of cells: an aggregate of spindle shaped cells in the upper right of the frame and a spherical adenoma in the lower left of the frame with some spindle shaped cells at its lower right border. Over time motile cells emerge from the lower adenoma, the adenoma involutes and the two collections of cells move closer together and interact.

An immediate concern was demonstrating if these motile, spindle-shaped cells were derived from adenoma cells and had undergone epithelial-mesenchymal transition, or if they were fibroblasts already present in the culture. Support from live cell imaging for them being transformed adenoma cells included their abundance (at 6 days after culture more than 85% of structures in the $Apc^{fl/fl}$ $Cdh1^{fl/fl}$ Ad-Cre+ cultures showed spindle-shaped morphology compared with less than 15% in the other cultures), and the observation that these motile cells emerged from an adenoma as it was changing shape and/or decreasing in size. Unfortunately the *Rosa-YFP* in the adenoma cells was not expressed strongly enough to detect it during live cell imaging which would have provided a definitive answer. Immunolabelling of formalin fixed adenomas following live cell imaging however confirmed that in the $Apc^{fl/fl}$ $Cdh1^{fl/fl}$ Ad-Cre+ cultures almost all these fibroblast like structures were *YFP* positive confirming they had originated from adenoma cells (Figure 69).

Immunolabelling was used to characterize the cellular changes. The spindle shaped cells had decreased or absent membrane bound E-cadherin. They were often, but not always, positive for Cre recombinase. They showed very low rates of cell division as assessed by EdU labelling (Figure 74) and apoptosis as assessed by cleaved caspase 3 (Figure 75). Nuclei, rather than being a uniform population as in normal adenomas, were heterogeneous. Some nuclei were large with prominent nucleoli and others pyknotic and fragmented. The spindle shaped cells without E-cadherin convincingly showed Wnt pathway upregulation with prominent cytoplasmic β-catenin and Axin2 and nuclear translocation of both markers. They were also positive for a number of EMT markers tested: Fibronectin, Twist and Vimentin. These changes are quantified in the next section.

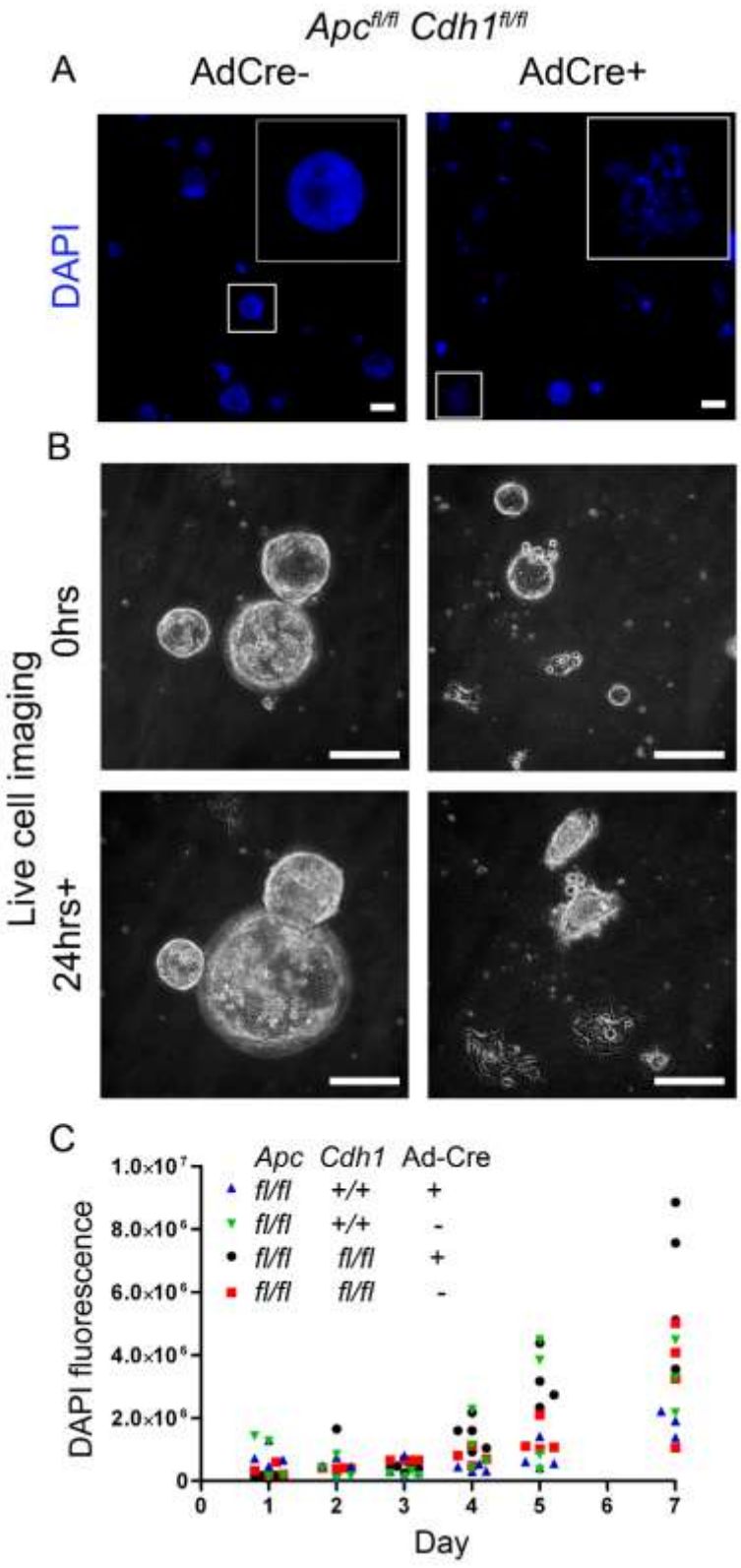

Figure 68. Ad-Cre treatment of adenomas from *Apc*$^{fl/fl}$ *Cdh1*$^{+/+}$ and *Apc*$^{fl/fl}$ *Cdh1*$^{fl/fl}$ animals
(**A**) Immunolabelling of cultured adenomas for DAPI showing dispersed appearance at low power of double homozygote cultures 4 days after treatment with Ad-Cre. (**B**) Morphological changes over 24 hours of live cell imaging of *Apc*$^{fl/fl}$ *Cdh1*$^{fl/fl}$ adenomas with or without Ad-Cre treatment. These still frames represent movies 2 and 3. (**C**) Attempt to assess adenoma growth using total DAPI fluorescence, ≥4 low power views of adenoma cultures assessed for each genotype at each timepoint. Scale bars 100µm.

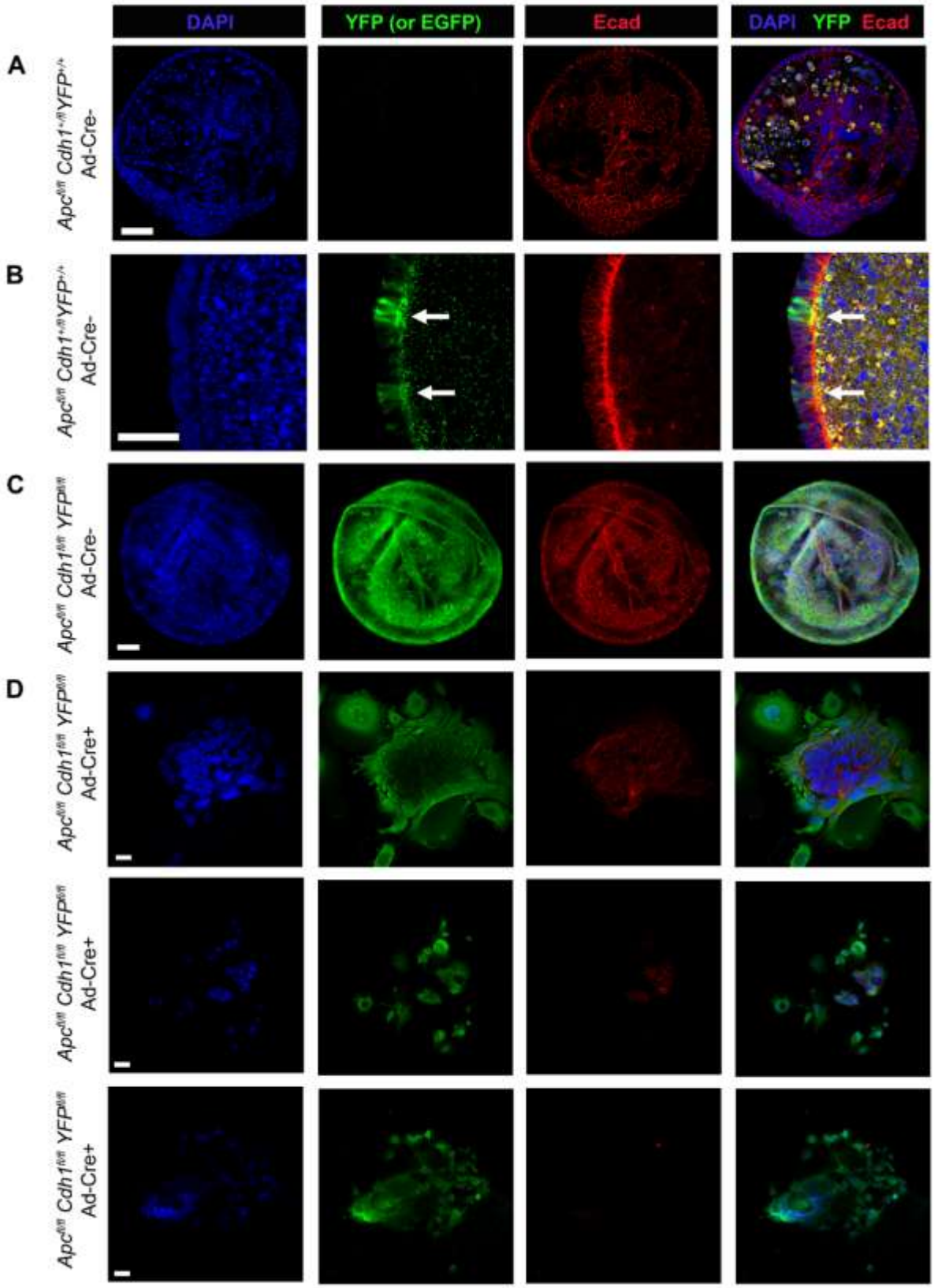

Figure 69. *Rosa-YFP* and *EGFP* expression in cultured adenomas

Rosa-YFP and EGFP expression detected by immunolabelling with anti-GFP antibody. Also immunolabelling for DAPI and E-cadherin. (**A**) and (**B**) show an adenoma wildtype for *Rosa-YFP* with no *YFP* expression, but positive EGFP expression in *Lgr5* cells at high magnification (white arrows). (**C**) $Apc^{fl/fl}$ $Cdh1^{fl/fl}$ $Rosa\text{-}YFP^{fl/fl}$ AdCre- adenoma with YFP expression. (**D**) Examples of $Apc^{fl/fl}$ $Cdh1^{fl/fl}$ $Rosa\text{-}YFP^{fl/fl}$ AdCre+ cultures showed cells with spindle-shaped projections, loss of E-cadherin and that are *RosaYFP* positive confirming these cells have originated from the adenoma. Scale bars 50µm

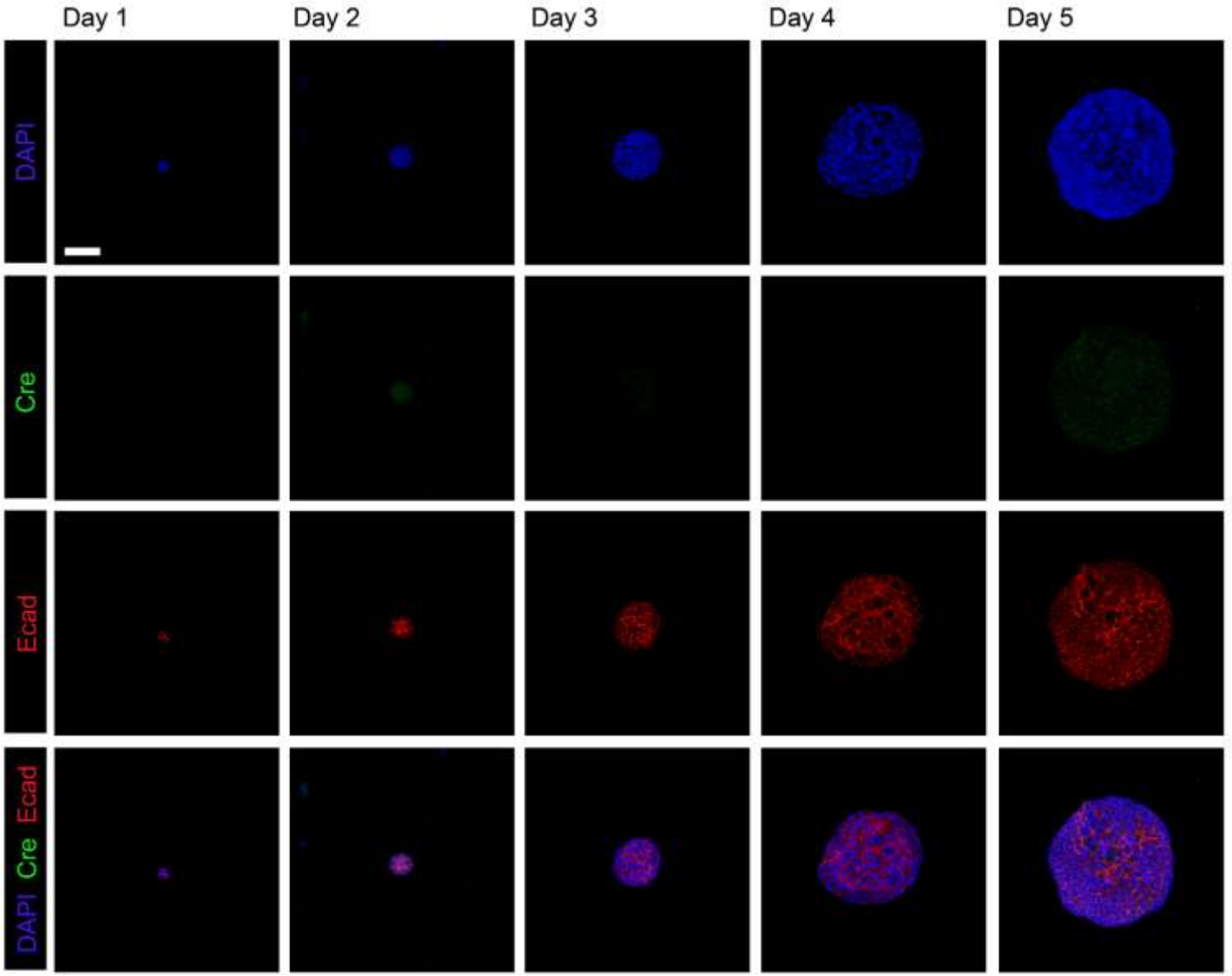

Figure 70. *Apc*$^{fl/fl}$ *Cdh1*$^{+/+}$ Ad-Cre- adenoma culture growth over 5 days
Immunolabelling of *Apc*$^{fl/fl}$ *Cdh1*$^{+/+}$ Ad-Cre- adenomas for DAPI, Cre recombinase and E-cadherin showing uniform growth over 5 days and no Cre recombinase expression. Scale bar 50µm.

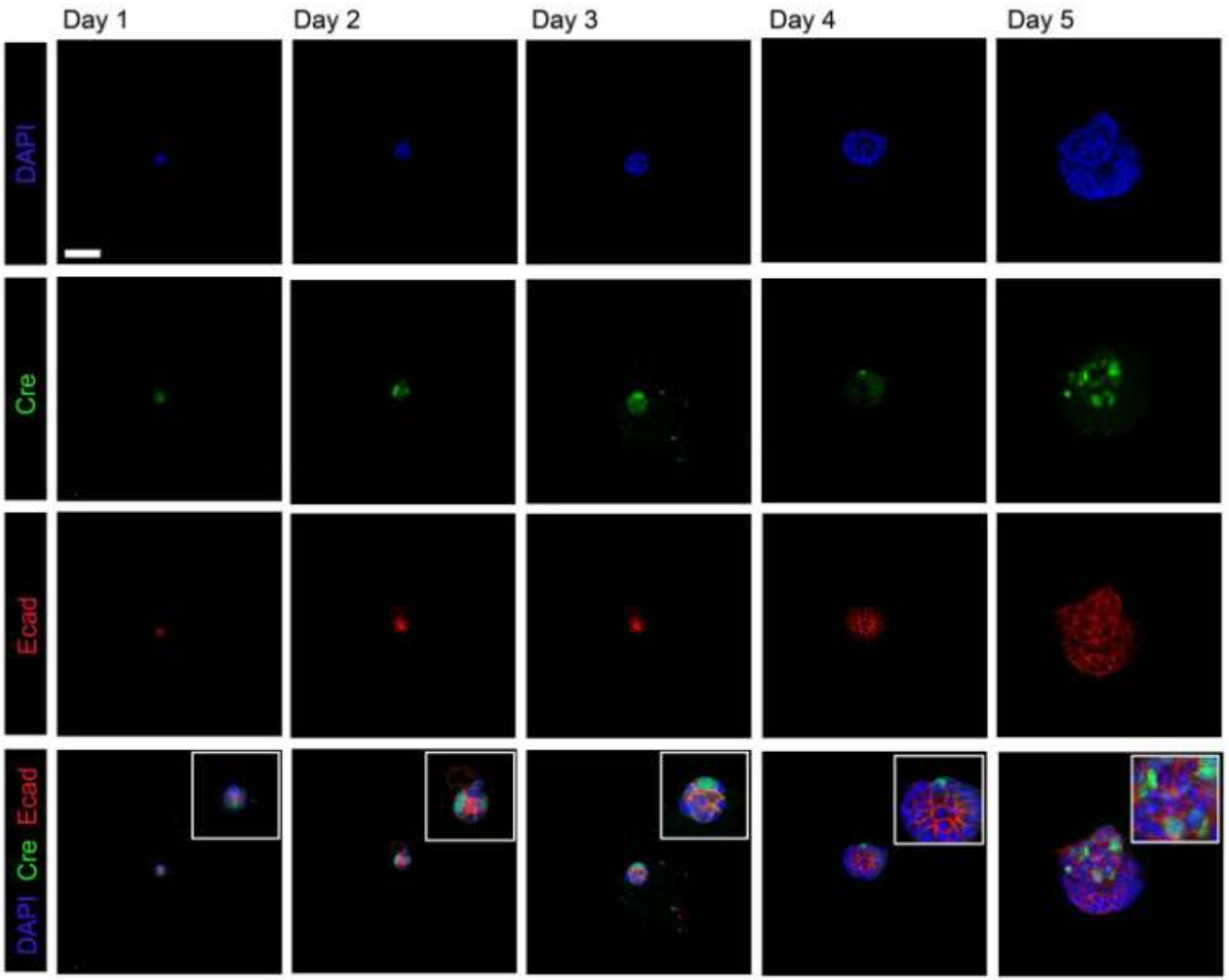

Figure 71. *Apc$^{fl/fl}$ Cdh1$^{+/+}$* Ad-Cre+ adenoma culture growth over 5 days
Immunolabelling of *Apc$^{fl/fl}$ Cdh1$^{+/+}$* Ad-Cre+ adenomas for DAPI, Cre recombinase and E-cadherin showing uniform growth over 5 days and positive Cre recombinase expression. The lower panel shows higher power views of Cre recombinase positive cells (in white boxes). Scale bar 50µm.

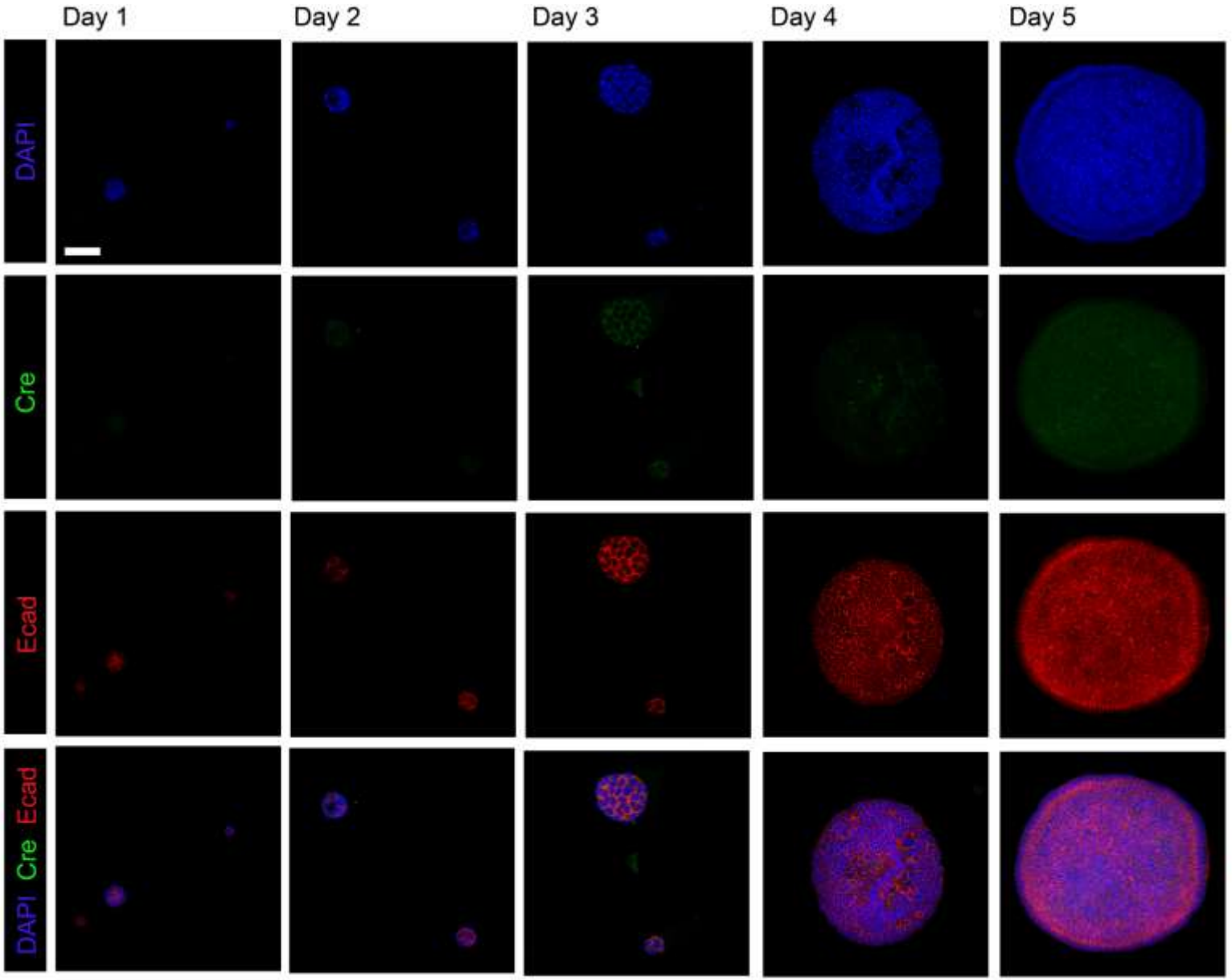

Figure 72. *Apc*$^{fl/fl}$ *Cdh1*$^{fl/fl}$ Ad-Cre- adenoma culture growth over 5 days
Immunolabelling of *Apc*$^{fl/fl}$ *Cdh1*$^{fl/fl}$ Ad-Cre- adenomas for DAPI, Cre recombinase and E-cadherin showing uniform growth over 5 days and no Cre recombinase expression. Scale bar 50µm.

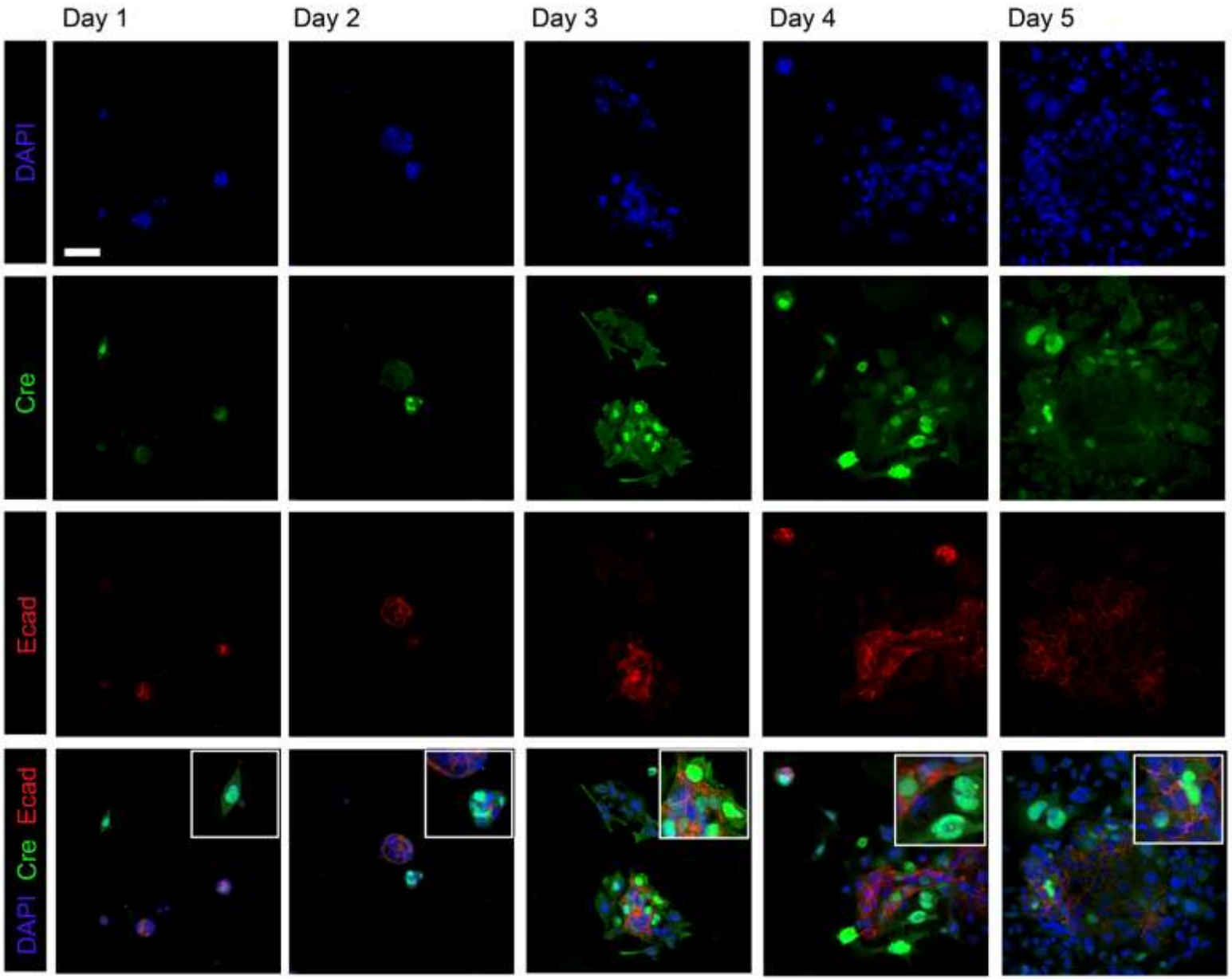

Figure 73. *Apc*$^{fl/fl}$ *Cdh1*$^{fl/fl}$ Ad-Cre+ adenoma culture growth over 5 days
Immunolabelling of *Apc*$^{fl/fl}$ *Cdh1*$^{fl/fl}$ Ad-Cre+ adenomas for DAPI, Cre recombinase and E-cadherin showing Cre-labelled cells that have disrupted or absent E-cadherin. There is also a heterogenous population of nuclei. The lower panel shows higher power views of Cre recombinase positive cells with disrupted E-cadherin (in white boxes). Scale bar 50µm.

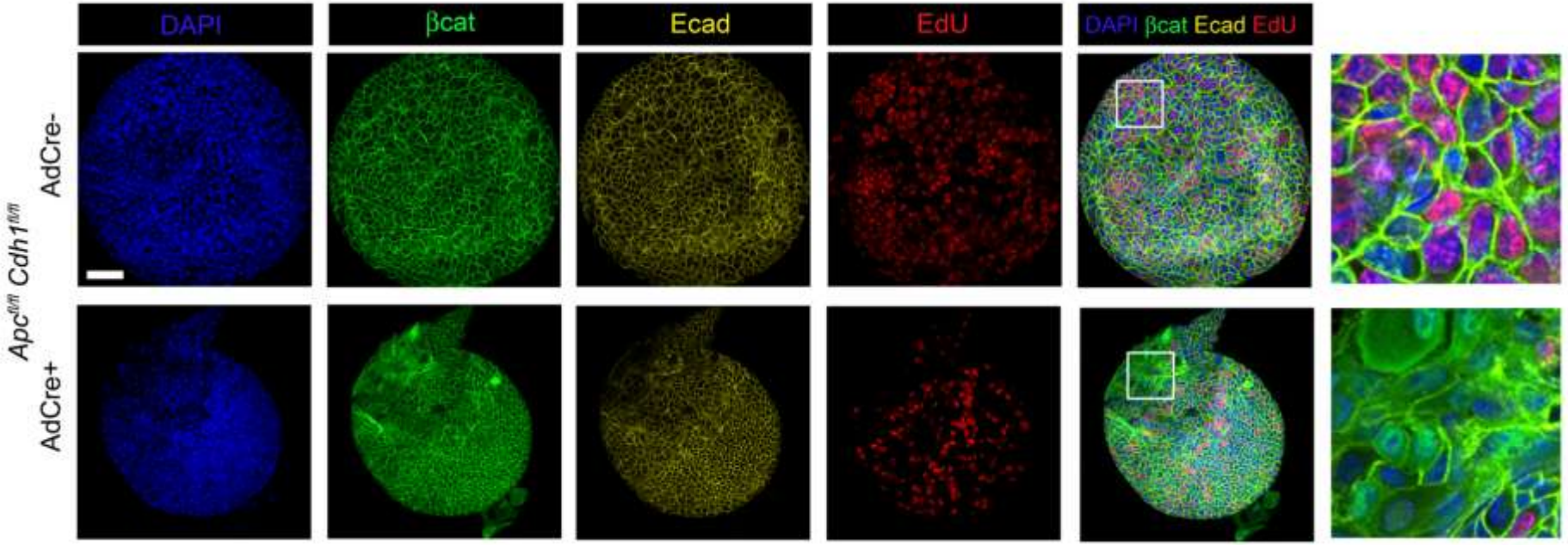

Figure 74. *Apc*$^{fl/fl}$ *Cdh1*$^{fl/fl}$ adenoma culture proliferation with or without Ad-Cre treatment

Cultured adenomas treated with EdU for 2 hours and then immunolabelled for DAPI, β-catenin, E-cadherin and EdU. The right panel shows higher power views of the areas marked with white boxes. In the *Apc*$^{fl/fl}$ *Cdh1*$^{fl/fl}$ AdCre- culture β-catenin and E-cadherin are colocalised at the cell membrane and EdU positive cells are present in all areas of the adenoma. In the *Apc*$^{fl/fl}$ *Cdh1*$^{fl/fl}$ AdCre+ there are very few EdU positive cells in the area of the adenoma with loss of membrane-bound E-cadherin and increased cytoplasmic and nuclear β-catenin. Scale bar 50μm

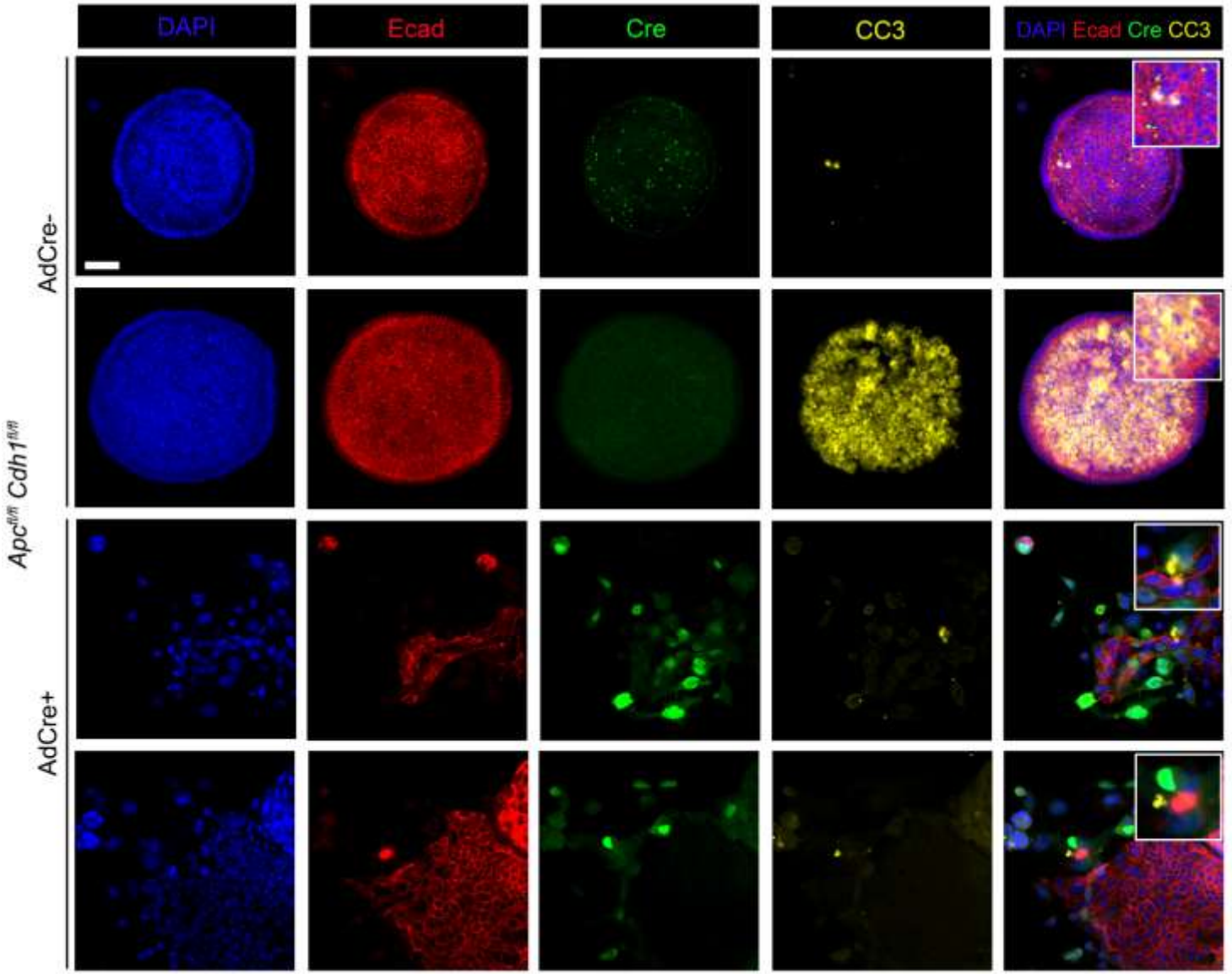

Figure 75. *Apc*$^{fl/fl}$ *Cdh1*$^{fl/fl}$ adenoma culture cleaved caspase 3 (CC3) labelling
Immunolabelling of *Apc*$^{fl/fl}$ *Cdh1*$^{fl/fl}$ adenoma cultures with or without AdCre treatment for DAPI, E-cadherin, Cre recombinase and CC3. In AdCre- adenomas there is occasional CC3 staining in outer adenoma epithelium and prominent necrotic cores one week following culture. In *Apc*$^{fl/fl}$ *Cdh1*$^{fl/fl}$ Ad-Cre+ adenomas CC3 positive cells are uncommon. Boxes outlined with white show higher power views of areas with CC3 positive cells. Scale bar 50µm

5.3.10 Characterisation of cellular changes using image analysis

As interpretation of immunolabelling results can be subjective, a method was developed to provide an objective assessment of the labelling of individual markers. For each marker, at least 4 adenomas were assessed from each of the $Apc^{fl/fl}$ $Cdh1^{fl/fl}$ Ad-Cre- and $Apc^{fl/fl}$ $Cdh1^{fl/fl}$ Ad-Cre+ groups. Figure 76 outlines the methodology. Figure 76A shows the original confocal image with 3 labelled channels: DAPI in blue, E-cadherin in red, and β-catenin in green. Using Olympus Fluoview viewer software, only the DAPI and E-cadherin channels were selected (Figure 76B) and based on the expression of E-cadherin the adenoma was divided into zones: an outer zone where there was no membrane bound E-cadherin, an inner zone where there was normal appearance of membrane bound E-cadherin, and a transition zone where cells had a mixture of intact and disrupted E-cadherin. Based on distance from the centre of the adenoma, the inner zone was divided into two: a central '50%' area and a surrounding '100%' area. The rationale for the 50/100 division was that because of the 3D structure of the adenomas, labelling of the central area was often inconsistent, with some central cores hollow and thus barely labelled, and others strongly labelled. $Apc^{fl/fl}$ $Cdh1^{fl/fl}$ Ad-Cre- adenomas did not have a transition or outer zone as all cells had intact membrane bound E-cadherin.

Once the adenoma was divided into zones, only the channel with the marker of interest (β-catenin in this example) was selected and this image was exported to ImageJ where it was converted to grayscale. ImageJ tools were then used to measure the fluorescence of the cells in each area and cells were manually counted to calculate a 'mean fluorescence per cell' measurement for each zone. For each marker at least 1000 cells were assessed, but often more (over 7000 in some cases). For each image the mean fluorescence per cell in each zone was normalized to that in the 100% zone.

For the Wnt targets β-catenin and Axin2, the location of the marker within the cell was also assessed. Using Olympus Fluoview software, DAPI was colored red and the marker of interest green. When the two were colocalised, the nucleus appeared yellow. For each cell I assessed whether staining of the marker of choice was predominantly cytoplasmic, predominantly nuclear or whether there was equal nuclear and cytoplasmic labelling. A cell with predominantly cytoplasmic staining was assigned a value of 0, equal cytoplasmic and

nuclear staining obtained a value of 1, and predominant nuclear staining was assigned a value of 2. Thus a total value could be generated for each area that reflected the proportion of cells with nuclear localization of the marker.

This data was represented as heatmaps generated using R software (*R Development Core Team*, 2008). For the average fluorescence per cell heat maps data underwent a log2 transformation.

5.3.11 Cdh1 loss in adenoma cells led to Wnt pathway upregulation and EMT

Figures 77 to 82 show immunolabelling for the Wnt target genes β-catenin and Axin2, and the EMT markers Fibronectin, Twist and Vimentin. $Apc^{fl/fl}$ $Cdh1^{+/+}$ adenomas show similar patterns of expression for each marker with or without Ad-Cre (Figure 77) and this pattern of expression is reproduced for each marker in $Apc^{fl/fl}$ $Cdh1^{fl/fl}$ Ad-Cre- adenomas (upper images in Figures 78-82). $Apc^{fl/fl}$ $Cdh1^{fl/fl}$ Ad-Cre+ adenomas show in the transition and outer zones, increased total and nuclear Axin2 and β-catenin demonstrating upregulation of the Wnt pathway, and increased expression of the EMT markers Fibronectin, Twist and Vimentin.

Flow cytometry analysis of adenomas 5 days after culture and treatment with Ad-Cre showed a population of cells in the $Apc^{fl/fl}$ $Cdh1^{fl/fl}$ Ad-Cre+ adenomas with decreased E-cadherin labelling compared to $Apc^{fl/fl}$ $Cdh1^{fl/fl}$ Ad-Cre- adenomas (Figure 83, lower two lines). This population of cells was not present in $Apc^{fl/fl}$ $Cdh1^{+/+}$ adenomas with or without Ad-Cre treatment (Figure 83, upper two lines). $Apc^{fl/fl}$ $Cdh1^{fl/fl}$ Ad-Cre+ cells with decreased E-cadherin expression showed increased β-catenin expression supporting increased Wnt signaling in these cells. They also showed increased cleaved caspase 3 activity suggesting E-cadherin loss may be associated with increased apoptosis, possibly anoikis-mediated. A limitation of flow cytometry analysis is the large number of cells required. Initial analysis was unreliable due to small cell numbers. Optimisation of the protocol and increased cell numbers achieved the results described here.

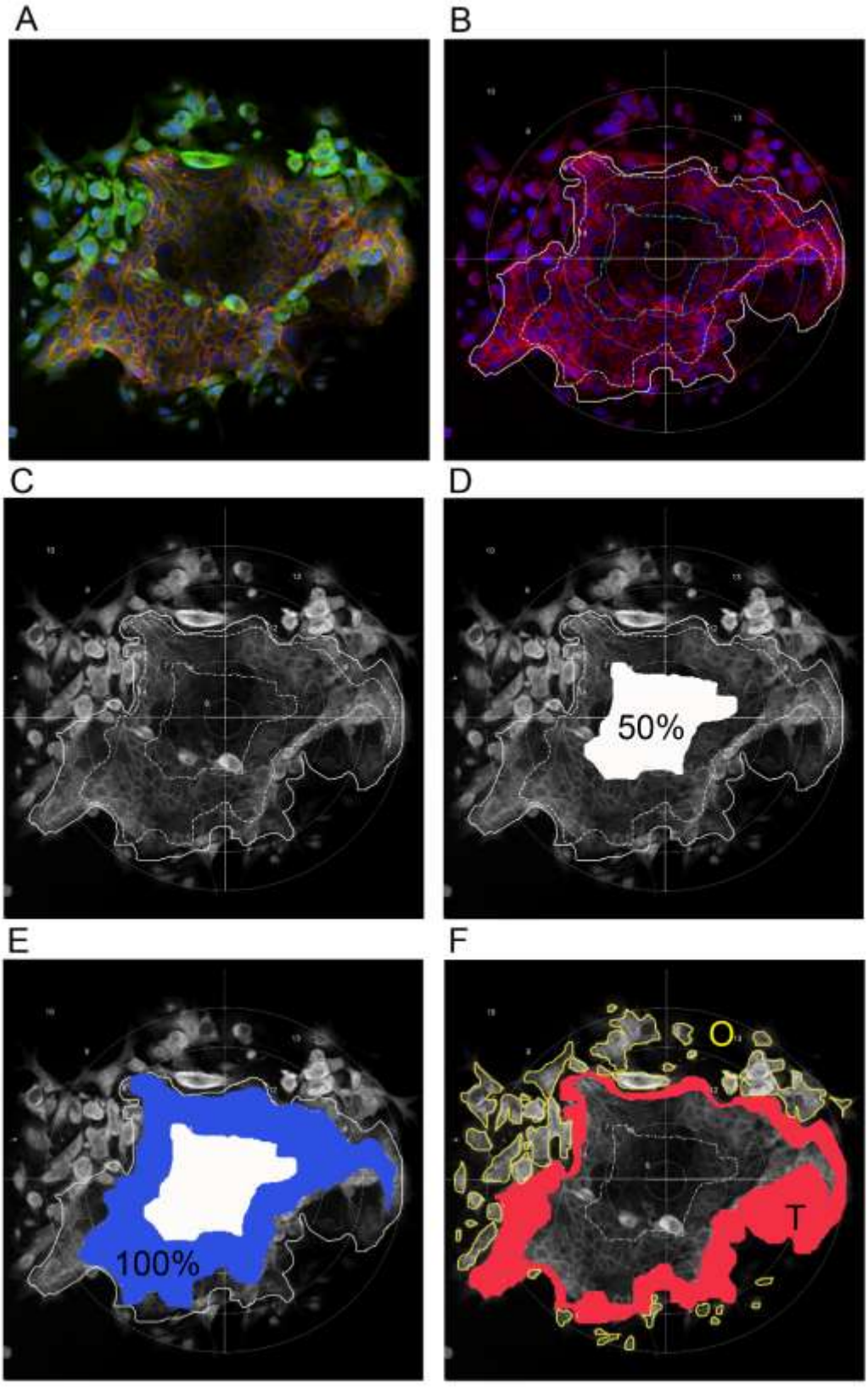

Figure 76. Image capture for heat map generation

(**A**) Original image with three channels shown (DAPI in blue, E-cadherin in red, β-catenin in green). (**B**) Image used to delineate boundaries between outer and transition zone (based on E-cadherin expression), and '100%' and '50%' zones based on distance from centre of the adenoma. (**C**) Gray scale image of (**B**) used for fluorescence analysis of marker of interest (β-catenin in this example). (**D**). '50%' area marked in white. (**E**) '100%' area marked in blue. (**F**) Transition zone ('T') marked in red and cells in outer zone ('O') outlined in yellow.

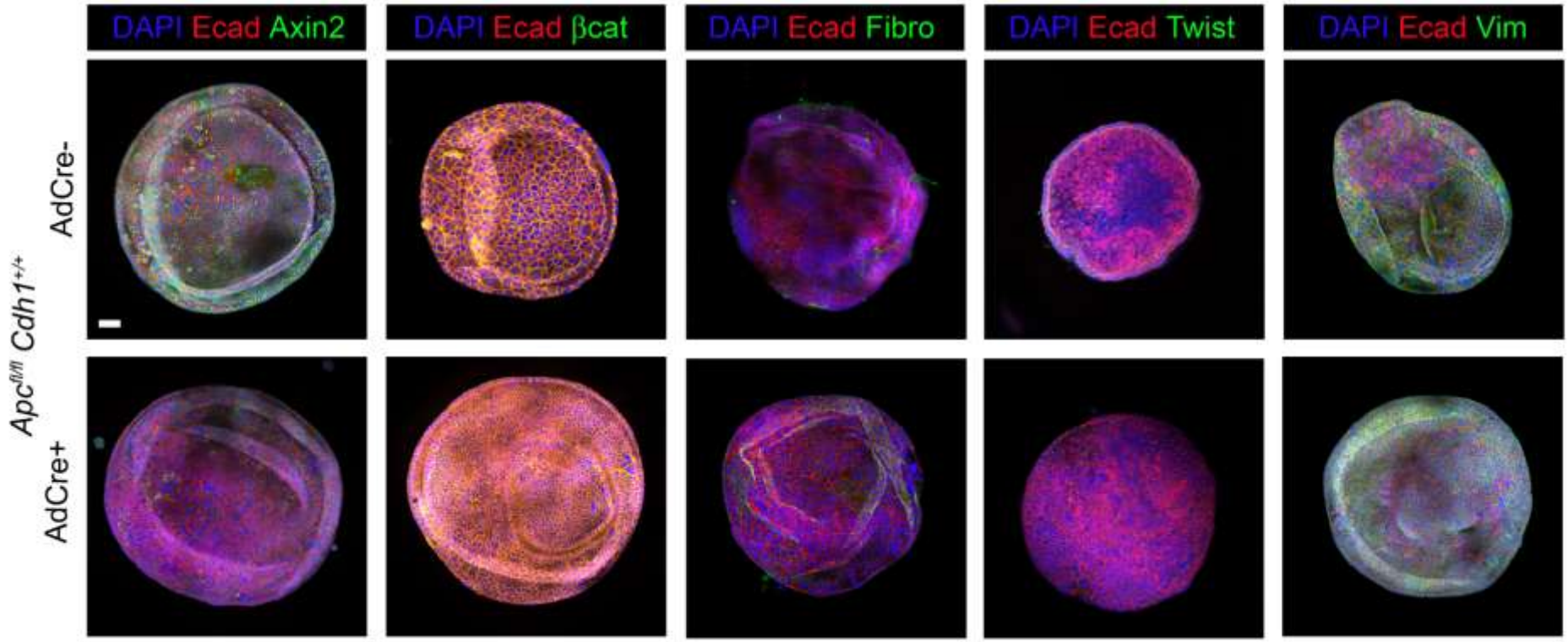

Figure 77. Immunolabelling of *Apc*$^{fl/fl}$ *Cdh1*$^{+/+}$ adenomas with or without Ad-Cre for Wnt and EMT markers

Immunolabelling of *Apc*$^{fl/fl}$ *Cdh1*$^{+/+}$ adenomas with or without Ad-Cre treatment for DAPI, E-cadherin and Axin2, β-catenin, fibronectin, twist or vimentin. There is no obvious difference in expression of these markers with or without AdCre. Scale bar 50µm

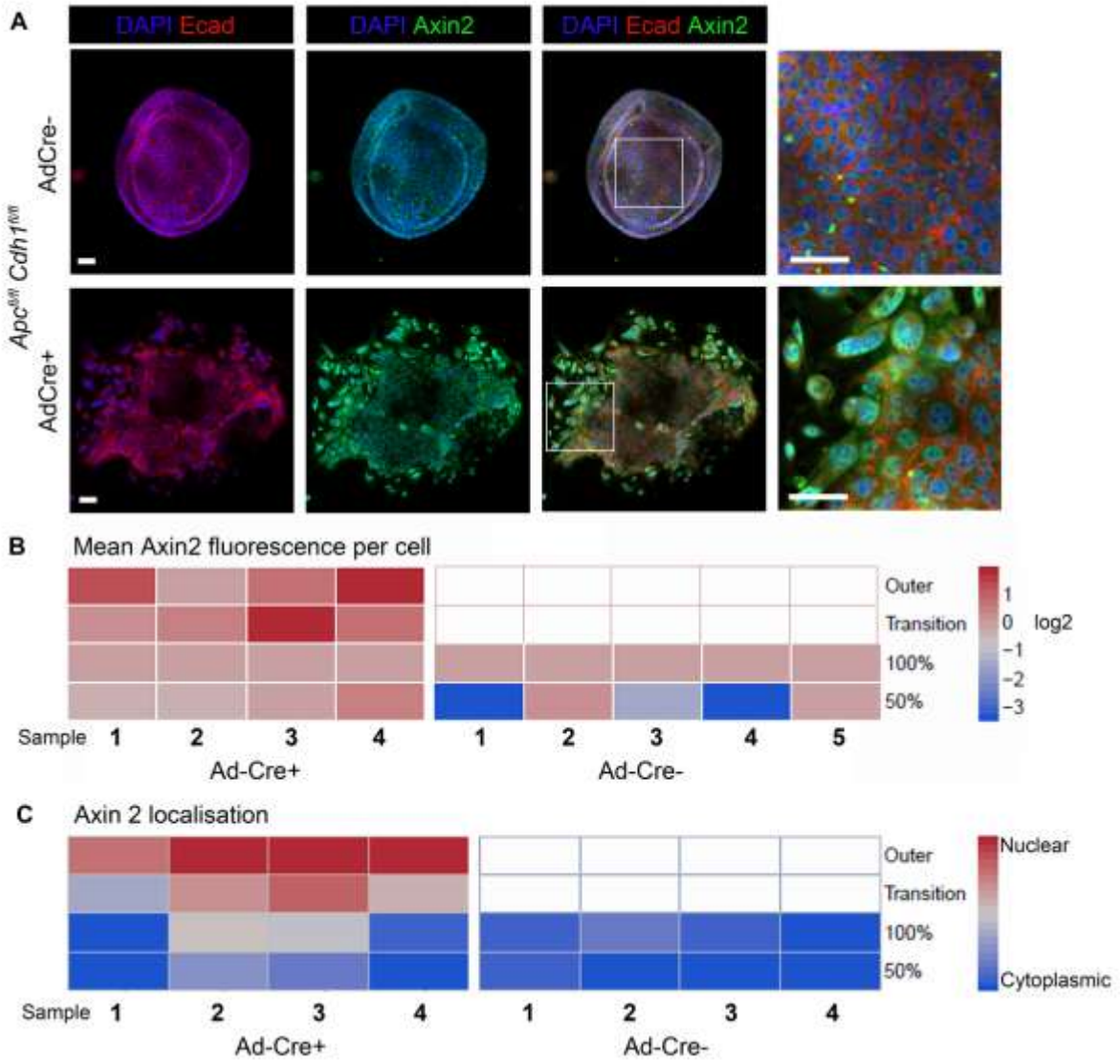

Figure 78. Immunolabelling of *Apc*$^{fl/fl}$ *Cdh1*$^{fl/fl}$ adenomas with or without Ad-Cre for Axin2
(**A**) Immunolabelling for DAPI, E-cadherin and Axin2 showing higher expression and nuclear localization of Axin2 in the outer cells of AdCre+ cultures lacking E-cadherin. Scale bars 50µm (**B**) Heat map for mean Axin2 fluorescence per cell, data log2 transformed, confirming increased Axin2 expression in AdCre+ cultures. (**C**) Heat map for cellular localization of Axin2 confirming increased nuclear localization in AdCre+ cultures.

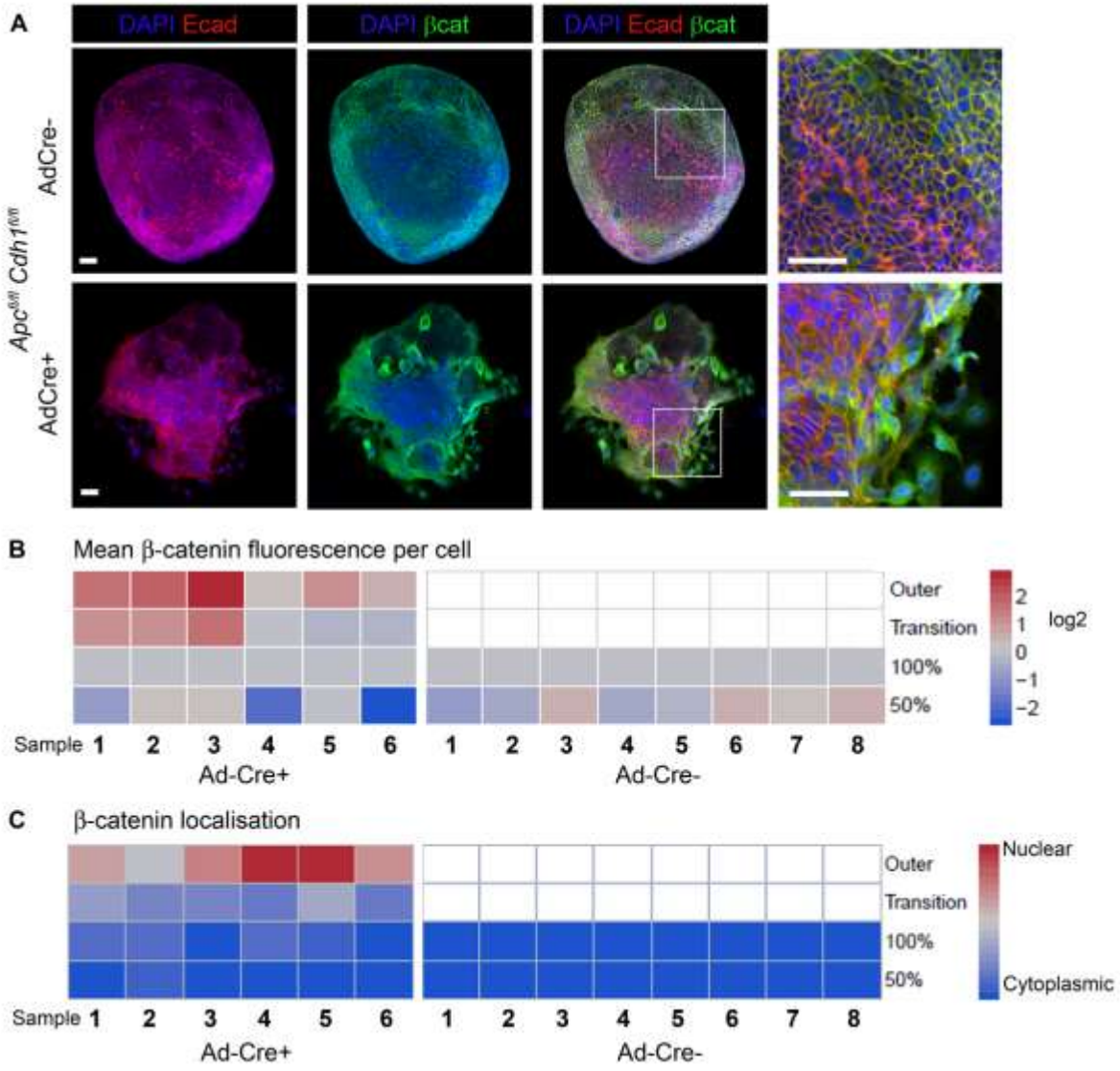

Figure 79. Immunolabelling of *Apc*$^{fl/fl}$ *Cdh1*$^{fl/fl}$ adenomas with or without Ad-Cre for β-catenin
(**A**) Immunolabelling for DAPI, E-cadherin and β-catenin showing higher expression and nuclear localization of β-catenin in the outer cells of AdCre+ cultures lacking E-cadherin. Scale bars 50μm (**B**) Heat map for mean β-catenin fluorescence per cell, data log2 transformed, confirming increased β-catenin expression in AdCre+ cultures. (**C**) Heat map for cellular localization of β-catenin confirming increased nuclear localization in AdCre+ cultures.

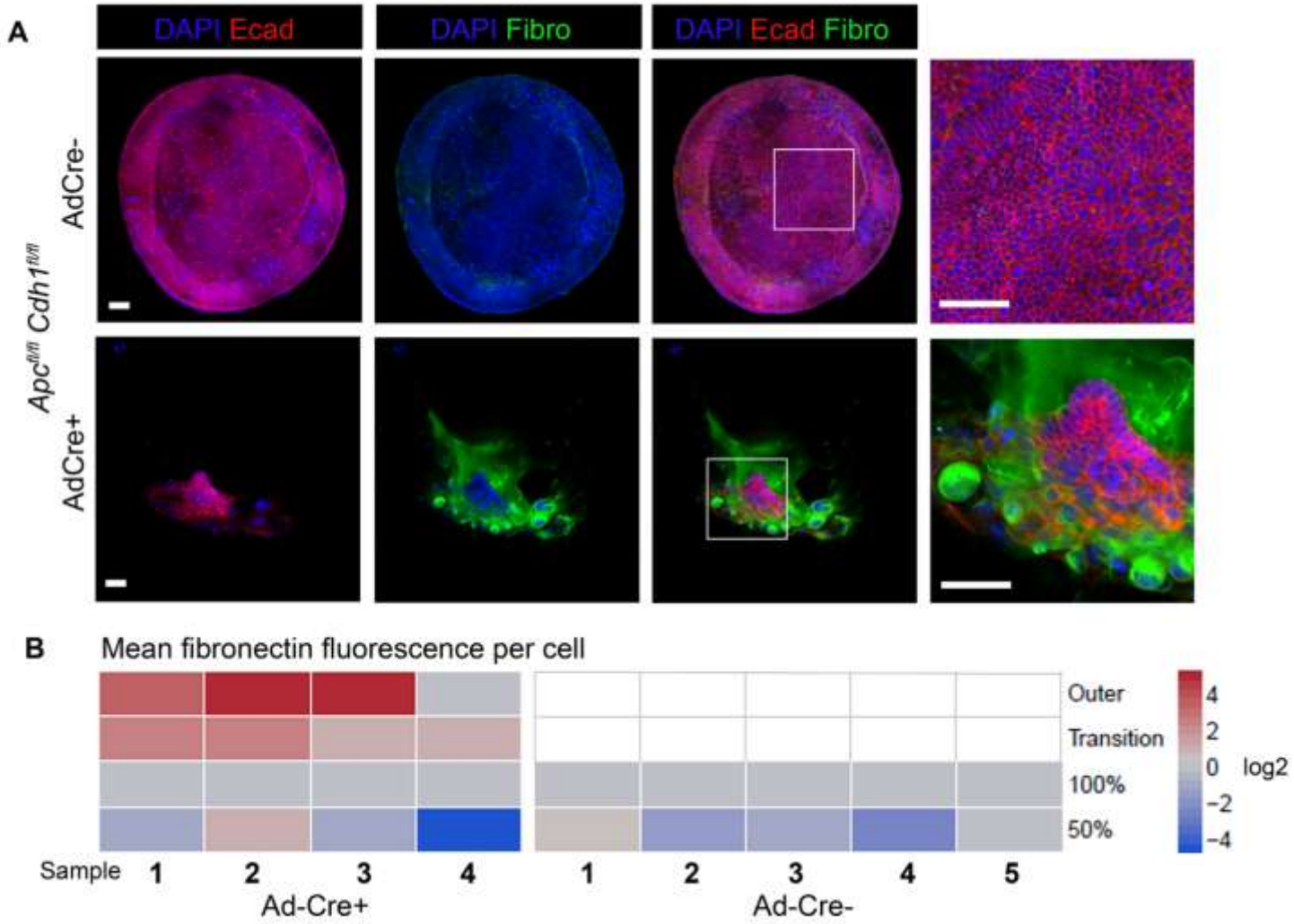

Figure 80. Immunolabelling of *Apc*$^{fl/fl}$ *Cdh1*$^{fl/fl}$ adenomas with or without Ad-Cre for Fibronectin

(**A**) Immunolabelling for DAPI, E-cadherin and fibronectin showing higher expression of fibronectin in the outer cells of AdCre+ cultures lacking E-cadherin. Scale bars 50µm (**B**) Heat map for mean fibronectin fluorescence per cell, data log2 transformed, confirming increased fibronectin expression in AdCre+ cultures.

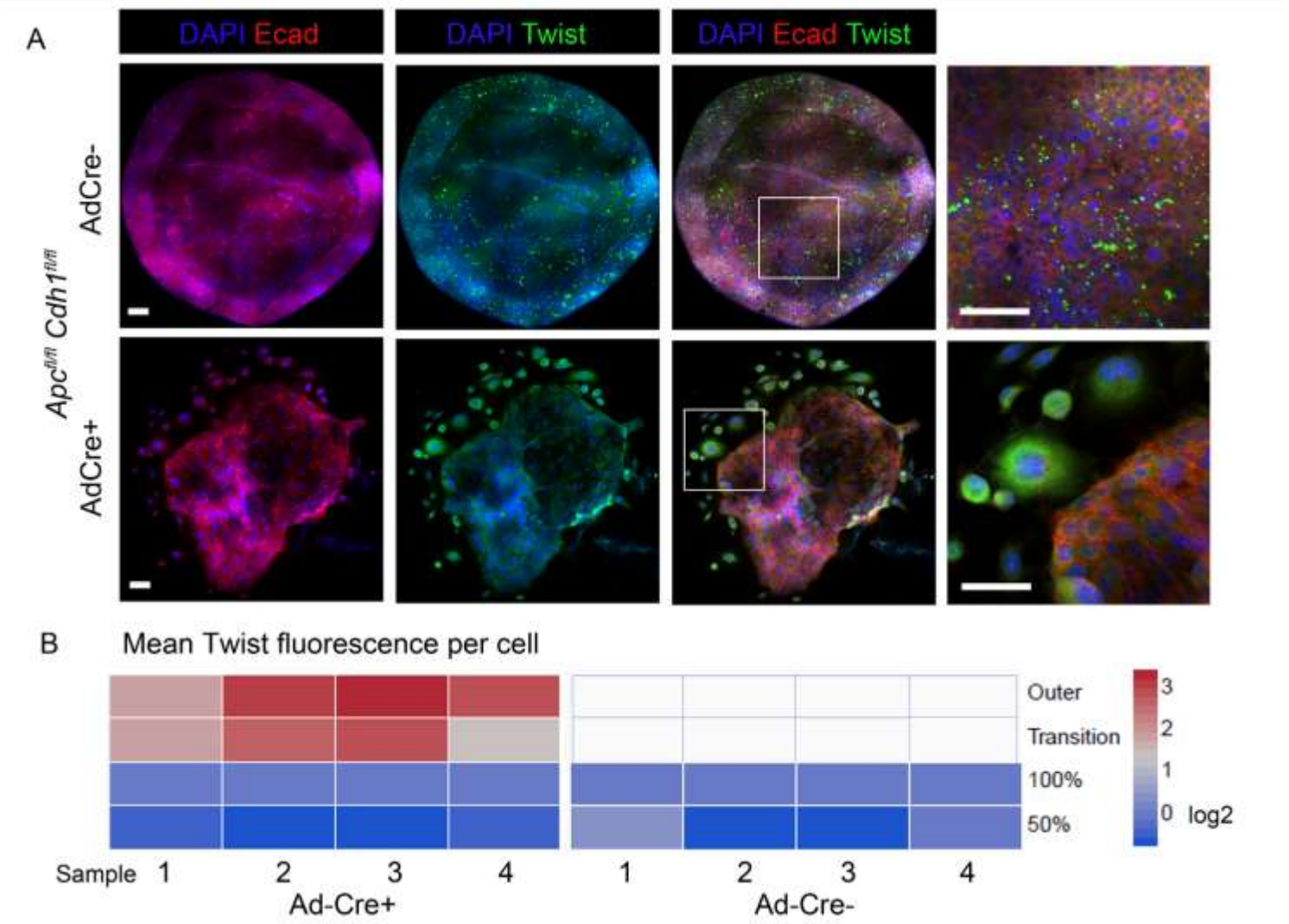

Figure 81. Immunolabelling of *Apc*$^{fl/fl}$ *Cdh1*$^{fl/fl}$ adenomas with or without Ad-Cre for Twist

(**A**) Immunolabelling for DAPI, E-cadherin and twist showing higher expression of twist in the outer cells of AdCre+ cultures lacking E-cadherin. Scale bars 50µm (**B**) Heat map for mean twist fluorescence per cell, data log2 transformed, confirming increased twist expression in AdCre+ cultures.

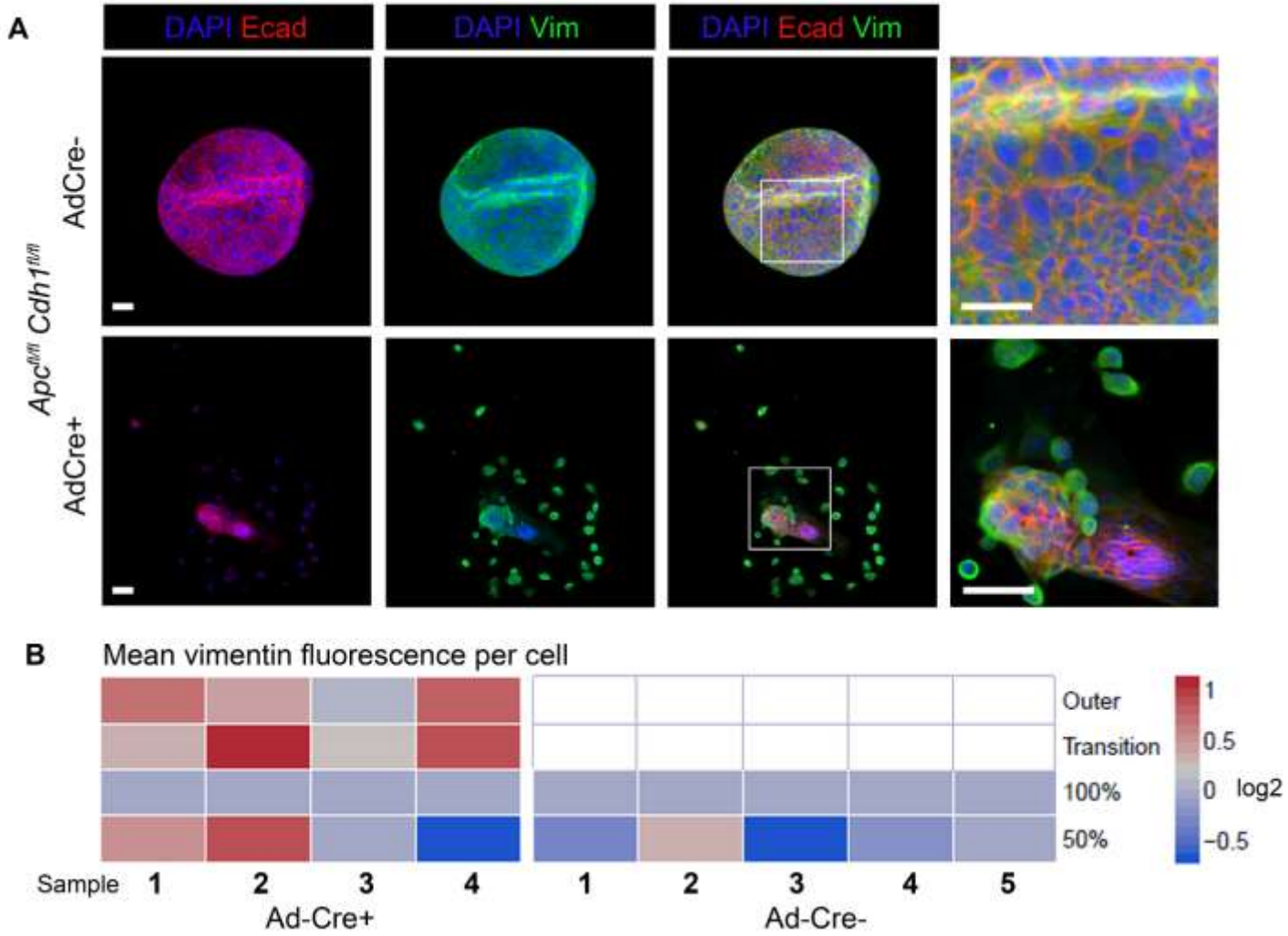

Figure 82. Immunolabelling of *Apc*$^{fl/fl}$ *Cdh1*$^{fl/fl}$ adenomas with or without Ad-Cre for Vimentin

(**A**) Immunolabelling for DAPI, E-cadherin and vimentin showing higher expression of vimentin in the outer cells of AdCre+ cultures lacking E-cadherin. Scale bars 50µm (**B**) Heat map for mean vimentin fluorescence per cell, data log2 transformed, confirming increased vimentin expression in AdCre+ cultures.

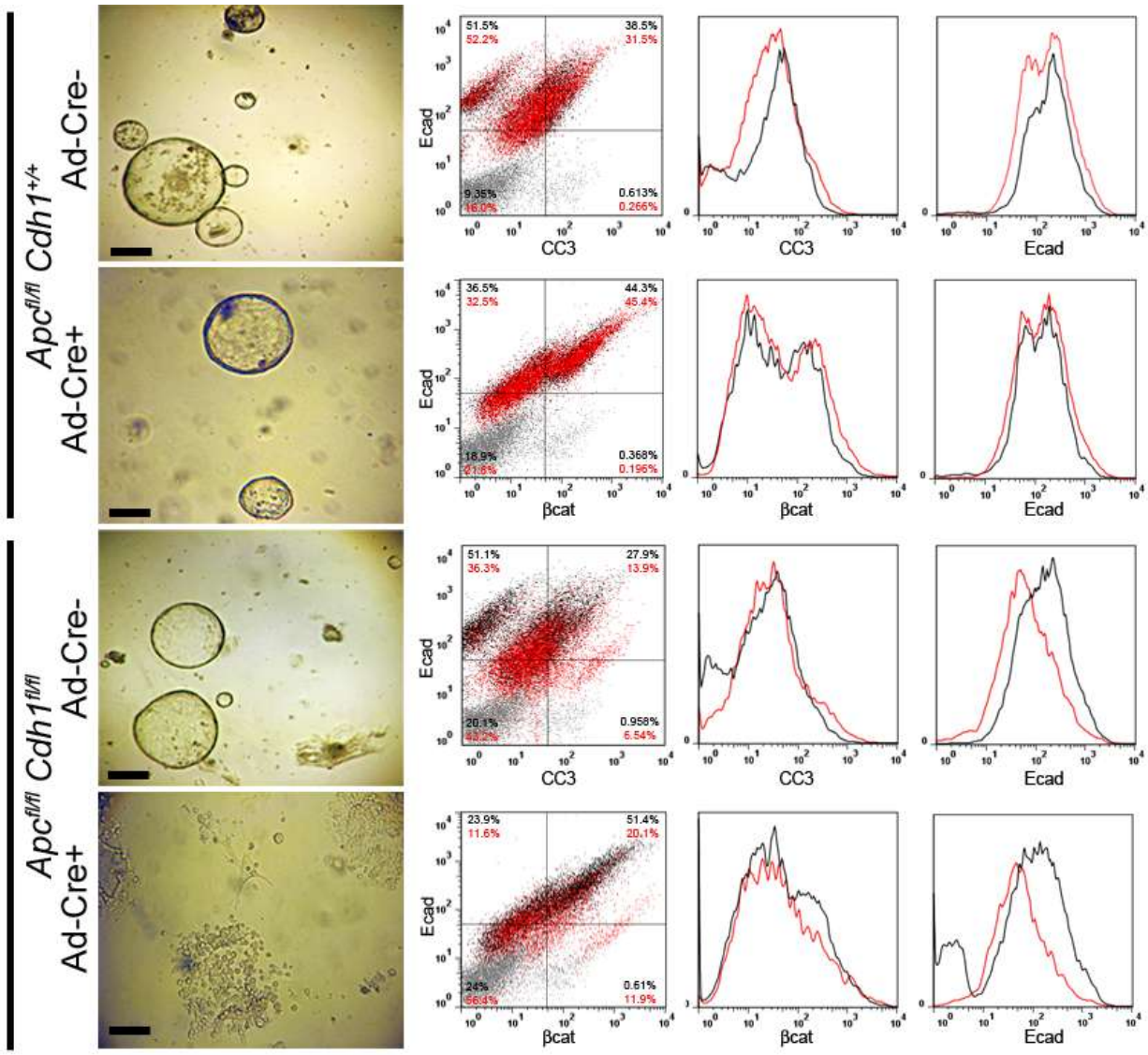

Figure 83. Flow cytometry analysis of adenomas

Flow cytometry analysis of adenoma cells from *Apc*$^{fl/fl}$ *Cdh1*$^{+/+}$ *Lgr5-Cre* (top two lines) or *Apc*$^{fl/fl}$ *Cdh1*$^{fl/fl}$ *Lgr5-Cre* (lower two lines) cultures, with or without Ad-Cre treatment (Ad-Cre+ or Ad-Cre-). Images in the left panel show the appearance of the adenoma cultures immediately prior to preparation for flow cytometry. Scale bars 200µm. For flow cytometry analysis cells have been labelled with E-cadherin (Ecad) and cleaved caspase 3 (CC3), or E-cadherin and β-catenin (βcat). Ad-Cre+ cells are represented in red. Ad-Cre- cells are represented in black. Isotype controls are shown in grey. The numbers indicate the proportion of cells in the relevant quadrant. For *Apc*$^{fl/fl}$ *Cdh1*$^{fl/fl}$ cultures there is an increase in the proportion of cells with reduced E-cadherin and increased CC3 expression, or reduced E-cadherin and increased CC3 expression (lower right quadrants).

5.4 Discussion

The principal findings of this chapter were that *Cdh1* was never completely lost in adenomas from *Apc*$^{fl/fl}$ *Cdh1*$^{fl/fl}$ *Lgr5-Cre* mice and this may be due to incomplete recombination or *Lgr5* positive cells with complete loss of *Cdh1* failing to survive. In culture *Cdh1* loss appeared to result in adenomas with Wnt pathway upregulation and epithelial mesenchymal transition.

5.4.1 Possible explanations for incomplete loss of Cdh1 *in* Apc$^{fl/fl}$ Cdh1$^{fl/fl}$ Lgr-Cre *adenomas*

Efficient recombination of *Apc* alleles using *Lgr5-Cre* was apparent from presence of the recombined allele by genotyping of adenoma cells and the presence of adenomas with β-catenin upregulation. Genotyping of *Apc*$^{fl/fl}$ *Cdh1*$^{fl/fl}$ adenomas showed expression of the recombined *Cdh1* allele, but also some expression of the full length loxP flanked allele showing incomplete recombination. Whilst E-cadherin expression was reduced in *Apc*$^{fl/fl}$*Cdh1*$^{fl/fl}$ adenomas as assessed by immunolabelling, it was never completely absent. Moreover RT-QPCR showed *Cdh1* mRNA levels between adenomatous and non-adenomatous tissue were very similar. This could be explained by different recombination efficiencies for the *Apc* and *Cdh1* alleles. Hans Clevers' group recently reported that recombination of the floxed *Apc* allele is more efficient than activation of the *Rosa26-Confetti* allele and personal discussion with other researchers using *Lgr5-Cre* has revealed difficulty obtaining efficient recombination or activation for multiple conditional alleles requiring up to 4 doses of tamoxifen (Schepers et al, 2012).

From the *Cdh1*$^{fl/fl}$ *Vil-CreER*^{T2} experiments we know that the floxed *Cdh1* allele is not particularly resistant to recombination. So, even if there are different recombination efficiencies in the *Lgr5* model it would seem unusual to never detect an adenoma cell (as identified by cytoplasmic β-catenin) with complete *Cdh1* loss. We hypothesised that cells with complete loss of *Cdh1* may not be able to survive. There was evidence for this from our earlier *Cdh1*$^{fl/fl}$ *Vil-CreER*^{T2} model showing increased caspase mediated apoptosis with *Cdh1* loss and detachment of cells lacking *Cdh1* and also from reports of E-cadherin loss being involved in the onset of anoikis (Fouquet et al, 2004).

Anoikis, the process of cell death specifically by detachment from the extracellular membrane, is poorly understood. Fouquet and colleagues investigated the role of E-cadherin in anoikis of intestinal epithelial cells using a model that detached epithelial cells from the underlying mesenchyme without disrupting cell-cell interactions. The epithelial cells underwent apoptosis rapidly, with 20-30% of nuclei apoptotic after 30 minutes. Apoptosis was slowed by treatment with Z-VAD, a pan-caspase inhibitor, indicating the process was at least in part caspase dependent. The loss of membrane bound E-cadherin was observed and correlated with nuclear morphology: within 30 minutes of detachment E-cadherin staining was diffuse in about half of the cells and whilst intact in some cells with normal nuclear morphology, was particularly faint in all cells showing apoptotic nuclei. Within 90 minutes E-cadherin was undetectable in about 90% of cells and of the thousands of cells analysed, intact E-cadherin staining and an apoptotic nucleus were always mutually exclusive. Z-VAD treatment or overexpression of Bcl-2 resulted in delay of apoptosis but had no significant effect on the loss of E-cadherin supporting the hypothesis that E-cadherin loss preceded the onset of apoptosis. The degradation of E-cadherin during anoikis was shown to happen through proteosomal and lysosomal pathways and subsequent work showed this was dependent on EGFR activation (Lugo-Martínez et al, 2009). Use of an antibody to the ectodomain of E-cadherin known to block E-cadherin mediated adhesion resulted in a two fold increase in apoptotic nuclei 30 minutes after detachment, and an E-cadherin-Fc chimera that acts as a functional E-cadherin ligand decreased the proportion of apoptotic nuclei by two fold, suggesting E-cadherin has a role in the control of anoikis.

It is possible that in our *Lgr5* model any cells with complete *Cdh1* loss were undergoing anoikis and thus only cells with Wnt pathway gain of function and residual *Cdh1* expression were able to progress to a tumour. It must be noted that Fouquet's experiments were done on intestinal epithelial cells, and the contribution of *Cdh1* loss to anoikis in intestinal stem cells may be different: given the differences in active signalling pathways they may be more or less sensitive to these cues.

5.4.2 Caecal tumours and ileocaecal intussusceptions

Large caecal tumours and distal ileal adenomas causing ileocaecal intussusception were common in $Apc^{fl/fl}$ *Lgr5-Cre* mice independent of *Cdh1* genotype and therefore whilst

interesting are of less importance in this experiment. Caecal tumours and ileocaecal intussusceptions had rarely been observed in Apc^{Min} and $Apc^{+/fl}$ *Vil-Cre* models. *Lgr5* mRNA expression and the number of *Lgr5+* cells are slightly higher in the distal part of the murine small intestine compared with the proximal and middle regions, but much lower in the caecum (Leedham et al, 2012) so higher recombination rates seems an unlikely explanation for the large caecal tumours.

The ileum and caecum mark a transition point from a relatively sterile small intestine to the colon where the microbiota plays a key role in the digestion of intestinal material and microbes make up 50% of faecal material (De Cruz et al, 2012). There is evidence for the microbiota being important in the development of inflammatory bowel disease, including from an IL-10 deficient mouse model where colitis only develops in the presence of resident enteric bacteria (Sellon et al, 1998) and the observation that antibiotic treatment often improves inflammation in Crohns disease and Ulcerative Colitis (Chamberlin et al, 2011; Ohkusa et al, 2010; Sartor, 2004; Talley et al, 2011). Further, in some mouse models of inflammatory bowel disease, tumour incidence is related to the presence of specific pathogens such as *Helicobacter hepaticus* (Fox et al, 2011).

The incidence of large caecal tumours and ileocaecal intussusceptions in our model may reflect inflammation at those sites of the intestine. The tumour burden and size is not influenced by *Cdh1* genotype and the animals are known to not be colonized with *Helicobacter hepaticus* so the mechanism is unknown. A simple way to evaluate if inflammation is likely to play a role in the development or progression of these tumours would be to assess the tumour phenotype when a cohort of the animals were treated with broad spectrum antibiotics. The caecal tumours were advantageous for culture because of their size and given their location may be more representative of human CRCs than the small intestinal adenomas traditionally studied using mouse models.

5.4.3 Interpretation of effect of EDTA treatment

As E-cadherin relies on calcium for its adhesive function, treatment with EDTA was undertaken to frame the effect of loss of the adhesive function of E-cadherin. Live cell imaging showed rapid changes in adenoma morphology within minutes, with involution of adenoma spheres,

and disaggregation of cells but was notable for the absence of highly motile, spindle shaped cells with filopodia as seen in the $Apc^{fl/fl}$ $Cdh1^{fl/fl}$ Ad-Cre+ cultures. Immunolabelling showed small rounded cells with loss of membrane bound E-cadherin, apoptotic nuclear changes and variable β-catenin and cleaved caspase 3 expression that did not bear resemblance to the EMT cells seen in $Apc^{fl/fl}$ $Cdh1^{fl/fl}$ Ad-Cre+ culture. This may represent anoikis. It has previously been shown using a mammary epithelial cell line that the loss of E-cadherin adhesion alone is not sufficient to activate EMT (Onder et al, 2008). Onder and colleagues used sh-RNA mediated knock-down of E-cadherin or expression of dominant negative truncated form of E-cadherin (DN-Ecad) that lacks the extracellular domain. Sh-RNA knock-down of E-cadherin resulted in cells with fibroblast morphology which was recoverable with reexpression of *Cdh1*.

5.4.4 Complete loss of Cdh1 in adenoma cells results in Wnt pathway upregulation and EMT

This work provides strong observation evidence that genetic loss of *Cdh1* contributes to Wnt pathway activation as assessed by nuclear localization of β-catenin and Axin2. There is also EMT as assessed by expression of the markers Fibronectin, Twist and Vimentin. The fibroblast like cells are *Rosa-YFP* positive indicating they originate from adenoma cells where recombination of *Apc* and activation of *Rosa-YFP* has taken place with tamoxifen *in vivo*. The cells with fibroblast appearance are motile and have very low rates of cell division and apoptosis. Senescence and resistance to apoptosis are both features of EMT that promote cell survival (Tiwari et al, 2012).

The ability of β-catenin originally bound to E-cadherin to contribute to Wnt signalling has been controversial. However mechanistically it is plausible that particularly in the context of an impaired β-catenin destruction complex, as in the setting of *Apc* loss, free β-catenin that has dissociated from a complex with E-cadherin could increase Wnt signalling. This is supported by recent evidence that our understanding of the degradation of β-catenin by the APC/Axin1 complex has been incorrect. Rather than Wnt signalling leading to inhibition of phosphorylation of β-catenin and disassembly of the APC/Axin complex, Wnt activation inhibits ubiquitination of β-catenin within the complex, saturating the complex with phosphorylated β-catenin resulting in newly synthesised unphosphorylated β-catenin being capable of contributing to Wnt

signalling (Li et al, 2012). This suggests that in the context of Wnt activation any increase in free cytoplasmic β-catenin, for example through release from the E-cadherin complex, could contribute to Wnt signalling as destruction complexes are saturated.

There has been much contention about the role of E-cadherin in EMT, specifically if loss or downregulation has the ability to initiate EMT or if it is merely a mediator of EMT when the process has been initiated by other factors. In epithelial cancers and developmental processes requiring EMT, multiple levels of regulation exist to control E-cadherin expression. A number of transcriptional repressors of E-cadherin are activated during EMT, including Slug, Snail, Twist, and ZEB-1 (Bolós et al, 2003; Cano et al, 2000; Peinado et al, 2007; Stemmler et al, 2003; von Burstin et al, 2009; Yang et al, 2004). MicroRNAs can strongly influence E-cadherin mRNA expression, for example in breast cancer cells miR-9, a C-Myc activated miRNA, directly targets E-cadherin (Ma et al, 2010) In cancer, transcription is also commonly modified by methylation of the E-cadherin promoter (Berx & van Roy, 2009; Hirohashi, 1998; Wheeler, 2005) and E-cadherin protein expression is often modulated by proteolysis (Schmeiser & Grand, 1999; Solanas et al, 2011; Steinhusen et al, 2001). Mutations in the *Cdh1* gene are common in diffuse hereditary gastric cancer (Guilford et al, 1999). As discussed in the introduction, two key mouse models have shown evidence for E-cadherin being important in initiating or preventing metastasis: a model of invasive lobular breast cancer with combined *p53* and *Cdh1* loss, and a model of pancreatic β-islet cell carcinogenesis where overexpression of E-cadherin prevented transition from adenoma to invasive carcinoma (Derksen et al, 2006; Perl et al, 1998). This study provides further evidence that in intestinal adenoma cells, loss of E-cadherin is implicated in an EMT phenotype in the context of Wnt pathway activation.

The study by Onder and colleagues using shRNA knock-down of E-cadherin provides some insights highly relevant to this work (Onder et al, 2008). They found that shRNA knockdown of E-cadherin in mammary epithelial cells (HMLER-shEcad) could activate EMT and cells were resistant to anoikis, but that expression of a dominant negative form of E-cadherin lacking the extracellular domain (HMLER-DN-Ecad) that could cause cellular dissociation was insufficient to activate EMT. Orthotopic transplant of these cells to the mammary fat pad led to numerous microscopic and macroscopic lung metastasis with HMLER-shEcad cells but no macroscopic lung

nodules with HMLER-DN-Ecad cells. Tail vein injection of tumour cells resulted in numerous lung metastases with HMLER-shEcad cells but no metastases with HMLER-DN-Ecad cells. β-catenin was shown to have a critical role in the phenotype. Levels of active cytoplasmic and nuclear β-catenin were increased with E-cadherin knock-down. Knock-down of β-catenin in HMLER-shEcad cells resulting in reduced growth rate and reduced expression of mesenchymal markers *in vitro,* and reduced ability to form lung metastases with tail vein injection of the cells. β-catenin activation alone was insufficient to induce EMT. Gene expression analysis of HMLER-shEcad and HMLER-DN-Ecad revealed that in HMLER-shEcad cells 19 genes were upregulated more than three-fold compared with controls and only 2 of these were also upregulated in HMLER-DN-Ecad cells. At least one of the 17 genes uniquely upregulated in HMLER-shEcad cells must therefore contribute to metastatic potential and Twist was shown to be vital to this process.

The *Apc*$^{fl/fl}$ *Cdh1*$^{fl/fl}$ *Lgr5-Cre in vivo* model induces loss of *Apc* and *Cdh1* simultaneously, whereas the *in vitro* model reflects more closely the sequence of genetic events proposed in human CRC development: initiating *APC* mutation followed by downregulation of *CDH1* during the late stage of tumour progression. An improved *in vivo* model would also be able to reflect this sequence. A possible way to do this would be to use an *Apc*$^{+/Min}$ model with *Cdh1*$^{fl/fl}$ *Vil-CreER*^{T2}, however it would rely on successfully titrating tamoxifen dose to achieve some recombination of *Cdh1* in adenomas but avoid the lethality seen with widespread *Cdh1* homozygosity in the adult intestine. A superior method would be to use two different conditional knock-out systems, for example the Cre-loxP system to achieve homozygous *Apc* loss using *Lgr5-CreER*^{T2} with tamoxifen, and a FLP-FRT system with a ligand binding domain other than the oestrogen receptor to achieve homozygous *Cdh1* loss at a later stage when you knew adenomas would be present. The FLP-FRT system uses flippase (FLP) recombinase, from the yeast Saccharomyces cerevisiae, to excise part of a gene of interest flanked by FLP recombinase target (FRT) sequences (Sadowski, 1995). As FLP-FRT is a much newer system there are fewer transgenic animals available and currently no intestinal or *Lgr5* specific inducible FLPs. The ability to culture adenomas in three dimensions however means the *in vitro* system is an increasingly appealing method of investigating these questions in a system that reflects *in vivo* adenoma

growth more closely than conventional cell culture without expensive and lengthy mouse engineering and breeding. Another way to investigate the metastatic potential of the $Apc^{fl/fl}Cdh1^{fl/fl}$ Ad-Cre+ cells would be by orthotopic transplant or tail-vein injection, however this would rely on successfully purifying the cells from matrigel. Also, as in these cells *Cdh1* loss has been achieved by knockout of the gene rather than through transcriptional downregulation or post-translational modification, the cells may not be capable of performing the mesenchymal-epithelial transition necessary to colonise a secondary organ with metastases.

The absence of metastatic disease or invasion in $Apc^{fl/fl}$ $Cdh1^{fl/fl}$ *Lgr5-Cre* animals may be due to the absence of any cells that have completely lost *Cdh1*, however this begs the question what determines a difference in survival *in vivo* versus *in vitro*? As discussed the cell type losing *Cdh1* may be important, as may be the sequence of loss of *Apc* and *Cdh1*. However we cannot exclude the role of the tumour microenvironment in modifying cellular behaviour. The culture model offers the potential to control factors such as cytokines and growth factors that may be important in the tumour microenvironment and see how this influences the EMT phenotype.

5.5 Future directions

5.5.1 Is the EMT and Wnt upregulation phenotype with Cdh1 loss reversible?

As distant metastases are the same tissue type as the primary tumour, if cancer cells undergo an EMT *in vivo* they must also undergo mesenchymal-epithelial transition (MET) when they establish themselves in a secondary organ. EMT is notoriously difficult to detect and prove in tumourigenesis *in vivo* and thus its existence remains controversial (De Wever et al, 2008).

Current work explores whether the EMT and Wnt upregulation phenotype seen with $Cdh1^{fl/fl}$ recombination in adenoma cells *in vitro* is reversible. A retroviral construct expressing murine E-cadherin was obtained from Professor Laurent Brossay (Brown University, USA). This construct was created by subcloning E-cadherin into the MSCV-IRES-GFP retroviral vector and successfully used to transduce T cells and fibroblasts (Tessmer et al, 2007). As the readout for Cre-recombination in $Apc^{fl/fl}$ $Cdh1^{fl/fl}$ Ad-Cre+ adenomas has been Cre-immunolabelling and loss of membrane bound E-cadherin, attempt to rescue the phenotype with this construct could be complicated by difficulty detecting cells where endogenous *Cdh1* has been recombined but

then been rescued by retroviral transduction with exogenous *Cdh1*. Although the construct has a GFP reporter, the adenomas already express YFP which we detect with an anti-GFP antibody. Also there are frequently spindle shaped cells that are YFP positive and have no membrane bound E-cadherin but are negative for immunolabelling of Cre recombinase suggesting that Cre detection by immunolabelling alone may not be reliable for detection of recombination.

To address this a second construct is being made with the MSCV-IRES-GFP backbone but replacing the GFP with tdtomato, and subcloning in a puromycin selection cassette and Cre recombinase. The tdtomato is a kind gift from Dr Shankar Srinivas (University of Oxford). This will allow for selection of only cells expressing Cre that will fluoresce red. By using mice that are wildtype for *RosaYFP* the GFP reporter from the E-cadherin construct will be reliable and cells expressing both Cre recombinase and exogenous E-cadherin will be detectable as yellow allowing characterization.

5.5.2 Determination of the contribution of loss of adhesion or β-catenin binding to the EMT phenotype

Cre-mediated recombination of $Cdh1^{fl/fl}$ excises exons 4 to 15 of *Cdh1* disrupting both the extracellular and cytoplasmic domains (Derksen et al, 2006). Loss of both domains in this model in the setting of Wnt pathway gain of function leads to Wnt upregulation and EMT. As the two domains have very specific functions, current work explores loss of only the adhesive function in an attempt to dissect out the role of loss of adhesion versus loss of β-catenin binding on Wnt pathway upregulation and EMT. To do this a retroviral vector expressing E-cadherin that is identical to that described in 5.5.1 is being constructed, except the highly conserved tryptophan residue (Trp2) that is vital for adhesion through strand swapping of the N-terminal extracellular domains of E-cadherin has been changed to an alanine residue. This mutation (W2A) has been shown to prevent strand swapping (Tamura et al, 1998). In addition to assessing if wildtype E-cadherin can rescue the $Apc^{fl/fl}$ $Cdh1^{fl/fl}$ Ad-Cre+ phenotype as outlined in section 5.5.1, I will also examine the effect of transduction with the mutant construct on the phenotype. For both of the above experiments in addition to characterization using immunolabelling, FACS analysis will be used, in particular labelling for E-cadherin, β-catenin, cleaved caspase 3 and detection of GFP and tdtomato fluorochromes.

6 The effect of combined *Smad4* and *Apc* homozygosity using *Lgr5-Cre*

6.1 Introduction

This chapter shows preliminary work investigating the effect of homozygous loss of another candidate gene involved in the progression of CRC, *Smad4*. *SMAD4* mutations are common in CRC and additionally *SMAD4* can influence transcription of *CDH1* (Takano et al, 2007). The $Apc^{fl/fl}$ *Lgr5-Cre* model used for the experiments described in Chapter 5 is used.

Smad family member 4 (Smad4) is a core protein involved in the TGFβ signaling pathway. In humans there are at least 42 members of the TGFβ superfamily, with Bone Morphogenetic Proteins (BMP) the largest subgroup with over 20 growth factors identified (Bragdon et al, 2011; Massagué et al, 2005). Much of our understanding of the pathway has come from *Drosophila* and *C. Elegans* models which have fewer numbers of known family members (Massagué et al, 2005). In fact the term *Smad* was coined when sequence homology was discovered between newly discovered human SMAD1, the *C. Elegans* Sma proteins and *Drosophila* Mad proteins (Liu et al, 1996). The TGFβ superfamily has a wide range of ligands involved in regulation of a broad range of cellular functions including cell growth, differentiation, migration, adhesion and apoptosis (Schmierer & Hill, 2007). Correct function is vital for embryogenesis, particularly germ-layer specification and patterning, and the pathway is often dysregulated in cancer.

6.1.1 SMAD4 structure, function and signalling

Smad4 is the only mammalian co-Smad and interacts with receptor-regulated R-Smads to form transcriptionally active complexes. A schematic of the basic TGF-β signalling pathway is outlined in Figure 84. TGFβ ligands bind to type I and II receptors to form active receptor complexes. The type II receptor kinase phosphorylates the type I receptor enabling the recruitment of receptor-regulated Smads 2 and 3. The type I receptor then phosphoylates the R-SMADs at the C-terminus and this facilitates binding to SMAD4 and formation of heteromeric complexes. The R-SMAD-SMAD4 complexes can translocate to the nucleus where they bind promoter regions

and transcriptional activators. The same process takes place for the BMP pathway: BMP ligands bind to BMPRI and BMPRII, forming an active complex that mediates phosphylation of R-SMADS 1, 5 and 8. These R-SMADs bind to SMAD4 and the complex translocates to the nucleus. Transcriptional regulation is modulated through association with a range of coactivators or corepressors. Additionally the inhibitory SMADs, SMAD6 and SMAD7, are upregulated by SMAD-mediated transcriptional pathways and can downregulate TGFβ and BMP signaling through diverse mechanisms including the recruitment of Smurfs, E3 ligases that facilitate ubiquitin-mediated degradation of receptors (Massagué et al, 2005; Schmierer & Hill, 2007).

The SMAD proteins share a similar basic structure. They are all about 500 amino acids in length and have two globular domains, Mad-homology 1 and 2 (MH1 and MH2), joined by a linker region (Shi & Massagué, 2003). The linker region varies substantially between the different proteins, but the MH1 domain is highly conserved in the R-SMADs and SMAD4 (but not the I-SMADs), and the MH2 domain is conserved in all SMADs. MH1 domains mediate DNA binding, the linker region is an important site for regulation by ubiquitination and phosphorylation and the MH2 domain is responsible for interactions with receptors, other SMADs and transcriptional cofactors. A region called the Smad4 activation domain (SAD) at the boundary between the linker and MH2 domain is the site for interactions with transcriptional activators and repressors (Massagué et al, 2005).

The mechanisms by which particular ligand and receptor combinations activate a complex range of transcriptional programmes that are cell-type and context specific by signaling through the Smads involves extensive regulation that remains incompletely understood (Schmierer & Hill, 2007). Additionally TGFβ activation can influence a number of SMAD-independent pathways, including phosphatidylinositol 3-kinase, mitogen-activated protein kinase and RhoA pathways (Bragdon et al, 2011).

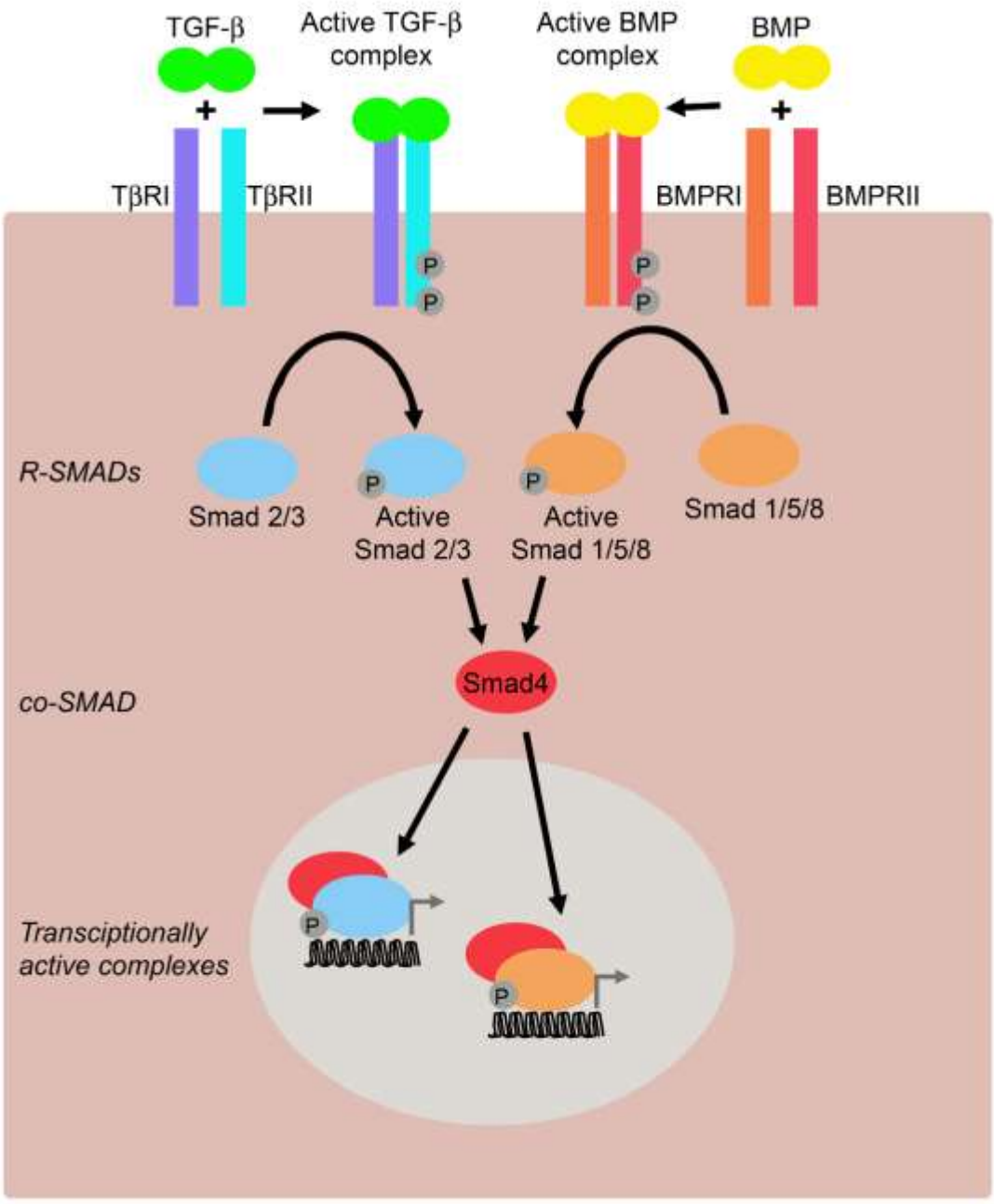

Figure 84. TGFβ and BMP signaling through the Smads

TGFβ or related ligands bind TβRI and TβRII to form an active complex. This active complex of serine-threonine kinase receptors can phosphorylate the receptor Smads 2 and 3. Active Smad2 and Smad3 are then able to form heteromeric complexes with Smad4 in the cytoplasm, translocate to the nucleus, interact the DNA binding proteins and activate transcription of target genes (Lagna et al, 1996). Similarly association of BMP ligand with BMPRI and BMPRII leads to an active complex that can phosphorylate Smads 1, 5 and 8. These Smads can then bind to Smad4 to form transcriptionally active complexes. Noggin is a BMP inhibitor used in intestinal crypt and adenoma culture. Adapted from (Radisky & Bissell, 2004)

6.1.2 TGFβ pathway in tumourigenesis

TGFβ pathway mutations are common in human cancers and the BMP pathway is inactive in 70% of CRCs (Kodach et al, 2008). TGFβ has conflicting roles in tumourigenesis: growth inhibition, but also, transcriptional activity that favours EMT and invasion (Akhurst & Balmain, 1999; Massagué, 2012). The mechanisms underlying the switch from one role to the other are poorly understood, but there is some evidence *Smad4* may be implicated. In MC38 cells, a *Smad4* null cell line, re-expression of *Smad4* restored growth inhibition induced by TGFβ and decreased their invasive ability, including in a splenic injection metastasis mouse model (Zhang et al, 2010). The results were confirmed using a human colon carcinoma cell line lacking *SMAD4*, suggesting *SMAD4* may have a role in influencing the switch of TGFβ from a tumour suppressor to a tumour promoter. Restoration of SMAD4 in a deficient colorectal cancer cell line has also been shown to transcriptionally induce E-cadherin expression (Müller et al, 2002) and in a pancreatic cancer cell line SMAD4 has been shown to mediate TGFβ induced downregulation of E-cadherin induced through Snail and Slug (Takano et al, 2007).

6.1.3 Smad4 and tumourigenesis

SMAD4 mutations have been identified in a number of cancers. *SMAD4* was first identified as a potential tumour suppressor gene through the study of allelic loss of chromosome 18q in pancreatic cancers, at which time it was called *DPC4* (Deleted in Pancreatic Carcinoma) (Hahn et al, 1996). Allelic loss of 18q21 is common in CRC, occurring in up to 60% of cases (Thiagalingam et al, 1996). A number of genes implicated in CRC are located here, including Deleted in Colorectal Cancer (*DCC*), *SMAD4* and *SMAD2*. Whilst *DCC* and *SMAD2* mutations are rare in human CRCs, *SMAD4* mutations have been implicated in about a third of CRCs showing 18q21 loss.

SMAD4 mutations have been confirmed as common driver mutations in human CRC in several large genomic studies including the recent comprehensive molecular characterization of human colon cancer (Cancer Genome Atlas Network, 2012; Network, 2012; Sjöblom et al, 2006; Wood et al, 2007). *Smad4* mutations are infrequent in early stage colorectal cancer (Mamot et al, 2003) but more common in advanced tumours (Miyaki et al, 1999), suggesting they have a role

in the later stages of adenoma-carcinoma transition. Screening of 44 CRC cell lines showed that loss of SMAD4 was common in lines without microsatellite instability (MSI) (44%), typically through loss of one allele and then mutation of the other, often in the MH2 domain. SMAD4 loss was however very uncommon in lines with MSI (0%) (Woodford-Richens et al, 2001a)

Familial syndromes have again been important in understanding this tumour suppressor gene. Juvenile polyposis syndrome (JPS) is a condition characterized by inflammatory gastrointestinal polyps and increased risk of colorectal cancer. Diagnostic criteria are the presence of five or more juvenile polyps in the colorectum, juvenile polyps throughout the gastrointestinal tract, or a positive family history of juvenile polyposis and any number of polyps (Jass et al, 1988). The condition is usually diagnosed by the age of 20, with patients presenting because of a family history or with rectal bleeding, rectal prolapse, anaemia or abdominal pain. Polyp frequency is variable, from less than 10 to hundreds of polyps. Whilst the polyps are usually benign, JPS confers an increased risk of colorectal cancer: a relative risk of 34 compared with the normal population and a cumulative life-time risk of 38.7% (Brosens et al, 2007).

Germline mutations in *SMAD4* or *BMPR1A* have been identified in 50-60% of patients with JPS (Brosens et al, 2011; Howe et al, 1998; Woodford-Richens et al, 2000a). Additionally *SMAD4* mutations are very common in people with combined JPS and hereditary haemorrhagic telangiectasia (HHT), who have an increased risk of early onset CRC (Schwenter et al, 2012). The majority of *SMAD4* mutations are point mutations or deletions of a small number of base pairs that result in proteins truncated at the carboxyl-terminus, however deletion of whole exons or the complete coding region account for about 15% of mutations; mutations in the *BMPR1A* promoter are seen in 10% of cases (Brosens et al, 2011; Calva-Cerqueira et al, 2010). Germline mutations can be sporadic, or inherited in an autosomal dominant manner. In the majority of JPS polyps with *SMAD4* mutations, there is LOH of the wildtype allele (Woodford-Richens et al, 2000b; Woodford-Richens et al, 2001b).

JPS polyps have histological characteristics distinct to adenomas. Whereas histological changes in adenomas are predominantly in the epithelial cells, classically JPS polyps are hamartomatous consisting of normal or dilated cystic crypts embedded in a prominent stroma with surface erosion and inflammatory changes (Jass et al, 1988; van Hattem et al, 2011). A minority of

polyps (about 20-40%) do not fit the classical description, with less prominent lamina propria, more epithelium and more frequent epithelial dysplasia (Jass et al, 1988; van Hattem et al, 2011). Atypical, epithelial-rich, polyps are more common with *SMAD4* mutation than *BMPR1A* mutation (van Hattem et al, 2011). JPS polyps are predominantly distributed in the colorectum, however can also be found in the upper gastrointestinal tract, the latter being more common with *SMAD4* mutation (Brosens et al, 2011).

The observation that the altered stromal environment may be responsible for increased CRC susceptibility in JSP led Kinzler and Vogelstein to postulate that rather than acting as a classic tumour suppressor with a 'gatekeeper' function to prevent excessive growth (such as *APC* in familial adenomatosis polyposis), or a 'caretaker' function involved in DNA repair (such as *MSH2* in HNPCC), *SMAD4* may have a 'landscaper' function, changing the terrain of epithelial cell growth (Kinzler & Vogelstein, 1998).

Additionally loss of *SMAD4* as assessed by immunohistochemistry may have potential as a prognostic indicator in CRC, particularly when predicting early recurrence or disease free survival after attempted curative surgery, or when combined with tumour-stroma ratio assessment (Ahn et al, 2011; Isaksson-Mettävainio et al, 2012; Kawakami et al, 2010; Mesker et al, 2009; Tanaka et al, 2006). The role of *SMAD4* downregulation in human adenomas prior to progression to adenocarcinomas is not known.

6.1.4 Mouse models targeting Smad4

Germline homozygosity of *Smad4* is embryonic lethal due to failure of gastrulation (Sirard et al, 1998; Yang et al, 1998). Heterozygote animals are viable and fertile but develop inflammatory polyps in the stomach and duodenum after 1 year of age that histologically closely resemble those seen in JPS, with stromal cell proliferation and prominent eosinophil and plasma cell infiltrates (Taketo & Takaku, 2000). The polyps had LOH of the wildtype *Smad4* allele but no Wnt pathway activation. No common mutations in *Kras*, *Hras*, *N-ras*, *p53* or *Pten* were identified in these lesions.

In the human *SMAD4* and *APC* are located on chromosomes 18 and 5 respectively however in the mouse *Smad4* and *Apc* are both located on chromosome 18, within 30cM of each other.

Combined $Apc^{\Delta 716}$ and *Smad4* heterozygosity resulted in tumours with a more malignant phenotype than those seen with $Apc^{\Delta 716}$ alone (Takaku et al, 1998). The tumours had LOH of both *Smad4* and *Apc*. The compound heterozygotes had fewer small intestinal polyps (only 12% of the total seen in the $Apc^{\Delta 716}$ heterozygotes), but more colonic polyps. The tumours with *Smad4* loss were significantly larger and showed advanced histological changes with early stromal proliferation and smooth muscle thickening developing into adenocarcinomas containing mucinous cells and showing submuscosal invasion. There was no evidence of metastasis by 14-20 weeks when the animals became unwell. This experiment was done on a mixed C57BL/6 and 129/Sv background. With increased backcrossing to C57BL/6J polyp numbers increased, however the invasive phenotype persisted.

Strengthening Kinzler and Vogelstein's 'landscaper' hypothesis, Kim and colleagues showed that conditional homozygous loss of *Smad4* in T cells resulted in spontaneous epithelial tumours throughout the gastrointestinal tract, whereas *Smad4* loss in epithelial cells did not give rise to tumours (Kim et al, 2006). Using Cre recombinase driven by the Lck or CD4 promoter they showed that T cell specific loss of *Smad4* produced a thickened intestinal mucosal surface, with pedunculated and sessile polyps notable for prominent stromal and mononuclear cell infiltrates resembling polyps seen in JPS. Invasive carcinomas with metastasis were observed. Epithelial cell specific loss of *Smad4* using Cre recombinase under the Mouse Mammary Tumour Virus (MMTV) or transthyretin promoter resulted in efficient loss of Smad4 in epithelial cells, but no epithelial tumours. Epithelial specific expression of a dominant-negative Smad4 known to completely disrupt TGF-β signalling through a truncated Smad4 lacking a DNA-binding MHI domain did not lead to intestinal tumourigenesis either.

A sleeping beauty transposon-based genetic in mice, that analysed over 16,000 transposon insertions in adenomas and adenocarcinomas identified 77 candidate genes for CRC, identifying *Smad4* as one of 15 genes most likely to be driver mutations in the disease (Starr et al, 2009).

6.1.5 Mouse models targeting other TGFβ components

A number of mouse models targeting components of the TGFβ superfamily have been described. This summary focuses on mutations in TGFβ components that have resulted in intestinal polyps, either alone or in combination with *Apc* mutations.

Mouse models investigating the effect of combined *Apc* and *Smad2* loss have shown conflicting results. Hamamato and colleagues showed that combined Apc^{580D} and *Smad2* heterozygosity resulted in tumours with a more malignant phenotype than those seen with Apc^{580D} alone (Hamamoto et al, 2002). There was no change in total adenoma number, but the compound heterozygotes had increased incidence of sudden death due to intestinal obstruction from large tumours, and tumours showed invasive features never seen with *Apc* loss alone. The changes were less marked than with *Smad4* mutation and unlike *Smad4*, heterozygous *Smad2* loss without *Apc* loss did not lead to tumourigenesis. However Takaku and colleagues showed *Smad2* loss in the $Apc^{\Delta 716}$ model had no effect on adenoma number, size or histopathology, unlike their observations for *Smad4* using the same system (Takaku et al, 1998; Takaku et al, 2002). Hamamato's study was on a C57BL/6 background and Takaku's used *Smad2* animals backcrossed three generations onto C57BL/6 and $Apc^{\Delta 716}$ animals backcrossed 13 generations suggesting strain dependent effects could be implicated.

$Smad3^{-/-}$ mice are viable and have no small intestinal abnormalities but develop colorectal tumours with lymph node metastasis between 18 and 24 weeks with 100% penetrance on a 129/Sv background and 30% penetrance on a hybrid 129/Sv and C57BL/6 background (Zhu et al, 1998). $Apc^{Min/+}$ $Smad3^{-/-}$ mice on a 129/Sv background develop tumours predominantly in the distal colon including invasive carcinomas (Sodir et al, 2006). Engle and colleagues used a model where $Rag2^{-/-}$ mice on a mixed strain background (97% 129S6 and 3% CF-1) developed spontaneous caecal and colonic hyperplasia that progressed to polyp formation (Engle et al, 1999). $Tgfb1^{-/-}$ $Rag^{-/-}$ animals rapidly developed adenomas and carcinomas, but no metastatic disease. This was despite no alteration in proliferation, inflammation or mismatch repair mechanisms.

Complete conditional loss of *Tgfbr2* in the intestine using *Villin-Cre* had no effect on cellular proliferation and did not induce spontaneous tumourigenesis (Muñoz et al, 2006). However when combined with $Apc^{1638N/+}$, animals developed more advanced adenocarcinomas than the adenomas seen with $Apc^{1638N/+}$ alone (Muñoz et al, 2006). In $Apc^{Min/+}$ mice, *Tgfbr1* heterozygosity conferred a two fold increase in adenoma numbers, and animals also developed adenocarcinomas of the colon (Zeng et al, 2009). These changes occurred without *Tgfbr1* LOH. The compound heterozygotes had increased cellular proliferation in colonic crypts and tumours. Conditional inactivation of *Bmpr1a* in the intestine using *Mx1-cre* lead to overgrowth of intestinal tissue with increased numbers of crypts and fused villi, with progression to polyps that histologically resembled JPS (He et al, 2004). Thus the majority of mouse models combining *Apc* heterozygosity and TGFβ or BMP pathway downregulation have shown higher grade tumours, but strain dependent effects have been apparent.

6.1.6 TGFβ and Wnt pathway crosstalk

Work in mice, *Drosophila* and *Xenopus* has shown that during embryogenesis, particular patterning and differentiation events rely on both Wnt and TGFβ signaling (Attisano & Labbé, 2004). For example both Smad4 and β-catenin are vital for correct anterior-posterior axis formation (Huelsken et al, 2000; Sirard et al, 1998). Evidence for cooperation between TGFβ and Wnt pathways in cancer comes mostly from mouse models of CRC discussed above. There is evidence from *Xenopus* models for a direct interaction between LEF-1 and the Smads, including R-Smads, Smad4, LEF-1 and β-catenin forming a transcriptional activation complex on the Xenopus twin gene (*Xtwn*) promoter during establishment of Spemann's organizer and maximal activation of *Xtwn* relying on all four components being present (Labbé et al, 2000).

A recent study looked specifically at the effect of loss of Smad4 on Wnt signaling, using β-catenin as a marker of Wnt activation (Freeman et al, 2012). They used a number of experimental modalities to show an association between Smad4 loss and upregulation of the Wnt pathway, including microarray analysis of *Smad4* and *β-catenin* expression in human CRC samples, expression analysis of β-catenin in colorectal cell lines with *Smad4* knocked down, and a mouse model combining $Apc^{\Delta 1638/+}$ with *Smad4* homozygosity achieved using the

tamoxifen-inducible, intestinal-specific *K19Cre^{ERT2} Apc$^{\Delta 1638/+}$ Smad4$^{fl/fl}$ K19Cre^{ERT2}* animals on a C57BL/6J background had a 10 fold increase in tumour burden 5 weeks following tamoxifen treatment, compared with vehicle treated animals. In the Smad4 null tumours there was a significant increase in nuclear β-catenin localization, and increased β-catenin, C-Myc and Axin2 expression measured by RT-QPCR of laser-captured tumour samples. Overall these results suggest that Smad4 signalling may suppress intestinal tumourigenesis through modulation of β-catenin levels and Wnt pathway activation, however the mechanism is currently unknown.

6.2 Methods

General methods are described in Chapter 2. Methods specific to this chapter are described below.

6.2.1 Breeding

The breeding for this experiment is outlined in Figure 85. *Smad4$^{fl/fl}$* mice were obtained from Professor Elizabeth Robertson (University of Oxford) and were on a 129/C57BL/6J background. Again whilst a C57BL/6J background would have been preferred for these experiments, the time required to backcross them was prohibitive. Animals wildtype for *Lgr5-Cre* were used as controls.

6.2.2 Activation of Cre-recombination

As described in Chapter 5, Lgr5-Cre recombination was activated in adult mice at 8-12 weeks of age by intraperitoneal injection of tamoxifen in corn oil. Two doses of 200mg/kg tamoxifen were given to each mouse IP on successive days.

6.2.3 Immunolabelling

Immunolabelling for Smad4 using a fluorescent secondary antibody was difficult to optimize therefore in the first instance immunohistochemistry using 3-,3-diaminobenzidine (DAB) substrate was performed to confirm SMAD4 loss. The protocol was identical to that described in Chapter 2, Section 2.8 until addition of the secondary antibody. At that point samples were incubated with a biotinylated secondary antibody (DAKO) diluted in PBS for one hour. They were then washed in TBS three times (5 minutes each), incubated with an avidin-biotin complex

kit (Vectastain Elite ABC kit) for 30 minutes, washed in TBS three times and incubated in DAB substrate for 5 minutes. After rinsing in tap water the slides were counterstained with haematoxylin, rinsed in water, dehydrated by passing them through an alcohol series, placed in xylene twice for 5 minutes each and coverslips were mounted with Depex mounting medium (Electron Microscopy Services).

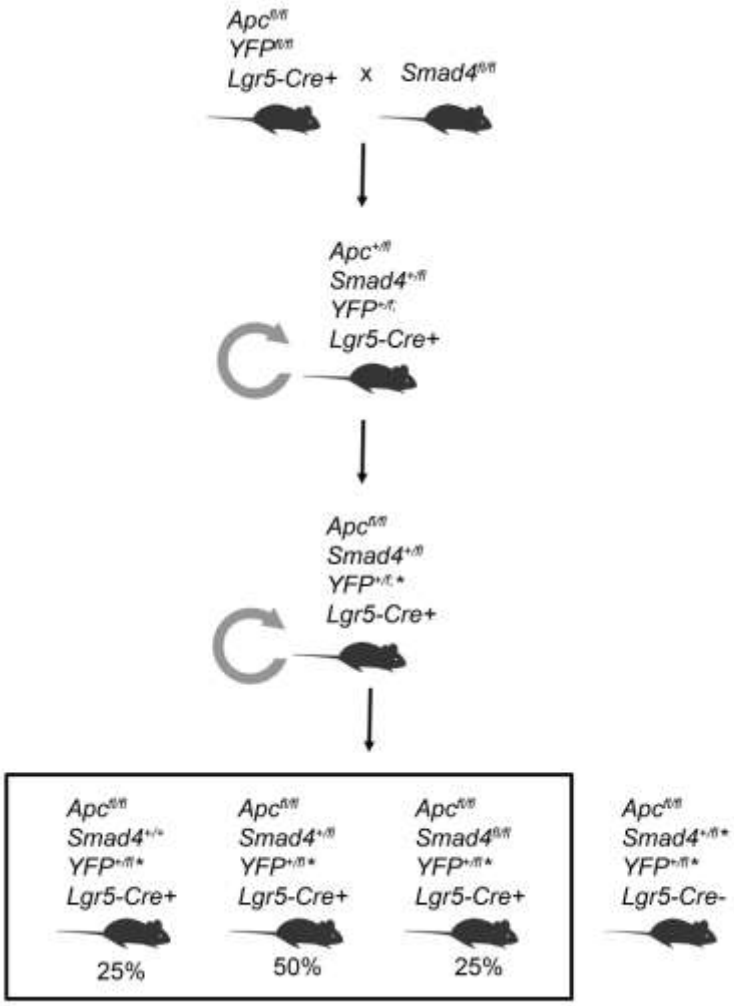

Figure 85. *Apc Smad4 Lgr5-Cre* breeding
Numbers below mice represent the expected Mendelian ratio of that genotype. *following a genotype (*YFP* in *Lgr5-Cre+* animals and *Smad4 and YFP* in *Lgr5-Cre-* animals) indicates that for simplicity only the most common heterozygous genotype has been represented in the figure, however wildtype or homozygous alleles were also generated. Circular arrows show intercross steps to breed the next generation of mice. The box outlines experimental animals.

6.3 Results

6.3.1 Altered survival and adenoma phenotype with Smad4 homozygosity

Apc$^{fl/fl}$ *Smad*$^{fl/fl}$ *Lgr5-Cre+* animals survived significantly longer than *Apc*$^{fl/fl}$ *Smad4*$^{+/+}$ *Lgr5-Cre+* animals (median survival 44 days and 26 days respectively, p=0.0113, log-rank test, Figure 86A). There was no significant difference in survival between *Apc*$^{fl/fl}$ *Smad4*$^{+/+}$ *Lgr5-Cre+* and *Apc*$^{fl/fl}$ *Smad4*$^{+/fl}$ *Lgr5-Cre+* animals, or *Apc*$^{fl/fl}$ *Smad4*$^{fl/fl}$ *Lgr5-Cre+* and *Apc*$^{fl/fl}$ *Smad4*$^{+/fl}$ *Lgr5-Cre+* animals.

Animals with homozygous *Smad4* loss had obvious differences in adenoma phenotype at dissection compared with animals heterozygous or wildtype for *Smad4.* Nearly all *Smad4* homozygotes had large caecal tumours with caecal weights greater than 0.5g (85% of animals), whereas tumours of this size these were seen rarely in *Smad4* heterozygotes (17% of animals) and never in animals with wildtype *Smad4* (Figure 86B-C). *Smad4* homozygotes also had a significantly lower adenoma burden in the small intestine than heterozygote or wildtype animals (mean adenoma count 42 and 55 for *Smad4* wildtype and hetereozygote animals respectively, compared with 8 for *Smad4* homozygote animals, p<0.001 one-way ANOVA with Bonferroni post-test. Figure 86D). There was no difference in colonic adenoma burden or the sizes of small intestinal and colonic tumours (Figure 86D). *Smad4* homozygotes had a significantly lower proportion of tumours in the proximal small intestine compared with the other genotypes (p=0.0278, one way ANOVA with Bonferroni post-test, Figure 86D). The large caecal tumours in the double homozygote animals could be related to their increased survival. Caecal weight was plotted against age at death for each genotype and linear regression analysis performed to generate a line of best fit (Figure 87). There was no significant difference between the slopes of the lines indicating tumour size did not correlate differently with age between the genotypes.

Preliminary assessment of histology by Professor Hans Morreau (Leiden University) has shown that *Apc*$^{fl/fl}$ *Smad4*$^{+/+}$ *Lgr5-Cre* animals usually have sessile adenomatosis and tubular adenomas care uncommon (documented in 2/8 small intestinal specimens). However in *Apc*$^{fl/fl}$ *Smad4*$^{+/fl}$ *Lgr5-Cre* and *Apc*$^{fl/fl}$ *Smad4*$^{fl/fl}$ *Lgr5-Cre* animals tubular adenomas are more common (3/7 and

4/6 specimens respectively, and the two *Smad4*$^{fl/fl}$ specimens without tubular adenomas showed either very small adenomas or no small intestinal adenomas). Small intestinal tumours were all low grade, regardless of genotype. Caecal tumour grades ranged widely independent of genotype, from low grade dysplasia to carcinoma *in situ*. Dirty necrosis was observed but inflammatory changes were otherwise not a prominent feature of the histology. I initially thought that large caecal tumours from *Smad4*$^{fl/fl}$ animals showed evidence of submucosal invasion similar to that shown in some *Smad4* mouse models where invasion had been reported (Figure 88), however on review by Professor Morreau he did not consider this true invasion.

6.3.2 Smad4 recombination using Lgr5-Cre is efficient

Immunolabelling of caecal tumours from *Apc*$^{fl/fl}$ *Smad*$^{fl/fl}$ *Lgr5+* animals confirmed Smad4 loss (Figure 89). Immunolabelling for *Smad4* using fluorescent secondary antibodies was challenging to optimize but preliminary staining showed *Smad4* loss in the same areas as increased cytoplasmic and nuclear β-catenin in *Apc*$^{fl/fl}$ *Smad4*$^{fl/fl}$ *Lgr5+* animals confirming loss of both *Apc* and *Smad4* (Figure 90).

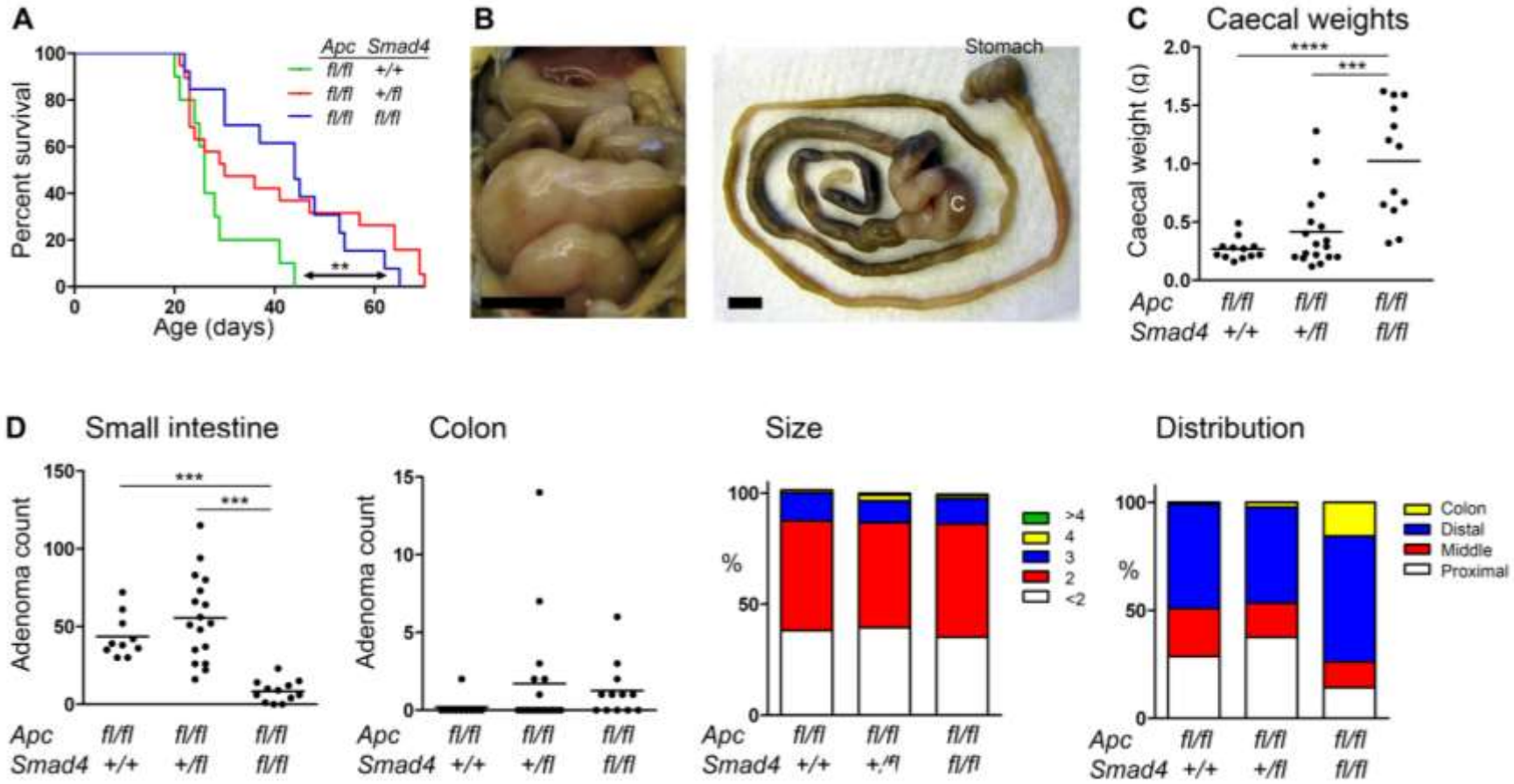

Figure 86. *Apc*$^{fl/fl}$ *Smad4*$^{fl/fl}$ *Lgr5-Cre* survival and adenoma phenotype

(**A**) Significant difference in survival with *Smad4* homozygosity. (**B**) Appearance of a large caecal tumour in an *Apc*$^{fl/fl}$ *Smad4*$^{fl/fl}$ *Lgr5-Cre+* mouse at dissection. Stomach and caecum (c) marked. Scale bars 1cm. (**C**) Significant difference in caecal weights between genotypes. (**D**) Small intestinal adenoma count significantly lower in *Apc*$^{fl/fl}$ *Smad4*$^{fl/fl}$ animals and a lower proportion of proximally distributed tumours. No difference in colonic adenoma numbers or adenoma sizes between genotypes. *Apc*$^{fl/fl}$*Smad4*$^{+/+}$ n=12, *Apc*$^{fl/fl}$*Smad4*$^{+/fl}$ n=18, *Apc*$^{fl/fl}$*Smad4*$^{fl/fl}$ n=13. Adenoma size measured in mm diameter. Log-rank test for survival analysis. One-way ANOVA with Bonferroni post-test for other analysis. ****=p<0.0001. ***=p<0.001. **=p<0.01

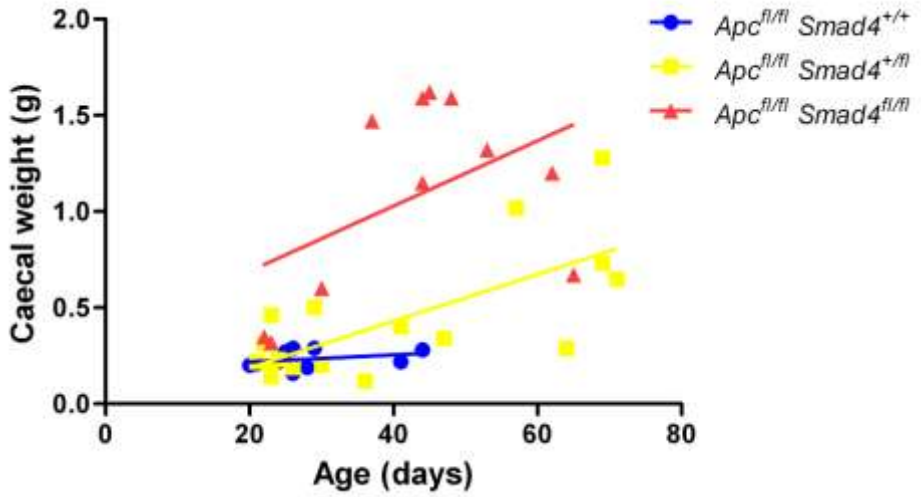

Figure 87. Comparison of caecal weight and age at death with or without *Smad4* loss
Graph shows age at death versus caecal weight for *Apc*$^{fl/fl}$ *Smad4*$^{+/+}$ *Lgr5-CreER*^{T2}, *Apc*$^{fl/fl}$ *Smad4*$^{+/fl}$ *Lgr5-CreER*^{T2} and *Apc*$^{fl/fl}$ *Smad4*$^{fl/fl}$ *Lgr5-CreER*^{T2} animals. Linear regression analysis was carried out to assess the correlation between age and caecal weight. There was no significant difference between slopes for the three genotypes, suggesting that the increased caecal weight with *Smad4* homozygosity may be related to increased survival.

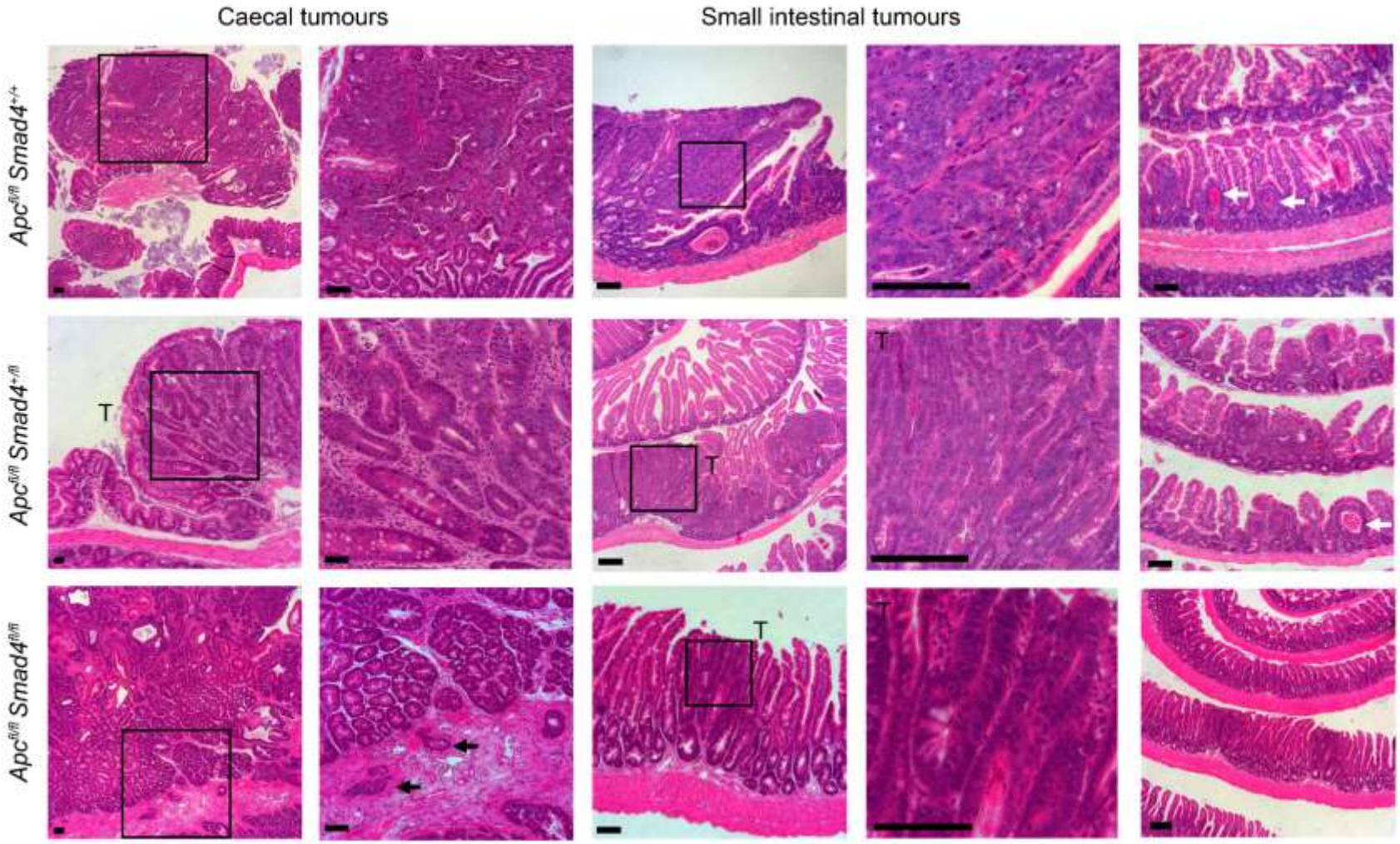

Figure 88. *Apc Smad4 Lgr5-Cre* histology

Representative examples of caecal tumour and small intestinal histology from *Apc*$^{fl/fl}$ *Smad4*$^{+/+}$ *Lgr5-CreER*^{T2}, *Apc*$^{fl/fl}$ *Smad4*$^{+/fl}$ *Lgr5-CreER*^{T2} and *Apc*$^{fl/fl}$ *Smad4*$^{fl/fl}$ *Lgr5-CreER*^{T2} animals. White arrows show examples of dirty necrosis. Black arrows show areas initially thought to be submucosal invasion. Examples of Tubular adenomas marked with **T.** Small intestinal diffuse adenomatosis apparent in *Apc*$^{fl/fl}$ *Smad4*$^{+/+}$ *Lgr5-CreER*^{T2} and *Apc*$^{fl/fl}$ *Smad4*$^{+/fl}$ *Lgr5-CreER*^{T2} images in right panel. Scale bars 100µm.

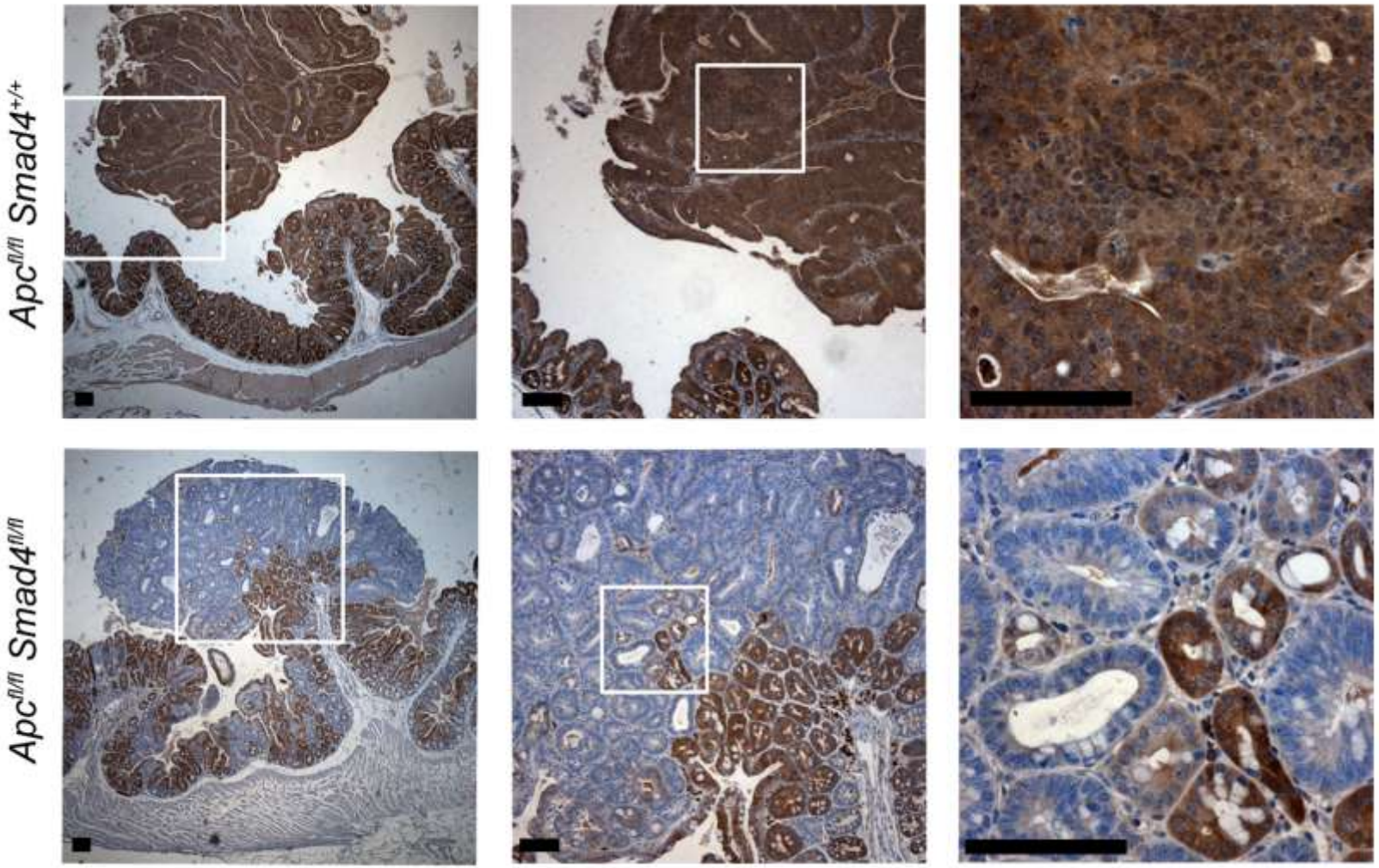

Figure 89. SMAD4 expression in *Apc$^{fl/fl}$ Smad4$^{fl/fl}$ Lgr5-CreER^{T2}* adenomas
Immunohistochemistry (DAB staining) of caecal tumours from *Apc$^{fl/fl}$ Smad4$^{+/+}$ Lgr5-CreER^{T2}* and *Apc$^{fl/fl}$ Smad4$^{fl/fl}$ Lgr5-CreER^{T2}* animals showing loss of SMAD4 protein expression with *Smad4* homozygosity. Areas in white boxes are shown at higher power in images to the right. Scale bars 100µm.

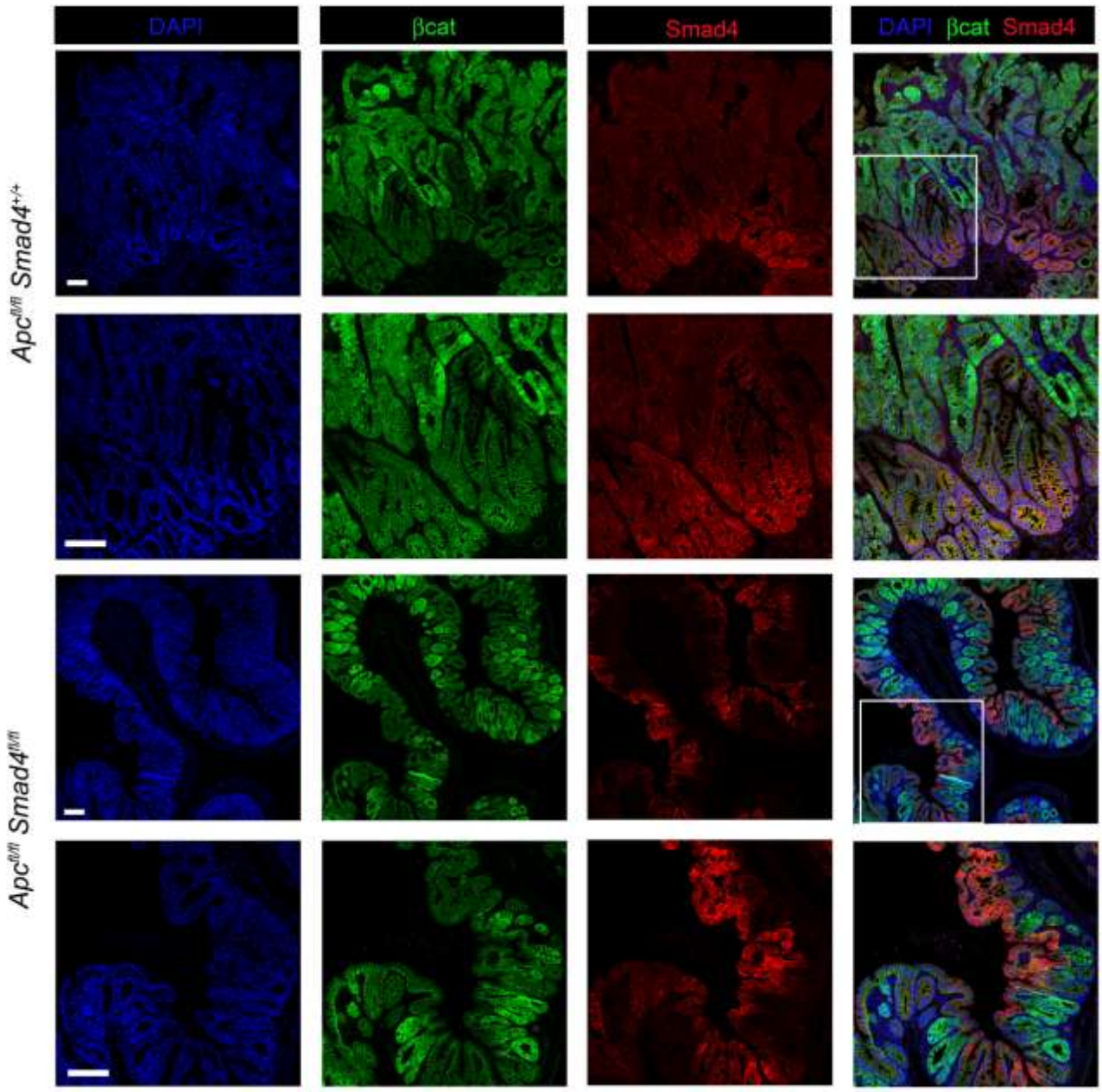

Figure 90. SMAD4 and β-catenin expression in *Apc$^{fl/fl}$ Smad4$^{fl/fl}$ Lgr5-CreER^{T2}* adenomas
Immunolabelling of caecum from *Apc$^{fl/fl}$ Smad4$^{+/+}$ Lgr5-CreER^{T2}* and *Apc$^{fl/fl}$ Smad4$^{fl/fl}$ Lgr5-CreER^{T2}* animals for DAPI, β-catenin and SMAD4 showing decreased SMAD4 expression in areas of the caecum with high β-catenin labelling. The areas marked with white boxes are shown at higher power in the following line. Scale bars 100μm.

6.4 Discussion

These results presented in this chapter are preliminary findings of an interesting phenotype. In an $Apc^{fl/fl}$ *Lgr5-Cre* model, *Smad4* homozygosity resulted in a significantly reduced number of small intestinal adenomas compared with *Smad4* heterozygosity or no *Smad4* loss. $Apc^{fl/fl}$ $Smad4^{fl/fl}$ animals survived longer than $Apc^{fl/fl}$ $Smad4^{+/+}$ animals, likely due to the reduced small intestinal adenoma burden. $Smad4^{fl/fl}$ animals developed large caecal tumours, possibly due to their extended survival. Preliminary analysis of tumour histology showed tubular adenomas were more common with *Smad4* loss, however there were no differences in tumour grade between genotypes.

The majority of mouse models combining TGFβ or BMP pathway inhibition and *Apc* loss have resulted in increased adenomatosis or increased invasiveness. Most of these models used *Apc* heterozygosity relying on a LOH event, and none used *Lgr5-Cre*. Our results in contrast show suppression of small intestinal adenomatosis with *Smad4* loss and no convincing increase in invasive tumours. It must however be noted that scoring of invasiveness in our study has been conservative compared to what is often seen in the mouse model literature.

The increased incidence of tubular adenomas (compared with villous or sessile adenomas) with *Smad4* loss suggests a role for BMP loss of function in the phenotype. Inactivation of *Bmpr1a* or overexpression of noggin, a BMP inhibitor, results in increased intestinal crypt formation (Haramis et al, 2004; He et al, 2004). Tubular adenomas have a glandular structure resembling tightly packed intestinal crypts. It is possible that these adenomas may be more difficult to identify on intestinal whole mounts than villous or sessile lesions during adenoma counting. Preliminary histological analysis however has reassuringly not shown a discrepancy with adenoma counts in $Apc^{fl/fl}$ $Smad4^{fl/fl}$ animals. Directed histological review with more samples is underway in an attempt to identify any subtle epithelial changes.

The observed phenotype may relate to the cell type in which recombination of $Apc^{fl/fl}$ and $Smad4^{fl/fl}$ has been activated. Maintenance of the intestinal stem cell requires crosstalk between a number of pathways including Wnt, BMP, Notch and Hedgehog (Crosnier et al, 2006). TGFβ/BMP pathway inhibition may have effects on intestinal stem cells (alone or in

combination with *Apc* loss) that are not seen in differentiated epithelial cells. For example in intestinal crypt culture BMP pathway inhibition with noggin is required to maintain the stem cell population (Sato et al, 2009). It is possible that an *Lgr5* positive stem cell with BMP pathway inactivation is unable to differentiate fully to form an adenoma.

This phenotype requires further characterization of the unexpected suppression of small intestinal adenomatosis with *Smad4* loss. A colleague is using crypt and adenoma culture systems to investigate this further.

7 Review and discussion

At the outset of this work it was known that in the mouse *Cdh1* homozygosity was embryonic lethal, and that *Cdh1* heterozygosity alone had no observable phenotype, but in combination with *Apc* heterozygosity it conferred a 9 fold increase in adenoma burden (Larue et al, 1994; Smits et al, 2000b). Germline *CDH1* mutations were implicated in hereditary diffuse gastric cancer and lobular breast cancer and downregulation of CDH1 was common in epithelial tumours as part of an EMT (Berx et al, 1995; Berx & van Roy, 2009; Guilford et al, 1998). In mouse models of pancreatic β-islet cell carcinogenesis and lobular breast cancer, *Cdh1* loss promoted invasion (Derksen et al, 2006; Perl et al, 1998). The ability of β-catenin bound to E-cadherin to contribute to Wnt signalling was controversial, despite evidence from *Drosophila* and *Xenopus* models that E-cadherin could modulate Wnt signalling through β-catenin availability, and cell culture experiments showing this was particularly so in the setting of Wnt activation (Gottardi et al, 2001; Heasman et al, 1994; Sanson et al, 1996; Stockinger et al, 2001).

In the past few years, dramatic advances have been made in both the understanding of intestinal biology and homeostasis, and regulation of the Wnt pathway. In particular, one must acknowledge the work by Hans Clevers' group identifying *Lgr5* as a stem cell marker, facilitating models where tumours can be generated quickly through stem-cell specific homozygous *Apc* deletion and the ability to reliably culture intestinal crypts and adenomas in 3D organoids (Barker et al, 2007; Sato et al, 2009). Additionally, just a few months ago, Clevers' group reported that our understanding of the degradation of β-catenin by the APC/Axin1 complex was incorrect (Li et al, 2012). Rather than Wnt signalling leading to inhibition of phosphorylation of β-catenin and disassembly of the APC/Axin complex, Wnt activation inhibited ubiquitination of β-catenin within the complex, saturating the complex with phosphorylated β-catenin, resulting in newly synthesised unphosphorylated β-catenin being capable of contributing to Wnt signalling. This suggests that in the context of Wnt activation any increase in free cytoplasmic β-catenin, for example through release from the E-cadherin complex, could contribute to Wnt signalling as destruction complexes are saturated.

The work in this thesis contributes to understanding the effect of loss of E-cadherin in the intestine, and particularly in the setting of *Apc* loss. It shows that E-cadherin loss in the visceral endoderm of the yolk sac likely leads to embryonic lethality. In the intestine, *Cdh1* loss with high levels of recombination has dramatic effects on the architecture of the crypt-villus unit, with disrupted barrier function and systemic bacteraemia. Both apoptosis and proliferation are increased, suggesting roles in anoikis of epithelial cells and attempted regeneration by the epithelium. *Cdh1* loss affects secretory cell lineages, most prominently through mislocalisation of Paneth cells that may be due to failed Eph-ephrin signalling usually mediated by E-cadherin. Despite upregulation of some Wnt target gene mRNA with *Cdh1* loss there is no convincing increase in cytoplasmic or nuclear β-catenin, consistent with *Cdh1* loss not contributing to Wnt signalling in the setting of a functional APC/Axin destruction complex. This work on *Cdh1* loss in the intestine supports the findings published by Schneider and colleagues during this study (Schneider et al, 2010).

Through detailed observational analysis, this thesis adds to the body of work supporting *Cdh1* loss being capable of modulating the supply of free cytoplasmic and nuclear β-catenin in the setting of *Apc* loss. Combined homozygous *Apc* and *Cdh1* loss with high levels of recombination resulted in phenotypic features seen with loss of each gene individually, and significantly increased nuclear β-catenin immunolabelling compared with *Apc* homozygosity alone. Heterozygous *Apc* models relying on LOH showed the potential for background strain to modify the effect of *Cdh1* heterozygosity. In a germline $Apc^{+/Min}$ model on a C57BL/6J background, germline *Cdh1* heterozygosity had no effect on adenoma phenotype, in contrast to previous reports on mixed backgrounds. In a conditional $Apc^{+/fl}$ *Vil-Cre* model on a mixed background, *Cdh1* heterozygosity conferred a significant increase in adenoma numbers but did not lead to invasive disease. In the *Vil-Cre* models survival was altered by background strain, independent of *Cdh1* loss. In the *Apc* heterozygosity models there was not convincing evidence that heterozygous *Cdh1* loss could modulate Wnt signalling.

Combined stem-cell specific homozygous *Apc* and *Cdh1* loss using *Lgr5-Cre* did not alter the adenoma phenotype, however genotyping, immunolabelling and RT-QPCR showed recombination of *Cdh1* was incomplete in these adenoma cells. One possibility for the absence

of any cells showing complete loss of E-cadherin was that cells with loss of both genes could not survive and underwent anoikis. An *in vitro* adenoma culture system was used to investigate this hypothesis and showed that complete recombination of *Cdh1* in adenoma cells resulted in cells with evidence of increased Wnt activation through measurement of nuclear β-catenin and Axin2, and epithelial mesenchymal transition through assessment of cell shape, motility and expression of the mesenchymal markers fibronectin, twist and vimentin. A strategy for definitively determining if this phenotype is due to *Cdh1* loss is underway and will include assessment of the specific contribution of E-cadherin adhesive function to the observed changes. The role of anoikis and apoptosis will also be assessed in more detail, as current results regarding this are inconclusive.

Smad4, an effector of the TGFβ and BMP pathways, is a known driver mutation in CRC. Additionally, it can influence *Cdh1* transcription during EMT. Most previous mouse models combining TGFβ pathway downregulation with *Apc* loss of function have shown an increase in adenoma numbers or adenomas with invasive features (Hamamoto et al, 2002; Muñoz et al, 2006; Sodir et al, 2006; Takaku et al, 1998). Stem-cell specific homozygous *Apc* and *Smad4* loss using *Lgr5-Cre* resulted in an unexpected phenotype: longer survival, a significant decrease in the number of small intestinal adenomas and no evidence of invasive disease. $Apc^{fl/fl}$ $Smad4^{fl/fl}$ animals were also noted to have large caecal tumours, however this may be related to their longer survival. *Smad4* loss was associated with tubular adenomas, which may suggest BMP downregulation is influencing the phenotype. The mechanism for tumour suppression in this mouse model is unknown. Further characterization is being undertaken using an *in vitro* organoid culture system.

Anoikis is cell death due to loss of attachment. Cell culture experiments have shown that upon detachment from the extracellular matrix epithelial cells undergo rapid anoikis mediated by loss of E-cadherin. Additionally, in colonic crypt epithelial cells, cells detached from the extracellular matrix are protected from anoikis provided cell-cell contacts are maintained (Hofmann et al, 2007). In this context, cell-cell adhesion appears to mediate cell survival mechanisms through β-catenin, Src and PI3K/Akt dependent pathways. Further, culture of human cancer tissue-originated spheroids (CTOSs) relies upon cell-cell adhesion: when colorectal cancer cells

were dissociated single cells showed increased cleaved caspase 3 and poly-ADP-ribose polymerase expression, whereas cells in clusters showed no activation of apoptosis (Kondo et al, 2011). Treatment of these CTOSs with an E-cadherin neutralising antibody resulted in cells dissociating and upregulation of apoptotic markers, results very similar to the effects seen in this study with EDTA treatment of adenomas.

In this work, homozygous *Cdh1* loss using *Vil-CreER^{T2}* resulted in increased intestinal cleaved caspase 3 activity compared with wildtype, including when combined with *Apc* loss. Anoikis is difficult to assess in this *in vivo* model. Quantification of CC3 was done on crypt-villus units from formalin fixed paraffin embedded tissue sections: cells that had already been extruded from the epithelium were not assayed. Indeed, in some sections from *Cdh1$^{fl/fl}$* animals, multiple CC3 positive cells were visible in the intestinal lumen, suggesting they were epithelial cells that had been shed into the lumen, however proving this or quantifying the loss of cells was not feasible. Both BrdU and Ki-67 labelling show increased proliferation in the crypt and villus structures of *Cdh1$^{fl/fl}$* animals, with BrdU proliferating cells nearing the villus tip by 2 hours, a process that in normal mouse epithelium takes 3 days. This suggests that despite the substantial increase in proliferation, the balance between the regeneration of new cells and the loss of cells was in favour of cell loss. Cell loss via anoikis thus seems plausible with *Cdh1* homozygosity.

In the *Apc$^{fl/fl}$ Cdh1$^{fl/fl}$ Vil-CreER^{T2}* model, apoptosis assayed by the number of CC3 positive cells per crypt villus unit is increased compared with wildtype, but is not significantly different to *Apc$^{fl/fl}$ Cdh1$^{+/+}$ Vil-CreER^{T2}* or *Apc$^{+/+}$ Cdh1$^{fl/fl}$ Vil-CreER^{T2}* animals. In the *in vitro* adenoma culture model, immunolabelling showed that cells that had both lost *Cdh1* and were positive for CC3 were rare. FACS analysis, however, showed a small population of cells with decreased CDH1 expression and increased CC3 expression. As anoikis can happen rapidly, it is possible that by using these assays that only measure a single timepoint we are missing occurrences of cell death. Increased anoikis with *Cdh1* loss is certainly possible. Further work would aim to provide better evidence of this *in vitro*, as the nature of anoikis makes it difficult to assay *in vivo*. A possible strategy for this would be *Cdh1$^{fl/fl}$* crypt culture and activation of recombination *in vitro* using Ad-Cre, or *Cdh1$^{fl/fl}$ Vil-CreER^{T2}* culture and activation of recombination *in vitro* using 4-hydroxy-tamoxifen.

Why then do at least some *Apc*$^{fl/fl}$ *Cdh1*$^{fl/fl}$ adenoma cells in culture survive when *Cdh1* is completely lost? It is likely that these cells have activation of survival pathways that make them resistant to anoikis. Indeed, one of the hallmarks of cancer defined by Hanahan and Weinberg is resistance to apoptosis, and resistance to anoikis is a specific feature of EMT (Hanahan & Weinberg, 2000; Tiwari et al, 2012). Further work could be based on the identification of such pathways as they may provide treatment targets for CRC. This *in vitro* model could be a valuable tool for assessing such therapies.

Why is *Cdh1* loss not associated with invasive disease in mouse models of *Apc* loss of function? The adenoma culture experiments demonstrated that loss of E-cadherin can lead to an EMT phenotype, though this was not observed *in vivo*. Complete loss of E-cadherin was not observed in any adenoma cells *in vivo*. As discussed, this is either due to incomplete recombination in every cell, or death of cells where recombination has been complete, or a combination of these two scenarios. If we postulate that *in vivo* there were adenoma cells with complete loss of *Cdh1* that were capable of evading cell death mechanisms, there are a number of possible explanations for the absence of invasive disease or metastasis. Firstly, the *in vitro* and *in vivo* environments are very different. *In vitro*, culture has high concentrations of growth factors including EGF that may promote survival. *In vivo*, additional factors may be required for effective invasion, for example, growth factors secreted by stromal cells at the leading edge of invasion. Further, effective metastasis based on the EMT model requires not only downregulation of E-cadherin to a motile mesenchymal phenotype, but also mesenchymal to epithelial transition (MET) when the circulating cancer cells colonise a secondary organ. Cells with complete genetic loss of *Cdh1* would be incapable of reexpressing E-cadherin and performing MET. This may explain the absence of homozygous mutations of *CDH1* in human cancers and the selection for transcriptional modulation of E-cadherin levels. Reexpression of E-cadherin may be required for efficient metastasis. Paradoxically, cancers with complete inactivation of the tumour suppressor gene E-cadherin may have reduced metastatic capability.

Whilst mouse models have greatly improved our understanding of molecular mechanisms underpinning CRC, they are imperfect models. As discussed previously, the distribution of tumours with *Apc* loss is different in the mouse to humans and mice rarely develop invasive or

metastatic disease. A mouse model phenocopying metastatic CRC would a huge asset to this field of research. In the absence of such a model, the *in vitro* culture system may be a valuable tool. The *in vitro* model used in this study reflects the accumulation of genetic changes in the adenoma to carcinoma transition more closely than inducing synchronous *Apc* and *Cdh1* loss *in vivo*. Additionally, culture systems have the advantages of being more cost-effective and faster than traditional mouse models.

A limit of this study has been reliable assays for Wnt pathway activation. Immunolabelling for β-catenin assays the Wnt pathway effector, but not the target gene response. RT-QPCR results for Wnt target genes have at times been inconsistent, despite optimisation of protocols to maximise the quality of RNA samples. Inconsistent RT-QPCR results have been reported in other studies also and the possibility of Wnt activation by effectors other than β-catenin suggested (Bondow et al, 2012). The use of reliable Wnt reporters, such as TOP-flash (a TCF reporter) *in vitro*, and *TOP-GAL* or *Axin2-LacZ in vivo,* would make this work more comprehensive and will be considered for future experiments.

The work in this thesis contributes to the understanding of the role of E-cadherin in the intestine. Using a mammalian system, it provides detailed observational evidence that genetic loss of E-cadherin can modulate Wnt pathway signalling through the supply of β-catenin, but suggests this only occurs when the Wnt pathway is already active. Further work delineating the particular contributions to the EMT phenotype of cell adhesion versus Wnt regulatory functions of E-cadherin are necessary. This future work could reveal potential treatment targets for CRC. As invasion and metastasis are the key determinants of mortality from this common disease, improved understanding of this stage in tumour progression could have far-reaching benefits.

Appendix: Genotyping PCR conditions

1.1 *AhCreER^T*

Primer name	Sequence (5'-3')
CRE A	TGACCGTACACCAAAATTTG
CRE B	ATTGCCCCTGTTTCACTATC

Table 1. *AhCreER^T* PCR reagent concentrations

Reagent	Working concentration	Volume (µl)
Buffer	1x	2.5
$MgCl_2$	2.5 mM	2.5
dNTP	0.4 mM	1
Primer	0.2 µM	0.05
Q solution	1x	0
ddH_2O		18.8
Taq	0.08 U/µl	0.1
Total Volume (µl)		25

PCR conditions

Step	Temp (°C)	Time
1	95	5 min
2	94	30 sec
3	60	30 sec
4	72	1 min
5		Repeat steps 2-4 further 29 cycles
6	72	5 min

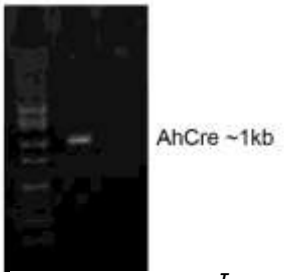

Figure 91. *AhCreER^T* genotyping

Products: Cre ~1kb
Reference: Adapted from personal communication with Owen Sansom

1.2 *Apc loxP*

Primer name	Sequence (5'-3')
APC P3	GTTCTGTATCATGGAAAGATAGGTGGTC
APC P4	CACTCAAAACGCTTTTGAGGGTTG
APC P5	GAGTACGGGGTCTCTGTCTCAGTGAA (for recombined product)

Table 2. *Apc*^{loxp} PCR reagent concentrations

Reagent	Working concentration	Volume (µl)
Buffer	1x	2.5
$MgCl_2$	2.5 mM	2.5
dNTP	0.4 mM	1
Primer	0.2 µM	0.05
Q solution	1x	0
ddH_2O		18.8
Taq	0.08 U/µl	0.1
Total Volume (µl)		25

PCR conditions

Step	Temp (°C)	Time
1	95	3 min
2	95	30 sec
3	60	30 sec
4	72	1 min
5		Repeat steps 2-4
further 29 cycles		
6	72	5 min

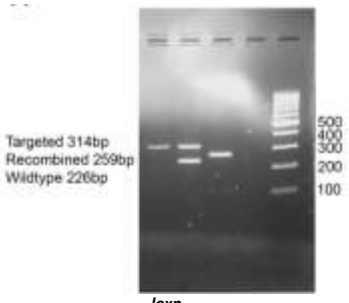

Figure 92. *Apc*^{loxp} genotyping

Products: WT 226bp, loxP 314bp, recombined 259bp
Reference: (Shibata et al, 1997). Adapted from personal communication with Owen Sansom

1.3 *Apc*^{Min}

Primer name	Sequence (5'-3')
Mapc 15	TTCCACTTTGGCATAAGGC
Mapc MT	TGAGAAAGACAGAAGTTA
Mapc 9	GCCATCCCTTCACGTTAG

Table 3. *Apc*^{Min} PCR reagent concentrations

Reagent	Working concentration	Volume (µl)
Buffer	1x	2.5
$MgCl_2$	2.5 mM	2.5
dNTP	0.4 mM	1
Primer	0.4 µM	0.1
Q solution	1x	0
ddH_2O		18.6
Taq	0.08U/µl	0.1
Total Volume (µl)		25

PCR conditions

Step	Temp (°C)	Time
1	94	5 min
2	94	1 min
3	55	1 min
4	72	1 min
5		Repeat steps 2-4 further 39 cycles
6	72	5 min

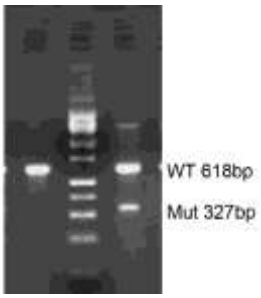

Figure 93. *Apc*^{Min} genotyping

Products: WT 618bp, Mut 327bp
Reference: (Su et al, 1992)

1.4 *Cdh1*

Primer name	Sequence
NewEcadF	CAAAATAAAACCGTCGGAGAA
EcadWtSR	AGCAAACACTGAGCTCGGGT
LL19R	GGGGATGTGCTGCAAGGCGATTA

Table 4. *Cdh1* PCR reagent concentrations

Reagent	Working concentration	Volume (µl)
Buffer	1x	2.5
$MgCl_2$	3 mM	3
dNTP	0.2 mM	0.5
Primer	0.2 µM	0.05
Q solution	1x	5
ddH_2O		13.775
Taq	0.1 U/µl	0.125
Total Volume (µl)		25

PCR conditions

Step	Temp (°C)	Time
1	95	5 min
2	94	1 min
3	58	1 min
4	72	1 min
5		Repeat steps 2-4
further 34 cycles		
6	72	5 min

Figure 94. *Cdh1* genotyping

Products: WT 600bp, Mut 700bp.

As WT and mutant bands were close together, separate PCR reactions were performed to detect each band (one reaction with primers NewEcadF and EcadWtSR to detect a WT band and a separate reaction with primers NewEcadF and LL19R to detect the mutant band).

Reference: (Larue et al, 1994)

1.5 *Cdh1loxp*

Primer name	Sequence
Cdh1p1	ACATGTTTGTATCGATCTCAG
Cdh1p2	CCATACACTGATAATGTCAGA
Cdh1p4	CCTGCCATGATTGTCATGGAC (for recombined product)

The above published primers were initially used (Derksen et al, 2006). According to the paper they should have given a 270bp product for the wildtype allele, and a 330bp product for the loxP allele. However as shown in

Figure 95 we failed to get the expected products, instead getting a product of less than 200bp for the wildtype allele, a product of 300bp for the loxP allele, and sometimes also a third band of about 350bp for the heterozygote animals.

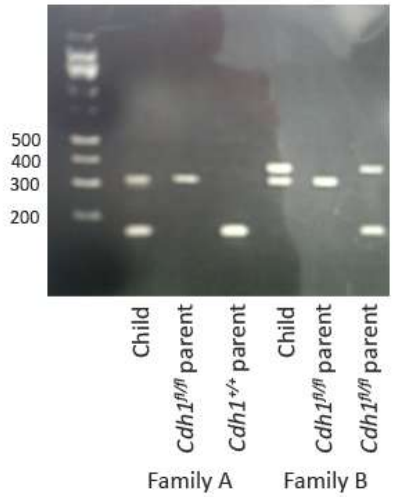

Figure 95. *Cdh1*^{fl} genotyping using published primers

Mapping of the primers showed that they should in fact give a product of 376bp for the wildtype allele (Figure 6). The loxP site would be expected to be 34bp long (two 13bp

palindromes separated by an 8bp asymmetric core sequence) thus the loxP allele should give a product of 410bp. Sequencing of the bands from Figure 5 showed that a 210bp length of sequence was being skipped due to presence a TCAGAAATAGTTCT repeat. Sequencing also showed that the insert including the loxP site was longer than expected at 144bp length. A new forward primer was designed to avoid the repeats as detailed below and shown in Figure 6. This gave an expected wildtype product of 124bp and a loxP product of 268bp (124+144) as shown in Figure 97.

Primer name	Sequence
Cdh1FJ	CCCCAAACTCGTTGATTGAT

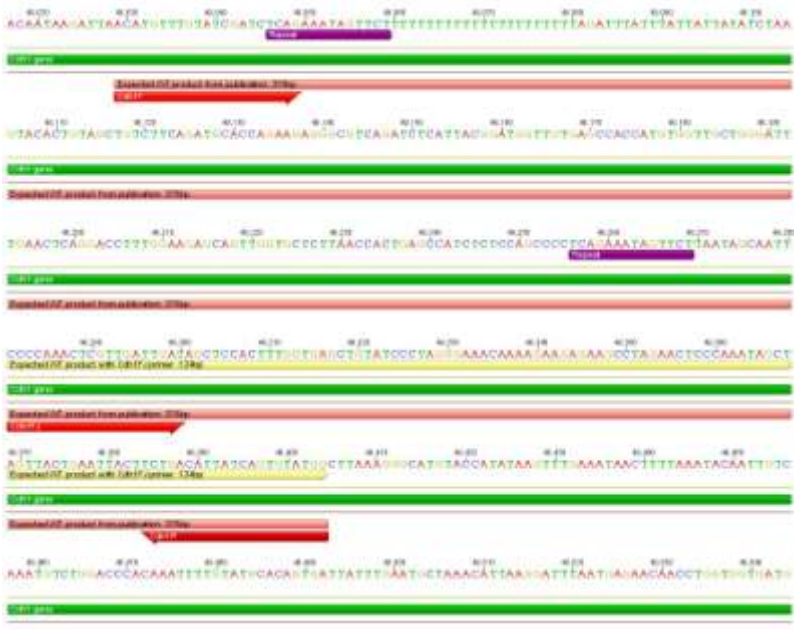

Figure 96. *Cdh1*^{fl} primer design
Original *Cdh1* primers (Cdh1F and Cdh1R) marked showing an expected wildtype product of 376 basepairs. A repeat region, marked in purple, was being skipped during PCR genotyping giving a shorter product than expected. A new forward primer avoiding this region (Cdh1FJ) was designed to give an expected wildtype product of 124 basepairs.

Table 5. *Cdh1*^{loxp} PCR reagent concentrations

Reagent	Working concentration	Volume (µl)
Buffer	1x	2.5
$MgCl_2$	2.5 mM	2.5
dNTP	0.125 mM	0.3125
Primer	0.5 µM	0.125
Q solution	1x	0
ddH_2O		10
Taq	0.24 U/µl	0.3125
Total Volume (µl)		25

PCR conditions

Step	Temp (°C)	Time
1	95	5 min
2	94	30 sec
3	62	30 sec
4	72	50 sec
5		Repeat steps 2-4 further 33 cycles
6	72	7 min

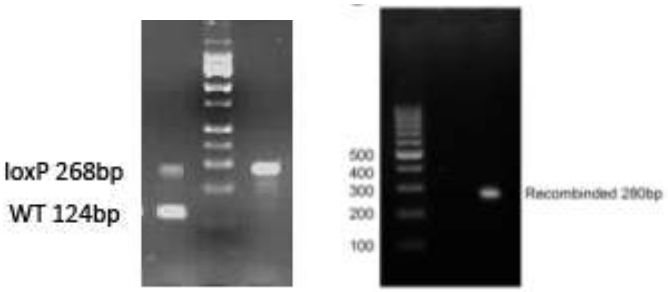

Figure 97. *Cdh1*^{fl} genotyping

1.6 *Lgr5-IRES-EGFP-CreER*^{T2}

Primer name	Sequence
Lgr5Klfor	CACTGCATTCTAGTTGTGG
Lgr5Klrev	CGGTGCCCGCAGCGAG

Table 6. *Lgr5-Cre* PCR reagents

Reagent	Working concentration	Volume (µl)
Buffer	1x	2.5
$MgCl_2$	2.5 mM	1.25
dNTP	0.2 mM	0.5
Primer	0.5 µM	0.125
Q solution	1x	0
ddH_2O		20.3125
Taq	0.08 U/µl	0.0625
Total Volume (µl)		25

PCR conditions

Step	Temp (°C)	Time
1	94	3 min
2	94	30 sec
3	58	30 sec
4	72	30 sec
5		Repeat steps 2-4 further 34 cycles
6	72	7 min

Products: Cre 180bp.

Reference: (Barker et al, 2007)

Figure 98. *Lgr5-CreET2* genotyping

1.7 *Rosa26YFP*

Primer name	Sequence
R26g2/F	TGTTATCAGTAAGGGAGCT
R26g2/Rmut	AAGACCGCGAAGAGTTTGT
R26g2/Rwt	CACACCAGGTTAGCCTTTA

Table 7. *Rosa26YFP* PCR reagent concentrations

Reagent	Working concentration	Volume (µl)
Buffer	1x	2.5
$MgCl_2$	2.5 mM	2.5
dNTP	0.2mM	0.5
Primer	0.2 µM	0.05
Q solution	1x	0
ddH_2O		19.25
Taq	0.08 U/µl	0.1
Total Volume (µl)		25

PCR conditions

Step	Temp (°C)	Time
1	94	7 min
2	94	30 sec
3	55	30 sec
4	72	30 sec
5		Repeat steps 2-4 further 39 cycles
6	72	5 min

Figure 99. *RosaYFP* genotyping

Products: WT 239bp, mut 301bp
Reference: Adapted from personal communication with Miguel Constancia

1.8 *Rosa26LacZ*

Primer name	Sequence
R26F2	AAAGTCGCTCTGAGTTGTTAT
R1295	GCGAAGAGTTTGTCCTCAACC
R523	GGAGCGGGAGAAATGGATATG

Table 8. *LacZ* PCR reagent concentrations

Reagent	Working concentration	Volume (µl)
Buffer	1x	2.5
$MgCl_2$	1.75 mM	1.25
dNTP	0.2 mM	0.5
Primer	0.8 µM	0.2
Q solution	1x	5
ddH_2O		15.55
Taq	0.08 U/µl	0.0625
Total Volume (µl)		25

PCR conditions

Step	Temp (°C)	Time
1	93	2 min
2	93	30 sec
3	58	40 sec
4	65	70 sec
5		Repeat steps 2-4 further 39 cycles
6	72	10 min

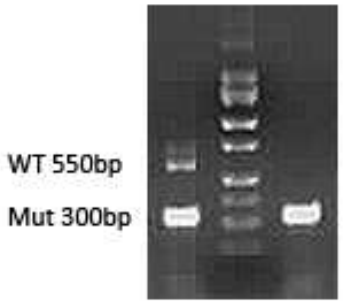

Figure 100. *Rosa26LacZ* genotyping

Products: WT 550bl, Mut 300bp.
Reference: (Soriano, 1999)

1.9 *Smad4*

Primer name	Sequence
Smad4R1	TACAAGTGCTATGTCTTCAGCG
Smad4F2	AAAATGGGAAAACCAACGAG

Table 9. *Smad4* PCR reagent concentrations

Reagent	Working concentration	Volume (µl)
Buffer	1x	2.5
$MgCl_2$	2.5 mM	2.5
dNTP	0.2mM	0.5
Primer	0.5 µM	0.125
Q solution	1x	0
ddH_2O		19.0625
Taq	0.08 U/µl	0.0625
Total Volume (µl)		25

PCR conditions

Step	Temp (°C)	Time
1	94	3 min
2	94	45 sec
3	54	45 sec
4	72	45 sec
5		Repeat steps 2-4 further 34 cycles
6	72	7 min

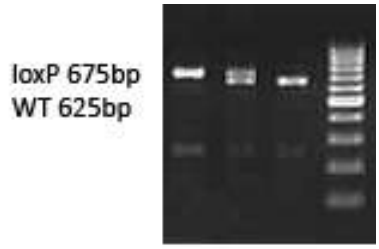

Figure 101. *Smad4* genotyping

Products: WT 625bp, loxP 675bp.
Reference: (Chu et al, 2004)

1.10 *Villin-Cre* and *Villin-CreER^{T2}*

Primer name	Sequence
S1X-A	GCATAACCAGTGAAACAGCATTGC TG
S1X-B	GGACATGTTCAGGGATCGCCAGGCG

Table 10. *Villin-Cre* and *Villin-CreER^{T2}* PCR reagent concentrations

Reagent	Working concentration	Volume (µl)
Buffer	1x	2.5
$MgCl_2$	2.5 mM	2.5
dNTP	0.2mM	0.5
Primer	0.5 µM	0.125
Q solution	1x	0
ddH_2O		19.0625
Taq	0.08 U/µl	0.0625
Total Volume (µl)		25

PCR conditions

Step	Temp (°C)	Time
1	94	3 min
2	94	30 sec
3	55	30 sec
4	65	1 min
5		Repeat steps 2-4 further 34 cycles
6	72	10 min

Products: Cre 280bp
Reference: (el Marjou et al, 2004)

Figure 102. *Villin-Cre* and *Villin-CreER^{T2}* genotyping

Bibliography

Abe K, Takeichi M (2008) EPLIN mediates linkage of the cadherin catenin complex to F-actin and stabilizes the circumferential actin belt. *Proc Natl Acad Sci U S A* **105:** 13-19

Aberle H, Bauer A, Stappert J, Kispert A, Kemler R (1997) beta-catenin is a target for the ubiquitin-proteasome pathway. *EMBO J* **16:** 3797-3804

Aberle H, Butz S, Stappert J, Weissig H, Kemler R, Hoschuetzky H (1994) Assembly of the cadherin-catenin complex in vitro with recombinant proteins. *J Cell Sci* **107 (Pt 12):** 3655-3663

Ahlgren U, Jonsson J, Jonsson L, Simu K, Edlund H (1998) beta-cell-specific inactivation of the mouse Ipf1/Pdx1 gene results in loss of the beta-cell phenotype and maturity onset diabetes. *Genes Dev* **12:** 1763-1768

Ahn BK, Jang SH, Paik SS, Lee KH (2011) Smad4 may help to identify a subset of colorectal cancer patients with early recurrence after curative therapy. *Hepatogastroenterology* **58:** 1933-1936

Ahrens T, Pertz O, Haussinger D, Fauser C, Schulthess T, Engel J (2002) Analysis of heterophilic and homophilic interactions of cadherins using the c-Jun/c-Fos dimerization domains. *J Biol Chem* **277:** 19455-19460

Akhurst RJ, Balmain A (1999) Genetic events and the role of TGF beta in epithelial tumour progression. *J Pathol* **187:** 82-90

Albuquerque C, Breukel C, van der Luijt R, Fidalgo P, Lage P, Slors FJ, Leitão CN, Fodde R, Smits R (2002) The 'just-right' signaling model: APC somatic mutations are selected based on a specific level of activation of the beta-catenin signaling cascade. *Hum Mol Genet* **11:** 1549-1560

Andreu P, Colnot S, Godard C, Gad S, Chafey P, Niwa-Kawakita M, Laurent-Puig P, Kahn A, Robine S, Perret C, Romagnolo B (2005) Crypt-restricted proliferation and commitment to the Paneth cell lineage following Apc loss in the mouse intestine. *Development* **132:** 1443-1451

Angst B, Marcozzi C, Magee A (2001) The cadherin superfamily: diversity in form and function. *J Cell Sci* **114:** 629-641

Aoki K, Taketo MM (2008) Tissue-specific transgenic, conditional knockout and knock-in mice of genes in the canonical Wnt signaling pathway. *Methods Mol Biol* **468:** 307-331

Ashery-Padan R, Marquardt T, Zhou X, Gruss P (2000) Pax6 activity in the lens primordium is required for lens formation and for correct placement of a single retina in the eye. *Genes Dev* **14:** 2701-2711

Ashton-Rickardt P, Dunlop M, Nakamura Y, Morris R, Purdie C, Steel C, Evans H, Bird C, Wyllie A (1989) High frequency of APC loss in sporadic colorectal carcinoma due to breaks clustered in 5q21-22. *Oncogene* **4:** 1169-1174

Attisano L, Labbé E (2004) TGFbeta and Wnt pathway cross-talk. *Cancer Metastasis Rev* **23:** 53-61

Bafico A, Liu G, Yaniv A, Gazit A, Aaronson SA (2001) Novel mechanism of Wnt signalling inhibition mediated by Dickkopf-1 interaction with LRP6/Arrow. *Nat Cell Biol* **3:** 683-686

Baki L, Marambaud P, Efthimiopoulos S, Georgakopoulos A, Wen P, Cui W, Shioi J, Koo E, Ozawa M, Friedrich VL, Jr., Robakis NK (2001) Presenilin-1 binds cytoplasmic epithelial cadherin, inhibits cadherin/p120 association, and regulates stability and function of the cadherin/catenin adhesion complex. *Proc Natl Acad Sci U S A* **98:** 2381-2386

Baran AA, Silverman KA, Zeskand J, Koratkar R, Palmer A, McCullen K, Curran WJ, Edmonston TB, Siracusa LD, Buchberg AM (2007) The modifier of Min 2 (Mom2) locus: embryonic lethality of a mutation in the Atp5a1 gene suggests a novel mechanism of polyp suppression. *Genome Res* **17:** 566-576

Barker N, Ridgway R, van Es J, van de Wetering M, Begthel H, van den Born M, Danenberg E, Clarke A, Sansom O, Clevers H (2009) Crypt stem cells as the cells-of-origin of intestinal cancer. *Nature* **457:** 608-611

Barker N, van de Wetering M, Clevers H (2008) The intestinal stem cell. *Genes Dev* **22:** 1856-1864

Barker N, van Es J, Kuipers J, Kujala P, van den Born M, Cozijnsen M, Haegebarth A, Korving J, Begthel H, Peters P, Clevers H (2007) Identification of stem cells in small intestine and colon by marker gene Lgr5. *Nature* **449:** 1003-1007

Barrett JC, Hansoul S, Nicolae DL, Cho JH, Duerr RH, Rioux JD, Brant SR, Silverberg MS, Taylor KD, Barmada MM, Bitton A, Dassopoulos T, Datta LW, Green T, Griffiths AM, Kistner EO, Murtha MT, Regueiro MD, Rotter JI, Schumm LP, Steinhart AH, Targan SR, Xavier RJ, Libioulle C, Sandor C, Lathrop M, Belaiche J, Dewit O, Gut I, Heath S, Laukens D, Mni M, Rutgeerts P, Van Gossum A, Zelenika D, Franchimont D, Hugot JP, de Vos M, Vermeire S, Louis E, Cardon LR, Anderson CA, Drummond H, Nimmo E, Ahmad T, Prescott NJ, Onnie CM, Fisher SA, Marchini J, Ghori J, Bumpstead S, Gwilliam R, Tremelling M, Deloukas P, Mansfield J, Jewell D, Satsangi J, Mathew CG, Parkes M, Georges M, Daly MJ, Consortium NIG, Consortium B-FI, Consortium WTCC (2008) Genome-wide association defines more than 30 distinct susceptibility loci for Crohn's disease. *Nat Genet* **40:** 955-962

Barrett JC, Lee JC, Lees CW, Prescott NJ, Anderson CA, Phillips A, Wesley E, Parnell K, Zhang H, Drummond H, Nimmo ER, Massey D, Blaszczyk K, Elliott T, Cotterill L, Dallal H, Lobo AJ, Mowat C, Sanderson JD, Jewell DP, Newman WG, Edwards C, Ahmad T, Mansfield JC, Satsangi J, Parkes M, Mathew CG, Donnelly P, Peltonen L, Blackwell JM, Bramon E, Brown MA, Casas JP, Corvin A, Craddock N, Deloukas P, Duncanson A, Jankowski J, Markus HS, McCarthy MI, Palmer CN, Plomin R, Rautanen A, Sawcer SJ, Samani N, Trembath RC, Viswanathan AC, Wood N, Spencer CC, Bellenguez C, Davison D, Freeman C, Strange A, Langford C, Hunt SE, Edkins S, Gwilliam R, Blackburn H, Bumpstead SJ, Dronov S, Gillman M, Gray E, Hammond N, Jayakumar A, McCann OT, Liddle J, Perez ML, Potter SC, Ravindrarajah R, Ricketts M, Waller M, Weston P, Widaa S, Whittaker P, Attwood AP, Stephens J, Sambrook J, Ouwehand WH, McArdle WL, Ring SM, Strachan DP, Consortium UIG, 2 WTCCC (2009) Genome-wide association study of ulcerative colitis identifies three new susceptibility loci, including the HNF4A region. *Nat Genet* **41:** 1330-1334

Batlle E, Henderson J, Beghtel H, van den Born M, Sancho E, Huls G, Meeldijk J, Robertson J, van de Wetering M, Pawson T, Clevers H (2002) Beta-catenin and TCF mediate cell positioning in the intestinal epithelium by controlling the expression of EphB/ephrinB. *Cell* **111:** 251-263

Batlle E, Sancho E, Franci C, Dominguez D, Monfar M, Baulida J, Garcia De Herreros A (2000) The transcription factor snail is a repressor of E-cadherin gene expression in epithelial tumour cells. *Nat Cell Biol* **2:** 84-89

Battle MA, Konopka G, Parviz F, Gaggl AL, Yang C, Sladek FM, Duncan SA (2006) Hepatocyte nuclear factor 4alpha orchestrates expression of cell adhesion proteins during the epithelial transformation of the developing liver. *Proc Natl Acad Sci U S A* **103:** 8419-8424

Beavon IR (2000) The E-cadherin-catenin complex in tumour metastasis: structure, function and regulation. *Eur J Cancer* **36:** 1607-1620

Bedzhov I, Liszewska E, Kanzler B, Stemmler MP (2012) Igf1r signaling is indispensable for preimplantation development and is activated via a novel function of E-cadherin. *PLoS Genet* **8:** e1002609

Behrens J, Jerchow BA, Wurtele M, Grimm J, Asbrand C, Wirtz R, Kuhl M, Wedlich D, Birchmeier W (1998) Functional interaction of an axin homolog, conductin, with beta-catenin, APC, and GSK3beta. *Science* **280:** 596-599

Behrens J, von Kries JP, Kühl M, Bruhn L, Wedlich D, Grosschedl R, Birchmeier W (1996) Functional interaction of beta-catenin with the transcription factor LEF-1. *Nature* **382:** 638-642

Berx G, Becker KF, Höfler H, van Roy F (1998) Mutations of the human E-cadherin (CDH1) gene. *Hum Mutat* **12:** 226-237

Berx G, Cleton-Jansen A, Nollet F, de Leeuw W, van de Vijver M, Cornelisse C, van Roy F (1995) E-cadherin is a tumour/invasion suppressor gene mutated in human lobular breast cancers. *EMBO J* **14:** 6107-6115

Berx G, Cleton-Jansen AM, Strumane K, de Leeuw WJ, Nollet F, van Roy F, Cornelisse C (1996) E-cadherin is inactivated in a majority of invasive human lobular breast cancers by truncation mutations throughout its extracellular domain. *Oncogene* **13:** 1919-1925

Berx G, van Roy F (2009) Involvement of members of the cadherin superfamily in cancer. *Cold Spring Harb Perspect Biol* **1:** a003129

Bhanot P, Brink M, Samos CH, Hsieh JC, Wang Y, Macke JP, Andrew D, Nathans J, Nusse R (1996) A new member of the frizzled family from Drosophila functions as a Wingless receptor. *Nature* **382:** 225-230

Bienz M (1999) APC: the plot thickens. *Curr Opin Genet Dev* **9:** 595-603

Bienz M (2002) The subcellular destinations of APC proteins. *Nat Rev Mol Cell Biol* **3:** 328-338

Blaschuk O, Sullivan R, David S, Pouliot Y (1990) Identification of a cadherin cell adhesion recognition sequence. *Dev Biol* **139:** 227-229

Bodmer WF, Bailey CJ, Bodmer J, Bussey HJ, Ellis A, Gorman P, Lucibello FC, Murday VA, Rider SH, Scambler P, et al. (1987) Localization of the gene for familial adenomatous polyposis on chromosome 5. *Nature* **328:** 614-616

Boggon T, Murray J, Chappuis-Flament S, Wong E, Gumbiner B, Shapiro L (2002) C-cadherin ectodomain structure and implications for cell adhesion mechanisms. *Science* **296:** 1308-1313

Bolós V, Peinado H, Pérez-Moreno MA, Fraga MF, Esteller M, Cano A (2003) The transcription factor Slug represses E-cadherin expression and induces epithelial to mesenchymal transitions: a comparison with Snail and E47 repressors. *J Cell Sci* **116:** 499-511

Bondow BJ, Faber ML, Wojta KJ, Walker EM, Battle MA (2012) E-cadherin is required for intestinal morphogenesis in the mouse. *Dev Biol* **371:** 1-12

Bosenberg M, Muthusamy V, Curley DP, Wang Z, Hobbs C, Nelson B, Nogueira C, Horner JW, Depinho R, Chin L (2006) Characterization of melanocyte-specific inducible Cre recombinase transgenic mice. *Genesis* **44:** 262-267

Boussadia O, Kutsch S, Hierholzer A, Delmas V, Kemler R (2002) E-cadherin is a survival factor for the lactating mouse mammary gland. *Mech Dev* **115:** 53-62

Brabletz T, Jung A, Hermann K, Gunther K, Hohenberger W, Kirchner T (1998) Nuclear overexpression of the oncoprotein beta-catenin in colorectal cancer is localized predominantly at the invasion front. *Pathol Res Pract* **194:** 701-704

Brabletz T, Jung A, Reu S, Porzner M, Hlubek F, Kunz-Schughart LA, Knuechel R, Kirchner T (2001) Variable beta-catenin expression in colorectal cancers indicates tumor progression driven by the tumor environment. *Proc Natl Acad Sci U S A* **98:** 10356-10361

Brabletz T, Jung A, Spaderna S, Hlubek F, Kirchner T (2005) Opinion: migrating cancer stem cells - an integrated concept of malignant tumour progression. *Nat Rev Cancer* **5:** 744-749

Bragdon B, Moseychuk O, Saldanha S, King D, Julian J, Nohe A (2011) Bone morphogenetic proteins: a critical review. *Cell Signal* **23:** 609-620

Brault V, Moore R, Kutsch S, Ishibashi M, Rowitch DH, McMahon AP, Sommer L, Boussadia O, Kemler R (2001) Inactivation of the beta-catenin gene by Wnt1-Cre-mediated deletion results in dramatic brain malformation and failure of craniofacial development. *Development* **128:** 1253-1264

Brieher W, Yap A, Gumbiner B (1996) Lateral dimerization is required for the homophilic binding activity of C-cadherin. *J Cell Biol* **135:** 487-496

Brooks-Wilson AR, Kaurah P, Suriano G, Leach S, Senz J, Grehan N, Butterfield YS, Jeyes J, Schinas J, Bacani J, Kelsey M, Ferreira P, MacGillivray B, MacLeod P, Micek M, Ford J, Foulkes W, Australie K, Greenberg C, LaPointe M, Gilpin C, Nikkel S, Gilchrist D, Hughes R, Jackson CE, Monaghan KG, Oliveira MJ, Seruca R, Gallinger S, Caldas C, Huntsman D (2004) Germline E-cadherin mutations in hereditary diffuse gastric cancer: assessment of 42 new families and review of genetic screening criteria. *J Med Genet* **41:** 508-517

Brosens LA, Langeveld D, van Hattem WA, Giardiello FM, Offerhaus GJ (2011) Juvenile polyposis syndrome. *World J Gastroenterol* **17:** 4839-4844

Brosens LA, van Hattem A, Hylind LM, Iacobuzio-Donahue C, Romans KE, Axilbund J, Cruz-Correa M, Tersmette AC, Offerhaus GJ, Giardiello FM (2007) Risk of colorectal cancer in juvenile polyposis. *Gut* **56:** 965-967

Buda A, Pignatelli M (2011) E-cadherin and the cytoskeletal network in colorectal cancer development and metastasis. *Cell Commun Adhes* **18:** 133-143

Cadigan KM, Peifer M (2009) Wnt signaling from development to disease: insights from model systems. *Cold Spring Harb Perspect Biol* **1:** a002881

Calva-Cerqueira D, Dahdaleh FS, Woodfield G, Chinnathambi S, Nagy PL, Larsen-Haidle J, Weigel RJ, Howe JR (2010) Discovery of the BMPR1A promoter and germline mutations that cause juvenile polyposis. *Hum Mol Genet* **19:** 4654-4662

Calì G, Zannini M, Rubini P, Tacchetti C, D'Andrea B, Affuso A, Wintermantel T, Boussadia O, Terracciano D, Silberschmidt D, Amendola E, De Felice M, Schütz G, Kemler R, Di Lauro R, Nitsch L (2007) Conditional inactivation of the E-cadherin gene in thyroid follicular cells affects gland development but does not impair junction formation. *Endocrinology* **148:** 2737-2746

Cancer Genome Atlas Network (2012) Comprehensive molecular characterization of human colon and rectal cancer. *Nature* **487:** 330-337

Cannon-Albright L, Skolnick M, Bishop D, Lee R, Burt R (1988) Common inheritance of susceptibility to colonic adenomatous polyps and associated colorectal cancers. *N Engl J Med* **319:** 533-537

Cano A, Perez-Moreno MA, Rodrigo I, Locascio A, Blanco MJ, del Barrio MG, Portillo F, Nieto MA (2000) The transcription factor snail controls epithelial-mesenchymal transitions by repressing E-cadherin expression. *Nat Cell Biol* **2:** 76-83

Castellone MD, Teramoto H, Williams BO, Druey KM, Gutkind JS (2005) Prostaglandin E2 promotes colon cancer cell growth through a Gs-axin-beta-catenin signaling axis. *Science* **310:** 1504-1510

Cavallaro U, Christofori G (2004) Cell adhesion and signalling by cadherins and Ig-CAMs in cancer. *Nat Rev Cancer* **4:** 118-132

Ceteci F, Ceteci S, Karreman C, Kramer BW, Asan E, Gotz R, Rapp UR (2007) Disruption of tumor cell adhesion promotes angiogenic switch and progression to micrometastasis in RAF-driven murine lung cancer. *Cancer Cell* **12:** 145-159

Chaffer CL, Thompson EW, Williams ED (2007) Mesenchymal to epithelial transition in development and disease. *Cells Tissues Organs* **185:** 7-19

Chamberlin W, Borody TJ, Campbell J (2011) Primary treatment of Crohn's disease: combined antibiotics taking center stage. *Expert Rev Clin Immunol* **7:** 751-760

Chappuis-Flament S, Wong E, Hicks L, Kay C, Gumbiner B (2001) Multiple cadherin extracellular repeats mediate homophilic binding and adhesion. *J Cell Biol* **154:** 231-243

Chen G, Fernandez J, Mische S, Courey AJ (1999) A functional interaction between the histone deacetylase Rpd3 and the corepressor groucho in Drosophila development. *Genes Dev* **13:** 2218-2230

Cheung AF, Carter AM, Kostova KK, Woodruff JF, Crowley D, Bronson RT, Haigis KM, Jacks T (2010) Complete deletion of Apc results in severe polyposis in mice. *Oncogene* **29:** 1857-1864

Christoffels VM, Grieskamp T, Norden J, Mommersteeg MT, Rudat C, Kispert A (2009) Tbx18 and the fate of epicardial progenitors. *Nature* **458:** E8-9; discussion E9-10

Chu GC, Dunn NR, Anderson DC, Oxburgh L, Robertson EJ (2004) Differential requirements for Smad4 in TGFbeta-dependent patterning of the early mouse embryo. *Development* **131:** 3501-3512

Clausen BE, Burkhardt C, Reith W, Renkawitz R, Förster I (1999) Conditional gene targeting in macrophages and granulocytes using LysMcre mice. *Transgenic Res* **8:** 265-277

Clevers H, Nusse R (2012) Wnt/β-catenin signaling and disease. *Cell* **149:** 1192-1205

Cliffe A, Hamada F, Bienz M (2003) A role of Dishevelled in relocating Axin to the plasma membrane during wingless signaling. *Curr Biol* **13:** 960-966

Colnot S, Niwa-Kawakita M, Hamard G, Godard C, Le Plenier S, Houbron C, Romagnolo B, Berrebi D, Giovannini M, Perret C (2004) Colorectal cancers in a new mouse model of familial adenomatous polyposis: influence of genetic and environmental modifiers. *Lab Invest* **84:** 1619-1630

Conacci-Sorrell M, Simcha I, Ben-Yedidia T, Blechman J, Savagner P, Ben-Ze'ev A (2003) Autoregulation of E-cadherin expression by cadherin-cadherin interactions: the roles of beta-catenin signaling, Slug, and MAPK. *J Cell Biol* **163:** 847-857

Cormier RT, Bilger A, Lillich AJ, Halberg RB, Hong KH, Gould KA, Borenstein N, Lander ES, Dove WF (2000) The Mom1AKR intestinal tumor resistance region consists of Pla2g2a and a locus distal to D4Mit64. *Oncogene* **19:** 3182-3192

Corso G, Marrelli D, Pascale V, Vindigni C, Roviello F (2012) Frequency of CDH1 germline mutations in gastric carcinoma coming from high- and low-risk areas: metanalysis and systematic review of the literature. *BMC Cancer* **12:** 8

Corso G, Pedrazzani C, Pinheiro H, Fernandes E, Marrelli D, Rinnovati A, Pascale V, Seruca R, Oliveira C, Roviello F (2011) E-cadherin genetic screening and clinico-pathologic characteristics of early onset gastric cancer. *Eur J Cancer* **47:** 631-639

Cortina C, Palomo-Ponce S, Iglesias M, Fernández-Masip JL, Vivancos A, Whissell G, Humà M, Peiró N, Gallego L, Jonkheer S, Davy A, Lloreta J, Sancho E, Batlle E (2007) EphB-ephrin-B interactions suppress colorectal cancer progression by compartmentalizing tumor cells. *Nat Genet* **39:** 1376-1383

Crosnier C, Stamataki D, Lewis J (2006) Organizing cell renewal in the intestine: stem cells, signals and combinatorial control. *Nat Rev Genet* **7:** 349-359

Cunningham D, Atkin W, Lenz H, Lynch H, Minsky B, Nordlinger B, Starling N (2010) Colorectal cancer. *Lancet* **375:** 1030-1047

Dahl U, Sjødin A, Semb H (1996) Cadherins regulate aggregation of pancreatic beta-cells in vivo. *Development* **122:** 2895-2902

Damsky WE, Curley DP, Santhanakrishnan M, Rosenbaum LE, Platt JT, Gould Rothberg BE, Taketo MM, Dankort D, Rimm DL, McMahon M, Bosenberg M (2011) β-catenin signaling controls metastasis in Braf-activated Pten-deficient melanomas. *Cancer Cell* **20:** 741-754

Daniels DL, Weis WI (2005) Beta-catenin directly displaces Groucho/TLE repressors from Tcf/Lef in Wnt-mediated transcription activation. *Nat Struct Mol Biol* **12:** 364-371

Dankort D, Filenova E, Collado M, Serrano M, Jones K, McMahon M (2007) A new mouse model to explore the initiation, progression, and therapy of BRAFV600E-induced lung tumors. *Genes Dev* **21:** 379-384

Davis MA, Ireton RC, Reynolds AB (2003) A core function for p120-catenin in cadherin turnover. *J Cell Biol* **163:** 525-534

De Cruz P, Prideaux L, Wagner J, Ng SC, McSweeney C, Kirkwood C, Morrison M, Kamm MA (2012) Characterization of the gastrointestinal microbiota in health and inflammatory bowel disease. *Inflamm Bowel Dis* **18:** 372-390

de Vries WN, Binns LT, Fancher KS, Dean J, Moore R, Kemler R, Knowles BB (2000) Expression of Cre recombinase in mouse oocytes: a means to study maternal effect genes. *Genesis* **26:** 110-112

De Vries WN, Evsikov AV, Haac BE, Fancher KS, Holbrook AE, Kemler R, Solter D, Knowles BB (2004) Maternal beta-catenin and E-cadherin in mouse development. *Development* **131:** 4435-4445

De Wever O, Pauwels P, De Craene B, Sabbah M, Emami S, Redeuilh G, Gespach C, Bracke M, Berx G (2008) Molecular and pathological signatures of epithelial-mesenchymal transitions at the cancer invasion front. *Histochem Cell Biol* **130:** 481-494

Derksen P, Liu X, Saridin F, van der Gulden H, Zevenhoven J, Evers B, van Beijnum J, Griffioen A, Vink J, Krimpenfort P, Peterse J, Cardiff R, Berns A, Jonkers J (2006) Somatic inactivation of E-cadherin and p53 in mice leads to metastatic lobular mammary carcinoma through induction of anoikis resistance and angiogenesis. *Cancer Cell* **10:** 437-449

Derksen PW, Braumuller TM, van der Burg E, Hornsveld M, Mesman E, Wesseling J, Krimpenfort P, Jonkers J (2011) Mammary-specific inactivation of E-cadherin and p53 impairs functional gland development and leads to pleomorphic invasive lobular carcinoma in mice. *Dis Model Mech* **4:** 347-358

Dietrich WF, Lander ES, Smith JS, Moser AR, Gould KA, Luongo C, Borenstein N, Dove W (1993) Genetic identification of Mom-1, a major modifier locus affecting Min-induced intestinal neoplasia in the mouse. *Cell* **75:** 631-639

Disson O, Grayo S, Huillet E, Nikitas G, Langa-Vives F, Dussurget O, Ragon M, Le Monnier A, Babinet C, Cossart P, Lecuit M (2008) Conjugated action of two species-specific invasion proteins for fetoplacental listeriosis. *Nature* **455:** 1114-1118

Dixon M, Seevaratnam R, Wirtzfeld D, McLeod R, Helyer L, Law C, Swallow C, Paszat L, Bocicariu A, Cardoso R, Mahar A, Bekaii-Saab T, Chau I, Church N, Coit D, Crane CH, Earle C, Mansfield P, Marcon N, Miner T, Noh SH, Porter G, Posner MC, Prachand V, Sano T, Van de Velde CJ, Wong S, Coburn N (2012) A RAND/UCLA Appropriateness Study of the Management of Familial Gastric Cancer. *Ann Surg Oncol*

Ducibella T, Albertini D, Anderson E, Biggers J (1975) The preimplantation mammalian embryo: characterization of intercellular junctions and their appearance during development. *Dev Biol* **45:** 231-250

Durand A, Donahue B, Peignon G, Letourneur F, Cagnard N, Slomianny C, Perret C, Shroyer NF, Romagnolo B (2012) Functional intestinal stem cells after Paneth cell ablation induced by the loss of transcription factor Math1 (Atoh1). *Proc Natl Acad Sci U S A* **109:** 8965-8970

el Marjou F, Janssen K, Chang B, Li M, Hindie V, Chan L, Louvard D, Chambon P, Metzger D, Robine S (2004) Tissue-specific and inducible Cre-mediated recombination in the gut epithelium. *Genesis* **39:** 186-193

Engle SJ, Hoying JB, Boivin GP, Ormsby I, Gartside PS, Doetschman T (1999) Transforming growth factor beta1 suppresses nonmetastatic colon cancer at an early stage of tumorigenesis. *Cancer Res* **59:** 3379-3386

Etienne-Manneville S, Hall A (2002) Rho GTPases in cell biology. *Nature* **420:** 629-635

Feinberg AP, Vogelstein B (1983) A technique for radiolabeling DNA restriction endonuclease fragments to high specific activity. *Anal Biochem* **132:** 6-13

Fiedler M, Mendoza-Topaz C, Rutherford TJ, Mieszczanek J, Bienz M (2011) Dishevelled interacts with the DIX domain polymerization interface of Axin to interfere with its function in down-regulating β-catenin. *Proc Natl Acad Sci U S A* **108:** 1937-1942

Finch PW, He X, Kelley MJ, Uren A, Schaudies RP, Popescu NC, Rudikoff S, Aaronson SA, Varmus HE, Rubin JS (1997) Purification and molecular cloning of a secreted, Frizzled-related antagonist of Wnt action. *Proc Natl Acad Sci U S A* **94:** 6770-6775

Fitzgerald RC, Hardwick R, Huntsman D, Carneiro F, Guilford P, Blair V, Chung DC, Norton J, Ragunath K, Van Krieken JH, Dwerryhouse S, Caldas C, Consortium IGCL (2010) Hereditary diffuse gastric cancer: updated consensus guidelines for clinical management and directions for future research. *J Med Genet* **47:** 436-444

Fodde R, Brabletz T (2007) Wnt/beta-catenin signaling in cancer stemness and malignant behavior. *Curr Opin Cell Biol* **19:** 150-158

Fodde R, Edelmann W, Yang K, van Leeuwen C, Carlson C, Renault B, Breukel C, Alt E, Lipkin M, Khan PM (1994) A targeted chain-termination mutation in the mouse Apc gene results in multiple intestinal tumors. *Proc Natl Acad Sci U S A* **91:** 8969-8973

Fodde R, Smits R, Clevers H (2001) APC, signal transduction and genetic instability in colorectal cancer. *Nat Rev Cancer* **1:** 55-67

Fouquet S, Lugo-Martínez VH, Faussat AM, Renaud F, Cardot P, Chambaz J, Pinçon-Raymond M, Thenet S (2004) Early loss of E-cadherin from cell-cell contacts is involved in the onset of Anoikis in enterocytes. *J Biol Chem* **279:** 43061-43069

Fox JG, Ge Z, Whary MT, Erdman SE, Horwitz BH (2011) Helicobacter hepaticus infection in mice: models for understanding lower bowel inflammation and cancer. *Mucosal Immunol* **4:** 22-30

Fre S, Huyghe M, Mourikis P, Robine S, Louvard D, Artavanis-Tsakonas S (2005) Notch signals control the fate of immature progenitor cells in the intestine. *Nature* **435:** 964-968

Fre S, Pallavi SK, Huyghe M, Laé M, Janssen KP, Robine S, Artavanis-Tsakonas S, Louvard D (2009) Notch and Wnt signals cooperatively control cell proliferation and tumorigenesis in the intestine. *Proc Natl Acad Sci U S A* **106:** 6309-6314

Frebourg T, Oliveira C, Hochain P, Karam R, Manouvrier S, Graziadio C, Vekemans M, Hartmann A, Baert-Desurmont S, Alexandre C, Lejeune Dumoulin S, Marroni C, Martin C, Castedo S, Lovett M, Winston J, Machado JC, Attié T, Jabs EW, Cai J, Pellerin P, Triboulet JP, Scotte M, Le Pessot F, Hedouin A, Carneiro F, Blayau M, Seruca R (2006) Cleft lip/palate and CDH1/E-cadherin mutations in families with hereditary diffuse gastric cancer. *J Med Genet* **43:** 138-142

Freeman TJ, Smith JJ, Chen X, Washington MK, Roland JT, Means AL, Eschrich SA, Yeatman TJ, Deane NG, Beauchamp RD (2012) Smad4-mediated signaling inhibits intestinal neoplasia by inhibiting expression of β-catenin. *Gastroenterology* **142:** 562-571.e562

Frisch SM, Francis H (1994) Disruption of epithelial cell-matrix interactions induces apoptosis. *J Cell Biol* **124:** 619-626

Fujita N, Jaye DL, Kajita M, Geigerman C, Moreno CS, Wade PA (2003) MTA3, a Mi-2/NuRD complex subunit, regulates an invasive growth pathway in breast cancer. *Cell* **113:** 207-219

Fujita Y, Krause G, Scheffner M, Zechner D, Leddy HE, Behrens J, Sommer T, Birchmeier W (2002) Hakai, a c-Cbl-like protein, ubiquitinates and induces endocytosis of the E-cadherin complex. *Nat Cell Biol* **4:** 222-231

Funayama N, Fagotto F, McCrea P, Gumbiner B (1995) Embryonic axis induction by the armadillo repeat domain of beta-catenin: evidence for intracellular signaling. *J Cell Biol* **128:** 959-968

Gaspar C, Fodde R (2004) APC dosage effects in tumorigenesis and stem cell differentiation. *Int J Dev Biol* **48:** 377-386

Glinka A, Wu W, Delius H, Monaghan AP, Blumenstock C, Niehrs C (1998) Dickkopf-1 is a member of a new family of secreted proteins and functions in head induction. *Nature* **391:** 357-362

Gottardi CJ, Gumbiner BM (2004) Distinct molecular forms of beta-catenin are targeted to adhesive or transcriptional complexes. *J Cell Biol* **167:** 339-349

Gottardi CJ, Wong E, Gumbiner BM (2001) E-cadherin suppresses cellular transformation by inhibiting beta-catenin signaling in an adhesion-independent manner. *J Cell Biol* **153:** 1049-1060

Gould KA, Dietrich WF, Borenstein N, Lander ES, Dove WF (1996) Mom1 is a semi-dominant modifier of intestinal adenoma size and multiplicity in Min/+ mice. *Genetics* **144:** 1769-1776

Grady WM, Willis J, Guilford PJ, Dunbier AK, Toro TT, Lynch H, Wiesner G, Ferguson K, Eng C, Park JG, Kim SJ, Markowitz S (2000) Methylation of the CDH1 promoter as the second genetic hit in hereditary diffuse gastric cancer. *Nat Genet* **26:** 16-17

Graham TA, Weaver C, Mao F, Kimelman D, Xu W (2000) Crystal structure of a beta-catenin/Tcf complex. *Cell* **103:** 885-896

Gregorieff A, Pinto D, Begthel H, Destree O, Kielman M, Clevers H (2005) Expression pattern of Wnt signaling components in the adult intestine. *Gastroenterology* **129:** 626-638

Guger KA, Gumbiner BM (1995) beta-Catenin has Wnt-like activity and mimics the Nieuwkoop signaling center in Xenopus dorsal-ventral patterning. *Dev Biol* **172:** 115-125

Guger KA, Gumbiner BM (2000) A mode of regulation of beta-catenin signaling activity in Xenopus embryos independent of its levels. *Dev Biol* **223:** 441-448

Guilford P, Blair V, More H, Humar B (2007) A short guide to hereditary diffuse gastric cancer. *Hered Cancer Clin Pract* **5:** 183-194

Guilford P, Hopkins J, Grady W, Markowitz S, Willis J, Lynch H, Rajput A, Wiesner G, Lindor N, Burgart L, Toro T, Lee D, Limacher J, Shaw D, Findlay M, Reeve A (1999) E-cadherin germline mutations define an inherited cancer syndrome dominated by diffuse gastric cancer. *Hum Mutat* **14:** 249-255

Guilford P, Hopkins J, Harraway J, McLeod M, McLeod N, Harawira P, Taite H, Scoular R, Miller A, Reeve AE (1998) E-cadherin germline mutations in familial gastric cancer. *Nature* **392:** 402-405

Guilford P, Humar B, Blair V (2010) Hereditary diffuse gastric cancer: translation of CDH1 germline mutations into clinical practice. *Gastric Cancer* **13:** 1-10

Gumbiner B (1996) Cell adhesion: the molecular basis of tissue architecture and morphogenesis. *Cell* **84:** 345-357

Hafner M, Wenk J, Nenci A, Pasparakis M, Scharffetter-Kochanek K, Smyth N, Peters T, Kess D, Holtkötter O, Shephard P, Kudlow JE, Smola H, Haase I, Schippers A, Krieg T, Müller W (2004) Keratin 14 Cre transgenic mice authenticate keratin 14 as an oocyte-expressed protein. *Genesis* **38:** 176-181

Hahn SA, Schutte M, Hoque AT, Moskaluk CA, da Costa LT, Rozenblum E, Weinstein CL, Fischer A, Yeo CJ, Hruban RH, Kern SE (1996) DPC4, a candidate tumor suppressor gene at human chromosome 18q21.1. *Science* **271:** 350-353

Haines J, Johnson V, Pack K, Suraweera N, Slijepcevic P, Cabuy E, Coster M, Ilyas M, Wilding J, Sieber O, Bodmer W, Tomlinson I, Silver A (2005) Genetic basis of variation in adenoma multiplicity in ApcMin/+ Mom1S mice. *Proc Natl Acad Sci U S A* **102:** 2868-2873

Hajra KM, Chen DY, Fearon ER (2002) The SLUG zinc-finger protein represses E-cadherin in breast cancer. *Cancer Res* **62:** 1613-1618

Halberg RB, Waggoner J, Rasmussen K, White A, Clipson L, Prunuske AJ, Bacher JW, Sullivan R, Washington MK, Pitot HC, Petrini JH, Albertson DG, Dove WF (2009) Long-lived Min mice develop advanced intestinal cancers through a genetically conservative pathway. *Cancer Res* **69:** 5768-5775

Hamamoto T, Beppu H, Okada H, Kawabata M, Kitamura T, Miyazono K, Kato M (2002) Compound disruption of smad2 accelerates malignant progression of intestinal tumors in apc knockout mice. *Cancer Res* **62:** 5955-5961

Hanahan D (1985) Heritable formation of pancreatic beta-cell tumours in transgenic mice expressing recombinant insulin/simian virus 40 oncogenes. *Nature* **315:** 115-122

Hanahan D, Weinberg R (2000) The hallmarks of cancer. *Cell* **100:** 57-70

Harada N, Tamai Y, Ishikawa T, Sauer B, Takaku K, Oshima M, Taketo MM (1999a) Intestinal polyposis in mice with a dominant stable mutation of the beta-catenin gene. *EMBO J* **18:** 5931-5942

Haramis AP, Begthel H, van den Born M, van Es J, Jonkheer S, Offerhaus GJ, Clevers H (2004) De novo crypt formation and juvenile polyposis on BMP inhibition in mouse intestine. *Science* **303:** 1684-1686

Harrison O, Corps E, Berge T, Kilshaw P (2005) The mechanism of cell adhesion by classical cadherins: the role of domain 1. *J Cell Sci* **118:** 711-721

Hart MJ, de los Santos R, Albert IN, Rubinfeld B, Polakis P (1998) Downregulation of beta-catenin by human Axin and its association with the APC tumor suppressor, beta-catenin and GSK3 beta. *Curr Biol* **8:** 573-581

Hassan A, Howell J (2000) Insulin-like growth factor II supply modifies growth of intestinal adenoma in Apc(Min/+) mice. *Cancer Res* **60:** 1070-1076

Hatta K, Okada T, Takeichi M (1985) A monoclonal antibody disrupting calcium-dependent cell-cell adhesion of brain tissues: possible role of its target antigen in animal pattern formation. *Proc Natl Acad Sci U S A* **82:** 2789-2793

Hawley SP, Wills MK, Jones N (2010) Adenovirus-mediated genetic removal of signaling molecules in cultured primary mouse embryonic fibroblasts. *J Vis Exp*

Hazan RB, Phillips GR, Qiao RF, Norton L, Aaronson SA (2000) Exogenous expression of N-cadherin in breast cancer cells induces cell migration, invasion, and metastasis. *J Cell Biol* **148:** 779-790

He TC, Sparks AB, Rago C, Hermeking H, Zawel L, da Costa LT, Morin PJ, Vogelstein B, Kinzler KW (1998) Identification of c-MYC as a target of the APC pathway. *Science* **281:** 1509-1512

He XC, Zhang J, Tong WG, Tawfik O, Ross J, Scoville DH, Tian Q, Zeng X, He X, Wiedemann LM, Mishina Y, Li L (2004) BMP signaling inhibits intestinal stem cell self-renewal through suppression of Wnt-beta-catenin signaling. *Nat Genet* **36:** 1117-1121

Heasman J, Crawford A, Goldstone K, Garner-Hamrick P, Gumbiner B, McCrea P, Kintner C, Noro CY, Wylie C (1994) Overexpression of cadherins and underexpression of beta-catenin inhibit dorsal mesoderm induction in early Xenopus embryos. *Cell* **79:** 791-803

Heldin CH, Westermark B (1999) Mechanism of action and in vivo role of platelet-derived growth factor. *Physiol Rev* **79:** 1283-1316

Hermiston M, Gordon J (1995a) In vivo analysis of cadherin function in the mouse intestinal epithelium: essential roles in adhesion, maintenance of differentiation, and regulation of programmed cell death. *J Cell Biol* **129:** 489-506

Hermiston ML, Gordon JI (1995b) Inflammatory bowel disease and adenomas in mice expressing a dominant negative N-cadherin. *Science* **270:** 1203-1207

Hermiston ML, Wong MH, Gordon JI (1996) Forced expression of E-cadherin in the mouse intestinal epithelium slows cell migration and provides evidence for nonautonomous regulation of cell fate in a self-renewing system. *Genes Dev* **10:** 985-996

Herzig M, Savarese F, Novatchkova M, Semb H, Christofori G (2007) Tumor progression induced by the loss of E-cadherin independent of beta-catenin/Tcf-mediated Wnt signaling. *Oncogene* **26:** 2290-2298

Hill DA, Hoffmann C, Abt MC, Du Y, Kobuley D, Kirn TJ, Bushman FD, Artis D (2010) Metagenomic analyses reveal antibiotic-induced temporal and spatial changes in intestinal microbiota with associated alterations in immune cell homeostasis. *Mucosal Immunol* **3:** 148-158

Hinck L, Näthke IS, Papkoff J, Nelson WJ (1994) Dynamics of cadherin/catenin complex formation: novel protein interactions and pathways of complex assembly. *J Cell Biol* **125:** 1327-1340

Hinoi T, Akyol A, Theisen BK, Ferguson DO, Greenson JK, Williams BO, Cho KR, Fearon ER (2007) Mouse model of colonic adenoma-carcinoma progression based on somatic Apc inactivation. *Cancer Res* **67:** 9721-9730

Hirano S, Kimoto N, Shimoyama Y, Hirohashi S, Takeichi M (1992) Identification of a neural alpha-catenin as a key regulator of cadherin function and multicellular organization. *Cell* **70:** 293-301

Hirohashi S (1998) Inactivation of the E-cadherin-mediated cell adhesion system in human cancers. *Am J Pathol* **153:** 333-339

Hoffmans R, Stadeli R, Basler K (2005) Pygopus and legless provide essential transcriptional coactivator functions to armadillo/beta-catenin. *Curr Biol* **15:** 1207-1211

Hofmann C, Obermeier F, Artinger M, Hausmann M, Falk W, Schoelmerich J, Rogler G, Grossmann J (2007) Cell-cell contacts prevent anoikis in primary human colonic epithelial cells. *Gastroenterology* **132:** 587-600

Hofmann M, Pircher H (2011) E-cadherin promotes accumulation of a unique memory CD8 T-cell population in murine salivary glands. *Proc Natl Acad Sci U S A* **108:** 16741-16746

Hoschuetzky H, Aberle H, Kemler R (1994) Beta-catenin mediates the interaction of the cadherin-catenin complex with epidermal growth factor receptor. *J Cell Biol* **127:** 1375-1380

Houlston R, Collins A, Slack J, Morton N (1992) Dominant genes for colorectal cancer are not rare. *Ann Hum Genet* **56:** 99-103

Houlston R, Webb E, Broderick P, Pittman A, Di Bernardo M, Lubbe S, Chandler I, Vijayakrishnan J, Sullivan K, Penegar S, Carvajal-Carmona L, Howarth K, Jaeger E, Spain S, Walther A, Barclay E, Martin L, Gorman M, Domingo E, Teixeira A, Kerr D, Cazier J, Niittymäki I, Tuupanen S, Karhu A, Aaltonen L, Tomlinson I, Farrington S, Tenesa A, Prendergast J, Barnetson R, Cetnarskyj R, Porteous M, Pharoah P, Koessler T, Hampe J, Buch S, Schafmayer C, Tepel J, Schreiber S, Völzke H, Chang-Claude J, Hoffmeister M, Brenner H, Zanke B, Montpetit A, Hudson T, Gallinger S, Campbell H, Dunlop M, Consortium CCAS, Consortium C, Consortium ICCGA (2008) Meta-analysis of genome-wide association data identifies four new susceptibility loci for colorectal cancer. *Nat Genet* **40:** 1426-1435

Howe JR, Roth S, Ringold JC, Summers RW, Järvinen HJ, Sistonen P, Tomlinson IP, Houlston RS, Bevan S, Mitros FA, Stone EM, Aaltonen LA (1998) Mutations in the SMAD4/DPC4 gene in juvenile polyposis. *Science* **280:** 1086-1088

Hsieh JC, Kodjabachian L, Rebbert ML, Rattner A, Smallwood PM, Samos CH, Nusse R, Dawid IB, Nathans J (1999) A new secreted protein that binds to Wnt proteins and inhibits their activities. *Nature* **398:** 431-436

Huang SM, Mishina YM, Liu S, Cheung A, Stegmeier F, Michaud GA, Charlat O, Wiellette E, Zhang Y, Wiessner S, Hild M, Shi X, Wilson CJ, Mickanin C, Myer V, Fazal A, Tomlinson R, Serluca F, Shao W, Cheng H, Shultz M, Rau C, Schirle M, Schlegl J, Ghidelli S, Fawell S, Lu C, Curtis D, Kirschner MW, Lengauer C, Finan PM, Tallarico JA,

Bouwmeester T, Porter JA, Bauer A, Cong F (2009) Tankyrase inhibition stabilizes axin and antagonizes Wnt signalling. *Nature* **461:** 614-620

Huber A, Stewart D, Laurents D, Nelson W, Weis W (2001) The cadherin cytoplasmic domain is unstructured in the absence of beta-catenin. A possible mechanism for regulating cadherin turnover. *J Biol Chem* **276:** 12301-12309

Huber AH, Nelson WJ, Weis WI (1997) Three-dimensional structure of the armadillo repeat region of beta-catenin. *Cell* **90:** 871-882

Huelsken J, Vogel R, Brinkmann V, Erdmann B, Birchmeier C, Birchmeier W (2000) Requirement for beta-catenin in anterior-posterior axis formation in mice. *J Cell Biol* **148:** 567-578

Hulsken J, Birchmeier W, Behrens J (1994) E-cadherin and APC compete for the interaction with beta-catenin and the cytoskeleton. *J Cell Biol* **127:** 2061-2069

Humar B, Blair V, Charlton A, More H, Martin I, Guilford P (2009) E-cadherin deficiency initiates gastric signet-ring cell carcinoma in mice and man. *Cancer Res* **69:** 2050-2056

Hyafil F, Babinet C, Jacob F (1981) Cell-cell interactions in early embryogenesis: a molecular approach to the role of calcium. *Cell* **26:** 447-454

Hyafil F, Morello D, Babinet C, Jacob F (1980) A cell surface glycoprotein involved in the compaction of embryonal carcinoma cells and cleavage stage embryos. *Cell* **21:** 927-934

Häussinger D, Ahrens T, Aberle T, Engel J, Stetefeld J, Grzesiek S (2004) Proteolytic E-cadherin activation followed by solution NMR and X-ray crystallography. *EMBO J* **23:** 1699-1708

Häussinger D, Ahrens T, Sass H, Pertz O, Engel J, Grzesiek S (2002) Calcium-dependent homoassociation of E-cadherin by NMR spectroscopy: changes in mobility, conformation and mapping of contact regions. *J Mol Biol* **324:** 823-839

Hülsken J, Birchmeier W, Behrens J (1994) E-cadherin and APC compete for the interaction with beta-catenin and the cytoskeleton. *J Cell Biol* **127:** 2061-2069

Ichii S, Horii A, Nakatsuru S, Furuyama J, Utsunomiya J, Nakamura Y (1992) Inactivation of both APC alleles in an early stage of colon adenomas in a patient with familial adenomatous polyposis (FAP). *Hum Mol Genet* **1:** 387-390

Ilyas M, Tomlinson IP, Hanby A, Talbot IC, Bodmer WF (1997) Allele loss, replication errors and loss of expression of E-cadherin in colorectal cancers. *Gut* **40:** 654-659

Ireland H, Kemp R, Houghton C, Howard L, Clarke AR, Sansom OJ, Winton DJ (2004) Inducible Cre-mediated control of gene expression in the murine gastrointestinal tract: effect of loss of beta-catenin. *Gastroenterology* **126:** 1236-1246

Ireton RC, Davis MA, van Hengel J, Mariner DJ, Barnes K, Thoreson MA, Anastasiadis PZ, Matrisian L, Bundy LM, Sealy L, Gilbert B, van Roy F, Reynolds AB (2002) A novel role for p120 catenin in E-cadherin function. *J Cell Biol* **159:** 465-476

Isaksson-Mettävainio M, Palmqvist R, Dahlin AM, Van Guelpen B, Rutegård J, Oberg A, Henriksson ML (2012) High SMAD4 levels appear in microsatellite instability and hypermethylated colon cancers, and indicate a better prognosis. *Int J Cancer* **131:** 779-788

Ishitani T, Ninomiya-Tsuji J, Nagai S, Nishita M, Meneghini M, Barker N, Waterman M, Bowerman B, Clevers H, Shibuya H, Matsumoto K (1999) The TAK1-NLK-MAPK-related pathway antagonizes signalling between beta-catenin and transcription factor TCF. *Nature* **399:** 798-802

Jamora C, DasGupta R, Kocieniewski P, Fuchs E (2003) Links between signal transduction, transcription and adhesion in epithelial bud development. *Nature* **422:** 317-322

Janda CY, Waghray D, Levin AM, Thomas C, Garcia KC (2012) Structural basis of Wnt recognition by Frizzled. *Science* **337:** 59-64

Jass JR, Williams CB, Bussey HJ, Morson BC (1988) Juvenile polyposis--a precancerous condition. *Histopathology* **13:** 619-630

Jen J, Powell S, Papadopoulos N, Smith K, Hamilton S, Vogelstein B, Kinzler K (1994) Molecular determinants of dysplasia in colorectal lesions. *Cancer Res* **54:** 5523-5526

Jenab M, McKay JD, Ferrari P, Biessy C, Laing S, Munar GM, Sala N, Peña S, Crusius JB, Overvad K, Jensen MK, Olsen A, Tjonneland A, Clavel-Chapelon F, Boutron-Ruault MC, Kaaks R, Linseisen J, Boeing H, Bergmann MM, Trichopoulou A, Georgila C, Psaltopoulou T, Mattiello A, Vineis P, Pala V, Palli D, Tumino R, Numans ME, Peeters PH, Bueno-de-Mesquita HB, Lund E, Ardanaz E, Sánchez MJ, Dorronsoro M, Sanchez CN, Quirós JR, Hallmans G, Stenling R, Manjer J, Régner S, Key T, Bingham S, Khaw KT, Slimani N, Rinaldi S, Boffetta P, Carneiro F, Riboli E, Gonzalez C (2008) CDH1 gene polymorphisms, smoking, Helicobacter pylori infection and the risk of gastric cancer in the European Prospective Investigation into Cancer and Nutrition (EPIC-EURGAST). *Eur J Cancer* **44:** 774-780

Jin T, George Fantus I, Sun J (2008) Wnt and beyond Wnt: multiple mechanisms control the transcriptional property of beta-catenin. *Cell Signal* **20:** 1697-1704

Johnson P, Ruffell B (2009) CD44 and its role in inflammation and inflammatory diseases. *Inflamm Allergy Drug Targets* **8:** 208-220

Jonkers J, Meuwissen R, van der Gulden H, Peterse H, van der Valk M, Berns A (2001) Synergistic tumor suppressor activity of BRCA2 and p53 in a conditional mouse model for breast cancer. *Nat Genet* **29:** 418-425

Jou T, Stewart D, Stappert J, Nelson W, Marrs J (1995) Genetic and biochemical dissection of protein linkages in the cadherin-catenin complex. *Proc Natl Acad Sci U S A* **92:** 5067-5071

Jovov B, Que J, Tobey NA, Djukic Z, Hogan BL, Orlando RC (2011) Role of E-cadherin in the pathogenesis of gastroesophageal reflux disease. *Am J Gastroenterol* **106:** 1039-1047

Jung A, Schrauder M, Oswald U, Knoll C, Sellberg P, Palmqvist R, Niedobitek G, Brabletz T, Kirchner T (2001) The invasion front of human colorectal adenocarcinomas shows co-localization of nuclear beta-catenin, cyclin D1, and p16INK4A and is a region of low proliferation. *Am J Pathol* **159:** 1613-1617

Kan NG, Stemmler MP, Junghans D, Kanzler B, de Vries WN, Dominis M, Kemler R (2007) Gene replacement reveals a specific role for E-cadherin in the formation of a functional trophectoderm. *Development* **134:** 31-41

Kanatsu-Shinohara M, Takehashi M, Takashima S, Lee J, Morimoto H, Chuma S, Raducanu A, Nakatsuji N, Fässler R, Shinohara T (2008) Homing of mouse spermatogonial stem cells to germline niche depends on beta1-integrin. *Cell Stem Cell* **3:** 533-542

Karayiannakis AJ, Syrigos KN, Efstathiou J, Valizadeh A, Noda M, Playford RJ, Kmiot W, Pignatelli M (1998) Expression of catenins and E-cadherin during epithelial restitution in inflammatory bowel disease. *J Pathol* **185:** 413-418

Karpowicz P, Willaime-Morawek S, Balenci L, DeVeale B, Inoue T, van der Kooy D (2009) E-Cadherin regulates neural stem cell self-renewal. *J Neurosci* **29:** 3885-3896

Katz B, Levenberg S, Yamada K, Geiger B (1998) Modulation of cell-cell adherens junctions by surface clustering of the N-cadherin cytoplasmic tail. *Exp Cell Res* **243:** 415-424

Kaurah P, MacMillan A, Boyd N, Senz J, De Luca A, Chun N, Suriano G, Zaor S, Van Manen L, Gilpin C, Nikkel S, Connolly-Wilson M, Weissman S, Rubinstein WS, Sebold C, Greenstein R, Stroop J, Yim D, Panzini B, McKinnon W, Greenblatt M, Wirtzfeld D, Fontaine D, Coit D, Yoon S, Chung D, Lauwers G, Pizzuti A, Vaccaro C, Redal MA, Oliveira C, Tischkowitz M, Olschwang S, Gallinger S, Lynch H, Green J, Ford J, Pharoah P, Fernandez B, Huntsman D (2007) Founder and recurrent CDH1 mutations in families with hereditary diffuse gastric cancer. *JAMA* **297:** 2360-2372

Kawakami M, Yamaguchi T, Takahashi K, Matsumoto H, Yasutome M, Horiguchi S, Hayashi Y, Funata N, Mori T (2010) Assessment of SMAD4, p53, and Ki-67 alterations as a predictor of liver metastasis in human colorectal cancer. *Surg Today* **40:** 245-250

Kazanskaya O, Glinka A, del Barco Barrantes I, Stannek P, Niehrs C, Wu W (2004) R-Spondin2 is a secreted activator of Wnt/beta-catenin signaling and is required for Xenopus myogenesis. *Dev Cell* **7:** 525-534

Kemler R, Babinet C, Eisen H, Jacob F (1977) Surface antigen in early differentiation. *Proc Natl Acad Sci U S A* **74:** 4449-4452

Kerkhoff E, Fedorov LM, Siefken R, Walter AO, Papadopoulos T, Rapp UR (2000) Lung-targeted expression of the c-Raf-1 kinase in transgenic mice exposes a novel oncogenic character of the wild-type protein. *Cell Growth Differ* **11:** 185-190

Kim BG, Li C, Qiao W, Mamura M, Kasprzak B, Kasperczak B, Anver M, Wolfraim L, Hong S, Mushinski E, Potter M, Kim SJ, Fu XY, Deng C, Letterio JJ (2006) Smad4 signalling in T cells is required for suppression of gastrointestinal cancer. *Nature* **441:** 1015-1019

Kim KA, Kakitani M, Zhao J, Oshima T, Tang T, Binnerts M, Liu Y, Boyle B, Park E, Emtage P, Funk WD, Tomizuka K (2005) Mitogenic influence of human R-spondin1 on the intestinal epithelium. *Science* **309:** 1256-1259

Kim TH, Escudero S, Shivdasani RA (2012) Intact function of Lgr5 receptor-expressing intestinal stem cells in the absence of Paneth cells. *Proc Natl Acad Sci U S A* **109:** 3932-3937

Kinzler K, Vogelstein B (1996) Lessons from hereditary colorectal cancer. *Cell* **87:** 159-170

Kinzler KW, Vogelstein B (1998) Landscaping the cancer terrain. *Science* **280:** 1036-1037

Kitagawa M, Natori M, Murase S, Hirano S, Taketani S, Suzuki S (2000) Mutation analysis of cadherin-4 reveals amino acid residues of EC1 important for the structure and function. *Biochem Biophys Res Commun* **271:** 358-363

Kizhatil K, Davis JQ, Davis L, Hoffman J, Hogan BL, Bennett V (2007) Ankyrin-G is a molecular partner of E-cadherin in epithelial cells and early embryos. *J Biol Chem* **282:** 26552-26561

Knudson A (1993) Antioncogenes and human cancer. *Proc Natl Acad Sci U S A* **90:** 10914-10921

Knudson AJ (1971) Mutation and cancer: statistical study of retinoblastoma. *Proc Natl Acad Sci U S A* **68:** 820-823

Kodach LL, Wiercinska E, de Miranda NF, Bleuming SA, Musler AR, Peppelenbosch MP, Dekker E, van den Brink GR, van Noesel CJ, Morreau H, Hommes DW, Ten Dijke P, Offerhaus GJ, Hardwick JC (2008) The bone morphogenetic protein pathway is inactivated in the majority of sporadic colorectal cancers. *Gastroenterology* **134:** 1332-1341

Kondo J, Endo H, Okuyama H, Ishikawa O, Iishi H, Tsujii M, Ohue M, Inoue M (2011) Retaining cell-cell contact enables preparation and culture of spheroids composed of pure primary cancer cells from colorectal cancer. *Proc Natl Acad Sci U S A* **108:** 6235-6240

Korswagen HC, Herman MA, Clevers HC (2000) Distinct beta-catenins mediate adhesion and signalling functions in C. elegans. *Nature* **406:** 527-532

Kostetskii I, Li J, Xiong Y, Zhou R, Ferrari VA, Patel VV, Molkentin JD, Radice GL (2005) Induced deletion of the N-cadherin gene in the heart leads to dissolution of the intercalated disc structure. *Circ Res* **96:** 346-354

Kotb AM, Hierholzer A, Kemler R (2011) Replacement of E-cadherin by N-cadherin in the mammary gland leads to fibrocystic changes and tumor formation. *Breast Cancer Res* **13:** R104

Kovacs EM, Ali RG, McCormack AJ, Yap AS (2002) E-cadherin homophilic ligation directly signals through Rac and phosphatidylinositol 3-kinase to regulate adhesive contacts. *J Biol Chem* **277:** 6708-6718

Kovtun IV, Harris KJ, Jatoi A, Jevremovic D (2011) Increased incidence of endometrioid tumors caused by aberrations in E-cadherin promoter of mismatch repair-deficient mice. *Carcinogenesis* **32:** 1085-1092

Kuphal F, Behrens J (2006) E-cadherin modulates Wnt-dependent transcription in colorectal cancer cells but does not alter Wnt-independent gene expression in fibroblasts. *Exp Cell Res* **312:** 457-467

Kuroda S, Fukata M, Nakagawa M, Fujii K, Nakamura T, Ookubo T, Izawa I, Nagase T, Nomura N, Tani H, Shoji I, Matsuura Y, Yonehara S, Kaibuchi K (1998) Role of IQGAP1, a target of the small GTPases Cdc42 and Rac1, in regulation of E-cadherin- mediated cell-cell adhesion. *Science* **281:** 832-835

Kwong LN, Shedlovsky A, Biehl BS, Clipson L, Pasch CA, Dove WF (2007) Identification of Mom7, a novel modifier of Apc(Min/+) on mouse chromosome 18. *Genetics* **176:** 1237-1244

Labbé E, Letamendia A, Attisano L (2000) Association of Smads with lymphoid enhancer binding factor 1/T cell-specific factor mediates cooperative signaling by the transforming growth factor-beta and wnt pathways. *Proc Natl Acad Sci U S A* **97:** 8358-8363

Lagna G, Hata A, Hemmati-Brivanlou A, Massagué J (1996) Partnership between DPC4 and SMAD proteins in TGF-beta signalling pathways. *Nature* **383:** 832-836

Lamlum H, Ilyas M, Rowan A, Clark S, Johnson V, Bell J, Frayling I, Efstathiou J, Pack K, Payne S, Roylance R, Gorman P, Sheer D, Neale K, Phillips R, Talbot I, Bodmer W, Tomlinson I (1999) The type of somatic mutation at APC in familial adenomatous polyposis is determined by the site of the germline mutation: a new facet to Knudson's 'two-hit' hypothesis. *Nat Med* **5:** 1071-1075

Larue L, Ohsugi M, Hirchenhain J, Kemler R (1994) E-cadherin null mutant embryos fail to form a trophectoderm epithelium. *Proc Natl Acad Sci U S A* **91:** 8263-8267

Laudet V, Stehelin D, Clevers H (1993) Ancestry and diversity of the HMG box superfamily. *Nucleic Acids Res* **21:** 2493-2501

Le TL, Yap AS, Stow JL (1999) Recycling of E-cadherin: a potential mechanism for regulating cadherin dynamics. *J Cell Biol* **146:** 219-232

Leckband D, Sivasankar S (2000) Mechanism of homophilic cadherin adhesion. *Curr Opin Cell Biol* **12:** 587-592

Lee E, Salic A, Kruger R, Heinrich R, Kirschner MW (2003) The roles of APC and Axin derived from experimental and theoretical analysis of the Wnt pathway. *PLoS Biol* **1:** E10

Lee PP, Fitzpatrick DR, Beard C, Jessup HK, Lehar S, Makar KW, Pérez-Melgosa M, Sweetser MT, Schlissel MS, Nguyen S, Cherry SR, Tsai JH, Tucker SM, Weaver WM, Kelso A, Jaenisch R, Wilson CB (2001) A critical role for Dnmt1 and DNA methylation in T cell development, function, and survival. *Immunity* **15:** 763-774

Leedham SJ, Rodenas-Cuadrado P, Howarth K, Lewis A, Mallappa S, Segditsas S, Davis H, Jeffery R, Rodriguez-Justo M, Keshav S, Travis SP, Graham TA, East J, Clark S, Tomlinson IP (2012) A basal gradient of Wnt and stem-cell number influences regional tumour distribution in human and mouse intestinal tracts. *Gut*

Lehembre F, Yilmaz M, Wicki A, Schomber T, Strittmatter K, Ziegler D, Kren A, Went P, Derksen PW, Berns A, Jonkers J, Christofori G (2008) NCAM-induced focal adhesion assembly: a functional switch upon loss of E-cadherin. *EMBO J* **27:** 2603-2615

Levy D, Smith K, Beazer-Barclay Y, Hamilton S, Vogelstein B, Kinzler K (1994) Inactivation of both APC alleles in human and mouse tumors. *Cancer Res* **54:** 5953-5958

Lewandoski M, Wassarman KM, Martin GR (1997) Zp3-cre, a transgenic mouse line for the activation or inactivation of loxP-flanked target genes specifically in the female germ line. *Curr Biol* **7:** 148-151

Lewis A, Davis H, Deheragoda M, Pollard P, Nye E, Jeffery R, Segditsas S, East P, Poulsom R, Stamp G, Wright N, Tomlinson I (2012) The C-terminus of Apc does not influence intestinal adenoma development or progression. *J Pathol* **226:** 73-83

Leyns L, Bouwmeester T, Kim SH, Piccolo S, De Robertis EM (1997) Frzb-1 is a secreted antagonist of Wnt signaling expressed in the Spemann organizer. *Cell* **88:** 747-756

Li G, Herlyn M (2000) Dynamics of intercellular communication during melanoma development. *Mol Med Today* **6:** 163-169

Li G, Satyamoorthy K, Herlyn M (2001) N-cadherin-mediated intercellular interactions promote survival and migration of melanoma cells. *Cancer Res* **61:** 3819-3825

Li Q, Ishikawa TO, Oshima M, Taketo MM (2005) The threshold level of adenomatous polyposis coli protein for mouse intestinal tumorigenesis. *Cancer Res* **65:** 8622-8627

Li VS, Ng SS, Boersema PJ, Low TY, Karthaus WR, Gerlach JP, Mohammed S, Heck AJ, Maurice MM, Mahmoudi T, Clevers H (2012) Wnt signaling through inhibition of β-catenin degradation in an intact Axin1 complex. *Cell* **149:** 1245-1256

Liu F, Hata A, Baker JC, Doody J, Cárcamo J, Harland RM, Massagué J (1996) A human Mad protein acting as a BMP-regulated transcriptional activator. *Nature* **381:** 620-623

Lock JG, Hammond LA, Houghton F, Gleeson PA, Stow JL (2005) E-cadherin transport from the trans-Golgi network in tubulovesicular carriers is selectively regulated by golgin-97. *Traffic* **6:** 1142-1156

Lock JG, Stow JL (2005) Rab11 in recycling endosomes regulates the sorting and basolateral transport of E-cadherin. *Mol Biol Cell* **16:** 1744-1755

Lugo-Martínez VH, Petit CS, Fouquet S, Le Beyec J, Chambaz J, Pinçon-Raymond M, Cardot P, Thenet S (2009) Epidermal growth factor receptor is involved in enterocyte anoikis through the dismantling of E-cadherin-mediated junctions. *Am J Physiol Gastrointest Liver Physiol* **296:** G235-244

Lum L, Clevers H (2012) Cell biology. The unusual case of Porcupine. *Science* **337:** 922-923

Luongo C, Moser A, Gledhill S, Dove W (1994) Loss of Apc+ in intestinal adenomas from Min mice. *Cancer Res* **54:** 5947-5952

Ma L, Young J, Prabhala H, Pan E, Mestdagh P, Muth D, Teruya-Feldstein J, Reinhardt F, Onder TT, Valastyan S, Westermann F, Speleman F, Vandesompele J, Weinberg RA (2010) miR-9, a MYC/MYCN-activated microRNA, regulates E-cadherin and cancer metastasis. *Nat Cell Biol* **12:** 247-256

MacPhee M, Chepenik KP, Liddell RA, Nelson KK, Siracusa LD, Buchberg AM (1995) The secretory phospholipase A2 gene is a candidate for the Mom1 locus, a major modifier of ApcMin-induced intestinal neoplasia. *Cell* **81:** 957-966

Madison BB, Braunstein K, Kuizon E, Portman K, Qiao XT, Gumucio DL (2005) Epithelial hedgehog signals pattern the intestinal crypt-villus axis. *Development* **132:** 279-289

Madison BB, Dunbar L, Qiao XT, Braunstein K, Braunstein E, Gumucio DL (2002) Cis elements of the villin gene control expression in restricted domains of the vertical (crypt) and horizontal (duodenum, cecum) axes of the intestine. *J Biol Chem* **277:** 33275-33283

Maher MT, Flozak AS, Stocker AM, Chenn A, Gottardi CJ (2009) Activity of the beta-catenin phosphodestruction complex at cell-cell contacts is enhanced by cadherin-based adhesion. *J Cell Biol* **186:** 219-228

Mamot C, Mild G, Reuter J, Laffer U, Metzger U, Terracciano L, Boulay JL, Herrmann R, Rochlitz C (2003) Infrequent mutation of the tumour-suppressor gene Smad4 in early-stage colorectal cancer. *Br J Cancer* **88:** 420-423

Mao B, Wu W, Davidson G, Marhold J, Li M, Mechler BM, Delius H, Hoppe D, Stannek P, Walter C, Glinka A, Niehrs C (2002) Kremen proteins are Dickkopf receptors that regulate Wnt/beta-catenin signalling. *Nature* **417:** 664-667

Mao J, Wang J, Liu B, Pan W, Farr GH, 3rd, Flynn C, Yuan H, Takada S, Kimelman D, Li L, Wu D (2001) Low-density lipoprotein receptor-related protein-5 binds to Axin and regulates the canonical Wnt signaling pathway. *Mol Cell* **7:** 801-809

Marambaud P, Shioi J, Serban G, Georgakopoulos A, Sarner S, Nagy V, Baki L, Wen P, Efthimiopoulos S, Shao Z, Wisniewski T, Robakis NK (2002) A presenilin-1/gamma-secretase cleavage releases the E-cadherin intracellular domain and regulates disassembly of adherens junctions. *EMBO J* **21:** 1948-1956

March HN, Rust AG, Wright NA, ten Hoeve J, de Ridder J, Eldridge M, van der Weyden L, Berns A, Gadiot J, Uren A, Kemp R, Arends MJ, Wessels LF, Winton DJ, Adams DJ (2011) Insertional mutagenesis identifies multiple networks of cooperating genes driving intestinal tumorigenesis. *Nat Genet* **43:** 1202-1209

Maretzky T, Reiss K, Ludwig A, Buchholz J, Scholz F, Proksch E, de Strooper B, Hartmann D, Saftig P (2005) ADAM10 mediates E-cadherin shedding and regulates epithelial cell-cell adhesion, migration, and beta-catenin translocation. *Proc Natl Acad Sci U S A* **102:** 9182-9187

Marino S, Vooijs M, van Der Gulden H, Jonkers J, Berns A (2000) Induction of medulloblastomas in p53-null mutant mice by somatic inactivation of Rb in the external granular layer cells of the cerebellum. *Genes Dev* **14:** 994-1004

Markowitz SD, Bertagnolli MM (2009) Molecular origins of cancer: Molecular basis of colorectal cancer. *N Engl J Med* **361:** 2449-2460

Marsh V, Winton D, Williams G, Dubois N, Trumpp A, Sansom O, Clarke A (2008) Epithelial Pten is dispensable for intestinal homeostasis but suppresses adenoma development and progression after Apc mutation. *Nat Genet* **40:** 1436-1444

Massagué J (2012) TGF-β signaling in development and disease. *FEBS Lett* **586:** 1833

Massagué J, Seoane J, Wotton D (2005) Smad transcription factors. *Genes Dev* **19:** 2783-2810

Masterson J, O'Dea S (2007) Posttranslational truncation of E-cadherin and significance for tumour progression. *Cells Tissues Organs* **185:** 175-179

Maxfield FR, McGraw TE (2004) Endocytic recycling. *Nat Rev Mol Cell Biol* **5:** 121-132

McCart AE, Vickaryous NK, Silver A (2008) Apc mice: models, modifiers and mutants. *Pathol Res Pract* **204:** 479-490

McMahon AP, Moon RT (1989) Ectopic expression of the proto-oncogene int-1 in Xenopus embryos leads to duplication of the embryonic axis. *Cell* **58:** 1075-1084

Mesker WE, Liefers GJ, Junggeburt JM, van Pelt GW, Alberici P, Kuppen PJ, Miranda NF, van Leeuwen KA, Morreau H, Szuhai K, Tollenaar RA, Tanke HJ (2009) Presence of a high amount of stroma and downregulation of SMAD4 predict for worse survival for stage I-II colon cancer patients. *Cell Oncol* **31:** 169-178

Mimata A, Fukamachi H, Eishi Y, Yuasa Y (2011) Loss of E-cadherin in mouse gastric epithelial cells induces signet ring-like cells, a possible precursor lesion of diffuse gastric cancer. *Cancer Sci* **102:** 942-950

Miyaki M, Iijima T, Konishi M, Sakai K, Ishii A, Yasuno M, Hishima T, Koike M, Shitara N, Iwama T, Utsunomiya J, Kuroki T, Mori T (1999) Higher frequency of Smad4 gene mutation in human colorectal cancer with distant metastasis. *Oncogene* **18:** 3098-3103

Miyashita Y, Ozawa M (2007) Increased internalization of p120-uncoupled E-cadherin and a requirement for a dileucine motif in the cytoplasmic domain for endocytosis of the protein. *J Biol Chem* **282:** 11540-11548

Miyoshi Y, Nagase H, Ando H, Horii A, Ichii S, Nakatsuru S, Aoki T, Miki Y, Mori T, Nakamura Y (1992) Somatic mutations of the APC gene in colorectal tumors: mutation cluster region in the APC gene. *Hum Mol Genet* **1:** 229-233

Moser AR, Dove WF, Roth KA, Gordon JI (1992) The Min (multiple intestinal neoplasia) mutation: its effect on gut epithelial cell differentiation and interaction with a modifier system. *J Cell Biol* **116:** 1517-1526

Moser AR, Pitot HC, Dove WF (1990) A dominant mutation that predisposes to multiple intestinal neoplasia in the mouse. *Science* **247:** 322-324

Moser AR, Shoemaker AR, Connelly CS, Clipson L, Gould KA, Luongo C, Dove WF, Siggers PH, Gardner RL (1995) Homozygosity for the Min allele of Apc results in disruption of mouse development prior to gastrulation. *Dev Dyn* **203:** 422-433

Muise AM, Walters TD, Glowacka WK, Griffiths AM, Ngan BY, Lan H, Xu W, Silverberg MS, Rotin D (2009) Polymorphisms in E-cadherin (CDH1) result in a mis-localised cytoplasmic protein that is associated with Crohn's disease. *Gut* **58:** 1121-1127

Muñoz Descalzo S, Martinez Arias A (2012) The structure of Wntch signalling and the resolution of transition states in development. *Semin Cell Dev Biol* **23:** 443-449

Muñoz NM, Upton M, Rojas A, Washington MK, Lin L, Chytil A, Sozmen EG, Madison BB, Pozzi A, Moon RT, Moses HL, Grady WM (2006) Transforming growth factor beta receptor type II inactivation induces the malignant transformation of intestinal neoplasms initiated by Apc mutation. *Cancer Res* **66:** 9837-9844

Müller N, Reinacher-Schick A, Baldus S, van Hengel J, Berx G, Baar A, van Roy F, Schmiegel W, Schwarte-Waldhoff I (2002) Smad4 induces the tumor suppressor E-cadherin and P-cadherin in colon carcinoma cells. *Oncogene* **21:** 6049-6058

Nagafuchi A, Takeichi M (1988) Cell binding function of E-cadherin is regulated by the cytoplasmic domain. *EMBO J* **7:** 3679-3684

Nagar B, Overduin M, Ikura M, Rini J (1996) Structural basis of calcium-induced E-cadherin rigidification and dimerization. *Nature* **380:** 360-364

National Cancer Institute N, DHHS, Bethesda. (April 2010) Trends Progress Report - 2009/2010 Update. Vol. 2010.

Network CGA (2012) Comprehensive molecular characterization of human colon and rectal cancer. *Nature* **487:** 330-337

Nieman MT, Prudoff RS, Johnson KR, Wheelock MJ (1999) N-cadherin promotes motility in human breast cancer cells regardless of their E-cadherin expression. *J Cell Biol* **147:** 631-644

Nnadi SC, Watson R, Innocent J, Gonye GE, Buchberg AM, Siracusa LD (2012) Identification of five novel modifier loci of ApcMin harbored in the BXH14 recombinant inbred strain. *Carcinogenesis* **33:** 1589-1597

Nollet F, Kools P, van Roy F (2000) Phylogenetic analysis of the cadherin superfamily allows identification of six major subfamilies besides several solitary members. *J Mol Biol* **299:** 551-572

Noren NK, Arthur WT, Burridge K (2003) Cadherin engagement inhibits RhoA via p190RhoGAP. *J Biol Chem* **278:** 13615-13618

Nose A, Tsuji K, Takeichi M (1990) Localization of specificity determining sites in cadherin cell adhesion molecules. *Cell* **61:** 147-155

Nusse R, Varmus HE (1982) Many tumors induced by the mouse mammary tumor virus contain a provirus integrated in the same region of the host genome. *Cell* **31:** 99-109

Nusslein-Volhard C, Wieschaus E (1980) Mutations affecting segment number and polarity in Drosophila. *Nature* **287:** 795-801

Nusslein-Volhard C, Wieschaus E, Kluding H (1984) Mutations affecting the pattern of the larval cuticle in Drosophila melanogaster. I. Zygotic loci on the second chromosome. *Roux's Arch Dev Biol* **193:** 267-282.

Ohkusa T, Kato K, Terao S, Chiba T, Mabe K, Murakami K, Mizokami Y, Sugiyama T, Yanaka A, Takeuchi Y, Yamato S, Yokoyama T, Okayasu I, Watanabe S, Tajiri H, Sato N, Group JUATS (2010) Newly developed antibiotic combination therapy for ulcerative colitis: a double-blind placebo-controlled multicenter trial. *Am J Gastroenterol* **105:** 1820-1829

Oikarinen SI, Cleveland AG, Cork KM, Bynoté KK, Rafter JJ, Gustafsson JA, Mutanen M, Gould KA (2009) Genetic mapping of Mom5, a novel modifier of Apc(Min)-induced intestinal tumorigenesis. *Carcinogenesis* **30:** 1591-1596

Oliveira C, Sousa S, Pinheiro H, Karam R, Bordeira-Carriço R, Senz J, Kaurah P, Carvalho J, Pereira R, Gusmão L, Wen X, Cipriano MA, Yokota J, Carneiro F, Huntsman D, Seruca R (2009) Quantification of epigenetic and genetic 2nd hits in CDH1 during hereditary diffuse gastric cancer syndrome progression. *Gastroenterology* **136:** 2137-2148

Onder TT, Gupta PB, Mani SA, Yang J, Lander ES, Weinberg RA (2008) Loss of E-cadherin promotes metastasis via multiple downstream transcriptional pathways. *Cancer Res* **68:** 3645-3654

Ormestad M, Astorga J, Landgren H, Wang T, Johansson BR, Miura N, Carlsson P (2006) Foxf1 and Foxf2 control murine gut development by limiting mesenchymal Wnt signaling and promoting extracellular matrix production. *Development* **133:** 833-843

Orsulic S, Huber O, Aberle H, Arnold S, Kemler R (1999) E-cadherin binding prevents beta-catenin nuclear localization and beta-catenin/LEF-1-mediated transactivation. *J Cell Sci* **112 (Pt 8):** 1237-1245

Oshima M, Oshima H, Kitagawa K, Kobayashi M, Itakura C, Taketo M (1995) Loss of Apc heterozygosity and abnormal tissue building in nascent intestinal polyps in mice carrying a truncated Apc gene. *Proc Natl Acad Sci U S A* **92:** 4482-4486

Overduin M, Harvey T, Bagby S, Tong K, Yau P, Takeichi M, Ikura M (1995) Solution structure of the epithelial cadherin domain responsible for selective cell adhesion. *Science* **267:** 386-389

Oyama T, Kanai Y, Ochiai A, Akimoto S, Oda T, Yanagihara K, Nagafuchi A, Tsukita S, Shibamoto S, Ito F (1994) A truncated beta-catenin disrupts the interaction between E-cadherin and alpha-catenin: a cause of loss of intercellular adhesiveness in human cancer cell lines. *Cancer Res* **54:** 6282-6287

Ozawa M, Engel J, Kemler R (1990a) Single amino acid substitutions in one Ca2+ binding site of uvomorulin abolish the adhesive function. *Cell* **63:** 1033-1038

Ozawa M, Kemler R (1990) Correct proteolytic cleavage is required for the cell adhesive function of uvomorulin. *J Cell Biol* **111:** 1645-1650

Ozawa M, Ringwald M, Kemler R (1990b) Uvomorulin-catenin complex formation is regulated by a specific domain in the cytoplasmic region of the cell adhesion molecule. *Proc Natl Acad Sci U S A* **87:** 4246-4250

Palacios F, Schweitzer JK, Boshans RL, D'Souza-Schorey C (2002) ARF6-GTP recruits Nm23-H1 to facilitate dynamin-mediated endocytosis during adherens junctions disassembly. *Nat Cell Biol* **4:** 929-936

Palacios F, Tushir JS, Fujita Y, D'Souza-Schorey C (2005) Lysosomal targeting of E-cadherin: a unique mechanism for the down-regulation of cell-cell adhesion during epithelial to mesenchymal transitions. *Mol Cell Biol* **25:** 389-402

Parisini E, Higgins J, Liu J, Brenner M, Wang J (2007) The crystal structure of human E-cadherin domains 1 and 2, and comparison with other cadherins in the context of adhesion mechanism. *J Mol Biol* **373:** 401-411

Parkin D, Bray F, Ferlay J, Pisani P (2005) Global cancer statistics, 2002. *CA Cancer J Clin* **55:** 74-108

Parviz F, Li J, Kaestner KH, Duncan SA (2002) Generation of a conditionally null allele of hnf4alpha. *Genesis* **32:** 130-133

Pece S, Gutkind JS (2000) Signaling from E-cadherins to the MAPK pathway by the recruitment and activation of epidermal growth factor receptors upon cell-cell contact formation. *J Biol Chem* **275:** 41227-41233

Peinado H, Olmeda D, Cano A (2007) Snail, Zeb and bHLH factors in tumour progression: an alliance against the epithelial phenotype? *Nat Rev Cancer* **7:** 415-428

Perez-Moreno M, Jamora C, Fuchs E (2003) Sticky business: orchestrating cellular signals at adherens junctions. *Cell* **112:** 535-548

Perez-Moreno MA, Locascio A, Rodrigo I, Dhondt G, Portillo F, Nieto MA, Cano A (2001) A new role for E12/E47 in the repression of E-cadherin expression and epithelial-mesenchymal transitions. *J Biol Chem* **276:** 27424-27431

Perl A, Wilgenbus P, Dahl U, Semb H, Christofori G (1998) A causal role for E-cadherin in the transition from adenoma to carcinoma. *Nature* **392:** 190-193

Pertz O, Bozic D, Koch A, Fauser C, Brancaccio A, Engel J (1999) A new crystal structure, Ca2+ dependence and mutational analysis reveal molecular details of E-cadherin homoassociation. *EMBO J* **18:** 1738-1747

Peyriéras N, Hyafil F, Louvard D, Ploegh H, Jacob F (1983) Uvomorulin: a nonintegral membrane protein of early mouse embryo. *Proc Natl Acad Sci U S A* **80:** 6274-6277

Pharoah PD, Guilford P, Caldas C, Consortium IGCL (2001) Incidence of gastric cancer and breast cancer in CDH1 (E-cadherin) mutation carriers from hereditary diffuse gastric cancer families. *Gastroenterology* **121:** 1348-1353

Pinto D, Clevers H (2005) Wnt, stem cells and cancer in the intestine. *Biol Cell* **97:** 185-196

Pollard P, Deheragoda M, Segditsas S, Lewis A, Rowan A, Howarth K, Willis L, Nye E, McCart A, Mandir N, Silver A, Goodlad R, Stamp G, Cockman M, East P, Spencer-Dene B, Poulsom R, Wright N, Tomlinson I (2009) The Apc 1322T mouse develops severe polyposis associated with submaximal nuclear beta-catenin expression. *Gastroenterology* **136:** 2204-2213.e2201-2213

Pontoriero GF, Smith AN, Miller LA, Radice GL, West-Mays JA, Lang RA (2009) Co-operative roles for E-cadherin and N-cadherin during lens vesicle separation and lens epithelial cell survival. *Dev Biol* **326:** 403-417

Portela-Gomes GM, Stridsberg M, Johansson H, Grimelius L (1999) Co-localization of synaptophysin with different neuroendocrine hormones in the human gastrointestinal tract. *Histochem Cell Biol* **111:** 49-54

Potten CS (1977) Extreme sensitivity of some intestinal crypt cells to X and gamma irradiation. *Nature* **269:** 518-521

Potten CS, Kovacs L, Hamilton E (1974) Continuous labelling studies on mouse skin and intestine. *Cell Tissue Kinet* **7:** 271-283

Powell S, Zilz N, Beazer-Barclay Y, Bryan T, Hamilton S, Thibodeau S, Vogelstein B, Kinzler K (1992) APC mutations occur early during colorectal tumorigenesis. *Nature* **359:** 235-237

Quesada CF, Kimata H, Mori M, Nishimura M, Tsuneyoshi T, Baba S (1998) Piroxicam and acarbose as chemopreventive agents for spontaneous intestinal adenomas in APC gene 1309 knockout mice. *Jpn J Cancer Res* **89:** 392-396

Qureshi HS, Linden MD, Divine G, Raju UB (2006) E-cadherin status in breast cancer correlates with histologic type but does not correlate with established prognostic parameters. *Am J Clin Pathol* **125:** 377-385

R Development Core Team. (2008) *R: A language and environment for statistical computing*. *R Foundation for Statistical Computing*, *Vienna, Austria*.

Radisky DC, Bissell MJ (2004) Cancer. Respect thy neighbor! *Science* **303:** 775-777

Rashid MG, Sanda MG, Vallorosi CJ, Rios-Doria J, Rubin MA, Day ML (2001) Posttranslational truncation and inactivation of human E-cadherin distinguishes prostate cancer from matched normal prostate. *Cancer Res* **61:** 489-492

Rasola A, Fassetta M, De Bacco F, D'Alessandro L, Gramaglia D, Di Renzo MF, Comoglio PM (2007) A positive feedback loop between hepatocyte growth factor receptor and beta-catenin sustains colorectal cancer cell invasive growth. *Oncogene* **26:** 1078-1087

Rattner A, Hsieh JC, Smallwood PM, Gilbert DJ, Copeland NG, Jenkins NA, Nathans J (1997) A family of secreted proteins contains homology to the cysteine-rich ligand-binding domain of frizzled receptors. *Proc Natl Acad Sci U S A* **94:** 2859-2863

Reardon SN, King ML, MacLean JA, Mann JL, DeMayo FJ, Lydon JP, Hayashi K (2012) CDH1 is essential for endometrial differentiation, gland development, and adult function in the mouse uterus. *Biol Reprod* **86:** 141, 141-110

Reya T, Morrison SJ, Clarke MF, Weissman IL (2001) Stem cells, cancer, and cancer stem cells. *Nature* **414:** 105-111

Reynolds A, Daniel J, McCrea P, Wheelock M, Wu J, Zhang Z (1994) Identification of a new catenin: the tyrosine kinase substrate p120cas associates with E-cadherin complexes. *Mol Cell Biol* **14:** 8333-8342

Riethmacher D, Brinkmann V, Birchmeier C (1995) A targeted mutation in the mouse E-cadherin gene results in defective preimplantation development. *Proc Natl Acad Sci U S A* **92:** 855-859

Rijsewijk F, Schuermann M, Wagenaar E, Parren P, Weigel D, Nusse R (1987) The Drosophila homolog of the mouse mammary oncogene int-1 is identical to the segment polarity gene wingless. *Cell* **50:** 649-657

Rimm D, Koslov E, Kebriaei P, Cianci C, Morrow J (1995) Alpha 1(E)-catenin is an actin-binding and -bundling protein mediating the attachment of F-actin to the membrane adhesion complex. *Proc Natl Acad Sci U S A* **92:** 8813-8817

Ringwald M, Schuh R, Vestweber D, Eistetter H, Lottspeich F, Engel J, Dölz R, Jähnig F, Epplen J, Mayer S (1987) The structure of cell adhesion molecule uvomorulin. Insights into the molecular mechanism of Ca2+-dependent cell adhesion. *EMBO J* **6:** 3647-3653

Rios-Doria J, Day KC, Kuefer R, Rashid MG, Chinnaiyan AM, Rubin MA, Day ML (2003) The role of calpain in the proteolytic cleavage of E-cadherin in prostate and mammary epithelial cells. *J Biol Chem* **278:** 1372-1379

Robanus-Maandag EC, Koelink PJ, Breukel C, Salvatori DC, Jagmohan-Changur SC, Bosch CA, Verspaget HW, Devilee P, Fodde R, Smits R (2010) A new conditional Apc-mutant mouse model for colorectal cancer. *Carcinogenesis* **31:** 946-952

Roth S, Weston J (1967) THE MEASUREMENT OF INTERCELLULAR ADHESION. *Proc Natl Acad Sci U S A* **58:** 974-980

Rubinfeld B, Souza B, Albert I, Muller O, Chamberlain SH, Masiarz FR, Munemitsu S, Polakis P (1993) Association of the APC gene product with beta-catenin. *Science* **262:** 1731-1734

Sadowski PD (1995) The Flp recombinase of the 2-microns plasmid of Saccharomyces cerevisiae. *Prog Nucleic Acid Res Mol Biol* **51:** 53-91

Sancho E, Batlle E, Clevers H (2004) Signaling pathways in intestinal development and cancer. *Annu Rev Cell Dev Biol* **20:** 695-723

Sangiorgi E, Capecchi MR (2008) Bmi1 is expressed in vivo in intestinal stem cells. *Nat Genet* **40:** 915-920

Sansom OJ, Meniel VS, Muncan V, Phesse TJ, Wilkins JA, Reed KR, Vass JK, Athineos D, Clevers H, Clarke AR (2007) Myc deletion rescues Apc deficiency in the small intestine. *Nature* **446:** 676-679

Sansom OJ, Reed KR, Hayes AJ, Ireland H, Brinkmann H, Newton IP, Batlle E, Simon-Assmann P, Clevers H, Nathke IS, Clarke AR, Winton DJ (2004) Loss of Apc in vivo immediately perturbs Wnt signaling, differentiation, and migration. *Genes Dev* **18:** 1385-1390

Sanson B, White P, Vincent JP (1996) Uncoupling cadherin-based adhesion from wingless signalling in Drosophila. *Nature* **383:** 627-630

Sartor RB (2004) Therapeutic manipulation of the enteric microflora in inflammatory bowel diseases: antibiotics, probiotics, and prebiotics. *Gastroenterology* **126:** 1620-1633

Sasai H, Masaki M, Wakitani K (2000) Suppression of polypogenesis in a new mouse strain with a truncated Apc(Delta474) by a novel COX-2 inhibitor, JTE-522. *Carcinogenesis* **21:** 953-958

Sato T, Stange DE, Ferrante M, Vries RG, Van Es JH, Van den Brink S, Van Houdt WJ, Pronk A, Van Gorp J, Siersema PD, Clevers H (2011a) Long-term expansion of epithelial organoids from human colon, adenoma, adenocarcinoma, and Barrett's epithelium. *Gastroenterology* **141:** 1762-1772

Sato T, van Es JH, Snippert HJ, Stange DE, Vries RG, van den Born M, Barker N, Shroyer NF, van de Wetering M, Clevers H (2011b) Paneth cells constitute the niche for Lgr5 stem cells in intestinal crypts. *Nature* **469:** 415-418

Sato T, Vries RG, Snippert HJ, van de Wetering M, Barker N, Stange DE, van Es JH, Abo A, Kujala P, Peters PJ, Clevers H (2009) Single Lgr5 stem cells build crypt-villus structures in vitro without a mesenchymal niche. *Nature* **459:** 262-265

Schepers AG, Snippert HJ, Stange DE, van den Born M, van Es JH, van de Wetering M, Clevers H (2012) Lineage tracing reveals Lgr5+ stem cell activity in mouse intestinal adenomas. *Science* **337:** 730-735

Schmeiser K, Grand RJ (1999) The fate of E- and P-cadherin during the early stages of apoptosis. *Cell Death Differ* **6:** 377-386

Schmierer B, Hill CS (2007) TGFbeta-SMAD signal transduction: molecular specificity and functional flexibility. *Nat Rev Mol Cell Biol* **8:** 970-982

Schneider MR, Dahlhoff M, Horst D, Hirschi B, Trülzsch K, Müller-Höcker J, Vogelmann R, Allgäuer M, Gerhard M, Steininger S, Wolf E, Kolligs FT (2010) A key role for E-cadherin in intestinal homeostasis and Paneth cell maturation. *PLoS One* **5:** e14325

Schuh R, Vestweber D, Riede I, Ringwald M, Rosenberg U, Jäckle H, Kemler R (1986) Molecular cloning of the mouse cell adhesion molecule uvomorulin: cDNA contains a B1-related sequence. *Proc Natl Acad Sci U S A* **83:** 1364-1368

Schuijers J, Clevers H (2012) Adult mammalian stem cells: the role of Wnt, Lgr5 and R-spondins. *EMBO J* **31:** 2685-2696

Schwenk F, Baron U, Rajewsky K (1995) A cre-transgenic mouse strain for the ubiquitous deletion of loxP-flanked gene segments including deletion in germ cells. *Nucleic Acids Res* **23:** 5080-5081

Schwenter F, Faughnan ME, Gradinger AB, Berk T, Gryfe R, Pollett A, Cohen Z, Gallinger S, Durno C (2012) Juvenile polyposis, hereditary hemorrhagic telangiectasia, and early onset colorectal cancer in patients with SMAD4 mutation. *J Gastroenterol* **47:** 795-804

Schönig K, Schwenk F, Rajewsky K, Bujard H (2002) Stringent doxycycline dependent control of CRE recombinase in vivo. *Nucleic Acids Res* **30:** e134

Sellon RK, Tonkonogy S, Schultz M, Dieleman LA, Grenther W, Balish E, Rennick DM, Sartor RB (1998) Resident enteric bacteria are necessary for development of spontaneous colitis and immune system activation in interleukin-10-deficient mice. *Infect Immun* **66:** 5224-5231

Shan W, Tanaka H, Phillips G, Arndt K, Yoshida M, Colman D, Shapiro L (2000) Functional cis-heterodimers of N- and R-cadherins. *J Cell Biol* **148:** 579-590

Shan W, Yagita Y, Wang Z, Koch A, Svenningsen A, Gruzglin E, Pedraza L, Colman D (2004) The minimal essential unit for cadherin-mediated intercellular adhesion comprises extracellular domains 1 and 2. *J Biol Chem* **279:** 55914-55923

Shapiro L, Fannon A, Kwong P, Thompson A, Lehmann M, Grübel G, Legrand J, Als-Nielsen J, Colman D, Hendrickson W (1995) Structural basis of cell-cell adhesion by cadherins. *Nature* **374:** 327-337

Shi Y, Massagué J (2003) Mechanisms of TGF-beta signaling from cell membrane to the nucleus. *Cell* **113:** 685-700

Shibata H, Toyama K, Shioya H, Ito M, Hirota M, Hasegawa S, Matsumoto H, Takano H, Akiyama T, Toyoshima K, Kanamaru R, Kanegae Y, Saito I, Nakamura Y, Shiba K, Noda T (1997) Rapid colorectal adenoma formation initiated by conditional targeting of the Apc gene. *Science* **278:** 120-123

Shimada S, Mimata A, Sekine M, Mogushi K, Akiyama Y, Fukamachi H, Jonkers J, Tanaka H, Eishi Y, Yuasa Y (2012) Synergistic tumour suppressor activity of E-cadherin and p53 in a conditional mouse model for metastatic diffuse-type gastric cancer. *Gut* **61:** 344-353

Shroyer NF, Helmrath MA, Wang VY, Antalffy B, Henning SJ, Zoghbi HY (2007) Intestine-specific ablation of mouse atonal homolog 1 (Math1) reveals a role in cellular homeostasis. *Gastroenterology* **132:** 2478-2488

Silverman KA, Koratkar R, Siracusa LD, Buchberg AM (2002) Identification of the modifier of Min 2 (Mom2) locus, a new mutation that influences Apc-induced intestinal neoplasia. *Genome Res* **12:** 88-97

Sirard C, de la Pompa JL, Elia A, Itie A, Mirtsos C, Cheung A, Hahn S, Wakeham A, Schwartz L, Kern SE, Rossant J, Mak TW (1998) The tumor suppressor gene Smad4/Dpc4 is required for gastrulation and later for anterior development of the mouse embryo. *Genes Dev* **12:** 107-119

Sjöblom T, Jones S, Wood LD, Parsons DW, Lin J, Barber TD, Mandelker D, Leary RJ, Ptak J, Silliman N, Szabo S, Buckhaults P, Farrell C, Meeh P, Markowitz SD, Willis J, Dawson D, Willson JK, Gazdar AF, Hartigan J, Wu L, Liu C, Parmigiani G, Park BH, Bachman KE, Papadopoulos N, Vogelstein B, Kinzler KW, Velculescu VE (2006) The consensus coding sequences of human breast and colorectal cancers. *Science* **314:** 268-274

Smalley-Freed WG, Efimov A, Burnett PE, Short SP, Davis MA, Gumucio DL, Washington MK, Coffey RJ, Reynolds AB (2010) p120-catenin is essential for maintenance of barrier function and intestinal homeostasis in mice. *J Clin Invest* **120:** 1824-1835

Smalley-Freed WG, Efimov A, Short SP, Jia P, Zhao Z, Washington MK, Robine S, Coffey RJ, Reynolds AB (2011) Adenoma formation following limited ablation of p120-catenin in the mouse intestine. *PLoS One* **6:** e19880

Smith K, Bui TD, Poulsom R, Kaklamanis L, Williams G, Harris AL (1999) Up-regulation of macrophage wnt gene expression in adenoma-carcinoma progression of human colorectal cancer. *Br J Cancer* **81:** 496-502

Smith K, Johnson K, Bryan T, Hill D, Markowitz S, Willson J, Paraskeva C, Petersen G, Hamilton S, Vogelstein B (1993) The APC gene product in normal and tumor cells. *Proc Natl Acad Sci U S A* **90:** 2846-2850

Smits R, Hofland N, Edelmann W, Geugien M, Jagmohan-Changur S, Albuquerque C, Breukel C, Kucherlapati R, Kielman MF, Fodde R (2000a) Somatic Apc mutations are selected upon their capacity to inactivate the beta-catenin downregulating activity. *Genes Chromosomes Cancer* **29:** 229-239

Smits R, Kielman MF, Breukel C, Zurcher C, Neufeld K, Jagmohan-Changur S, Hofland N, van Dijk J, White R, Edelmann W, Kucherlapati R, Khan PM, Fodde R (1999) Apc1638T: a mouse model delineating critical domains of the adenomatous polyposis coli protein involved in tumorigenesis and development. *Genes Dev* **13:** 1309-1321

Smits R, Ruiz P, Diaz-Cano S, Luz A, Jagmohan-Changur S, Breukel C, Birchmeier C, Birchmeier W, Fodde R (2000b) E-cadherin and adenomatous polyposis coli mutations are synergistic in intestinal tumor initiation in mice. *Gastroenterology* **119:** 1045-1053

Sodir NM, Chen X, Park R, Nickel AE, Conti PS, Moats R, Bading JR, Shibata D, Laird PW (2006) Smad3 deficiency promotes tumorigenesis in the distal colon of ApcMin/+ mice. *Cancer Res* **66:** 8430-8438

Solanas G, Cortina C, Sevillano M, Batlle E (2011) Cleavage of E-cadherin by ADAM10 mediates epithelial cell sorting downstream of EphB signalling. *Nat Cell Biol* **13:** 1100-1107

Soriano P (1999) Generalized lacZ expression with the ROSA26 Cre reporter strain. *Nat Genet* **21:** 70-71

Sparks AB, Morin PJ, Vogelstein B, Kinzler KW (1998) Mutational analysis of the APC/beta-catenin/Tcf pathway in colorectal cancer. *Cancer Res* **58:** 1130-1134

Srinivas S, Watanabe T, Lin C, William C, Tanabe Y, Jessell T, Costantini F (2001) Cre reporter strains produced by targeted insertion of EYFP and ECFP into the ROSA26 locus. *BMC Dev Biol* **1:** 4

Staal FJ, Noort Mv M, Strous GJ, Clevers HC (2002) Wnt signals are transmitted through N-terminally dephosphorylated beta-catenin. *EMBO Rep* **3:** 63-68

Starr T, Allaei R, Silverstein K, Staggs R, Sarver A, Bergemann T, Gupta M, O'Sullivan M, Matise I, Dupuy A, Collier L, Powers S, Oberg A, Asmann Y, Thibodeau S, Tessarollo L, Copeland N, Jenkins N, Cormier R, Largaespada D (2009) A transposon-based genetic screen in mice identifies genes altered in colorectal cancer. *Science* **323:** 1747-1750

Starr TK, Scott PM, Marsh BM, Zhao L, Than BL, O'Sullivan MG, Sarver AL, Dupuy AJ, Largaespada DA, Cormier RT (2011) A Sleeping Beauty transposon-mediated screen identifies murine susceptibility genes for adenomatous polyposis coli (Apc)-dependent intestinal tumorigenesis. *Proc Natl Acad Sci U S A* **108:** 5765-5770

Steinhusen U, Weiske J, Badock V, Tauber R, Bommert K, Huber O (2001) Cleavage and shedding of E-cadherin after induction of apoptosis. *J Biol Chem* **276:** 4972-4980

Stemmler MP, Bedzhov I (2010) A Cdh1HA knock-in allele rescues the Cdh1-/- phenotype but shows essential Cdh1 function during placentation. *Dev Dyn* **239:** 2330-2344

Stemmler MP, Hecht A, Kemler R (2005) E-cadherin intron 2 contains cis-regulatory elements essential for gene expression. *Development* **132:** 965-976

Stemmler MP, Hecht A, Kinzel B, Kemler R (2003) Analysis of regulatory elements of E-cadherin with reporter gene constructs in transgenic mouse embryos. *Dev Dyn* **227:** 238-245

Stephenson RO, Yamanaka Y, Rossant J (2010) Disorganized epithelial polarity and excess trophectoderm cell fate in preimplantation embryos lacking E-cadherin. *Development* **137:** 3383-3391

Stockinger A, Eger A, Wolf J, Beug H, Foisner R (2001) E-cadherin regulates cell growth by modulating proliferation-dependent beta-catenin transcriptional activity. *J Cell Biol* **154:** 1185-1196

Su L, Kinzler K, Vogelstein B, Preisinger A, Moser A, Luongo C, Gould K, Dove W (1992) Multiple intestinal neoplasia caused by a mutation in the murine homolog of the APC gene. *Science* **256:** 668-670

Su LK, Vogelstein B, Kinzler KW (1993) Association of the APC tumor suppressor protein with catenins. *Science* **262:** 1734-1737

Sugioka K, Mizumoto K, Sawa H (2011) Wnt regulates spindle asymmetry to generate asymmetric nuclear β-catenin in C. elegans. *Cell* **146:** 942-954

Suraweera N, Haines J, McCart A, Rogers P, Latchford A, Coster M, Polanco-Echeverry G, Guenther T, Wang J, Sieber O, Tomlinson I, Silver A (2006) Genetic determinants modulate susceptibility to pregnancy-associated tumourigenesis in a recombinant line of Min mice. *Hum Mol Genet* **15:** 3429-3435

Syder AJ, Karam SM, Mills JC, Ippolito JE, Ansari HR, Farook V, Gordon JI (2004) A transgenic mouse model of metastatic carcinoma involving transdifferentiation of a gastric epithelial lineage progenitor to a neuroendocrine phenotype. *Proc Natl Acad Sci U S A* **101:** 4471-4476

Taddei ML, Giannoni E, Fiaschi T, Chiarugi P (2012) Anoikis: an emerging hallmark in health and diseases. *J Pathol* **226:** 380-393

Takahashi K, Suzuki K (1996) Density-dependent inhibition of growth involves prevention of EGF receptor activation by E-cadherin-mediated cell-cell adhesion. *Exp Cell Res* **226:** 214-222

Takaku K, Oshima M, Miyoshi H, Matsui M, Seldin M, Taketo M (1998) Intestinal tumorigenesis in compound mutant mice of both Dpc4 (Smad4) and Apc genes. *Cell* **92:** 645-656

Takaku K, Wrana JL, Robertson EJ, Taketo MM (2002) No effects of Smad2 (madh2) null mutation on malignant progression of intestinal polyps in Apc(delta716) knockout mice. *Cancer Res* **62:** 4558-4561

Takano S, Kanai F, Jazag A, Ijichi H, Yao J, Ogawa H, Enomoto N, Omata M, Nakao A (2007) Smad4 is essential for down-regulation of E-cadherin induced by TGF-beta in pancreatic cancer cell line PANC-1. *J Biochem* **141:** 345-351

Takeichi M (1977) Functional correlation between cell adhesive properties and some cell surface proteins. *J Cell Biol* **75:** 464-474

Takeichi M (1995) Morphogenetic roles of classic cadherins. *Curr Opin Cell Biol* **7:** 619-627

Taketo MM, Takaku K (2000) Gastrointestinal tumorigenesis in Smad4 (Dpc4) mutant mice. *Hum Cell* **13:** 85-95

Talley NJ, Abreu MT, Achkar JP, Bernstein CN, Dubinsky MC, Hanauer SB, Kane SV, Sandborn WJ, Ullman TA, Moayyedi P, Force ACoGIT (2011) An evidence-based systematic review on medical therapies for inflammatory bowel disease. *Am J Gastroenterol* **106 Suppl 1:** S2-25; quiz S26

Tamai K, Zeng X, Liu C, Zhang X, Harada Y, Chang Z, He X (2004) A mechanism for Wnt coreceptor activation. *Mol Cell* **13:** 149-156

Tamura K, Shan W, Hendrickson W, Colman D, Shapiro L (1998) Structure-function analysis of cell adhesion by neural (N-) cadherin. *Neuron* **20:** 1153-1163

Tanaka T, Watanabe T, Kazama Y, Tanaka J, Kanazawa T, Kazama S, Nagawa H (2006) Chromosome 18q deletion and Smad4 protein inactivation correlate with liver metastasis: A study matched for T- and N- classification. *Br J Cancer* **95:** 1562-1567

Tepass U, Gruszynski-DeFeo E, Haag TA, Omatyar L, Török T, Hartenstein V (1996) shotgun encodes Drosophila E-cadherin and is preferentially required during cell rearrangement in the neurectoderm and other morphogenetically active epithelia. *Genes Dev* **10:** 672-685

Tessmer MS, Fugere C, Stevenaert F, Naidenko OV, Chong HJ, Leclercq G, Brossay L (2007) KLRG1 binds cadherins and preferentially associates with SHIP-1. *Int Immunol* **19:** 391-400

Thiagalingam S, Lengauer C, Leach FS, Schutte M, Hahn SA, Overhauser J, Willson JK, Markowitz S, Hamilton SR, Kern SE, Kinzler KW, Vogelstein B (1996) Evaluation of candidate tumour suppressor genes on chromosome 18 in colorectal cancers. *Nat Genet* **13:** 343-346

Thiery J (2002) Epithelial-mesenchymal transitions in tumour progression. *Nat Rev Cancer* **2:** 442-454

Thiery JP (2003) Epithelial-mesenchymal transitions in development and pathologies. *Curr Opin Cell Biol* **15:** 740-746

Thompson B, Townsley F, Rosin-Arbesfeld R, Musisi H, Bienz M (2002) A new nuclear component of the Wnt signalling pathway. *Nat Cell Biol* **4:** 367-373

Thoreson MA, Reynolds AB (2002) Altered expression of the catenin p120 in human cancer: implications for tumor progression. *Differentiation* **70:** 583-589

Tian H, Biehs B, Warming S, Leong KG, Rangell L, Klein OD, de Sauvage FJ (2011) A reserve stem cell population in small intestine renders Lgr5-positive cells dispensable. *Nature* **478:** 255-259

Tichelaar JW, Lu W, Whitsett JA (2000) Conditional expression of fibroblast growth factor-7 in the developing and mature lung. *J Biol Chem* **275:** 11858-11864

Tinkle CL, Lechler T, Pasolli HA, Fuchs E (2004) Conditional targeting of E-cadherin in skin: insights into hyperproliferative and degenerative responses. *Proc Natl Acad Sci U S A* **101:** 552-557

Tinkle CL, Pasolli HA, Stokes N, Fuchs E (2008) New insights into cadherin function in epidermal sheet formation and maintenance of tissue integrity. *Proc Natl Acad Sci U S A* **105:** 15405-15410

Tiwari N, Gheldof A, Tatari M, Christofori G (2012) EMT as the ultimate survival mechanism of cancer cells. *Semin Cancer Biol* **22:** 194-207

Tolwinski NS, Wehrli M, Rives A, Erdeniz N, DiNardo S, Wieschaus E (2003) Wg/Wnt signal can be transmitted through arrow/LRP5,6 and Axin independently of Zw3/Gsk3beta activity. *Dev Cell* **4:** 407-418

Tomita K, van Bokhoven A, van Leenders GJ, Ruijter ET, Jansen CF, Bussemakers MJ, Schalken JA (2000) Cadherin switching in human prostate cancer progression. *Cancer Res* **60:** 3650-3654

Townsley FM, Cliffe A, Bienz M (2004) Pygopus and Legless target Armadillo/beta-catenin to the nucleus to enable its transcriptional co-activator function. *Nat Cell Biol* **6:** 626-633

Tronche F, Kellendonk C, Kretz O, Gass P, Anlag K, Orban PC, Bock R, Klein R, Schütz G (1999) Disruption of the glucocorticoid receptor gene in the nervous system results in reduced anxiety. *Nat Genet* **23:** 99-103

Trotman LC, Niki M, Dotan ZA, Koutcher JA, Di Cristofano A, Xiao A, Khoo AS, Roy-Burman P, Greenberg NM, Van Dyke T, Cordon-Cardo C, Pandolfi PP (2003) Pten dose dictates cancer progression in the prostate. *PLoS Biol* **1:** E59

Trowe MO, Maier H, Petry M, Schweizer M, Schuster-Gossler K, Kispert A (2011) Impaired stria vascularis integrity upon loss of E-cadherin in basal cells. *Dev Biol* **359:** 95-107

Truett G, Heeger P, Mynatt R, Truett A, Walker J, Warman M (2000) Preparation of PCR-quality mouse genomic DNA with hot sodium hydroxide and tris (HotSHOT). *Biotechniques* **29:** 52, 54

Tunggal JA, Helfrich I, Schmitz A, Schwarz H, Günzel D, Fromm M, Kemler R, Krieg T, Niessen CM (2005) E-cadherin is essential for in vivo epidermal barrier function by regulating tight junctions. *EMBO J* **24:** 1146-1156

van de Wetering M, Barker N, Harkes IC, van der Heyden M, Dijk NJ, Hollestelle A, Klijn JG, Clevers H, Schutte M (2001) Mutant E-cadherin breast cancer cells do not display constitutive Wnt signaling. *Cancer Res* **61:** 278-284

Van den Bossche J, Bogaert P, van Hengel J, Guérin CJ, Berx G, Movahedi K, Van den Bergh R, Pereira-Fernandes A, Geuns JM, Pircher H, Dorny P, Grooten J, De Baetselier P, Van Ginderachter JA (2009) Alternatively activated macrophages engage in homotypic and heterotypic interactions through IL-4 and polyamine-induced E-cadherin/catenin complexes. *Blood* **114:** 4664-4674

Van der Flier LG, Sabates-Bellver J, Oving I, Haegebarth A, De Palo M, Anti M, Van Gijn ME, Suijkerbuijk S, Van de Wetering M, Marra G, Clevers H (2007) The Intestinal Wnt/TCF Signature. *Gastroenterology* **132:** 628-632

van Es JH, van Gijn ME, Riccio O, van den Born M, Vooijs M, Begthel H, Cozijnsen M, Robine S, Winton DJ, Radtke F, Clevers H (2005) Notch/gamma-secretase inhibition turns proliferative cells in intestinal crypts and adenomas into goblet cells. *Nature* **435:** 959-963

van Hattem WA, Langeveld D, de Leng WW, Morsink FH, van Diest PJ, Iacobuzio-Donahue CA, Giardiello FM, Offerhaus GJ, Brosens LA (2011) Histologic variations in juvenile polyp phenotype correlate with genetic defect underlying juvenile polyposis. *Am J Surg Pathol* **35:** 530-536

van Roy F, Berx G (2008) The cell-cell adhesion molecule E-cadherin. *Cell Mol Life Sci* **65:** 3756-3788

Vandesompele J, De Preter K, Pattyn F, Poppe B, Van Roy N, De Paepe A, Speleman F (2002) Accurate normalization of real-time quantitative RT-PCR data by geometric averaging of multiple internal control genes. *Genome Biol* **3:** RESEARCH0034

Vasioukhin V, Bauer C, Yin M, Fuchs E (2000) Directed actin polymerization is the driving force for epithelial cell-cell adhesion. *Cell* **100:** 209-219

Vasioukhin V, Degenstein L, Wise B, Fuchs E (1999) The magical touch: genome targeting in epidermal stem cells induced by tamoxifen application to mouse skin. *Proc Natl Acad Sci U S A* **96:** 8551-8556

Vendome J, Posy S, Jin X, Bahna F, Ahlsen G, Shapiro L, Honig B (2011) Molecular design principles underlying β-strand swapping in the adhesive dimerization of cadherins. *Nat Struct Mol Biol* **18:** 693-700

Voiculescu O, Charnay P, Schneider-Maunoury S (2000) Expression pattern of a Krox-20/Cre knock-in allele in the developing hindbrain, bones, and peripheral nervous system. *Genesis* **26:** 123-126

von Burstin J, Eser S, Paul MC, Seidler B, Brandl M, Messer M, von Werder A, Schmidt A, Mages J, Pagel P, Schnieke A, Schmid RM, Schneider G, Saur D (2009) E-cadherin regulates metastasis of pancreatic cancer in vivo and is suppressed by a SNAIL/HDAC1/HDAC2 repressor complex. *Gastroenterology* **137:** 361-371, 371.e361-365

Wang F, Wang J, Liu D, Su Y (2010) Normalizing genes for real-time polymerase chain reaction in epithelial and nonepithelial cells of mouse small intestine. *Anal Biochem* **399:** 211-217

Wang S, Krinks M, Lin K, Luyten FP, Moos M, Jr. (1997) Frzb, a secreted protein expressed in the Spemann organizer, binds and inhibits Wnt-8. *Cell* **88:** 757-766

Watabe M, Nagafuchi A, Tsukita S, Takeichi M (1994) Induction of polarized cell-cell association and retardation of growth by activation of the E-cadherin-catenin adhesion system in a dispersed carcinoma line. *J Cell Biol* **127:** 247-256

Wells JM, Melton DA (1999) Vertebrate endoderm development. *Annu Rev Cell Dev Biol* **15:** 393-410

Wheeler JM (2005) Epigenetics, mismatch repair genes and colorectal cancer. *Ann R Coll Surg Engl* **87:** 15-20

Willert K, Jones KA (2006) Wnt signaling: is the party in the nucleus? *Genes Dev* **20:** 1394-1404

Wong HC, Bourdelas A, Krauss A, Lee HJ, Shao Y, Wu D, Mlodzik M, Shi DL, Zheng J (2003) Direct binding of the PDZ domain of Dishevelled to a conserved internal sequence in the C-terminal region of Frizzled. *Mol Cell* **12:** 1251-1260

Wood LD, Parsons DW, Jones S, Lin J, Sjöblom T, Leary RJ, Shen D, Boca SM, Barber T, Ptak J, Silliman N, Szabo S, Dezso Z, Ustyanksky V, Nikolskaya T, Nikolsky Y, Karchin R, Wilson PA, Kaminker JS, Zhang Z, Croshaw R, Willis J, Dawson D, Shipitsin M, Willson JK, Sukumar S, Polyak K, Park BH, Pethiyagoda CL, Pant PV, Ballinger DG, Sparks AB, Hartigan J, Smith DR, Suh E, Papadopoulos N, Buckhaults P, Markowitz SD, Parmigiani G, Kinzler KW, Velculescu VE, Vogelstein B (2007) The genomic landscapes of human breast and colorectal cancers. *Science* **318:** 1108-1113

Woodford-Richens K, Bevan S, Churchman M, Dowling B, Jones D, Norbury CG, Hodgson SV, Desai D, Neale K, Phillips RK, Young J, Leggett B, Dunlop M, Rozen P, Eng C, Markie D, Rodriguez-Bigas MA, Sheridan E, Iwama T, Eccles D, Smith GT, Kim JC, Kim KM, Sampson JR, Evans G, Tejpar S, Bodmer WF, Tomlinson IP, Houlston RS (2000a) Analysis of genetic and phenotypic heterogeneity in juvenile polyposis. *Gut* **46:** 656-660

Woodford-Richens K, Williamson J, Bevan S, Young J, Leggett B, Frayling I, Thway Y, Hodgson S, Kim JC, Iwama T, Novelli M, Sheer D, Poulsom R, Wright N, Houlston R, Tomlinson I (2000b) Allelic loss at SMAD4 in polyps from juvenile polyposis patients and use of fluorescence in situ hybridization to demonstrate clonal origin of the epithelium. *Cancer Res* **60:** 2477-2482

Woodford-Richens KL, Rowan AJ, Gorman P, Halford S, Bicknell DC, Wasan HS, Roylance RR, Bodmer WF, Tomlinson IP (2001a) SMAD4 mutations in colorectal cancer probably occur before chromosomal instability, but after divergence of the microsatellite instability pathway. *Proc Natl Acad Sci U S A* **98:** 9719-9723

Woodford-Richens KL, Rowan AJ, Poulsom R, Bevan S, Salovaara R, Aaltonen LA, Houlston RS, Wright NA, Tomlinson IP (2001b) Comprehensive analysis of SMAD4 mutations and protein expression in juvenile polyposis: evidence for a distinct genetic pathway and polyp morphology in SMAD4 mutation carriers. *Am J Pathol* **159:** 1293-1300

Wu ZQ, Brabletz T, Fearon E, Willis AL, Hu CY, Li XY, Weiss SJ (2012) Canonical Wnt suppressor, Axin2, promotes colon carcinoma oncogenic activity. *Proc Natl Acad Sci U S A* **109:** 11312-11317

Xu Q, Wang Y, Dabdoub A, Smallwood PM, Williams J, Woods C, Kelley MW, Jiang L, Tasman W, Zhang K, Nathans J (2004) Vascular development in the retina and inner ear: control by Norrin and Frizzled-4, a high-affinity ligand-receptor pair. *Cell* **116:** 883-895

Yamamoto E, Suzuki H, Takamaru H, Yamamoto H, Toyota M, Shinomura Y (2011) Role of DNA methylation in the development of diffuse-type gastric cancer. *Digestion* **83:** 241-249

Yanagawa S, Matsuda Y, Lee JS, Matsubayashi H, Sese S, Kadowaki T, Ishimoto A (2002) Casein kinase I phosphorylates the Armadillo protein and induces its degradation in Drosophila. *EMBO J* **21:** 1733-1742

Yang J, Mani SA, Donaher JL, Ramaswamy S, Itzykson RA, Come C, Savagner P, Gitelman I, Richardson A, Weinberg RA (2004) Twist, a master regulator of morphogenesis, plays an essential role in tumor metastasis. *Cell* **117:** 927-939

Yang J, Weinberg R (2008) Epithelial-mesenchymal transition: at the crossroads of development and tumor metastasis. *Dev Cell* **14:** 818-829

Yang L, Lin C, Liu ZR (2006) P68 RNA helicase mediates PDGF-induced epithelial mesenchymal transition by displacing Axin from beta-catenin. *Cell* **127:** 139-155

Yang Q, Bermingham NA, Finegold MJ, Zoghbi HY (2001) Requirement of Math1 for secretory cell lineage commitment in the mouse intestine. *Science* **294:** 2155-2158

Yang X, Li C, Xu X, Deng C (1998) The tumor suppressor SMAD4/DPC4 is essential for epiblast proliferation and mesoderm induction in mice. *Proc Natl Acad Sci U S A* **95:** 3667-3672

Yap A, Brieher W, Pruschy M, Gumbiner B (1997) Lateral clustering of the adhesive ectodomain: a fundamental determinant of cadherin function. *Curr Biol* **7:** 308-315

Yap AS, Crampton MS, Hardin J (2007) Making and breaking contacts: the cellular biology of cadherin regulation. *Curr Opin Cell Biol* **19:** 508-514

Yoshida C, Takeichi M (1982) Teratocarcinoma cell adhesion: identification of a cell-surface protein involved in calcium-dependent cell aggregation. *Cell* **28:** 217-224

Yoshida-Noro C, Suzuki N, Takeichi M (1984) Molecular nature of the calcium-dependent cell-cell adhesion system in mouse teratocarcinoma and embryonic cells studied with a monoclonal antibody. *Dev Biol* **101:** 19-27

Young P, Boussadia O, Berger P, Leone DP, Charnay P, Kemler R, Suter U (2002) E-cadherin is required for the correct formation of autotypic adherens junctions of the outer mesaxon but not for the integrity of myelinated fibers of peripheral nerves. *Mol Cell Neurosci* **21:** 341-351

Young P, Boussadia O, Halfter H, Grose R, Berger P, Leone DP, Robenek H, Charnay P, Kemler R, Suter U (2003) E-cadherin controls adherens junctions in the epidermis and the renewal of hair follicles. *EMBO J* **22:** 5723-5733

Zeng Q, Phukan S, Xu Y, Sadim M, Rosman DS, Pennison M, Liao J, Yang GY, Huang CC, Valle L, Di Cristofano A, de la Chapelle A, Pasche B (2009) Tgfbr1 haploinsufficiency is a potent modifier of colorectal cancer development. *Cancer Res* **69:** 678-686

Zhang B, Halder SK, Kashikar ND, Cho YJ, Datta A, Gorden DL, Datta PK (2010) Antimetastatic role of Smad4 signaling in colorectal cancer. *Gastroenterology* **138:** 969-980.e961-963

Zhu W, Leber B, Andrews DW (2001) Cytoplasmic O-glycosylation prevents cell surface transport of E-cadherin during apoptosis. *EMBO J* **20:** 5999-6007

Zhu Y, Richardson JA, Parada LF, Graff JM (1998) Smad3 mutant mice develop metastatic colorectal cancer. *Cell* **94:** 703-714